PHOSPHORUS BIDENTATE LIGAND INTERACTION AT PLATINUM GROUP METALS: A CATALYTIC AND SOLID STATE STUDY

by

Dumisani Vincent Kama

A dissertation submitted to meet the requirements for the degree of

MAGISTER SCIENTIAE

In the

DEPARTMENT OF CHEMISTRY

FACULTY OF NATURAL AND AGRICULTURAL SCIENCES

At the

UNIVERSITY OF THE FREE STATE

SUPERVISOR: PROF. HENDRIK G. VISSER

CO-SUPERVISOR: DR. ALICE BRINK

FEBRUARY 2015

Acknowledgements

Firstly, I would like to thank God for all the knowledge, understanding and wisdom He equipped me with, to ensure that no challenge was big enough for me through this journey. I believe with all my heart that I'm nothing without You. Thank You!

Secondly, I would like to express my deepest gratitude for the help and support I obtained from the following persons, whom I have no doubt have contributed greatly to the success of this study.

To Prof. André Roodt. Firstly I'm honored to have known a person of your caliber in my life. Thank you for giving me such an opportunity. Your guidance and support is highly appreciated.

To Prof. Deon Visser. Thank you for believing in me and for all your guidance, comments, suggestions and support. Everything you did for me is greatly appreciated.

To Dr. Alice Brink. Thank you for your time, effort, guidance, support and advices. You made me believe in myself and for that I would always respect.

To Ilana, Marietjie, Carla and Renier, thank you for your support. You were always available to assist me from the beginning of this project. Thank you!

To the Inorganic group, thank you for all for sharing your knowledge and for encouraging nothing but excellence. Without you none of this would have been possible.

To Nthabiseng, Sibongile, Orbett, Penny, Lebohang and Daniel, thank you for all the joy, jokes, encouragement and support. You have made this journey worth traveling.

To my family, without your unconditional love and support I wouldn't be where I am today. I will always love you.

Financial assistance from the University of the Free State and SASOL towards this research is also gratefully acknowledged.

Table of Contents

Abbreviations and Symbols

Label	Definitions
Å	Angstrom
δ	Chemical shift
ν	Stretching frequency on IR
°	Degrees
°C	Degrees Celsius
T	Temperature
g	Gram
M	$Mol.dm^{-3}$
π	Pi
α	Alpha
γ	Gamma
σ	Sigma
β	Beta
λ	Wavelength
Z	Number of asymmetric units per unit cell
θ	Theta
$\theta_{N\text{-}sub}$	Effective Tolman-based N-substituent steric effect
s	Singlet
d	Doublet
m	Multiplet
ppm	(Unit of chemical shift) Parts per million
NMR	Nuclear magnetic resonance
$CDCl_3$	Deuterated chloroform
CD_2Cl_2	Deuterated dichloromethane
DCM	Dichloromethane
IR	Infrared spectroscopy
PNP	Bis(diphenylphosphino)alkylamine
Ph	Ph Phenyl
CO	Carbonyl
cod	Cyclooctadiene
Cl-Ph-PNP	*N*,*N*-Bis(diphenylphosphino)-4-chloroaniline
F-Ph-PNP	*N*,*N*-Bis(diphenylphosphino)-4-fluoroaniline
CH_3-Ph-PNP	*N*,*N*-Bis(diphenylphosphino)-*p*-toluidine
5-*p*-tolyl-PNP	*N*,*N*-Bis(di-*p*-tolylphosphino)-*p*-toluidine
4-*p*-tolyl-*o*-tol	*N*,*N*-Bis(di-*p*-tolylphosphino)-*o*-toluidine
Chzyl-4-*p*-tolyl	*N*,*N*-Bis(di-*p*-tolylphosphino)cyclohexylamine
Cbutyl-4-*p*-tolyl	*N*,*N*-Bis(di-*p*-tolylphosphino)cyclobutylamine

Summary

Hydroformylation of alkenes (olefins) is one of the world's leading aldehyde producing process. The resulting aldehydes can easily be converted to secondary products such as alcohols for production of plasticizers and detergents. Recent studies are directed towards the production of highly selective catalysts as linear aldehydes are the most desired products. A number of phosphine ligands have been investigated regarding this process, showing that fine tuning of the ligands electronic and steric properties significantly affects the activity and selectivity of a catalyst.

A range of diphosphinoamine (PNP) ligands with various substituents on the nitrogen atom were synthesized and characterized, namely (**1**) *N*,*N*-Bis(diphenylphosphino)-*p*-toluidine [CH_3-Ph-PNP],(**2**) *N*,*N*-Bis(diphenylphosphino)-4-chloroaniline [Cl-Ph-PNP], (**3**) *N*,*N*-Bis(diphenylphosphino)-4-fluoroaniline [F-Ph-PNP], (**4**) *N*,*N*-Bis(di-*p*-tolylphosphino)-*p*-toluidine [5-*p*-tolyl-PNP], (**5**) *N*,*N*-Bis(di-*p*-tolylphosphino)-*o*-toluidine [4-*p*-tolyl-*o*-tol], (**6**) *N*,*N*-Bis(di-*p*-tolylphosphino)cyclohexylamine [Chzyl-4-*p*-tolyl] and (**7**) *N*,*N*-Bis(di-*p*-tolylphosphino)cyclobutylamine [Cbutyl-4-*p*-tolyl] (see **Figure 1**). These ligands were systematically synthesized to induce different steric and electronic properties on the nitrogen atom. All the ligands were coordinated to Pt(II) and Pd(II) metals to serve as models for Rh(I) pre-catalysts systems to be used in hydroformylation of 1-octene. Metal complexes which produced crystals suitable for X-ray data analysis were (**A**) Dichloro-[*N*,*N*-Bis(di-*p*-tolylphosphino)-*p*-toluidine-κ^2*P,P'*]platinum(II) [Pt(5-*p*-tolyl-PNP)Cl_2], (**B**) Dichloro-[*N*,*N*-Bis(di-*p*-tolylphosphino)-*o*-toluidine-κ^2*P,P'*]platinum(II) [Pt(4-*p*-tolyl-*o*-tol)Cl_2], (**C**) Dichloro-[*N*,*N*-Bis(diphenylphosphino)-4-chloroaniline-κ^2*P,P'*]palladium(II) [Pd(Cl-Ph-PNP)Cl_2], (**D**) Dichloro-[*N*,*N*-Bis(diphenylphosphino)-*p*-toluidine-κ^2*P,P'*]palladium(II) [Pd(5-*p*-tolyl-PNP)Cl_2], (**E**) Dichloro-[*N*,*N*-Bis(di-*p*-tolylphosphino)cyclobutylamine-κ^2*P,P'*]platinum(II) [Pt(Cbutyl-4-*p*-tolyl)Cl_2] and (**F**) Dichloro-[*N*,*N*-Bis(di-*p*-tolylphosphino)cyclohexylamine-κ^2*P,P'*]palladium(II) [Pd(Chzyl-4-*p*-tolyl)Cl_2] (see **Figure 2**). This data provided information regarding the coordination modes of the ligands.

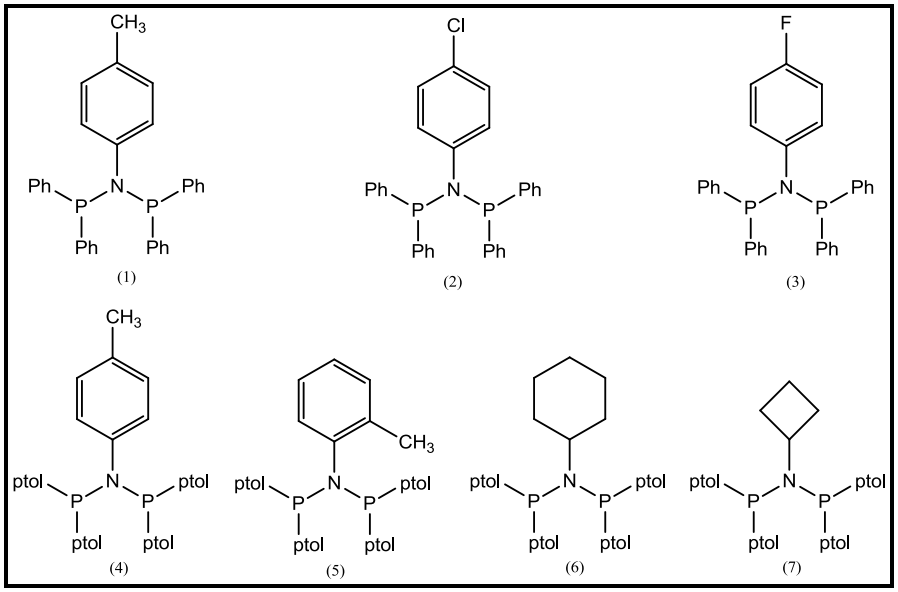

Figure 1: Diphosphinoamine (PNP) ligands synthesized and used in this study. (**1**) [CH_3-Ph-PNP]; (**2**) [Cl-Ph-PNP]; (**3**) [F-Ph-PNP]; (**4**) [5-*p*-tolyl-PNP]; (**5**) [4-*p*-tolyl-*o*-tol]; (**6**) [Chzyl-4-*p*-tolyl]; (**7**) [Cbutyl-4-*p*-tolyl].

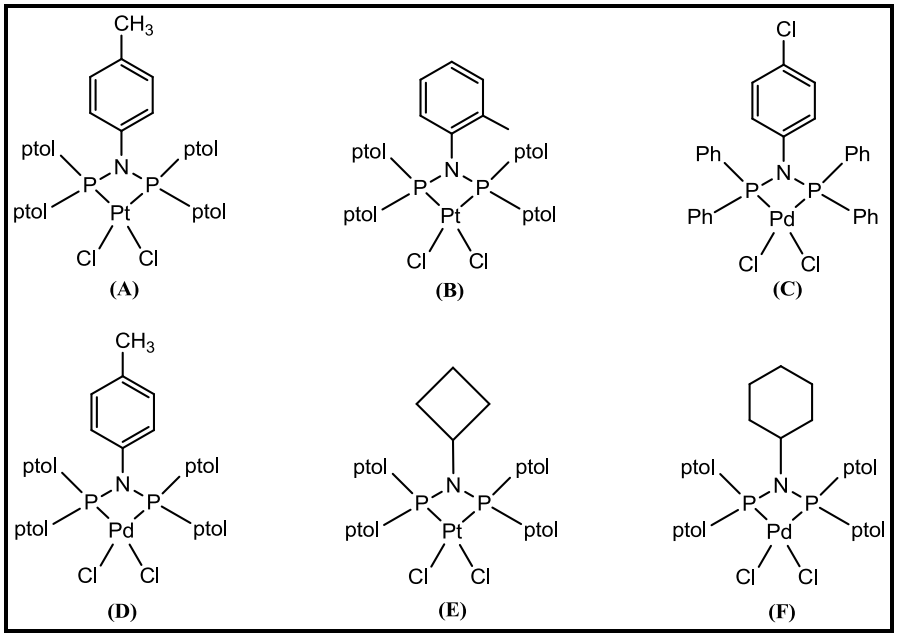

Figure 2: Metal complexes that provided single crystals, which were analyzed by X-ray diffraction. (**A**) [Pt(5-*p*-tolyl-PNP)Cl_2], (**B**) [Pt(4-*p*-tolyl-*o*-tol)Cl_2], (**C**) [Pd(Cl-Ph-PNP)Cl_2], (**D**) [Pd(5-*p*-tolyl-PNP)Cl_2], (**E**) [Pt(Cbutyl-4-*p*-tolyl)Cl_2], (**F**) [Pd(Chzyl-4-*p*-tolyl)Cl_2].

A total of six crystal structures were solved, which allowed the calculation of the steric demand on the nitrogen atom defined by the *Effective Tolman-based N-substituent steric effect* ($\theta_{N\text{-}sub}$).

Summary

To evaluate the electronic properties of ligand **1**, **2** and **3**, the first order coupling constants *J*(Pt-P) were determined and correlated.

Hydroformylation of 1-octene was performed using a Rh(I)-PNP catalyst. An increase in linear product yield was observed when the ligand electron withdrawing ability and the steric bulk on the nitrogen were systematically increased. The highest recorded linear product yield was 35.1 % with Ligand **3** and the lowest was 20.3 % with ligand **4** in the first three hours of the sampling period. The highest calculated $\theta_{\text{N-sub}}$ was 80.6 ° for ligand **6** and gave a linear product of 28.5%. The lowest recorded $\theta_{\text{N-sub}}$ was 33.7 ° for ligand **4**. These results showed that both the electronic and the steric properties have a significant influence on the catalysts selectivity.

Keywords: Hydroformylation, 1-Octene, Aldehydes, Diphosphinoamine, Steric bulk, X-ray data analysis, Catalysts.

Opsomming

Hidroformilering van alkene (olefiene) is een van die wêreld se belangrikste aldehied-vervaardigingsprosesse. Die gevolglike aldehiede kan maklik na sekondêre produkte soos alkohole vir die vervaardiging van plastiseerders en skoonmaakmiddels omgeskakel word. Onlangse studies is gerig op die vervaardiging van hoogs selektiewe kataliste aangesien liniêre aldehiede die mees gesogde produkte is. `n Aantal fosfienligande is ondersoek rakende hierdie proses, en die studies het aangedui dat verfyning van die elektroniese en steriese eienskappe van ligande `n beduidende uitwerking op die aktiwiteit en selektiwiteit van `n katalis het.

`n Reeks difosfinoamien (PNP) ligande met verskeie substituente op die stikstofatoom is vervaardig en gekarakteriseer, naamlik (**1**) *N*,*N*-Bis(difenielfosfino)-*p*-toluïdien [CH_3-Ph-PNP],(**2**) *N*,*N*-Bis(difenielfosfino)-4-chlooranilien [Cl-Ph-PNP], (**3**) *N*,*N*-Bis(difenielfosfino)-4-fluooranilien [F-Ph-PNP], (**4**) *N*,*N*-Bis(di-*p*-tolielfosfino)-*p*-toluïdien [5-*p*-toliel-PNP], (**5**) *N*,*N*-Bis(di-*p*-tolielfosfino)-*o*-toluïdien [4-*p*-toliel-*o*-tol], (**6**) *N*,*N*-Bis(di-*p*-tolielfosfino)sikloheksiel-amien [Chzyl-4-*p*-toliel] en (**7**) *N*,*N*-Bis(di-*p*-tolielfosfino)siklobutielamien [Cbutiel-4-*p*-toliel] (sien **Figuur 1**). Hierdie ligande is sistematies vervaardig om verskillende steriese en elektroniese eienskappe op die stikstofatoom te induseer. Alle ligande is aan Pt(II) en Pd(II) metale gekoördineer om as modelle te dien in Rh(I) pre-katalitiese stelsels vir gebruik in hidroformilering van 1-okteen. Metaalkomplekse wat geskikte kristalle vir X-straaldiffraksie gevorm het is (**A**) Dichloor-[*N*,*N*-Bis(di-*p*-tolielfosfino)-*p*-toluïdien-κ^2P,P']platinum(II) [Pt(5-toliel-PNP)Cl_2], (**B**) Dichloor-[*N*,*N*-Bis(di-*p*-tolielfosfino)-*o*-toluïdien-κ^2P,P']platinum(II) [Pt(4-toliel-tol)Cl_2], (**C**) Dichloor-[*N*,*N*-Bis(difenielfosfino)-4-chlooranilien-κ^2P,P']palladium(II) [Pd(Cl-Ph-PNP)Cl_2], (**D**) Dichloor-[*N*,*N*-Bis(difenielfosfino)-*p*-toluïdien-κ^2P,P']palladium(II) [Pd(5-*p*-toliel-PNP)Cl_2], (**E**) Dichloor-[*N*,*N*-Bis(di-*p*-tolielfosfino)siklobutielamien-κ^2P,P'] platinum(II) [Pt(Cbutiel-4-*p*-toliel)Cl_2] en (**F**) Dichloor-[*N*,*N*-Bis(di-*p*-tolielfosfino)sikloheksiel-amien-κ^2P,P']palladium(II) [Pd(Chzyl-4-*p*-toliel)Cl_2] (sien **Figuur 2**). Hierdie data het inligting rakende die koördineringsmodusse van die ligande verskaf.

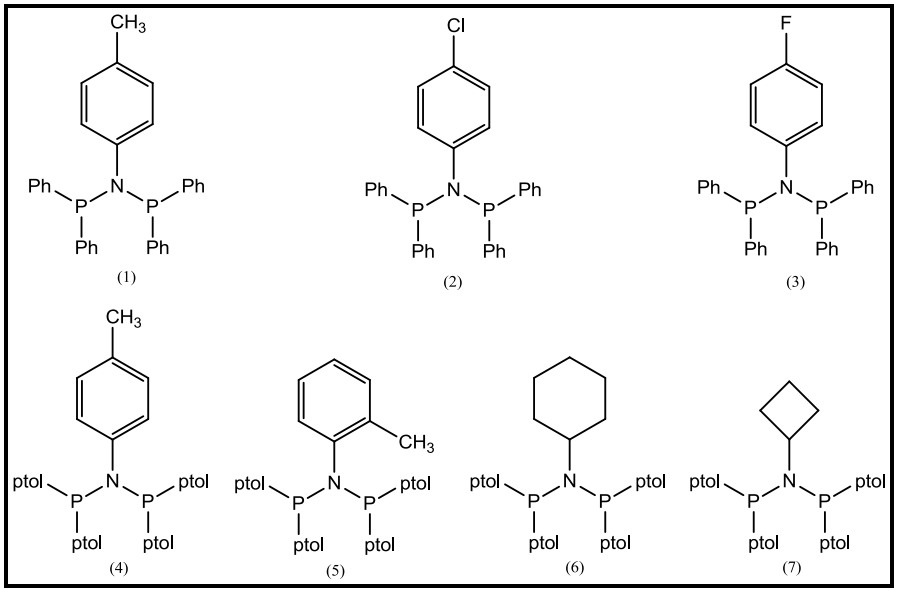

Figuur 1: Difosfinoamien (PNP) ligande vervaardig en gebruik in hierdie studie. (**1**) [CH_3-Ph-PNP]; (**2**) [Cl-Ph-PNP]; (**3**) [F-Ph-PNP]; (**4**) [5-*p*-toliel-PNP]; (**5**) [4-*p*-toliel-*o*-tol]; (**6**) [Chzyl-4-*p*-toliel]; (**7**) [Cbutiel-4-*p*-toliel].

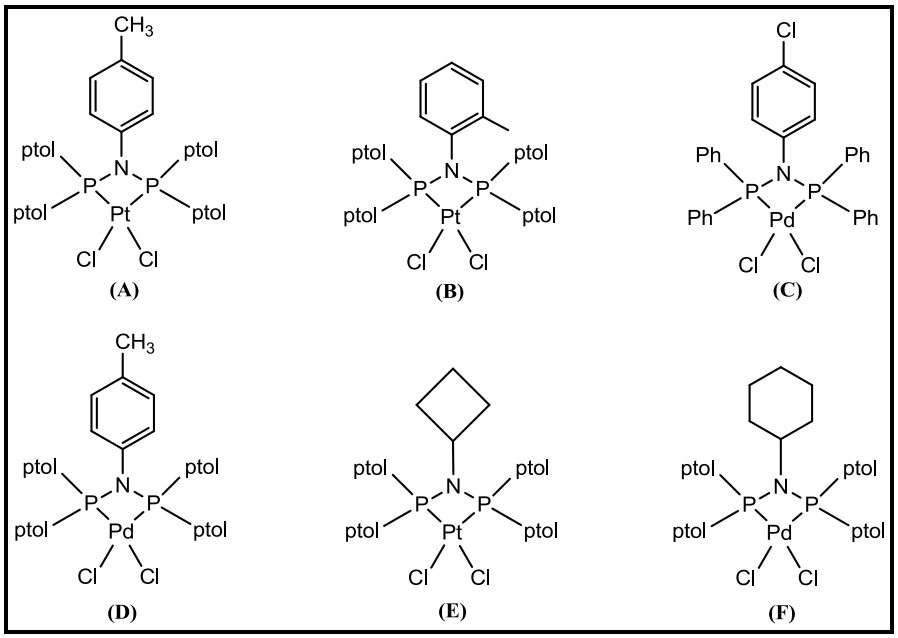

Figuur 2: Metaalkomplekse wat enkelkristalle gevorm het en met behulp van X-straaldiffraksie ontleed is. (**A**) [Pt(5-*p*-toliel-PNP)Cl_2], (**B**) [Pt(4-*p*-toliel-*o*-tol)Cl_2], (**C**) [Pd(Cl-Ph-PNP)Cl_2], (**D**) [Pd(5-*p*-toliel-PNP)Cl_2], (**E**) [Pt(Cbutiel-4-*p*-toliel)Cl_2], (**F**) [Pd(Chzyl-4-*p*-toliel)Cl_2].

`n Totaal van ses kristalstrukture is opgelos wat die berekening van steriese aanvraag op die stikstofatoom, soos gedefinieer deur die *Effektiewe Tolman-gebaseerde N-substituent steriese*

effek ($\theta_{N\text{-}sub}$), toelaat. Om die elektroniese eienskappe van ligand **1**, **2** en **3** te evalueer is die eerste orde koppelingskonstantes *J*(Pt-P) vasgestel en gekorreleer.

Hidroformilering van 1-okteen is uitgevoer deur middel van `n Rh(I)-PNP katalis. `n Toename in liniêre produkopbrengs is waargeneem namate die ligand se elektron-onttrekkende eienskappe en die steriese invloed op die stikstofatoom sistematies verhoog is. Die hoogste waargenome liniêre produkvorming was 35.1 % met ligand **3** en die laagste was 20.3 % met ligand **4** in die eerste drie ure van die steekproeftydperk. Die hoogste berekende $\theta_{N\text{-}sub}$ was 80.6 ° vir ligand **6** en het `n liniêre produk van 28.5 % opgelewer. Die laagste aangetekende $\theta_{N\text{-}sub}$ was 33.7 ° vir ligand **4**. Hierdie resultate toon aan dat beide die elektroniese en steriese eienskappe beduidende invloed op katalisselektiwiteit het.

Sleutelwoorde: Hidroformilering, 1-Okteen, Aldehiede, Difosfinoamien, Steriese grootte, X-straal data-analise, Kataliste.

1 Aim of the study

Abstract

In this chapter, the aim of the study is discussed in detail. A brief overview of the history of homogeneous catalysis and background information on selected platinum group metals is also presented.

1.1 Introduction

It is widely accepted that the world is in dire need of new environmentally-friendly bulk chemicals producing processes to help eradicate current issues such as global warming, water and environmental pollution. Thus, there's a need to either develop new processes or improve old processes by designing new highly selective "green" catalysts. In most current processes, switching from old to new would not be economically-friendly; hence a number of studies are being directed at improving the existing processes by modifying their current catalysts.

1.1.1 Homogeneous Catalysis

The addition of a substance to a chemical reaction to increase the rate of the reaction is coined catalysis.[1] A catalyst is defined as a substance that increases the rate of a reaction by providing a pathway with low activation energy and achieving this without itself sustaining a permanent chemical change.[2,3] When a catalyst is presented in the same phase as the reactants, the catalyst is said to be a homogeneous catalyst.[4,5] The oldest homogeneous catalyzed reaction known is the production of sulphuric acid through a chemical process known as the "lead chamber process".[2]

[1] R.A. Sheldon, *Pure Appl. Chem*., **2000**, *72*, 1233.

[2] P.W.N.M. Van Leeuwen, *Homogeneous Catalysis: Understanding the Art*, Dordrecht: Kluwer Academic Publishers, **2004**.

[3] G. Rothenberg, *Catalysis: Concepts and Green Applications*, Weinheim: Wiley-VCH Publishers, **2008**.

[4] T. Richardson, *Principles of Catalyst Development*, New York: Plenum Press, **1989**.

[5] G.C. Bond, *Heterogeneous catalysis*, Oxford: Claredon Press, **1974**.

In this process sulphur dioxide (SO_2) is oxidized to trioxide by nitrogen oxides (NO/NO_2) and the NO is oxidized by air back to the initial NO_2. Thus, NO and NO_2 are the catalysts and since both the reactants and the catalysts are in the same gas phase, this process can be called a homogeneous catalyzed reaction.[2]

A number of homogeneous catalyzed processes have since been found and applied industrially, which includes methanol carbonylation via cobalt based catalyst (BASF),[6,7] epoxidation of propene (Halcon Corporation),[8] hydrocyanation via nickel based catalyst (Dupont)[9,10] and cobalt catalyzed hydroformylation.[11] In recent years, it has been shown that the ligand effects play a vital role in homogeneous catalysis especially when an organometallic catalyst is used.[12,13] For an example, **Figure 1.1** shows various catalytic reactions that can be performed on butadiene with resulting products using a range of nickel based catalysts.

[6] C.E. Hickey, P.M. Maitlis, *J. Chem. Soc. Chem. Commun..*, **1984**, 1609.

[7] C.M. Lukehart, *Fundamental Transition Metal Organometallic Chemistry*, California: Brooks/Cole Publishing Company, **1985**.

[8] B. Cornils, W.A. Herrmann, *Applied Homogeneous Catalysis with Organometallic Compounds*, 2nd Ed, Weinheim, Willey-VCH Publishers, **2002**.

[9] F.A. Cotton, G. Wilkinson, P.L. Gaus, *Basic Inorganic Chemistry*, 3rd Ed., New York: John Wiley & Sons, Inc, **1995.**

[10] A. Falk, A.L. Goderz, H.G. Schmalz. *Angew. Chem. Int. Ed*., **2013**, *52*, 1576.

[11] M. Haumann, R. Meijboom, J.R. Moss, A. Roodt. *Dalton Trans*., **2004**, *11*, 1679.

[12] A. Roodt, S. Otto, G. Steyl, *Coord. Chem. Rev*., **2003**, *245*, 121.

[13] R.G. Wilkins, *Kinetics and Mechanisms of Reactions of Transition Metal Complexes*, New York: VCH Publishers, 2nd Ed, **1991**.

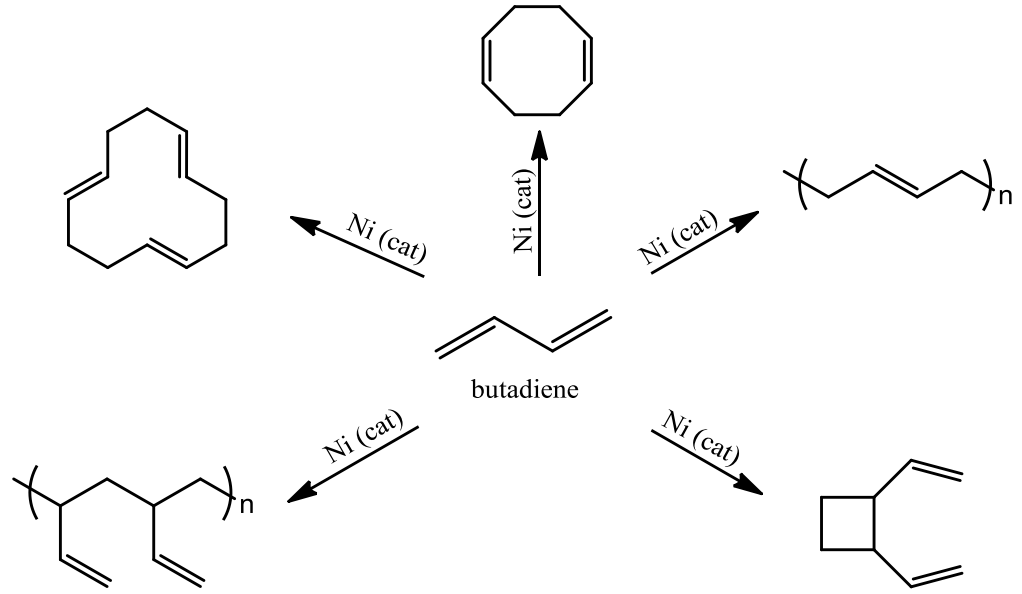

Figure 1.1: Various ligand effects in the nickel-based catalyzed reaction of butadiene and their resulting products, "cat" stands for "catalyst".[2]

From **Figure 1.1** it is clear that by changing the ligands around a single metal centre, one can obtain a variety of products. It is therefore safe to say, the most convenient way of refining the properties of an organometallic catalyst is to manipulate the characters of the coordinated ligands. Distinct ligand effects on a number of catalytic processes will be discussed in detail in **Chapter 2**.

Homogeneous catalyzed reactions can nowadays be easily studied in detail using advanced analytical tools such as Nuclear Magnetic Resonance (NMR) spectroscopy, Ultraviolet-Visible spectroscopy, X-ray diffraction (XRD) and Infrared spectroscopy to understand the mechanism of the catalytic cycle.

1.1.2 Platinum Group Metals (PMG's)

Platinum group metals (PMG's) consists of six metallic elements namely platinum, ruthenium, rhodium, palladium, osmium and iridium.[14] These metallic elements are found on the transition metals category on the periodic table, lying in the "d" block elements. They have similar physical and chemical properties such as a partly field *d* or *f* shells in their most common

[14] L.B. Hunt, F.M. Lever, *Platinum Metals Rev.*, **1969**, *13* (4), 126.

oxidation states.[15] Some of the properties of PMG's include corrosion resistant, high melting points, high lustre and most interestingly their catalytic tendencies. The world's main suppliers of PGM's are located in South Africa, followed by Russia and Canada.[15]

Platinum metal was discovered in South America by Ulloa in 1735.[15] It is one of the rarer earth elements, and usually found accompanied by all of its group members in the same ore (i.e. Merensky and UG2).[15,16] The metal is commonly used in corrosion resistant materials, jewelleries, thermocouples, wires and dentistry. It has also been extensively studied as a catalyst in chemical reactions such as the cracking of petroleum products, production of ammonia (Haber process) and production of aromatics.[4,15,17] The first Pt(II)-containing chemotherapy drugs was a square-planar *cis*-platin ([*cis*-$(PtCl_2(NH_3)_2]$). The platinum metal can occur in four different oxidation states namely +1, +2, +3 and +4, with +2 and +4 being the most common oxidation states.[15,18]

Palladium metal was discovered in 1803 by Wollaston.[15] It is found along with other platinum group metals. Natural occurring palladium consists of six stable isotopes ^{102}Pd, ^{104}Pd, ^{105}Pd, ^{106}Pd, ^{108}Pd, and ^{110}Pd. It is a steel-white metal that does not tarnish when exposed to air and has the lowest melting point among its group members. At room temperature palladium absorbs up to 900 times its own volume of hydrogen and this character of palladium is used as a method of purifying the gas. The palladium metal is commonly used in production of surgical instruments and electrical contacts. The metal has also been extensively studied as a catalyst by automobile companies, mostly as automotives catalyst converters.[15] Common oxidation states of the palladium metal are 0, +1, +2 and +4.[18]

Rhodium metal was also discovered by Wollaston in 1803. It occurs naturally among other platinum metals. It has a silver white colour and has a higher boiling point than platinum. The major use of rhodium is to harden platinum and palladium as an alloying agent. It is one of the rarer earth elements and has lately been extensively studied as a catalyst in chemical synthesis

[15] D.R. Lide, *Handbook of Chemistry and Physics*, 84th Ed, CRC Press LLC, **2004**.

[16] R.E. Phillips, R.T. Jones, P. Chennells, *J. S. Afr. Inst. Min. Metall*., **2008**, *64*, 141.

[17] H. J. Wolfenden, *J. Chem. Edu.*, **1967**, *44* (5), 299.

[18] N.N. Greenwood, A. Earnshaw, *Chemistry of the Elements*, 2nd Ed., Great Britain: Pergamon Press, **1997**.

such as alkene hydroformylation and the Haber process. The metal has six oxidation states namely +1, +2, +3, +4, +5 and +6, with +1 and +3 being the most common states. Rh(I) has a d^8 electron configuration with either a bipyrimidal 5-coordinate or a 4-coordinate square planar conformation, while Rh(III) has a d^6 electron configuration with an octahedral conformation.[15,17]

1.2 Aim of the study

In chemistry, hydroformylation is defined as the addition of a formyl group (CHO) on olefins to form aldehydes. This chemical process was discovered by Otto Roelen in 1938.[19] It is one of the world's leading aldehyde producing process, with over 12 million tons of aldehydes produced each year through this process.[20] The resulting aldehydes can easily be converted to secondary products such as alcohols for production of plasticizers and detergents. Recent research is directed towards the production of highly selective catalysts, as linear aldehydes are the most desired aldehyde products.[12]

The first generation of a hydroformylation catalyst was a cobalt based catalyst of the form $[CoH(CO)_4]$.[21] In the early 1960's Shell replaced the CO ligand with a tertiary phosphine (PPh_3) and observed an increase in the selectivity of a catalyst.[19] Since then, a number of phosphine modified catalysts have been investigated in many catalytic reactions.[19,22,23,24] Recent studies have shown that varying the steric bulk on a range of diphosphinoamine (PNP) ligands increased the selectivity of a chromium based catalyst in ethylene tri- and tetramerisation reactions.[25,26,27]

[19] R. Meijboom, M. Haumann, A. Roodt, L. Damoense, *Helv. Chim. Acta*., **2005**, *88* , 676.

[20] G.D. Frey, *J. Organomet. Chem*., **2014**, *754*, 5.

[21] C. Erkey, D.R. Palo, S. Haji, *Fuel. Chem. Div. Prep.*, **2002**, *47*, 144.

[22] P.J. Barcelli, E. Lujano, M. Modrono, A.C. Marrero, Y.M. Garcia, A. Fuentes, R.A. Sanchez-Delgado, *Organomet. Chem*., **2004**, *689*, 3782.

[23] P.W.N.M. van Leeuwen, C.F. Roobeek, *J. Organomet. Chem*., **1983**, *258*, 343.

[24] A. van Rooy, J.N.H. de Bruijn, C.F. Roobeek, P.C. Kamer, P.W.N.M. van Leeuwen, *J. Organomet. Chem*., **1996**, *507*, 69.

[25] N. Cloete, H.G. Visser, I. Engelbrecht, M.J. Overett, W.F. Gabrielli, A. Roodt, *Inorg. Chem*., **2013**, *52*, 2268.

[26] S. Kuhlmann, K. Blann, A. Bollmann, J.T. Dixon, E, Killian, M.C. Maumela, H. Maumela, D.H. Morgan, M. Pretorius, *J. Catal*., **2007**, *245*, 279.

[27] M.J. Overett, K. Blann, A. Bollman, J.T. Dixon, D. Haasbroek, E. Killian, H. Maumela, D.S. McGuinness, D.H. Morgan, *J. Am. Chem. Soc*., **2005**, *127*, 10723.

Based on the information described above, an investigation of distinct PNP-ligands with various substituents on the nitrogen atom and their catalytic behaviour in hydroformylation of 1-octene was instigated. The main objective of this study was focused on the systematic synthesis of the ligands, platinum group metal interactions and solid state characterization to gain more information on the general behaviour of these ligands and metal complexes.

For this reason, a number of PNP ligands have been synthesized based on varying steric and electronic properties. These ligands were then coordinated to both Pt(II) and Pd(II) metals. Complexing various PNP ligands with metal cations such as Pt(II) and Pd(II) will provide vital information regarding the coordination chemistry of these ligands and these complexes will also serve as models for Rh-PNP pre-catalysts. In addition, the reaction involving 1-octene hydroformylation with various Rh-PNP complexes was investigated. A comparison of these various Rh catalysts could provide vital information for future Rh-based catalysts in hydroformylation of alkenes.

Proceeding from the previous paragraphs, the following stepwise goals were set for this study:

1. Synthesize systematically an array of diphosphinoamine ligands with different steric and electronic properties.
2. Synthesize and fully characterise metal-PNP complexes (metal = Pt(II) and Pd(II)) and collect single crystal X-ray crystallographic data.
3. From the crystallographic data, calculate the *Effective Tolman-based N-substituent* steric parameter and correlate these values to the catalysts selectivity, during the hydroformylation of 1-octene.
4. Design a systematic approach to evaluating catalysis by integrating X-ray crystallographic data and the *Effective Tolman-based N-substituent* steric parameter in order to improve future ligand and catalysts design methods.

A brief overview on the discovery and development of alkene (olefin) hydroformylation is presented in the following chapter, followed by a presentation and discussion of the experimental results.

2 General aspects of Catalysis

Abstract

A brief overview on the discovery and development of catalysis in particular hydroformylation, as well as fundamental ligand properties and effects on catalysis is presented in this chapter.

2.1 Introduction

Catalysis is important in the industrial production of bulk chemicals and liquid fuels such as production of oil and conversion of petrochemicals.[1] Catalyst selectivity is based on many things, which include the selectivity and rate influence of the catalyst towards the desired product, amount of waste produced, amount of resources needed and robustness of the catalyst.[2] Homogeneous catalyzed hydroformylation ("oxo" synthesis) is one of the biggest aldehyde producing chemical processes in the world with over 12 million tons of secondary, together with, primary products produced in 2012 only.[3,4,5] This catalytic process was first discovered in 1938.[6] The majority of the products coming from this process goes to the polymer industries as a form of plasticizers, surfactants, preservatives and detergents.[7,8] The first generation of hydroformylation processes were conducted using a cobalt based catalyst [$CoH(CO)_4$,

[1] P.W.N.M. Van Leeuwen. *Homogeneous Catalysis: Understanding the Art*, Dordrecht: Kluwer Academic Publishers, **2004**.

[2] G. Rothenberg. *Catalysis: Concepts and Green Applications*, Weinheim: Wiley-VCH Publishers, **2008**.

[3] L.A. Van der Veen, P.C.J. Kamer, P.W.N.M. Van Leeuwen. *Angew. Chem. Int. Ed*., **1999**, *38*, 3.

[4] G.D. Frey. *J. Organomet. Chem*., **2014**, *754*, 5.

[5] C. Erkey, D.R. Palo, S. Haji. *Fuel. Chem. Div. Prep.*, **2002**, *47*, 144.

[6] M. Haumann, R. Meijboom, J.R. Moss, A. Roodt. *Dalton Trans*., **2004**, *11*, 1679.

[7] P.W.N.M Van Leeuwen, C. Claver., (Eds.), *Rhodium Catalyzed Hydroformylation*, Dordrecht: Kluwer Academics Publishers, **2000**.

[8] B. Cornils, W.A. Herrmann. *Applied Homogeneous Catalysis with Organometallic Compounds*, 2nd Ed, Weinheim: Willey-VCH Publishers, **2002**.

$CoH(CO)_3PBu_3$].[6] The cobalt based catalyst was later replaced by the more effective rhodium based catalyst [$RhH(CO)(PR_3)_3$].[8,9] Ligand modification has been the main tool for catalyst modification especially after the discovery made by Shell researchers regarding phosphine ligands in homogeneous catalysis.[10] These phosphine modified catalysts were found to be less reactive when compared to the unmodified ones but very selective towards the desired linear products.[11] A range of phosphine ligands have since been applied in many catalytic reactions due to this discovery. After Berzelius discovery, [12] a number of studies on catalyst production and catalyst modification emerged and the birth of organometallic catalysts greatly changed this field. Organometallic catalysts are those catalysts in which organic (or inorganic) groups called ligands are connected to central metal atoms. Organometallic chemistry success owe it to the fact that the simplest and most convenient way of catalyst modification is the modification of ligands; and this can be easily performed in organometallic catalysts.[1] For transition metal complexes, the general order of catalytic activity for hydroformylation reaction shows the following trend Rh >> Co > Ru or Ir > Os > Pt > Pd > Fe > Ni.[8]

2.2 Catalysis

The addition of a substance to a chemical reaction to increase the rate of the reaction is coined catalysis.[13] According to Ostwald, a substance is considered a catalyst if it forces a chemical reaction to proceed through a different pathway from that of a non-catalyzed one without itself being consumed.[1] Ostwald's definition is so broad that it suggests that a catalyzed reaction can either be slower or faster than the general non-catalyzed one. Hence, his definition implicated that a negative catalyst would slow down the reaction while a positive catalyst speeds it up by lowering the activation energy, but neither a positive nor a negative catalyst alters the thermodynamics of a reaction.[1] Presently, a catalyst is referred to as *a substance that increases the rate of a reaction by providing "a different pathway with low activation energy without itself sustaining a permanent chemical change"* (see **Figure 2.1**).[1,2] Catalyzed reactions are classified

[9] J.A. Osborn, G. Wilkinson, J.F. Young. *J. Chem. Soc., Chem. Commun*, **1965**, 17.

[10] R. Meijboom, M. Haumann, A. Roodt, L. Damoense. *Helv. Chim. Acta*., **2005**, *88* , 676.

[11] M. Beller, B. Cornils, C.D. Frohning, C.W. Kohlpainter. *J. Mol. Catal. A: Chem*., **1995**, *104*, 17.

[12] J.J. Berzelius. *Trans. R. Swed. Sci. A., 1830, 49*, 49

[13] R.A. Sheldon. *Pure Appl. Chem*., **2000**, *72*, 1233.

into two categories: homogeneous and heterogeneous catalytic reaction. In a homogeneous catalytic reaction the catalyst is in the same phase as the reactants whereas in a heterogeneous catalytic reaction the catalyst is in a different phase from that of the reactants.[14,15] Biocatalysis is a third form of catalysis through which natural species like enzymes are used as catalysts.[2] For stability reasons, catalysts are normally added to chemical reactions in their inactive forms coined Catalyst Precursors. There are three important terminologies in catalysis, namely the turnover number (TON), turnover frequency (TOF) and substrate to catalyst ratio. Calculations for TON differ from one catalytic system to the other. For a homogeneously catalyzed reaction TON is defined as the number of times a catalyst loops through a cycle before deactivation occurs. For a heterogeneously catalyzed reaction TON is defined per active site, and in biocatalysis TON is also defined per active site since most enzymes are much larger than the substrates. TOF is simply TON over time (minute/second/hour).[2] Apart from enzymology, the substrate of most catalyzed reactions is usually bigger in concentrations than the catalyst, thus when interpreting a catalytic reaction the ratio of substrate to catalyst is an important factor. A good catalyst will not only generate the desired product faster with less resources but it would also minimize the production of by-products. An undesirable catalyst generates less desired product and is susceptible to poison. In catalysis a poison is a substance that kills a catalyst and an inhibitor is a substance that decelerates a catalytic reaction.[1]

[14] G.C. Bond., *Heterogeneous catalysis*, Oxford: Claredon Press, **1974**.

[15] T. Richardson, *Principles of Catalyst Development*, New York: Plenum Press, **1989**.

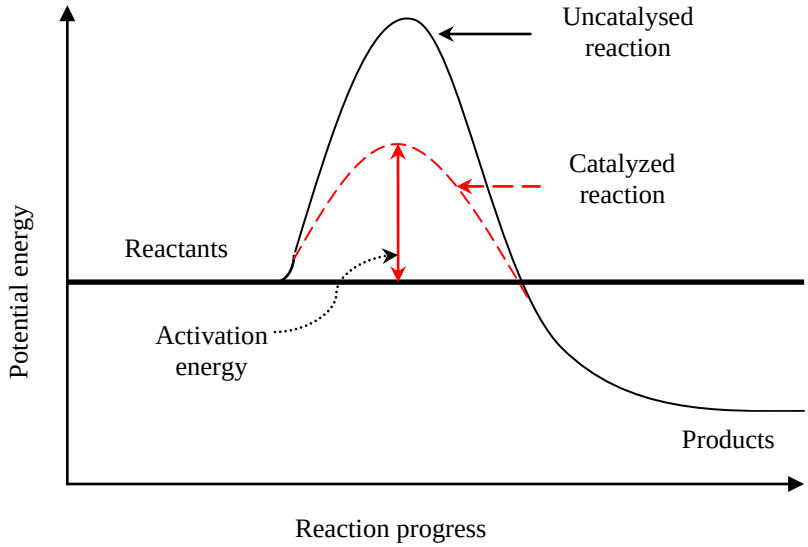

Figure 2.1: Reaction profile for a catalyzed chemical reaction and non-catalyzed chemical reaction.[16]

As previously indicated, catalyst selectivity is crucial in catalysis. There are four different kinds of catalyst product selectivity (see **Figure 2.2**), namely regioselectivity, chemoselectivity, enantioselectivity and diastereoselectivity. In simple terms:[2]

a) *Regio*-selectivity: denotes a chemical reaction where a single substrate can be attacked on more than one region leading to different products;

b) *Chemo*-selectivity: denotes a situation where there is a possibility of more than one chemical reaction on a single substrate;

c) *Enantio*-selectivity: an enantio-pure catalyst converts an achiral substrate to a specific enantiomer product;

d) *Diastereo*-selectivity: a stereogenic centre containing substrate is converted to two diastereomers, the selectivity in this scenario is coined diastereoselectivity.

[16] K.J. Laidler, J.H. Meiser, B.C. Sanctuary. *Physical Chemistry*, 4th Ed, Boston: Houghton Mifflin Publishers, **2003**.

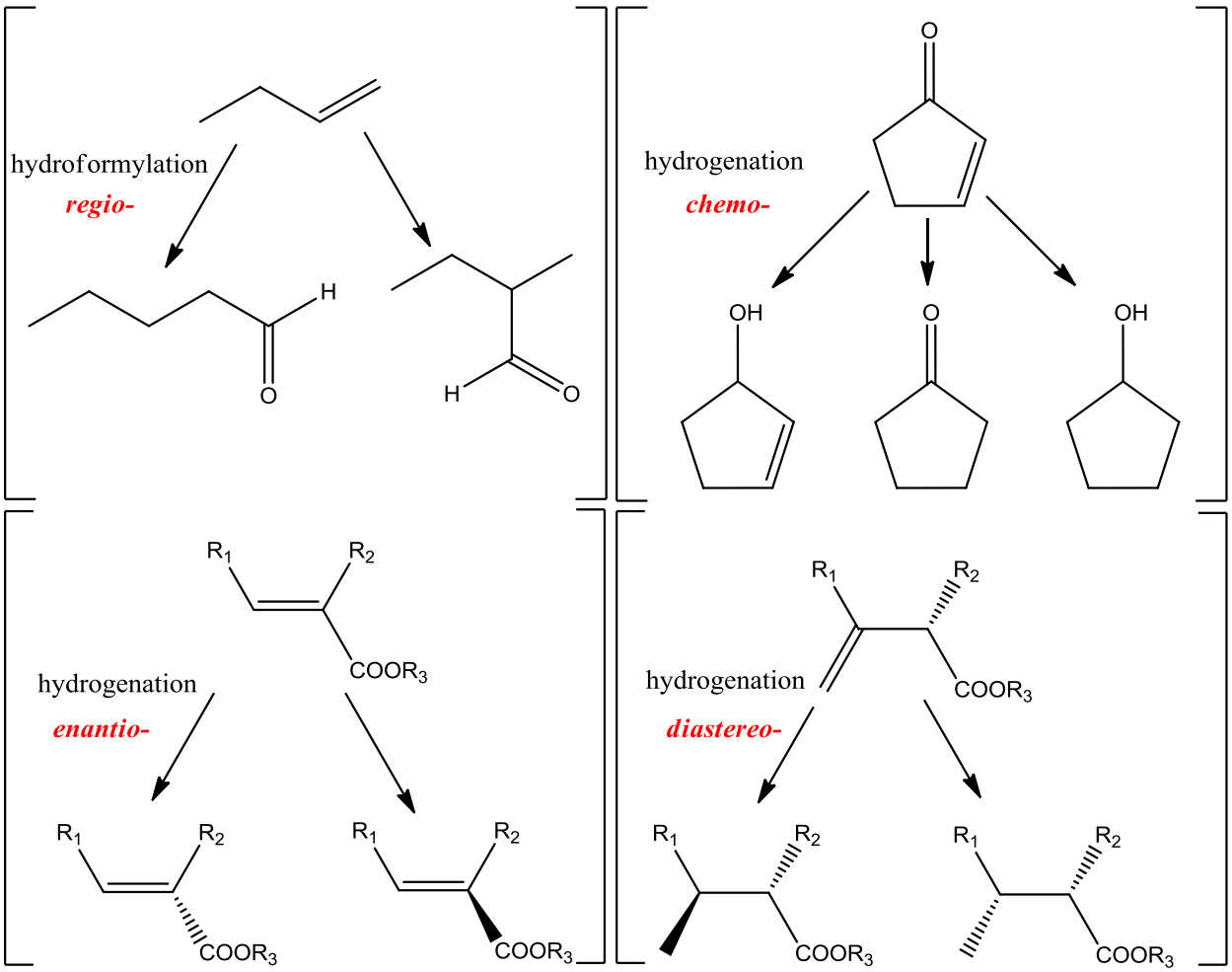

Figure 2.2: Examples of regioselectivity (*region*-), chemoselectivity (*chemo*-), enantionselectivity (*enantio*-) and diastereoselectivity (*diastereo*-).[1]

2.3 Homogeneous *versus* Heterogeneous Catalysis

2.3.1 Introduction

As mentioned before, homogeneous catalysis refers to a chemical reaction in which a catalyst is presented in the same phase as the reactants whereas heterogeneous catalysts are insoluble in reaction mixtures. For economic reasons, homogeneous catalysts are mostly commercialized for a certain reaction when there is no heterogeneous catalyst available or when selectivity to a

desired product is higher than in a heterogeneous process. A comparison between homogeneous and heterogeneous catalysis is shown in **Table 2.1**.[17]

Table 2.1: Comparison of heterogeneous and homogeneous catalysis.[17,18,19,20]

	Homogeneous	**Heterogeneous**
Catalyst phase	Metal complex	Solid (e.g. Metal oxides)
Selectivity	Can be tuned	Poor
Stability	Often decompose <100 °C	Very stable even at high temperatures
Recyclability	Often difficult	Often easy
Solvent	Usually required	Usually not required
Mode of use	Dissolved in a reaction mixture	Slurry or Fixed bed

2.3.2 Homogeneous Catalysis

Homogeneous catalysts are normally dissolved together with the other reactants into a single reaction medium. Separation of the products from the reactants (including the catalyst) can be extremely difficult. However, a range of catalytic processes listed below can now be produced at a high selectivity using homogeneous catalysts with carefully selected ligands and metal centres:[8,17,21,22]

- Methanol carbonylation (BASF, Monsanto and Cativa Processes)[23,24]
- Hydroformylation (cobalt and rhodium catalysts)[25]
- Hydrogenation (Wilkinson's catalyst)[26]
- Co-oligomerization[27]

[17] D.J. Cole-Hamilton, R.P. Tooze. *Catalyst separation, recovery and recycling: Chemistry and process Design*, Dordrecht: Springer Publishers, **2006**.

[18] B. Cornils, J. Falbe. *4th Int. Symp. Homogeneous Catalysis*, Leningrad, Preprints, **1984**.

[19] W. A. Henmann. *Hoechst. High. Chem*, Frankfurt., **1992**, *13*, 19.

[20] A. Behr, W. Keim. *Erdol. Erdga., Kohle*, **1987**, *103*, 126.

[21] C.C. Tzschucke, C. Markert, W. Bannwarth, S. Roller, A. Hebel, R. Haag. *Angew. Chem. Int. Ed.*, **2002**, *41*, 3964.

[22] D. J. Cole-Hamilton. *Science*, **2003**, 299, 1702.

[23] C.E. Hickey, P.M. Maitlis. *J. Chem. Soc. Chem. Commun..*, **1984**, 1609.

[24] C.M. Lukehart. *Fundamental Transition Metal Organometallic Chemistry*, California: Brooks/Cole Publishing Company, **1985**.

[25] W.A. Hermann, B. Cornils. *Angew. Chem., Int. Ed.*, **1997**, *36*, 1048.

[26] R.H. Crabtree. *The Organometallic Chemistry of the Transition Metals*, New York, John Wiley & Sons., **1988**.

- Isomerisation
- Alkene metathesis (Schrock's and Grubbs' catalyst)[28,29,30]
- CO Hydrogenation
- Hydrocarbonylation
- Hydrocyanation (Nickel phosphite complex)[31,32]
- Methoxycarbonylation
- Methanol homologation
- Co-polymerisation
- Polymerisation

2.3.3 Heterogeneous catalysis

Heterogeneous catalysts are generally solids in the form of metal oxides and are known to be unselective. They have a low surface area as compared to homogeneous catalysts and they are highly stable towards high pressures and heat. A number of heterogeneously catalyzed processes are listed below:[15,17]

- Haber process (Pt, Pd or Rh catalysts)[33]
- Contact process (V_2O_5)[34]
- Fischer – Tropsch process (Cobalt and iron catalyst)[35,36,37]
- Heterogeneous photocatalysis (semiconductors)
- Exhaust clean up (Pt, Pd on oxides as catalyst)

---

[27] J.T. Dixon, C. Grově, A. Ranwell, *WO 01/83447 (Sasol Tehnology (Pty) Ltd)*, November 8, **2001**.

[28] R.R. Schrock, J.S. Murdzek, G.C. Bazan, J. Robbins, M. DiMare, M. O'Regan., *J. Am. Chem. Soc*., **1990**, *112*, 3875.

[29] R.H. Grubbs, S. Chang, *Tetrahedron*, **1988**, *54*, 4413.

[30] R.H. Grubbs, *Tetrahedron*, **2004**, *60*, 7117.

[31] F.A. Cotton, G. Wilkinson, P.L. Gaus, *Basic Inorganic Chemistry*, 3rd Ed., New York: John Wiley & Sons, Inc., **1995**.

[32] A. Falk, A.L. Goderz, H.G. Schmalz. *Angew. Chem. Int. Ed*. **2013**, *52*, 1576.

[33] H. J. Wolfenden. *J. Chem. Edu.*, **1967**, *44*(5), 299.

[34] H. B. Pulsifer. *J. Am. Chem. Soc.*, **1904**, *26*,1387.

[35] R. Agrawal, N.R. Singh, F.H. Ribeiro, W.N. Delgass. *Proc. Natl. Acad. Sci*., **2007**, *104*, 4828.

[36] N. Fischer, B. Clapham, T. Feltes, M. Claeys.,*ACS Catal*., **2015**, *5*, 113.

[37] G.P. Van der Laan, A.A.C.M. Beenackers., *Catal.Rev.–Sci.Eng*., **1999**, 41, 255.

- Oil cracking (Zeolites)[38]
- Oxidation of ethylene (Ag on support)
- Polyethelene (Cr, Ti, Ziegler–Natta catalyst)[39]
- Hydrogenation of oils (Ni catalyst)
- Hydrocracking (Pt on zeolites)[40]
- Dehydrogenation (Pt, Al_2O_3)
- Alkylation (Zeolited, silicates,solid acids)[41]
- Methanation (Ni catalyst)
- Methanol synthesis (Cu, ZnO, Al_2O_3)[42]
- Production of aromatics (Pt catalyst on Al_2O_3)

The primary focus of this study is on the catalytic hydroformylation of 1-octene using a Rh-phosphine complex. Thus, the discussion that follows would be based on hydroformylation and the phosphine ligand effects on this process.

2.4 Hydroformylation

2.4.1 Introduction

In chemistry, the addition of a formyl group (CHO) on alkenes (olefins) to form an aldehyde (see **Figure 2.3**) is coined hydroformylation (also known as the "oxo" synthesis). This chemical process was first discovered by Otto Roelen in 1938 while working as a research director at Ruhrchemie AG.[10] In 1960 Heck and Breslow proposed a reaction mechanism for this process.[43] It is one of the world's largest aldehyde producing processes; in 2012 over 12 million tons of aldehydes were produced.[3,5,4]

[38] B.W. Wojciechowski. *Catal. Rev. – Sci. Eng*., **1998**, 40, 209.

[39] J. Huang, G.L. Rempel. *Prog. Polym. Sci*., **1995**, 20, 459.

[40] J.H. Gary, G.E. Handwerk. *Petroleum Refining: Technology and Economics*, CRC Press, Boca Raton, **2001**.

[41] A. Feller, J.A. Lercher. *Adv. Catal*., **2004**, 48, 229.

[42] K. Klier. *Adv. Catal*. **1982**, 30, 243.

[43] B. Cornils, W. A. Henmann, M. Rasch, *Angew. Chem*. **1994**, 106, 2219.

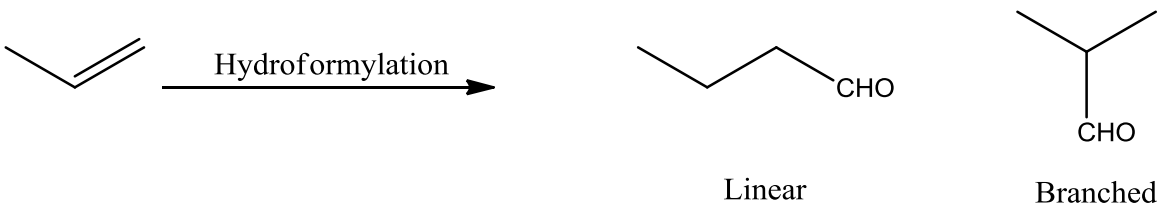

Figure 2.3: Schematic representation of a hydroformylation reaction of 1-propene, showing the formation of branched (Isobutyraldehyde) and a linear (butanal) product. Production of small aldehydes ($\leq C_5$) mostly utilizes a rhodium based catalyst.[5]

The success of this chemical process owes it to the rapid growth of the detergent and the petrochemical industries in the early 1960's.[8] To date, the detergent industry remains the largest primary and secondary hydroformylation product consumer followed by the polymer industry.[10] Hydroformylation is a valuable process, because from its primary "aldehyde" product a number of secondary products can be produced (see **Figure 2.4**).[8]

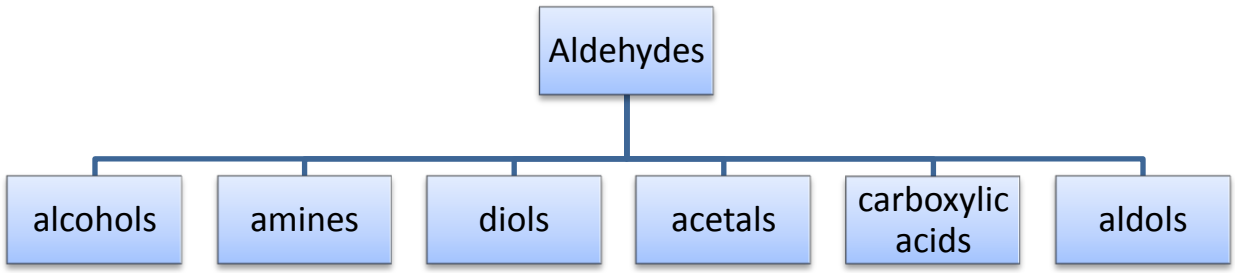

Figure 2.4: Organization chart representing products and compounds obtainable through hydroformylation catalytic process.[8]

The first organometallic catalyst used in large scale hydroformylation processes was a cobalt based catalyst of the form $[CoH(CO)_4]$ by Ruhrchemie AG and later by BASF.[5] Even with the success shown by these two large companies, there was still a need for catalyst improvement. In the early 1960's Shell replaced the CO moiety with a tertiary phosphine ligand, increasing the steric bulk of the ligand and the catalyst activity significantly.[10] This discovery increased the level of knowledge regarding the effects of various ligands with different electronic and steric properties in catalyst modification. The second and third catalyst developments that changed and

improved catalyst modification were the transition from cobalt to rhodium metal centers and the use of water soluble phosphine ligands respectively. In the early 1970s the first rhodium-phosphine hydroformylation catalyst was commercialized by the Hoechst Corporation, the world's leading acetyl products producing company.[1]

Current hydroformylation processes are conducted with either a cobalt or a rhodium based catalyst $[CoH(CO)_4]$, $[RhH(CO)(PR_3)_3]$ and $[CoH(CO)_3PBu_3]$, and current researches is focused on improving catalyst selectivity towards the desired linear products. Despite the fact that this process has been intensively examined, there is still a room for further enhancement. [6,10,44,45,46,47,48]

[44] H. Janecko, A.M. Trzeciak, J.J. Ziolkowski. *J. Mol. Cat.*, **1984**, *26*, 355.

[45] A. Polo, J. Real, C. Claver, S. Castillon, J.C. Bayon. *J. Chem. Soc., Chem. Commun*., **1990**, 600.

[46] A. van Rooy, J.N.H. de Bruijn, C.F. Roobeek, P.C. Kamer, P.W.N.M. van Leeuwen. *J. Organomet. Chem*., **1996**, *507*, 69.

[47] P.W.N.M. van Leeuwen, C.F. Roobeek. *J. Organomet. Chem*., **1983**, *258*, 343.

[48] P.J. Barcelli, E. Lujano, M. Modrono, A.C. Marrero, Y.M. Garcia, A. Fuentes, R.A. Sanchez-Delgado. *Organomet. Chem*., **2004**, *689*, 3782.

2.4.2 Mechanism

The basic hydroformylation reaction mechanism using a cobalt tetracarbonyl based catalyst proposed by Heck is indicated below. The mechanism is believed to hold also for a rhodium based catalyst and is illustrated below in **Figure 2.5**.[49,50]

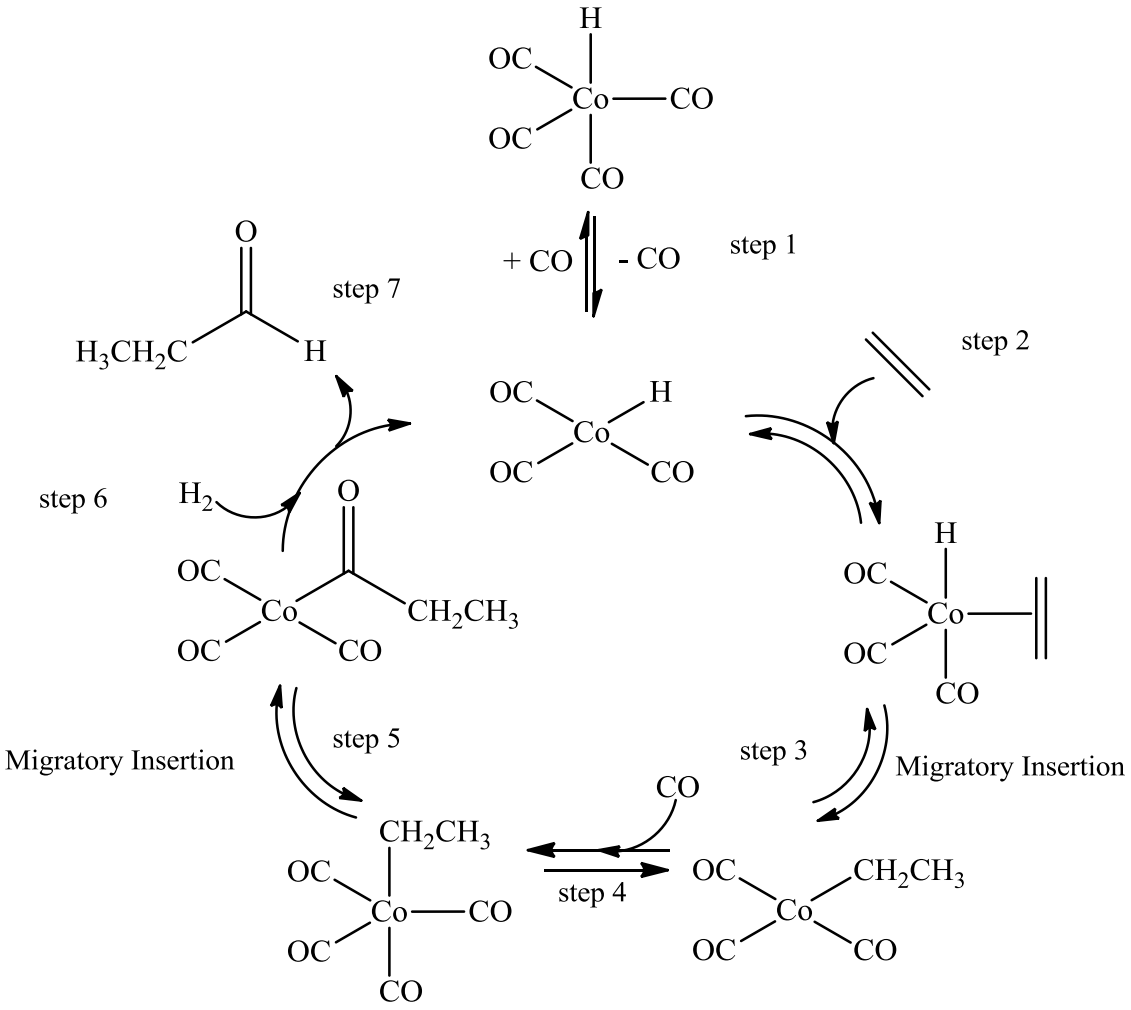

Figure 2.5: Reaction mechanism for hydroformylation of ethylene using a cobalt tetracarbonyl based catalyst. With the exception of the final step (the release of the aldehyde), all steps are reversible.[1,8]

In the above mentioned catalytic cycle, **(1)**, the first step is the formation of a $16e^-$ catalytic species of the form $[HCo(CO)_3]$ from a $18e^-$ catalyst $[HCo(CO)_4]$. **(2)** The second step is the

[49] R.F. Heck. *Acc. Chem. Res*., **1969**, *2*, 10.

[50] D. Evans, G. Yagupsky, G. Wilkinson. *J. Chem. Soc.* (A)., **1968**, 2660.

binding of the alkene and the hydrogen transfer to form a hydro-alkene complex ($18e^-$) **(3)**. The migratory insertion step resulting in a $16e^-$ alkyl cobalt species then follows. **(4)** The forth step involves the addition of CO, preparing the complex for an anti-Markovnikov product, resulting in an $18e^-$complex. **(5)** This is then followed by another migratory insertion step to form a carbonyl complex ($16e^-$). **(6)** The second last step is the oxidative addition step by H_2 to form an $18e^-$ complex, **(7)**. The final step is the reductive elimination step producing the product and the initial $16e^-$ catalyst.

With the exception of the final step (the release of the aldehyde) all steps are reversible. The release of the aldehyde has always been the topic under continuous discussion, but studies has shown that step four which is the addition of the CO moiety to the alkyl cobalt species is the step where conditions for both linear and branched products are formed. It is reported that rhodium carbonyl catalysts undergo similar chemical kinetics as the above discussed cobalt carbonyl species.[51,52]

2.5 Rhodium in catalysis

In organometallic chemistry, rhodium and cobalt have been widely studied as metal centers in catalysts for processes such as:[53]

- Hydroformylation
- Isomerisation of alkenes
- Ethylene tri- and tetramerisation
- Hydrogenation
- Hydrogen atom exchange
- Carbonylation

However, given that rhodium is ten thousand times more active than cobalt, reactions performed under a rhodium-based catalyst are thus operated at significantly moderate pressures and temperatures than the ones performed under a cobalt-based catalyst.[5] For instance, the BASF

[51] J.F. Young, J.A. Osborn, F.A. Jardine, G. Wilkinson., *J. Chem. Soc. Chem. Commun*., **1965**, 131.

[52] J.A. Osborn, G. Wilkinson, D. Evans., *J. Chem. Soc*., (A), **1968**, 3133.

[53] P.W.N.M. Van Leeuwen, J.C. Chadwick. *Homogeneous Catalysis: Activity-Selectivity-Deactivation*, Weinheim: Wiley-VCH Publishers, **2011**.

hydroformylation of 1-octene with a cobalt-based catalyst operates in the temperature and pressure range of 160-190 °C and 250-300 bar respectively, whereas the UCC hydroformylation of propene with a rhodium-based catalyst is operated at the temperature and pressure range of about 85-90 °C and 18 bar respectively. Thus switching from cobalt to rhodium would be cost effective for most hydroformylation industrial companies.

Changing from a cobalt to a rhodium based catalyst is delayed by the difficulty on the separation of the products and catalyst from the reaction mixture, especially for higher olefins since the boiling points of long chained aldehydes are very high. Intense studies are devoted to synthesizing new rhodium-based catalyst that can surpass this problem.[5]

2.6 General ligand properties: Steric *versus* Electronic

2.6.1 Introduction

Changing the ligand properties on a catalyst can result in high activity and selectivity for a catalyst, but the opposite may also be true. Relating the catalyst behavior to the steric and electronic properties remains the classical approach followed by chemist and engineers on analyzing a catalyst.[54] A number of studies have been conducted on this, and it is believed that ligand modification is the main tool for modification of homogeneous catalysts. A few tools used to analyze ligand characters will be described in the following sections.

2.6.2 Electronic properties

Infrared (IR) spectroscopy is a branch of spectroscopic technique concerned with molecular vibration and can be used to indirectly measure the electronic properties of a number of phosphine ligands. In a metal-ligand coordinated complex, a carbonyl ligand absorption band can be easily identified in the IR spectrum. This information can then be used for measuring electronic properties of the other coordinated ligand on the same complex as described by Strohmeier and Horrocks.[55,56] Carbonyl frequencies of the CO ligands are used to determine the

[54] N. Fey, A.G. Orpen, J.N. Harvey. *Coord. Chem. Rev*., **2009**, *253*, 704.

[55] W. Strohmeier, F.J. Müller. *Chem. Ber*., **1967**, *100*, 2812.

[56] W.D. Horrocks Jr, R.C. Taylor. *Inorg. Chem*., **1963**, *2*, 273.

acidity and basicity of phosphorus ligands, a strong sigma-donor ligand increases the electron density on the metal centre causing dominant back-donation effect to the CO ligands. This effect shortens the C-O bond length and increases the M-C bond length resulting in a low IR frequency. On the other hand a strong π-acceptor ligand is a contender for the electrons responsible for the back-donation effect, thus will compete with the CO ligand on electron back-donation resulting in a higher CO ligand IR frequency (see **Figure 2.6**).[57,58]

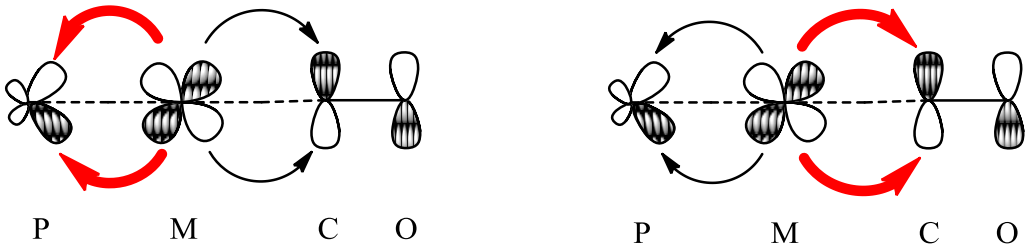

strong π-acceptor, high *v*(CO) week π-acceptor, low *v*(CO)

Figure 2.6: Electronic effects of a phosphine ligand.

2.6.3 Steric properties

A wide variety of scientific models have been developed to describe and calculate the steric properties of ligands. However, the well-known parameter used is the classical Tolman cone angle (θ) developed for phosphine ligands by Tolman in 1977.[58] To measure the size or steric bulk of a phosphine ligand, Tolman constructed a 3-D space filing model of a simple phosphine ligand as illustrated in **Figure 2.7**. The phosphorus atom was placed at a distance of about 2.28 Å away from the metal and the cylindrical cone was constructed as shown in **Figure 2.7** touching the Van der Waals radii of the outermost atoms of the model. For non symmetric phosphorus ligands the Tolman cone angle scenario is mimicked as shown in **Figure 2.7-B** and can be calculated using **Equation 2.1**.[58]

$$\theta = \frac{2}{3}\sum_{i=1}^{3}\frac{\theta_i}{2} \qquad \textbf{Equation 2.1}$$

[57] A. Muller, S. Otto, A. Roodt. *Dalton Trans*., **2008**, 650.

[58] C.A. Tolman. *Chem. Rev*., **1977**, *77*, 313.

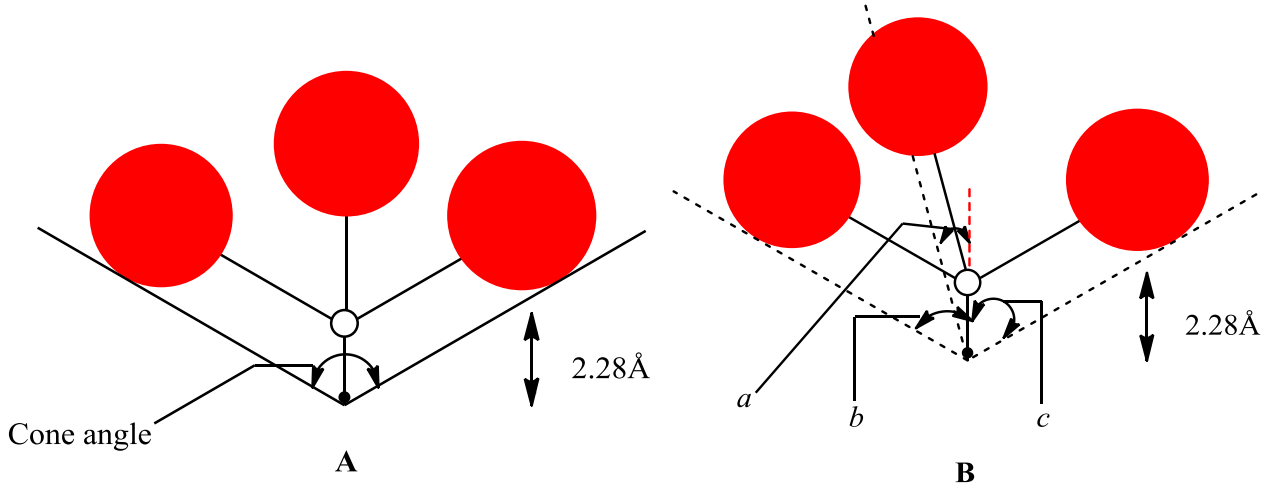

Figure 2.7: Tolman cone angle measurements for a symmetrical (A) and a non-symmetrical (B) ligands. *a*, *b* and *c* represent the angles $\theta_1/2$ $\theta_2/2$ $\theta_3/2$ *respectively*.[58]

2.6.3.1 The Effective Tolman-Based N-substituent ($\theta_{N\text{-}sub}$)

The *Effective Tolman-Based N-substituent* ($\theta_{N\text{-}sub}$) is a modified steric parameter used to calculate the steric bulk of a diphosphinoamine (PNP) ligand at the nitrogen atom. This parameter is designed for both metal-coordinated and free PNP ligands. It can be calculated for both the free and metal-coordinated PNP ligand derived from crystallographic data and computational analysis. After being calculated, this parameter can be linked to the behaviour of a catalyst and from this data new enhanced ligands can be designed.[59] To calculate $\theta_{N\text{-}sub,}$ a tangent line is created from the N atom to the Van der Waals radii of the outermost atoms of the species above the N atom as shown in **Figure 2.8** and **Equation 2.1** is utilized. This parameter was designed for the quantification of steric effects of phosphine ligands (PNP) on the N atom.

[59] N. Cloete, H.G. Visser, I. Engelbrecht, M.J. Overett, W.F. Gabrielli, A. Roodt. *Inorg. Chem*., **2013**, *52*, 2268.

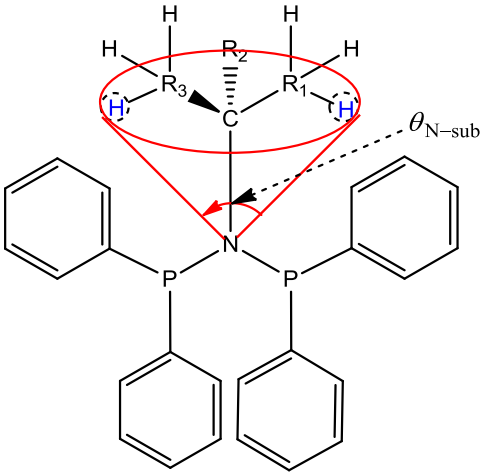

Figure 2.8: The Effective Tolman-Based N-substituent ($\theta_{N\text{-}sub}$) is a steric parameter.[59]

2.7 Phosphine ligand effects in catalysis

2.7.1 Introduction

Ligand properties play a key role on the overall properties of an organometallic catalyst. A good knowledge of ligand characters increases the understanding of a catalyst. Scientists would like to reach a level of knowledge whereby they can predict catalyst's behavior prior to the actual synthesis. However, separation of these properties for analysis turns out to be a difficult task due to their close relation. A complete description of all variations is considered beyond the scope of this study, therefore only the electronic and the steric effects will be evaluated.

2.7.2 Electronic effects

An electronic effect defines the electron donating and accepting property of molecules. Tertiary phosphine (PR_3) types of ligands are an important class of ligands in organometallic chemistry in that their electronic properties can be altered in a predictable way.[60,61] These phosphine ligands are good σ-donors, given that they have a lone pair on the P atom like the N atom on amines. When the R groups coordinated to the phosphine atom are electron withdrawing, they can act as

[60] F. Maseras, A. Lledós (Eds.). *Computational modeling of homogeneous catalysis*, Dordrecht: Kluwer Academic Publishers, **2002**.

[61] P.W.N.M van Leeuwen, K. Morokuma, J.H. van Lenthe (Eds.). *Theoretical aspects of homogeneous catalysis, Applications of Ab Initio molecular orbital theory*, Dordrecht: Kluwer Academic Publishers, **1995**.

moderate π-acceptors. By varying the R group in PR_3 you can change the electronic properties of a ligand significantly, making tertiary phosphine ligands one of the most versatile ligands in organometallic chemistry. The trend of donating ability of tertiary phosphines follows the order below:[62]

$$PMe_3 \approx P(NR_2)_3 < PAr_3 < P(OMe)_3 < P(OAr)_3 < PCl_3 < PF_3 \approx CO$$

Me = CH_3 Ar = 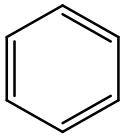

Using these ligand characters, Tolman correlated the electronic properties of phosphine and carbonyl (CO) ligand containing metal complexes to the stretching frequency of the CO in the corresponding $[Ni(CO)_3L]$ complexes (with L = monodentate phosphine ligand).[58,63] This is still one of the most frequently used methods of calculating electronic properties of a ligand. Tolman's observation led to the development of new phosphine ligands with different electronic characters particularly the trialkylphosphines and dialkyl(2-biphenyl)phosphines.[64,65,66,67,68]

Developments made by Buchwald and Hartwig changed the complexity of phosphine ligands significantly (see **Figure 2.9**).[67,68] A large number of phosphine ligands with various electronic effects can now be easily synthesized using the Buchwald-Hartwig cross coupling reactions.[69,70,71,72,73]

[62] M.S. Davies, M.J. Aroney, I.E. Buys, T.W. Hambley, J.L. Calvert. *Inorg. Chem*., **1995**, *34*, 330.

[63] D.J.M. Snelders, G. Van Koten, R.J.M.K Gebbink. *Chem. Eur. J*., **2011**, *17*, 42

[64] L.L. Hill, J.M. Smith, W.S. Brown, L.R. Moore, P.Guevera,E.S. Pair, J. Porter, J. Chou b, C.J. Wolterman, R. Craciun, D.A. Dixon, K.H. Shaughnessy. *Tetrahedron*., **2008**, *64*, 6920.

[65] T. Hundertmark, A.F. Littke, S.L. Buchwald, G.C. Fu. *Org. Lett.* **2000**, *2*, 1729.

[66] R.B. King, J.C. Cloyd, Jr, R.H. Reimann. *J. Org. Chem*., 1976, *41*, 6.

[67] K.W. Anderson, R.E. Tundel, T. Ikawa, R.A. Altman, S.L. Buchwald. *Angew.Chem., Int. Ed.*, **2006**, *45*, 6523

[68] S. Harkal, K. Kumar, D. Michalik, A. Zapf, R. Jackstell, F. Rataboul, T. Riermeier, A. Monseesb, M. Bellera, *Tetrahedron Lett*, **2005**, *46*, 3237.

[69] J. P. Wolfe, S. Wagaw, S.L. Buchwald. *J. Am. Chem. Soc.*, **1996**, *118*, 7215.

[70] M.C. Harris, X. Huang, S.L. Buchwald. *Org. Lett.*, **2002**, *4*, 2885.

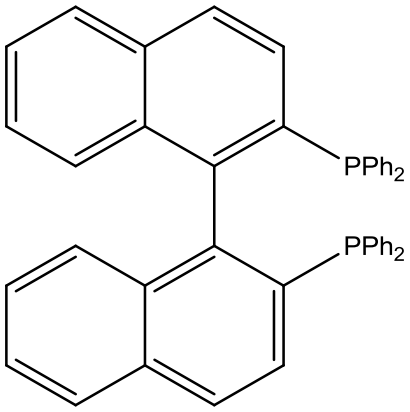

BINAP (1)

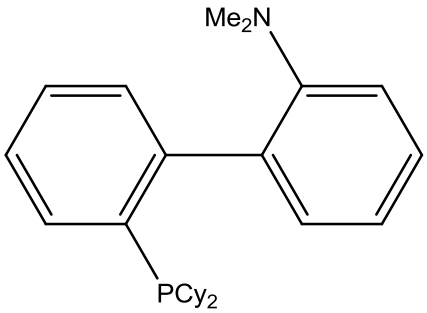

(2)

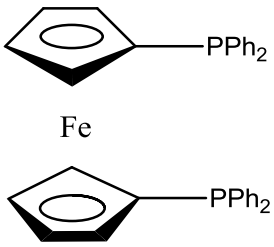

dppf (3)

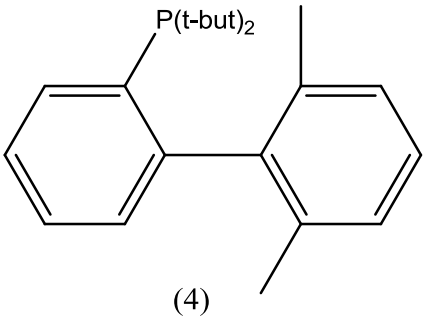

(4)

Figure 2.9: Examples of more complex phosphine ligands that have been used in catalysis. **(1)** 2,2'-Bis(diphenylphosphino)-1,1'-binaphthyl **(2)** 2-(dicyclohexylphosphino)-2'-(*N*,*N*-dimethylamino)biphenyl **(3)** 1,1'-Bis(diphenylphosphino)ferrocene **(4)** 2-(di-tert-butylphosphino)-2',6'-(dimethyl)biphenyl. [74,75,76,77,78]

Studies of ligand electronic effects in homogeneous catalysis are few in numbers. However, some reliable methods have been developed to illustrate this effect. One of these methods uses coupling constants of various NMR active nuclei to evaluate the electronic effects of phosphine ligands. For instance, Allen *et al*. measured the coupling constants between ^{31}P and ^{77}Se of phosphine selenide compounds to demonstrate the uses of $^{1}J_{P\text{-}Se}$ in determining the basicity of the

[71] M.S. Driver, J.F. Hartwig. *J. Am. Chem. Soc.*, **1996**, *118*, 7217.

[72] D.W. Old, J.P. Wolfe, S.L. Buchwald. *J. Am. Chem. Soc.*, **1998**, *120*, 9722.

[73] H. Tomori, J. M. Fox, S. L. Buchwald. *J. Org. Chem.*, **2000**, *65*, 5334.

[74] J. P. Wolfe, S. Wagaw, S. L. Buchwald. *J. Am. Chem. Soc.*, **1996**, *118*, 7215.

[75] M. C. Harris, X. Huang, S. L. Buchwald. *Org. Lett.*, **2002**, *4*, 2885.

[76] M. S. Driver, J. F. Hartwig. *J. Am. Chem. Soc.*, **1996**, *118*, 7217.

[77] D. W. Old, J. P. Wolfe, S.L. Buchwald. *J. Am. Chem. Soc.*, **1998**, *120*, 9722.

[78] H. Tomori, J. M. Fox, S. L. Buchwald. *J. Org. Chem.*, **2000**, *65*, 5334.

phosphine ligand.[79,80,81,82] This method was later utilized by Otto *et al*. for bicyclic phosphine ligands upon illustrating the electronic effect of various bicyclic phosphine ligands. This study proved that although the steric demands of different *cis,cis*-1,5cyclooctadiene (Phoban group) isomers were quite similar, the electronic properties were significantly different.[83] Studies by Brink *et al.* showed that phosphine electronic effects had a significant influence on the oxidative addition of CH_3I to tertiary phosphine modified rhodium(I)acetylacetonato complexes.[84] In this study it was noted that although a systematic increase of the electronic effect was observed, the kinetic results did not follow a systematic pattern. This suggested that a small variation on the electronic demand of a catalyst may affect the behavior of a catalytic system significantly.[84]

2.7.3 Steric effects

Electronic and steric properties are very difficult to separate, and they both play a key role in the overall properties of a metal complex. The steric effects of a tertiary phosphine ligand can also be altered in a systematic way similar to the electronic effect, by changing the R group(s) of a PR_3 ligand. The Tolman cone angle remains the most frequently used parameter defining the steric character of phosphine ligands. An alternative and refined model such as the *Effective Tolman-Based N-substituent* ($\theta_{N\text{-}sub}$) and Solid cone angle have also been reported.[59,63] Extensive researches have been dedicated into designing phosphine ligands with various steric properties since the birth of the Tolman cone angle parameter. **Figure 2.10** shows a range of PR_3 kinds of ligands with an increasing order of steric bulk.

[79] P. Nicpon, D.W. Meek. *Inorg. Chem*., **1966**, *5*, 1297.

[80] A.H. Cowley, M.C. Damasco., *J. Am. Chem. Soc.,* **1971**, *93*, 6815.

[81] D.W. Allen, B.F. Taylor. *J. Chem. Soc. Dalton Trans.,* **1982**, 51.

[82] D.W. Allen, I.W. Nowel. B.F. Taylor. *J. Chem. Soc. Dalton Trans.,* **1985**, 2505.

[83] P.N. Bungu, S. Otto. *J. Organomet. Chem.,* **2007**, *692*, 3370

[84] A. Brink, A. Roodt, G. Steyl, H.G. Visser. *Dalton Trans.*, **2010**, 39, 5572.

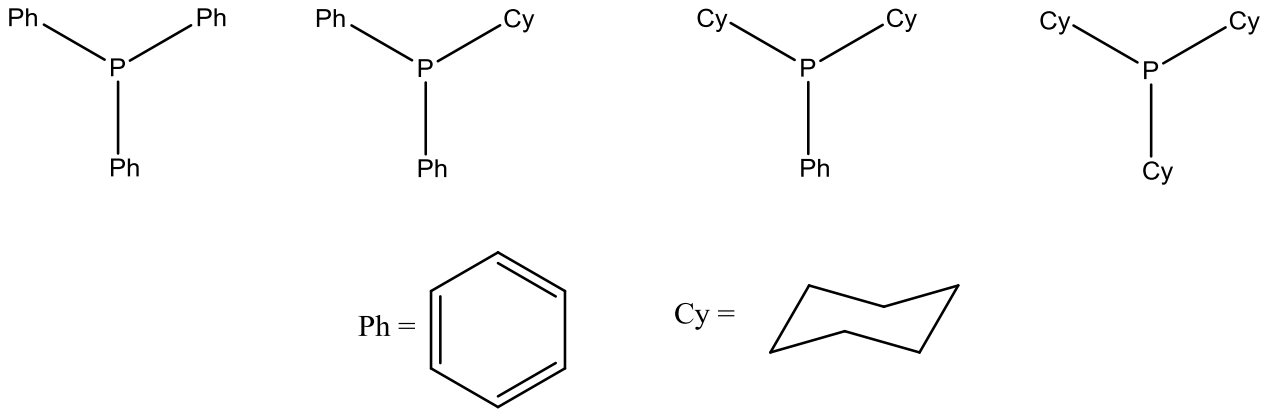

Figure 2.10: Phosphine ligands with increasing steric effect from left to right.[84]

The importance of steric effects was first illustrated by Pruett and Smith when they used a rhodium-phosphite modified catalyst for a hydroformylation reaction and obtained higher catalyst reactivity.[85] This opened access to hydroformylation of branched olefins which were known to be unreactive under normal Rh-PPh_3 modified catalysts.[86,87,88,89,90] A study comparing a conventional PPh_3 ligand and a bulky tris-(2-tert-butyl-4-methylphenyl) phosphite ligand on rhodium catalysed hydroformylation showed that the bulky ligand was more reactive than the less bulky one when a substrate such as 1,2 or 2,2-dialkylalkenes was subjected to hydroformylation.[47]

The significance of a ligand steric parameter was further illustrated by the effect of bicyclic phosphine ligands in cobalt catalysed hydroformylation. A significant increase on the reaction rate and the selectivity towards the desired products was observed when a PBu_3 (Bu = butyl) ligand was compared to a range of bicyclic phosphine ligands derived from *cis*,*cis*-1,5-cyclooctadiene (Phoban group, see **Figure 2.11**) despite both ligands having similar electronic

[85] R.L. Pruett, J. A. Smith. *J. Org. Chem*., **1969**, *34*, 327.

[86] R. Kadyrov, D. Heller and R. Selke. *Tetrahedron: Asymmetry*, **1998**, *9*, 329.

[87] Z. Freixa, M. M. Pereira, J. C. Bayon, A. M. S. Silva, J. A. R. Salvador, A. M. Beja, J. A. Paixao, M. Ramos. *Tetrahedron: Asymmetry*, **2001**, *12*, 1083.

[88] M.A. Freeman, D. A. Young. *Inorg. Chem*., **1986**, *25*, 1556.

[89] T. Yoshida, T. Okano, Y. Ueda and S. Otsuka, *J. Am. Chem. Soc*., **1981**, *103*, 3411.

[90] A. van Rooy, J.N.H. de Bruijn, K.F. Roobeek, P.C.J. Kamer, P.W.N.M. van Leeuwen, *J. Organomet. Chem*., **1996**, *507*, 69.

properties.[91] The only difference between the two groups were the steric properties, PBu_3 had a cone angle of ~132 ° while the phoban groups had approximately 165 °. Sufficient evidence was obtained to conclude that the steric bulk of the phoban groups played a key role on the rate of the reaction increment.

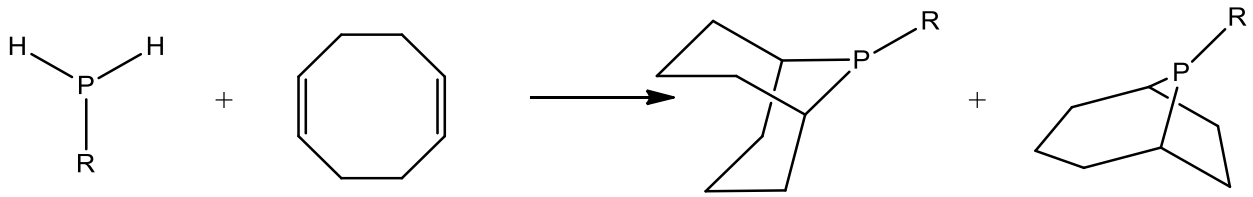

Figure 2.11: Synthesis of bicyclic phosphine ligands from *cis,cis*-1,5-cyclooctadiene (Phoban group).

Another class of phosphine ligands that further illustrated the importance of a ligand steric parameter is the so called diphosphinoamine (PNP) ligands. Ever since the discovery of the effectiveness of a modified catalyst with these ligands in ethylene tri- and tetra-merization reactions, recent researches are directed towards exploring these ligands.[92] In 2004, a tetramerization reaction was conducted under a Cr-PNP catalyst and a methyaluminoxane based activator by Wasserscheid *et al*.[93] Good activity and selectivity was observed towards 1-hexene and 1-octene with PNP ligands containing a cyclopentyl and a cyclohexyl moiety.[93] Wasserscheid *et al.* further illustrated the significant reduction of side products when the steric bulk of the cyclohexyl containing ligand was increased by substitution at the second position of the cyclohexyl skeleton.[94]

[91] P.N. Bungu, S. Otto. *Dalton Trans*., **2007**, 2876.

[92] W.W. du Mont, R.G. Gimeno, D. Lungu, R.M. Birzon, C.G. Daniliuc, C. Goers, A. Riecke, R. Bartsch. *Pure Appl. Chem*., **2013**, *85*, 633.

[93] A. Bollmann, K. Blann, J.T. Dixon, F.M. Hess, E. Killian, H. Maumela, D.S. McGuinness, D.H. Morgan, A. Neveling, S. Otto, M. Overett, A. M.Z. Slawin, P. Wasserscheid, S. Kuhlmann. *J. Am. Chem. Soc*., **2004**, *126*, 14712.

[94] S. Kuhlmann, K. Blann, A. Bollmann, J.T. Dixon, E, Killian, M.C. Maumela, H. Maumela, D.H. Morgan, M. Pretorius. *J. Cat*., **2007**, *245*, 279.

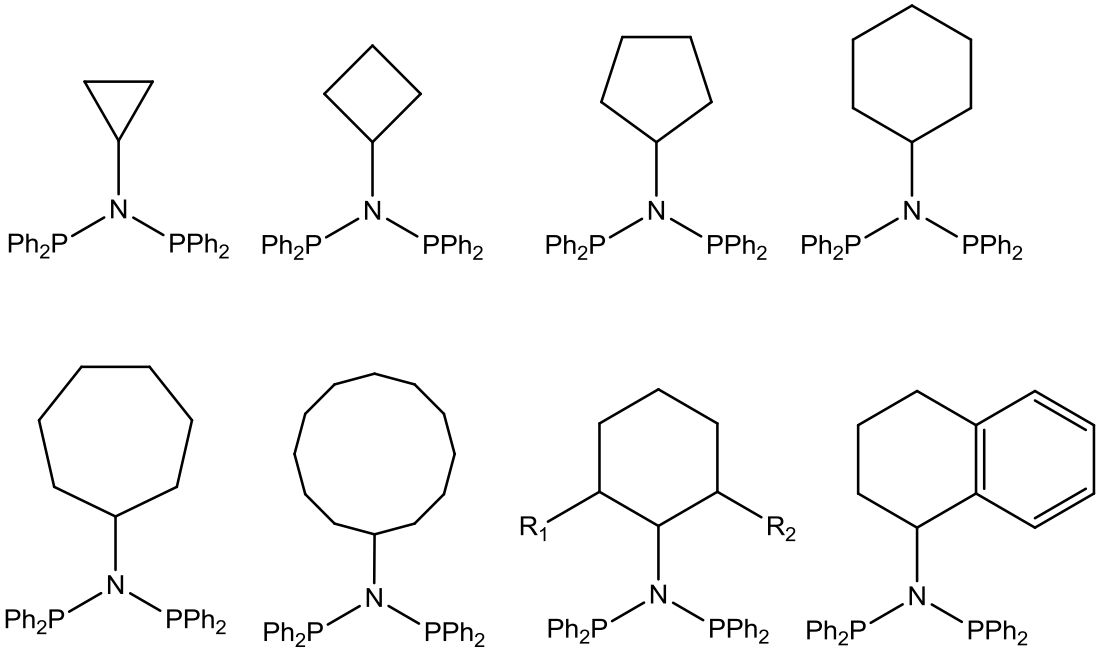

Figure 2.12: Diphosphinoamine ligands synthesized by Wasserschheid *et al.*[94]

A recent study on ethylene tri- and tetramerisation by Cloete *et al.* illustrated that an increase in the steric bulk of the PNP ligands, particularly on the N atom influenced the catalyst productivity and selectivity of 1-hexene and 1-octene significantly.[59,95] A well-established tetramerisation mechanism (see **Figure 2.13 and 2.14**) was used to explain the observed results. These observations showed that at maximum steric bulk 1-hexene formation was favoured whereas as the steric bulk was decreased the catalytic reaction favoured the formation of 1-octene and cyclic by-products.

[95] N. Cloete. PhD thesis, University of the Free State, Bloemfontein, Free State, **2009**.

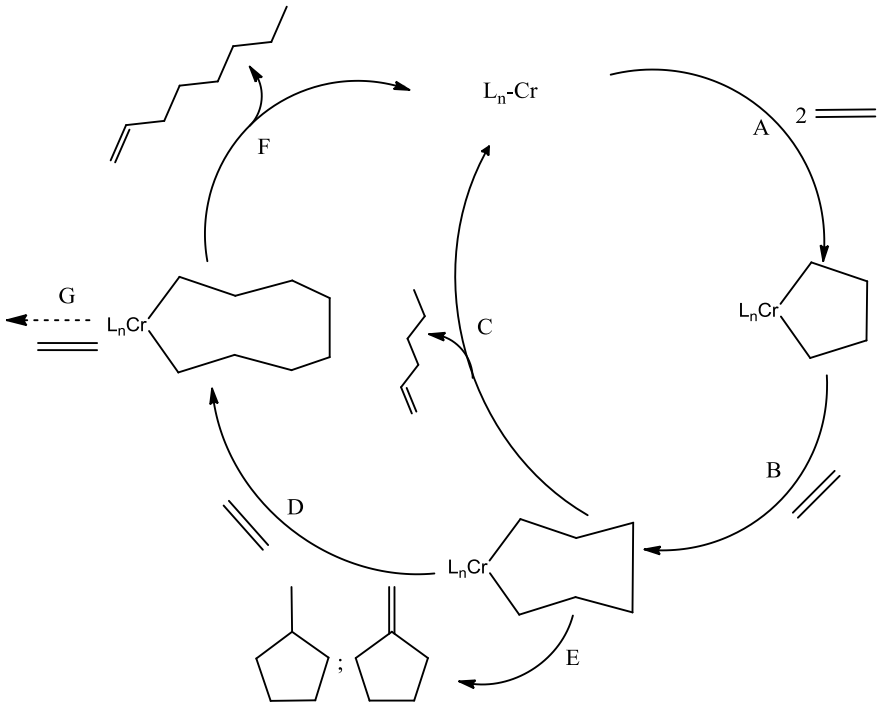

Figure 2.13: Ethylene tetramerization catalytic cycle, Step G represents further insertion elimination to give 1-C_{10}, 1-C_{12}, etc.[59,96]

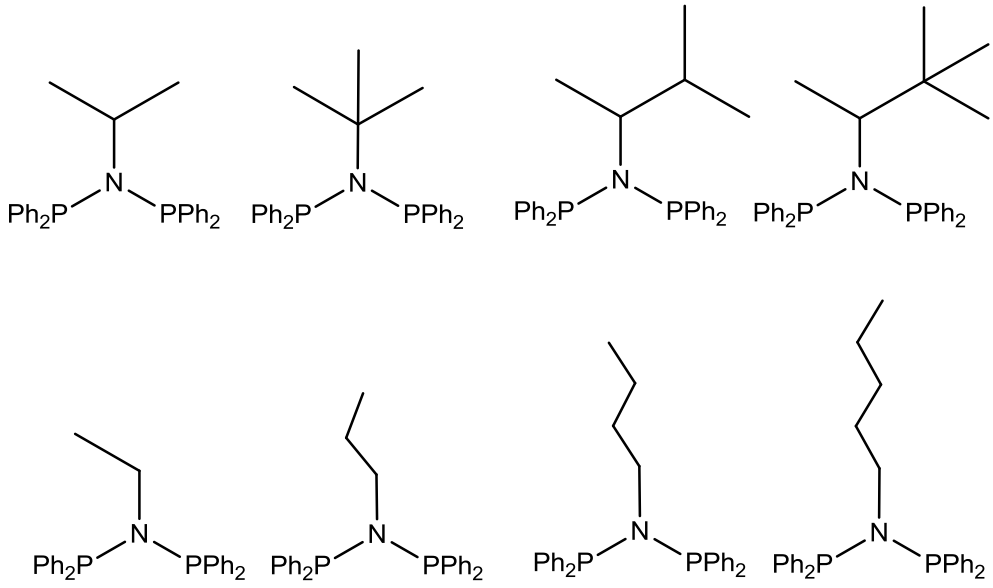

Figure 2.14: Diphosphinoamine ligands synthesized during a study by Cloete *et al*.[59,95]

[96] M.J. Overett, K. Blann, A. Bollman, J.T. Dixon, D. Haasbroek, E. Killian, H. Maumela, D.S. McGuinness, D.H. Morgan. *J. Am. Chem. Soc*., **2005**, *127*, 10723.

A variety of trialkylphosphines and dialkyl(2-biphenyl)phosphines ligands have been developed and tested in a number of catalytic processes.[64,65,66,67,68] However, studies on the diphosphinoamine influence on hydroformylation are low in numbers as compared to ethylene tri- and tetramerization. A study done by del Rio *et al.* on the hydroformylation of styrene was only on determining the enantiomeric excess influence of chiral diphosphine ligands.[97] A recent study by Kumar *et al*. used density functional calculations to determine phosphine ligand effects on the regioselectivity of rhodium-diphosphine catalyzed hydroformylation and observed that ligand-ligand and ligand-substrate non-bonding interactions played a key role on the region-selectivity of a catalyst, particularly when the phosphine ligands used were on an equatorial-equatorial positions.[98] Another recent study used a phosphine tetradentate (tris-[2-(diphenylphosphino)ethyl]phosphine) ligand during hydroformylation and with this study a range of 55-75 % yield of the aldehydes under the following conditions: 35 bar, 80 °C and 500 rpm within 5-8 h was observed.[99] Other examples involve, the investigations in Suzuki cross coupling and Heck reaction by Akba *et al.* using tris-[2-(*N*,*N*-bis(diphenylphosphino)aminoethyl] amine derivatives on Pd(II) complexes observing desirable yields for biphenyls and stilbenes respectively.[100,101,102]

2.8 Conclusion

In this chapter, some general aspects of catalysis were discussed in terms of the road to discovery, various homogeneous and heterogeneous processes, factors contributing to the final properties of an organometallic catalyst and the industrial significance of rhodium-based catalyst. A comparison between homogeneous and heterogeneous catalysis was also included.

The importance of organometallic catalyst enhancement *via* ligand modification was also illustrated in this chapter. This means advancement in the area of organometallic catalyst

[97] I. del Rio, W.G.J. de Lange, P.W.N.M. van Leeuwen, C. Claver., *J. Chem. Soc., Dalton Trans*., **2001**, 1293.

[98] M. Kumar, R. V. Chaudhari, B Subramaniam, T. A. Jackson., *Organomet*., **2014**, *33*(16), 4183.

[99] K. Saikia, B. Deb, D. K. Dutta., *J. Mol. Catal. A: Chem*, **2014**, *381*, 188.

[100] M. Aydermir, A. Baysal, B. Gumgum., *J. Organomet. Chem*., **2008**, *693*, 3810.

[101] O. Akba, F. Durap, M. Aydemir, A. Baysal, B. Gumgum, S. Ozkar., *J. Organomet. Chem*., **2009**, *694*, 731.

[102] C. Kayan, N. Biricik, M. Aydemir, R. Scopelliti., *Inorg. Chem. Acta*., **2012**, *385*, 164.

especially those used in homogeneous catalyzed processes may not only be through altering of the metal centres but also through thorough investigation of the appropriate ligands surrounding these metal centres. Therefore, the properties of an organometallic catalyst are determined by both the metal centres and the surrounding ligands.

The versatility of phosphine ligands make them one of the most interesting ligands to investigate. In this study, different PNP ligands will be synthesized, characterized and evaluated as potential ligands for 1-octene hydroformylation reaction, with rhodium as the catalyst's metal center. To evaluate the coordination chemistry of these PNP ligands, Pt(II) and Pd(II)-PNP complexes will be synthesized and analyzed by X-ray diffraction. Despite the fact that only rhodium-PNP complexes will be investigated as potential catalysts in this study, studies of both Pt(II) and Pd(II)-PNP complexes as potential catalysts will also be investigated in future.

Chapter 3 will discuss in detail all the analytical instruments that would be used for chemical analysis.

3 Basic Theory of Solid and Solution State Characterization

Abstract

A brief overview of the characterisation techniques such as Infrared spectroscopy (IR), X-ray Diffraction (XRD) and Nuclear Magnetic Resonance (NMR) spectroscopy is described in this chapter.

3.1 Introduction

In catalytic studies, accurate identification of starting materials, final products and intermediates are vital objectives. Non-destructive techniques such as UV-Vis, IR and XRD helps in identifying these components while indirectly assist on the determination of the reaction mechanism. A range of metal complexes synthesized in this study were fully characterized by various spectroscopic techniques and the theories of these techniques are described in this section. Of great importance are the six complexes that were characterized by X-ray diffraction. These complexes play a key role in this study and will be discussed in **Chapter 5**.

3.2 X-ray crystallography

3.2.1 Introduction

X-rays are electromagnetic radiations having a wavelength range of 0.02 – 100 Å while X-ray diffraction is a manner used in determining the molecular structure of a compound utilizing the compound's crystallinity.[1] In the late 1660's, the first crystal symmetry determination was investigated by the Danish scientist N. Steno.[2] A greater understanding of crystallography came

[1] W. Clegg, *Crystal Structure Determination*, New York: Oxford University Press, Inc., **1998**.

[2] W. Friedrich, P. Knipping, M. von Laue, *Interferenz-Erscheinungen bie Rontgenstrahlen*, **1912**, 202.

through the work of Bragg and his son in 1912.[3] X-ray crystallography celebrated its 100 year of existence in 2013 and in 2014 the United Nations declared the year as the International Year of Crystallography (IYCr2014). This illustrated the world wide importance of this analytical tool in the field of science.

3.2.2 X-rays

Before the discovery of X-rays, scientists made their crystallographic assumptions regarding the arrangement of atoms in a molecule from angle measurements between its crystal faces. Some crystallographers used molecular properties, such as the reactivity, chemical formula and number of isomers to obtain indirect information regarding the molecular structure. The discovery of X-rays made it possible for crystallographers to obtain sufficient information to produce a detailed three dimensional image of a crystalline compound. X-rays have small wavelengths and this makes it easy for them to penetrate though the surface of matter. This feature makes it useful in the medical field for internal structure determination and in the chemistry field for molecular structural determination.

Although X-rays and radioactivity were discovered between the 18th century and the First World War, the birth of X-ray crystallography came through the work of Sir William Henry Bragg and his son Sir W. Lawrence Bragg in 1912.[4] It is through William and Lawrence work that crystallographers can now determine accurately the arrangement of atoms in a crystal. A single crystal being defined as the primary objective required in X-ray crystallography. It is defined as a solid material with highly ordered constituents forming three dimensional structural moieties that are repeated through a unit cell. Unit cells dimensions can be described using the three bond angles (α, β, γ) and edge lengths (*a*, *b*, *c*).[5] Cartesian coordinates are used to describe the position of atoms in a unit cell. In a crystal lattice the description of directions and planes is coined the Miller indices (hkl). The symmetry of a unit cell is described by a crystal space group and there

[3] A. Compton, *Physical Review*, **1923**, *21*, 483.

[4] P. Ball, *The birth of Crystallography*, Crystallography–Feature, Spring/Summer, **2013**, Available at http://www.astbury.leeds.ac.uk/about/Ball.pdf. Last downloaded on the 6th-January-**2015**.

[5] D.W.A. Sharpe, *The Penguin Dictionary of Chemistry*, 3rd Ed., London: Penquin Books Ltd., **2003**.

can only be 230 different types. These space group variations have been thoroughly studied and are listed in the International Tables for Crystallography.[6]

X-ray crystallography is based on the basic principle of X-ray diffraction. When crystalline molecular structures are exposed to X-rays, electrons within the crystal diffract these X-rays resulting in a diffraction pattern. This diffraction pattern is transformed into a electron density map from which the position of electrons can be obtained.

3.2.3 Bragg's law

When a crystal is exposed to X-rays, phenomena such as constructive and destructive interferences are observed. Atoms in a crystal interact with these X-rays to produce these interferences. Figure **3.1** illustrates how X-rays from a beam of monochromatic X-rays are reflected according to the Bragg's law model when shined at a shallow angle (θ) to a crystalline molecular structure. From **Figure 3.1** it is evident that these X-rays are diffracted by certain planes coined "lattice planes" within an atom. These planes are parallel to one another and intersect the axis of the crystallographic unit cell. Any lattice plane with in a crystal can be indexed by the triple *hkl* integer or the so called Miller indices.

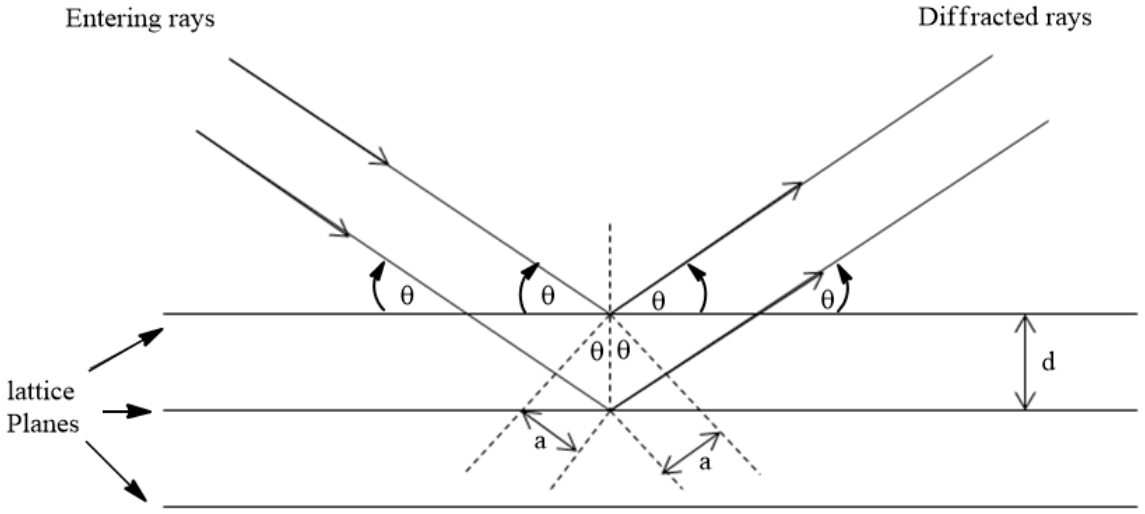

Figure 3.1: Crystallographic lattice planes occupied by atoms in a crystal used to visualize the Bragg equation $n\lambda = 2d\sin\theta$.

[6] *International Tables for Crystallography*, A, 5th Ed., Kluwer Academic Publishers, **2002**.

The distance between two successive lattice planes is represented by the interplanar spacing d_{hkl}.[7] According to Bragg, to observe maximum intensity in the diffraction pattern, **Equation 3.1** and **3.2** must be satisfied were *n* is an inter number, λ represents the wavelength and θ is the incident and the reflected angle.

$$n\lambda = 2dsin\theta \qquad \textbf{Equation 3.1}$$

$$2a = 2dsin\theta;\ a = dsin\theta \qquad \textbf{Equation 3.2}$$

$$n\lambda = 2a \qquad \textbf{Equation 3.3}$$

Equation **3.1** is known as the Bragg's law for X-ray diffraction.[8] This equation is used to correct the resulting difference due to reflections from different planes.[9] From this **Equation 3.1** it is evident that if the wavelength and the angle are known, the distance between successive planes can be calculated. Further exposure will result in identification of more and more planes then finally the unit cell can be calculated and the crystal structure solved. For constructive interference **Equation 3.3** must be satisfied and from **Equation 3.3** it is clear that for a reflection to be indexed the scattering angle must be equal to 2θ and its miller indices (*hkl* values) be identified from known wavelengths.

If the miller indices can be assign to each diffraction spot then the so called Laue class can be assigned to the crystal. This class is assigned to a crystal from the relation of the intensity weighted reciprocal lattice. The systematic extinctions occurring in the reciprocal space are then used for space group determination. These systematic extinctions are determined from structural factors in that space group and these structural factors will be discussed comprehensively in **Section 3.2.2**.[6] Correct space group assignment increases the chances of solving the crystal structure.

[7] J.M. Buerger, *X-Ray Crystallography*, London, Academic Press, **1971**.

[8] U.W. Arndt, A.J. Wonacott, *The Rotation Method in Crystallography*, North-Holland, **1997**.

[9] M.F.C. Ladd, R.A. Palmer, *Structure Determination by X-ray Crystallography*, New York: Plenum Press, **1977**.

3.2.4 Structure factor

Geometrical ordering of atoms on a crystallographic plane is known to be indicated by the fractional coordinates (h, k, l) which are also known as the Miller indices. Each coordinate can have a number between 0 and 1 while the cell edges are defined by the vectors *a*, *b*, and *c*. The position of an atom in terms of these fractional coordinated can be expressed as:

$$r = hx + ky + Iz \qquad \textbf{Equation 3.4}$$

The structure factor (F_{hkl}) indicates the overall scattering of all atoms (j) in the unit cell relative to that of a single electron. The equation indicating this is expressed as:

$$F_{hkl} = \sum_{j=1}^{N} f_j \exp\left[i2\pi\left(hx_j + ky_j + lz_j\right)\right] \qquad \textbf{Equation 3.5}$$

Where f_j represents the scattering factor for each N atoms and (x_j, y_j, z_j) represents the coordinates of each individual atom within the unit cell. From **Equation 3.5** it is clear that the structural factor's magnitude depends only on the relative atoms position and these atoms scattering factors. Each term on this equation represents a wavelet having an amplitude f_j and phase $\Phi_j = 2\pi(hxj + ky_j + lz_j)$ expressing the path length for each scattered wavelet. From the above explanations, the structure is then simply the resultant of wavelets scattered by N number of atoms within the unit cell.[10] Equation **3.5** can also be expressed as:

$$F_{hkl} = \sum_{j=1}^{N} f_j\left[cos2\pi\left(hx_j + ky_j + lz_j\right) + isin2\pi\left(hx_j + ky_j + lz_j\right)\right] \qquad \textbf{Equation 3.6}$$

In a cosine wave, energy is proportional to the square of the wave's amplitude or in other words the square of the absorbance. In X-ray diffraction, the intensity [I_0(hkl)] of the scattered wave is

[10] L.V. Azaroff, *Elements of X-ray Crystallography*, New York: McGraw-Hill, Inc., **1968**.

used to represent the experimentally observed quantity. Thus, this intensity function can be used to represent the ideal intensity $|F_{hkl}|^2$. Therefore:

$$I_0(hkl) \propto |F_0(hkl)|^2 \qquad \textbf{Equation 3.7}$$

Equation **3.7** allows direct relation of experimental intensity values [I_0(hkl)] to the structure properties represented by $|F_{hkl}|$. Atoms having high atomic numbers give greater electron concentration than those with low atomic numbers. Thus the crystal structure can be determined from the diffraction patterns created by electrons associated with these atoms. Electron density is a function of position and can be expressed as ρ(X, Y, Z). The relationship between the structure factor and the electron density can be expressed as:

$$F_{hkl} = \int \rho(x,y,z) exp\,[i2\pi(hx_n + ky_n + lz_n)]\,dV \qquad \textbf{Equation 3.8}$$

3.2.5 Phase Problem

Accurate analysis of a crystal structure using X-ray diffraction depends on the precise determination of the modulus $|F_{hkl}|$ which is obtained from the intensity data (**Equation 3.7**) and the phase (Φ_{hkl}) corresponding this modulus $|F_{hkl}|$. However, the corresponding phase (Φ_{hkl}) cannot be directly determined. For this reason, a Fourier transform method is applied to this function to invert it, making it possible for us to see the electron density map on a computer. To obtain back the original function, the inverted function needs to be run through another transformer called the inverse Fourier transformer to give the original function. This is where the problem arises; to obtain this the actual amplitude and phase of the diffracted waves needs to be known and there is no practical way of obtaining this relative phase angles. This problem is known as the 'Phase Problem'. Two approaches have been developed to overcome this problem and will be discussed in **Section 3.2.6** and **3.2.7**.

3.2.6 Direct Method

In the direct method approach, the initial and the expanding phase angles from measured X-ray intensities is estimated using a mathematical formulae such as the triple phase relation, the Sayre equation and the tangent formula.[11] A ranged of small light molecule crystals having up to 1000 atoms in an asymmetric unit have been successfully solved in literature using this method. For this reason this method is preferred for light atoms. The Patterson method is use for compounds containing heavier atoms.

3.2.7 Patterson Function

As mentioned before, the Patterson Function approach is used for compounds containing heavier atoms or when major parts of the crystal structure are known. To get the Patterson Function, all phase angles are set to zero and Fourier transformed amplitudes are squared resulting in the equation below:

$$P(u,v,w) = V^{-1} \sum_h \sum_k \sum_l (F_{hkl})^2 \exp\left[-2\pi i(hu + kv + lw)\right] \qquad \textbf{Equation 3.9}$$

Where V represents the volume of the unit cell.[12] The Patterson Function does not represent the actual position of atoms in a crystal structure but rather the electron density map with peaks of positive electron density in various positions. For every peak at (u, v, w) position, there are two atoms laying relative to each other in the structure whose x coordinates differ by *u*, *y* coordinates differ by *v* and *z* coordinates differ by *w*. Thus, these peaks only produce information about atoms laying relative to each other and not to the unit cell origin. The Patterson Function gives an indication of the atom size involved in the unit cell and then the rest of the structure can be analyzed by other techniques.

[11] G.M. Sheldrick, *Classical direct methods*, Gottingen, **2008**. Available at shelx.uni-ac.gwdg.de/SHELX/classic-dm.pdf. Last downloaded on the 6th-January-**2015**.

[12] G.H. Stout, L.H. Jensen, *X-ray Structure Determination: A Practical Guide*, London: The Macmillan Company, **1968**.

3.2.8 Least Square Refinement

The least square refinement is a system used to compare the calculated diffraction pattern and the experimentally observed diffraction pattern in order to obtain the degree of similarity between them. The comparison between the experimental data $|F_0|$ and the calculated structure factor $|F_c|$ for a certain crystal structure is described in terms of *residual inde*x or R-*factor* represented by **Equation 3.10** below:[12]

$$R = \frac{\sum ||F_0| - |F_c||}{\sum |F_0|} \qquad \textbf{Equation 3.10}$$

A range of 0.02-0.07 of the R-factor is an indication of a complete and correct crystal structure determination through experimental data of good quality.

To obtain an even better refinement of the crystal structure, the weighing factor (w) can be incorporated for each reflection. This new factor gives a reliability factor for different measured data. Adding the weighing factor (w) results in the equation below:

$$wR^2 = \frac{\sum w(F_0^2 - F_c^2)^2}{\sum w(F_0^2)^2} \qquad \textbf{Equation 3.11}$$

The three basic steps in crystal structure analysis:

- Grow good crystals suitable for X-ray diffraction. (Easier said than done!)
- Collect crystal data using an X-ray diffractometer.
- Refine your structure using available structural refinement software. "*this requires long hours of practice, the more you practice the better you become*"

3.3 Nuclear Magnetic Resonance Spectroscopy

3.3.1 History

Nuclear Magnetic Resonance (NMR) spectroscopy was developed in the late 1940s and early 1950s by E.M Purcell and F. Bloch together with their respective groups in Harvard University and Stanford University respectively. This analytical instrument is used to analyze chemical compounds and elucidate their structures.

3.3.2 NMR spectroscopy

In chemistry, one of the most commonly used instruments to study a molecular structure is the so called NMR spectroscopy. This instrument is closely related to the Magnetic Resonance Imaging (MRI) used by the medical faculties.[13] It is based on the nuclear magnetic spin of several atoms such as ^{1}H, ^{13}C, ^{31}P, ^{19}F, and so forth. When compared to other analytical techniques such as the IR spectroscopy and Mass spectrometer, NMR gives the most detailed information regarding the molecular structure.

All atom nucleus have magnetic properties that when manipulated can give chemical information regarding the respective atom. The subatomic particle such as protons, neutrons and electrons can be viewed as spinning along their own axes. For some atoms, the spins are paired against each other and for other like ^{1}H, ^{13}C, ^{31}P, ^{19}F the spins are not. If the spins are paired, the nucleus has no overall spin while others like those mentioned above contain nuclei with an overall spin. This overall spin (I) is important and to determine it the following rules can be used:

- The nucleus has no net spin if the number of protons and the number of neutrons are both even.
- If the addition of the number of protons and the number of neutrons gives an odd number, the nucleus has a half-integer spin i.e. 1/2, 3/2, 5/2, and so forth.
- If the number of protons and the number of neutrons are both odd, then the nucleus has an integer spin of 1, 2, 3, and so forth.

[13] J.C. Kotz, P.M. Treichel, J.R. Townsend, *Chemistry and Chemical Reactivity*, Thomson Brooks/Cole publishers, Canada, **2009**.

Quantum mechanics states that a nucleus with a spin of I will have (2I + 1) possible orientations. Thus, a nucleus with spin 1/2 half will have two possible orientations (+1/2 which is parallel to the applied field and -1/2 which is anti-parallel to the applied field. These orientations have equal energy when a magnetic field is not applied. If a magnetic field is applied, the energy levels will split with each level being given by a quantum number (m) as shown in **Figure 3.2**.

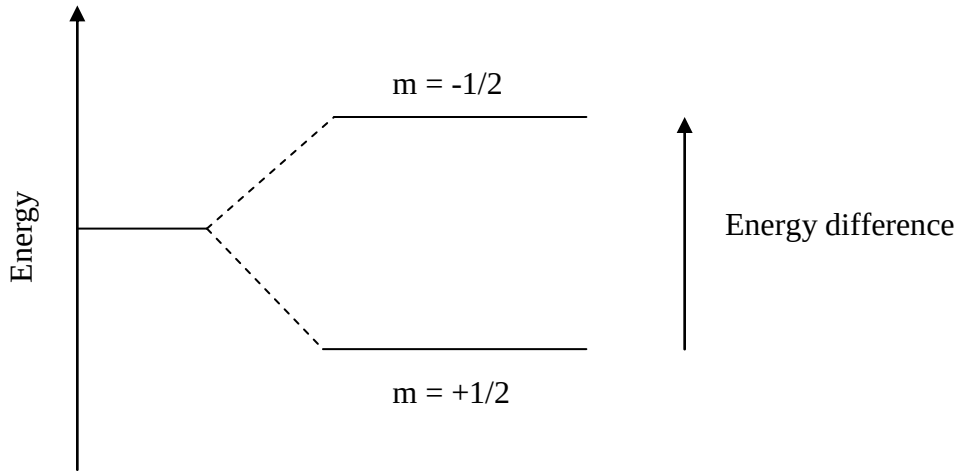

Figure 3.2: Energy difference for a nucleus with spin quantum number 1/2.

Each level is represented by the magnetic quantum number (m) and because the nucleus is positively charged, it can generate its own magnetic field. The resulting spin-magnet has a magnetic moment (μ) which is proportional to its spin (I) as shown in **Equation 3.12** below.

$$\mu = \frac{\gamma I h}{2\pi} \qquad \textbf{Equation 3.12}$$

Where h represents Planck's constant and γ represents the magnetogyric ratio. This magnetic moment is the fundamental nuclear constant and is different for every nucleus.

Strong magnetic fields are necessary for NMR spectroscopy. In the presence of a magnetic field, the nucleus spins on its own axis with this axis processing around this magnetic field as shown in **Figure 3.3**.

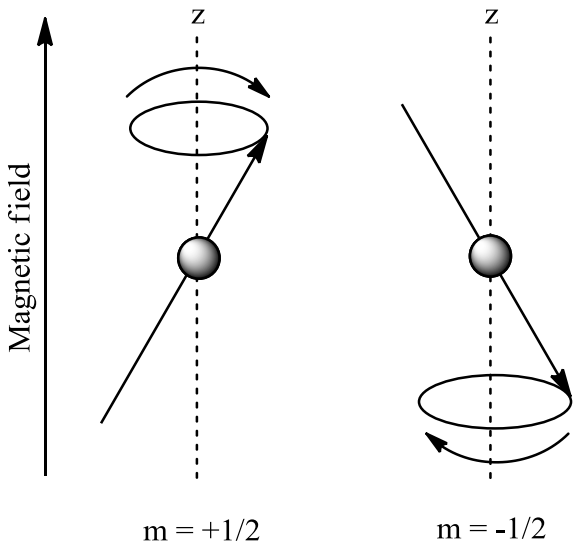

Figure 3.3: Axis of rotation processing around the magnetic field

The frequency of this precession is called the Larmor frequency and it is identical to the transition frequency which is given by **Equation 3.13** below:

$$E = -\mu B cos\theta \qquad \textbf{Equation 3.13}$$

Where θ represents the angle between the direction of the applied magnetic field and axis of nuclear rotation. If the nucleus absorbs energy, this angle will change. This means that in a nucleus with spin 1/2, this will result in 180^o flip of the magnetic moment thus opposing the applied field and moving to the higher energy state.

Due to the shielding of electrons around the nucleus, the magnetic field encountered at the nucleus is not equal to this applied magnetic field. This shielding generated by the s orbital electrons around the nucleus reduces the net magnetic moment; the difference in magnetic field

strength coursed is called the nuclear shielding. Thus, for the nucleus to absorb at its transition frequency the applied field has to be increased. This is an up-field shift which is also called the diamagnetic shift.

Unlike the electrons in the s orbital, the electrons in the p orbital produces relatively large magnetic field. These results in low field shift commonly referred to as deshielding or paramagnetic shifts.

An adjacent atom nuclear spins influences one another and the results are manifested in the resonance signals. This small interaction between groups in molecules is called coupling and is transmitted from one atom to the other through connecting bonds in all directions. The coupling mentioned above is measured in Hertz and termed the coupling constant (J).

3.4 Infrared Spectroscopy

3.4.1 Introduction

Infrared (IR) spectroscopy is an instrument used to determine functional groups such as the CO, CN, COR (where R is an alkyl group), COOR, and so forth present in a molecule. This instrument uses the similarity between the energies in infra-red radiation and energies involved in bond vibrations to analyse chemical compounds.

3.4.2 How IR spectroscopy works

To obtain an infrared spectrum, an infrared radiation is passed through the chemical sample then the fraction of radiation absorbed is calculated. The frequency (υ) which is calculated as the number of wave cycles passing through a point per second and the wavelength () which is calculated as the length of a one complete wave cycle is related according to the equation illustrated below:

$$\upsilon = \frac{c}{\lambda}$$ **Equation 3.14**

Where c = 3 x 10^8 ms^{-1} represents the speed of light. Equation **3.15** is then used for energy calculation which is proportional to the frequency (υ).

$$E = hv = \frac{hc}{\lambda}$$ **Equation 3.15**

Where *h* represents the Planck's constant.

Graphs of IR spectrum are widely represented in a unit called the wavenumber ($\bar{\upsilon}$) which is represented by **Equation 3.16**. This equation represents the number of waves in a length of one centimeter.

$$\bar{\upsilon} = \frac{1}{\lambda} = \frac{v}{c}$$ **Equation 3.16**

As mentioned before, the IR instrument works on the basis of rotations of atoms and the molecular dipoles associated with bond vibrations. To visualize this, a molecule is viewed as an arrangement of atoms connected through bonds with spring like properties.

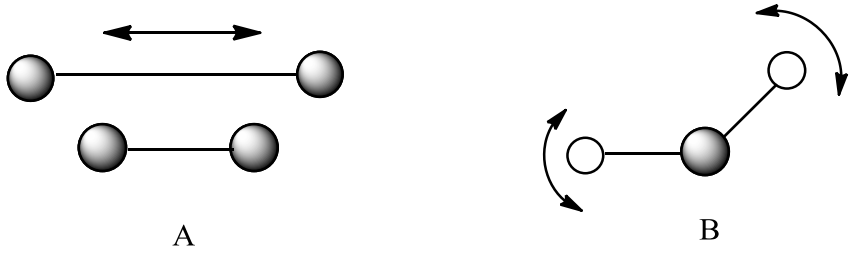

Figure 3.4: Virtualization of bonds spring like properties, scheme **A** represents vibrations due to bond stretching and contracting while scheme **B** represents the vibrations due to bond bending.

From **Figure 3.4** it is clear that vibrations involve either a change in bond length due to stretching or a change in bond angles due to bond bending. When bond stretching between two atoms is in phase the stretching is said to be symmetrical and when out-of-phase is said to be asymmetric stretching. Homonuclear molecules such as H_2 and O_2 do not show infrared

absorption. Only those molecules that possess an electric dipole moment which changes during vibrations show infrared absorption. From these vibrations molecular vibration energy will be generated when molecules absorb infrared radiation. The absorption of IR radiation results in the excitation of vibrational and rotational transitions of covalent bonds, but this energy is not enough for electron excitation to take place. When interpreting the IR spectrum, the energy of any peak corresponds to the respective frequency of vibration of a certain part of a molecule.[14,15] Excluding chiral molecules, all unique molecular species have corresponding unique IR spectra.

3.5 Conclusion

In conclusion, a detailed description of the analytical instruments that were used to reach the objectives of this project is presented in this chapter. X-ray diffractometer was used to elucidate the solid state structures of some Pt(II) and Pd(II)-PNP complexes synthesized in this study, while a 300 MHz NMR was used to analyze free and coordinated PNP ligands and IR spectroscopy was used to analyze carbonyl group containing rhodium complexes. The results obtained from these tools will be described in detail on the following chapters.

[14] J. Coates, *Encyclopedia of Analytical Chemistry; Interpretation of infrared Spectra, A Practical Approach*, 10815, **2000**.

[15] K. Nakamoto, *Infrared Spectra of Inorganic and Coordination Compounds*, 2nd Ed, New York: John Wiley & Sons Inc., **1970**.

4 Synthesis and characterization of free diphosphinoamine (PNP) ligands and Pt, Pd metal complexes

Abstract

In this chapter the synthesis of various diphosphinoamine (PNP) ligands and their coordination to palladium [Pd(II)] and platinum [Pt(II)] metals will be described in detail.

4.1 Introduction

A number of diphosphinoamine (PNP) ligands were synthesized onto which various substituents on both the N and P atoms were systematically varied from one ligand to the other (**Figure 4.1** and **Figure 4.2**). The PNP ligands were coordinated to Pt(II) and Pd(II) transition metals for the purpose of studying their coordination properties. Each of these free ligands were used in the hydroformylation catalytic reaction of 1-octene to gain information regarding their impact on the chemical process based on the different steric and electronic properties (see **Chapter 6**). A simplified PNP ligand synthetic mechanism is shown in Scheme **4.1**.

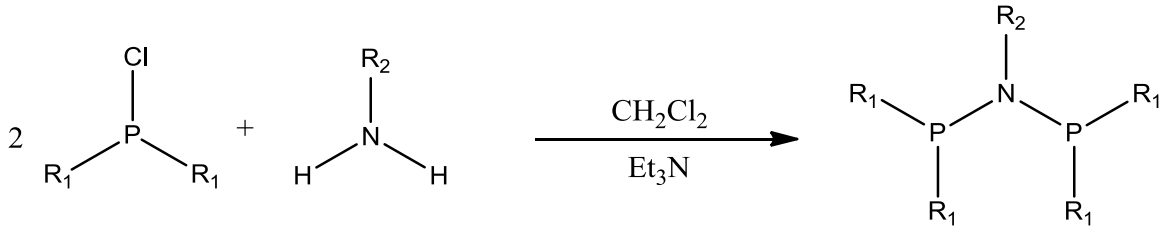

Scheme 4.1: General method for the synthesis of diphosphinoamine (PNP) ligands.[1,2]

[1] M.S. Balakrishna, T.K. Prakasha, S.S. Krishnamurthy, *J. Organomet. Chem*., **1990**, *390* (2), 203.

[2] S. Kuhlmann, K. Blann, A. Bollmann, J.T. Dixon, E. Killian, M.C. Maumela, H. Maumela, D.H. Morgan, M. Pretorius, N. Taccardi, P. Wasserscheid, *J. Catal*., **2007**, *245*, 279.

In **Table 4.1** a summary of all the compounds naming and abbreviations is presented. A number of similar ligands have been reported in literature and will be compared to those synthesized in this study.[3,4,5,6,7,8]

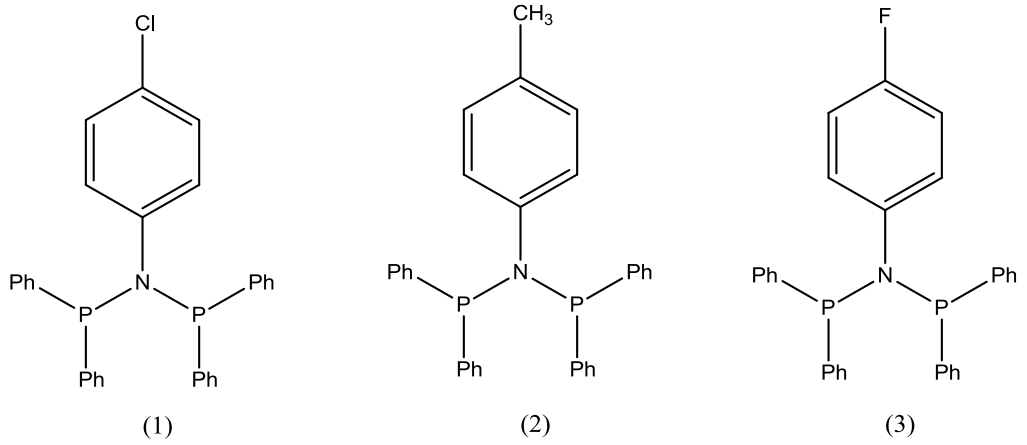

Figure 4.1: Diphosphinoamine ligands (PNP ligands) with significantly different electronic effects on the N atom synthesized in this study: **1** Cl-Ph-PNP, **2** CH_3-Ph-PNP, **3** F-Ph-PNP.

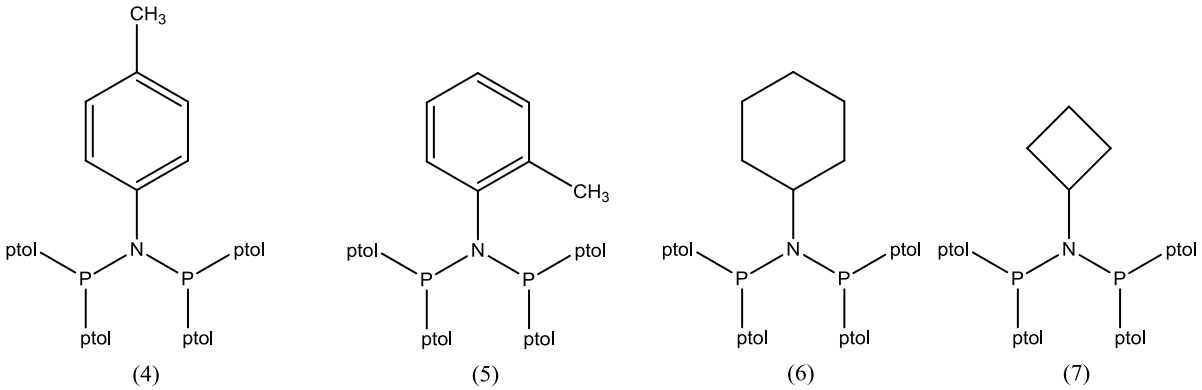

Figure 4.2: Diphosphinoamine ligands (PNP ligands) with significantly different steric bulkiness on the N atom synthesized in this study: **4** 5-*p*-tolyl-PNP, **5** 4-*p*-tolyl-*o*-tol, **6** Chzyl-4-*p*-tolyl and **7** Cbutyl-4-*p*-tolyl.

[3] A.N.J. Blok, P.H.M. Budzelaar, A.W. Gal, *Organometallics*, **2003**, *22*, 2564.

[4] S. Kuhlmann, K. Blann, A. Bollmann, J.T. Dixon, E. Killian, M.C. Maumela, H. Maumela, D.H. Morgan, M. Pretorius, N. Taccardi, P. Wasserscheid, *J. Catal*., **2007**, *245*, 277.

[5] F.A. Cotton, F.E. Kuhn, A. Yokochi, *Inorg. Chim. Acta*, **1996**, *252*, 251.

[6] Z. Fei, R. Scopeleti, P.J. Dyson, *J. Chem. Soc. Dalton Trans*., **2003**, 2772.

[7] N. Cloete, H.G. Visser, A. Roodt. J.T. Dixon, K. Blann, *Acta Cryst*., **2008**, *E64*, o480.

[8] N.Cloete, PhD thesis, University of the Free State, Free State, Bloemfontein, **2009**.

Table 4.1: Abbreviations and definition of all complexes shown in **Figure 4.1** and **4.2**.

No:	Abbreviations	Definition
1	Cl-Ph-PNP	*N*,*N*-Bis(diphenylphosphino)-4-chloroaniline
2	CH_3-Ph-PNP	*N*,*N*-Bis(diphenylphosphino)-*p*-toluidine
3	F-Ph-PNP	*N*,*N*-Bis(diphenylphosphino)-4-fluoroaniline
4	5-*p*-tolyl-PNP	*N*,*N*-Bis(di-*p*-tolylphosphino)-*p*-toluidine
5	4-*p*-tolyl-*o*-tol	*N*,*N*-Bis(di-*p*-tolylphosphino)-*o*-toluidine
6	Chzyl-4-*p*-tolyl	*N*,*N*-Bis(di-*p*-tolylphosphino)cyclohexylamine
7	Cbutyl-4-*p*-tolyl	*N*,*N*-Bis(di-*p*-tolylphosphino)cyclobutylamine

4.2 Materials and Methods

All chemicals (with the exception of solvents) were reagent grade and were used without further purification. Triethylamine, 1,5-cyclo-octadiene and chlorodiphenylphosphine were purchased from Sigma Aldrich, while potassium tetrachloroplatinate(II) (K_4PtCl_4) and palladium(II) chloride ($PdCl_2$) were purchased from Next Chimica, South Africa. For dry conditions all solvents involved were purified and dried using methods prescribed in literature.[9,10] All reactions that were either air or moisture sensitive were performed under standard Schlenk conditions.

All Nuclear Magnetic Resonance (NMR) data were obtained on a Bruker 300 MHz NMR spectrometer (operating at 300 and 121 MHz for ^1H and ^{31}P respectively) using either deuterated solvent or samples spiked with deuterated solvent. Chemical shifts, δ, are reported in parts per million (ppm) using tetramethylsilane (TMS) as internal standard for ^1H NMR and 85 % H_3PO_4 as external standard in a tightly closed capillary (0 ppm) for ^{31}P NMR. Coupling constants, *J*, are reported in Hertz (Hz).

Free PNP ligands were synthesized by reacting each respective amine with its respective phosphine-chloride precursor as described in the literature.[1,2]

[9] D.D. Perrin, W.L.F. Armarego. *Purification of laboratory chemicals*, 3rd Ed, Great Britain: Butterworth-Heinemann Publishers, **1988**.

[10] D.D. Perrin, W.L.F. Armarego. *Purification of laboratory chemicals*, 5th Ed, Great Britain: Butterworth-Heinemann Publishers, **2003**.

4.3 Ligand Synthesis

4.3.1 *N,N*-Bis(di-*p*-tolylphosphino)-*p*-toluidine (4)

p-Toluidine (0.2154 g, 0.002010 mol) was dissolved in dichloromethane (15 ml); the reaction mixture was placed in an ice bath and stirred. Triethylamine (2.2 ml, 0.01578 mol) was added to the mixture with stirring, followed by chloro-di(*p*-toly)phosphine (909.0 µl, 0.004021 mol). The mixture was stirred further for 1 h, before the ice bath was removed. The reaction was stirred for an additional 14 hours at room temperature (~ 27 °C). The mixture was dried under vacuum and the remaining solid was dissolved with hot dichloromethane. The solution was loaded on to the column containing neutral activated alumina (~35 g). The solvent of the eluent was removed under reduced pressure and the solid product was washed with 1.2-dichloroethaneand giving a yield of (0.9511 g, 89.0 %). ^{1}H NMR (300 MHz CD_2Cl_2) δ_H 2.18 (3 H, s, CH_3), 2.33 (12 H, s, 4 CH_3), 6.49 (2 H, d, *J* = 8.4 Hz, 2 CH), 6.75 (2 H, d, *J* = 8.4 Hz, 2 CH), 7.09 (8 H, m, 8 CH), 7.19 (8 H, m, 8 CH). ^{31}P NMR (121.49 MHz, CD_2Cl_2) δ_P 67.36 (s).

4.3.2 *N,N*-Bis(di-*p*-tolylphosphino)-*o*-tolueneamine (5)

The procedure was analogous to that described in **Section 4.4.1** except *o*-Toluidine (213.7 µl, 0.002010 mol) was used. Yield (0.6550 g, 61.3 %). ^{1}H NMR (600 MHz CD_2Cl_2) δH 2.66 (3 H, s, CH_3), 2.35 (12 H, s, 4 CH_3), 6.59 (1 H, d, *J* = 7.9 Hz, 1 CH), 6.84 (1 H, m, 1 CH), 7.02 (10 H, m, 10 CH), 7.19 (4 H, s, 4 CH), 7.32 (4 H, m, 4 CH). ^{31}P NMR (121.49 MHz, CD_2Cl_2) δP 59.90 (s).

Note: at 2.5 ppm we expected a singlet peak integrating to 12 protons however a multiplet peak was observed. At 7.02 ppm an overlapping of two peaks is observed. Once more, we expected a singlet peak around 7.1 -7.4 integrating to 8 protons but 2 distinct peaks, each integrating to 4 protons were observed. However, no abnormalities were observed on the ^{31}P NMR. The successful syntheses of this ligand will be further proven by X-ray diffraction studies in **Chapter 5**.

4.3.3 *N,N*-Bis(diphenylphosphino)-4-fluoroanilineamine (3)

4-Fluoroaniline (480 µl, 0.0051 mol) was dissolved in dichloromethane (15 ml) and the mixture was placed in an ice bath (0 °C) with stirring. Triethylamine (2 ml, 0.014 mol) was added to the

mixture while stirring followed by chlorodiphenylphosphine (2.0 ml, 0.011 mol). The reaction was stirred further for 1 hour, before the removal of the ice bath. The mixture was stirred for and additiona 14 h at room temperature (~ 27 °C). The formed salt ammonium salt was filtered and the filtrate was left to recrystallize as a white powder. A yield of (2.318 g, 94.8 %) was recorded. ^{1}H NMR (300 MHz CD_2Cl_2) δ_H 6.59 (4 H, m, 4 CH), 7.34 (20 H, m, 20 CH). ^{31}P NMR (121.49 MHz, CD_2Cl_2) δ_P 70.59 (s).

4.3.4 *N,N*-Bis(diphenylphosphino)-4-chloroanilineamine (1)

The procedure was analogous to that presented in **Section 4.4.3** utilizing 4-chloroaniline (0.6379 g, 0.0050 mol). White crystals (1.825 g, 73.6 %) were obtained. ^{1}H NMR (300 MHz CD_2Cl_2) δ_H 6.58 (2 H, d, *J* = 8.7 Hz, 2 CH), 6.90 (2 H, d, *J* = 8.7 Hz, 2 CH), 7.33 (20 H, m, 20 CH). ^{31}P NMR (121.49 MHz, CD_2Cl_2) δ_P 69.86 (s).

4.3.5 *N,N*-Bis(diphenylphosphino)-*p*-tolueneamine (2)

The procedure was analogous to that presented in **Section 4.4.3** utilizing *p*-toluidine (0.5355 g, 0.0050 mol). White powder (2.068 g, 87.0 %) was obtained. ^{1}H NMR (300 MHz CD_2Cl_2) δ_H 6.52 (2 H, d, *J* = 8.1 Hz, 2 CH), 6.77 (2 H, d, *J* = 8.1 Hz, 2 CH), 7.31 (20 H, m, 20 CH). ^{31}P NMR (121.49 MHz, CD_2Cl_2) δ_P 68.64 (s).

4.3.6 *N,N*-Bis(di-*p*-tolylphosphino)cyclohexylamine (6)

Cyclohexylamine (230.0 µl, 0.002011 mol) was dissolved in dichloromethane (10 ml) and the reaction was placed in an ice bath (0 °C) with vigorous stirring. Triethylamine (846 µl, 0.006069 mol) was added to this mixture while stirring followed by chloro-di(*p*-toly)phosphine (909.0 µl, 0.004021 mol). The reaction was stirred further for 1 hour, before the removal of the ice bath. The mixture was stirred for additional 14 hours at room temperature. The mixture was dried under vacuum and the remaining solid was dissolved with a solvent mixture of hexane (20 ml) and toluene (2 ml). The solution was loaded on to the column containing neutral activated alumina (~35 g). The solvent of the eluent was removed under reduced pressure and the solid product was washed with 1.2-dichloroethane and giving a yield of (0.4275 g, 40.6 %) was obtained. ^{1}H NMR (300 MHz CD_2Cl_2) δ_H 1.05 (3 H, m, 3 CH), 1.50 (5 H, m, 5 CH), 1.86 (2 H,

m, 2 CH), 2.36 (12 H, m, 4 CH_3), 3.22 (1 H, m, 1 CH), 7.16 (16 H, m, 16 CH). ^{31}P NMR (121.49 MHz, CD_2Cl_2) δ_P 49.69 (s).

4.3.7 *N,N*-Bis(di-*p*-tolylphosphino)cyclobutylamine (7)

The procedure was analogous to that presented in **Section 4.3.6** utilizing cyclobutylamine (171.7 µl, 0.002011 mol). The product was obtained as a white solid with a yield of (0.4117 g, 41.3 %). ^{1}H NMR (300 MHz CD_2Cl_2) δ_H 1.38 (1 H, m, CH), 1.72 (4 H, m, 4 CH), 2.35 (12 H, s, 4 CH_3), 2.51 (2 H, m, 2 CH), 3.99 (1 H, m, 1 CH), 7.18 (16 H, m, 16 CH). ^{31}P NMR (121.49 MHz, CD_2Cl_2) δ_P 48.14 (s).

4.4 Synthesis of [M(cod)Cl_2] (M = Pd(II), Pt(II))

4.4.1 *cis*-(η4-Cycloocta-1,5-diene-dichloridopalladium(II)) ([Pd(cod)Cl_2])

Palladium(II) chloride (2.00g, 0.0113 mol) was dissolved in a hot (~ 85 °C) hydrochloric acid (5.0 ml, 10 M) while stirring. The solution was then left to cool to room temperature. Ethanol (150 ml) was then added to the vigorously stirring solution followed by 1,5-cyclooctadiene (3.0 ml, 0.0113 mol), resulting in an immediate orange yellow colour and precipitate formation. The precipitate was filtered after 10 minutes and washed four times with diethyl ether (25 ml). A yield of 2.50 g (77.7 %) was obtained. ^{1}H NMR (300 MHz CD_2Cl_2) δ_H 2.56 (4 H, m, 2 CH_2); 2.88 (4 H, m, 2 CH_2); 6.26 (4 H, m, 4 CH).

4.4.2 *cis*-(η4-Cycloocta-1,5-diene-dichloridoplatinum(II)) ([Pt(cod)Cl_2])

Potassium tetrachloroplatinate(II) (1.0 g, 2.4 mmol) was dissolved in a mixture of *n*-propanol (11 ml) and distilled water (16 ml) with stirring. 1,5-Cyclooctadiene (2 ml, $2.4x10^{-3}$ mol) and tin(II) chloride (15.0 mg, $2.4x10^{-3}$ mol) were added to the reaction mixture and then left to stir at room temperature for 48 h. The solvent was evaporated and the product extracted with hot dichloromethane and left to recrystallize resulting in light yellow coloured crystals. Yield (0.702 g, 77.6 %). ^{1}H NMR (300 MHz $CDCl_3$) δ_H 2.27 (4 H, m, 2 CH_2), 2.71 (4 H, m, 2 CH_2), 5.61 (4 H, m, 4 CH).

4.5 Pt(II) – PNP Complex Synthesis

4.5.1 Dichloro-[*N*,*N*-bis(di-*p*-tolylphosphino)-*p*-toluidine-κ^2*P*,*P'*]platinum(II)

N,*N*-Bis(di-*p*-tolylphosphino)-*p*-toluidine (28.44 mg, 5.35×10^{-5} mol) was added to a solution of $Pt(cod)Cl_2$ (20 mg, 5.35×10^{-5} mol) in dry dichloromethane (10 ml) and stirred for 14 h. The volume of the reaction mixture was reduced to approximately 2 ml. Thereafter, diethyl ether (20 ml) was added, resulting in light yellow precipitate which was filtered and dried. Dissolving the light yellow product in dichloromethane and layering the solution with methanol resulted in orange crystals (25.0 mg, 58.6 %) suitable for X-ray diffraction. ^{1}H NMR (300 MHz CD_2Cl_2) δ_H 2.17 (3 H, s, CH_3), 2.43 (12 H, s, 4 CH_3), 6.34 (2 H, d, *J* = 8.0 Hz, 2 CH), 6.85 (2 H, d, *J* = 8.0 Hz, 2 CH), 7.32 (8 H, m, 8 CH), 7.69 (8 H, m, 8 CH). ^{31}P NMR (121.49 MHz, $CDCl_3$) δ_P 19.7 (t, *J*(Pt-P) = 1678.4 Hz).

4.5.2 Dichloro-[*N*,*N*-bis(di-*p*-tolylphosphino)-*o*-toluidine-κ^2*P*,*P'*]platinum(II)

The procedure was analogous to that presented in **Section 4.5.1** except *N*,*N*-Bis(di-*p*-tolylphosphino)-*o*-toluidine (28.44 mg, 5.35×10^{-5} mol) was used. Dissolving the product in dichloromethane and layering the solution with methanol resulted in light yellow crystals (19.8 mg, 46.4 %) suitable for X-ray diffraction. ^{1}H NMR (300 MHz CD_2Cl_2) δ_H 2.44 (15 H, s, 5 CH_3), 6.59 (1 H, d, *J* = 8.2 Hz, 1 CH), 6.96 (1 H, t, *J* = 7.4 Hz, 1 CH), 7.04 (1 H, d, *J* = 7.5 Hz, 1 CH), 7.23 (1 H, t, *J* = 7.6 Hz, 1 CH), 7.31 (8H, m, 8 CH), 7.78 (8H, m, 8 CH). ^{31}P NMR (121.49 MHz, $CDCl_3$) δ_P 20.37 (t, *J*(Pt-P) = 1683.9 Hz).

4.5.3 Dichloro-[*N*,*N*-bis(di-*p*-tolylphosphino)cyclohexylamine-κ^2*P*,*P'*]platinum(II)

The procedure was analogous to that presented in **Section 4.5.1** except *N*,*N*-Bis(di-*p*-tolylphosphino)cyclohexylamine (7.00 mg, 1.34×10^{-5} mol) was used. Dissolving the product in dichloromethane layering the solution with methanol resulted in colourless crystals. Yield of (8.60 mg, 81.3%). ^{1}H NMR (600 MHz CD_2Cl_2) δ_H 0.71 (1 H, m, 1 CH), 0.88 (4 H, m, 4 CH), 1.35 (5 H, m, 5 CH), 2.46 (12 H, s, 4 CH_3), 3.10 (1 H, m, 1 CH), 7.39 (8 H, d, *J* = 7.2 Hz, 8 CH), 7.90 (8 H, m, 8 CH). ^{31}P NMR (243 MHz, CD_2Cl_2) δ_P 13.83 (t, *J*(Pt-P) = 1650.0 Hz).

4.5.4 Dichloro-[*N*,*N*-bis(di-*p*-tolylphosphino)cyclobutylamine-κ^2*P*,*P'*]platinum(II)

The procedure was analogous to that presented in **Section 4.5.1** except *N*,*N*-Bis(di-*p*-tolylphosphino)cyclobutylamine (6.70 mg, 1.34×10^{-5} mol) was used. Dissolving the product in dichloromethane layering the solution with methanol resulted in colourless crystals suitable for X-ray diffraction. Yield of (8.92 mg, 87.5%). ^{1}H NMR (600 MHz CD_2Cl_2) δ_H 1.32 (2 H, m, 2 CH), 1.73 (4 H, m, 4 CH), 2.49 (12 H, s, 4 CH_3), 3.73 (1 H, m, 1 CH), 7.42 (8 H, d, *J* = 7.2 Hz, 8 CH), 7.83 (8 H, m, 8 CH). ^{31}P NMR (243 MHz, CD_2Cl_2) δ_P 13.49 (t, *J*(Pt-P) = 1654.8 Hz).

4.5.5 Dichloro-[*N*,*N*-bis(diphenylphosphino)-4-fluoroaniline-κ^2*P*,*P'*]platinum(II)

The procedure was analogous to that presented in **Section 4.5.1** except *N*,*N*-Bis(diphenylphosphino)-4-fluoroaniline (12.83 mg, 2.675×10^{-5} mol) was used. Yield (13.5 mg, 67.7 %). ^{1}H NMR (300 MHz CD_2Cl_2) δ_H 6.40 (2 H, m, 2 CH), 6.77 (2 H, m, 2 CH), 7.53 (8 H, m, 8 CH), 7.66 (4 H, m, 4 CH), 7.81 (8 H, m, 8 CH). ^{31}P NMR (121.49 MHz, CD_2Cl_2) δ_P 20.30 (t, *J*(Pt-P) = 1684.46 Hz).

4.5.6 Dichloro-[*N*,*N*-bis(diphenylphosphino)-4-chloroaniline-κ^2*P*,*P'*]platinum(II)

The procedure was analogous to that presented in **Section 4.5.1** except *N*,*N*-Bis(diphenylphosphino)-4-chloroaniline (13.27 mg, 2.675×10^{-5} mol) was used. Yield (16.5 mg, 81.0 %). ^{1}H NMR (300 MHz CD_2Cl_2) δ_H 6.40 (2 H, m, 2 CH), 7.06 (2 H, m, 2 CH), 7.55 (8 H, m, 8 CH), 7.68 (4 H, m, 4 CH), 7.84 (8 H, m, 8 CH). ^{31}P NMR (121.49 MHz, CD_2Cl_2) δ_P 21.91 (t, *J*(Pt-P) = 1683.24 Hz).

4.5.7 Dichloro-[*N*,*N*-bis(diphenylphosphino)-*p*-toluidine-κ^2*P*,*P'*]platinum(II)

The procedure was analogous to that presented in **Section 4.5.1** except *N*,*N*-Bis(diphenylphosphino)-*p*-toluidine (12.72 mg, 2.675×10^{-5} mol) was used. Yield (14.9 mg, 75.1 %). ^{1}H NMR (300 MHz CD_2Cl_2) δ_H 2.18 (3 H, m, CH_3), 6.31 (2 H, d, *J* = 8.4 Hz, 2 CH), 6.85 (2

H, d, *J* = 8.5 Hz, 2 CH), 7.51 (8 H, m, 8 CH), 7.63 (4 H, m, 4 CH), 7.81 (8 H, m, 8 CH). ^{31}P NMR (121.49 MHz, CD_2Cl_2) δ_P 20.84 (t, *J*(Pt-P) = 1665.63 Hz).

4.6 Pd(II) – PNP Complex Synthesis

4.6.1 Dichloro-[*N*,*N*-bis(di-*p*-tolylphosphino)-*p*-toluidine-κ^2*P*,*P'*]palladium(II)

N,*N*-Bis(di-*p*-tolylphosphino)-*p*-toluidine (37.24 mg, 7.01x10^{-5} mol) was added to a solution of [Pd(cod)Cl_2] (20 mg, 7.01x10^{-5} mol) in dry dichloromethane (10 ml) and stirred for 14 h. The volume of the reaction mixture was reduced to approximately 2 ml. Diethyl ether (20 ml) was added, resulting in a deep orange precipitate which was filtered and dried. Dissolving the product in dichloromethane and layering the solution with methanol resulted in orange crystals (31.0 mg, 62.4 %) suitable for X-ray diffraction. ^{1}H NMR (300 MHz CD_2Cl_2) δ_H 2.19 (3 H, s, CH_3), 2.42 (12 H, s, 4 CH_3), 6.41 (2 H, d, *J* = 8.0 Hz, 2 CH), 6.86 (2 H, d, *J* = 8.1 Hz, 2 CH), 7.34 (8 H, m, 8 CH), 7.74 (8 H, m, 8 CH). ^{31}P NMR (121.49 MHz, $CDCl_3$) δ_P 34.26 (s).

4.6.2 Dichloro-[*N*,*N*-bis(di-*p*-tolylphosphino)-*o*-toluidine-κ^2*P*,*P'*]palladium(II)

The procedure was analogous to that presented in **Section 4.6.1** utilizing *N*,*N*-Bis(diphenylphosphino)-*o*-toluidine (37.24 mg, 7.01x10^{-5} mol) was used. Dissolving the product in dichloromethane and layering the solution with methanol resulted in orange crystals (36.5 mg, 73.5 %) suitable for X-ray diffraction. ^{1}H NMR (300 MHz CD_2Cl_2) δ_H 2.41 (15 H, s, 5 CH_3), 6.56 (1 H, d, *J* = 8.1 Hz, 1 CH), 6.97 (2 H, m, 2 CH), 7.19 (1 H, dt, 1 CH), 7.29 (8H, m, 8 CH), 7.77 (8H, m, 8 CH). ^{31}P NMR (121.49 MHz, $CDCl_3$) δ_P 35.25 (s).

4.6.3 Dichloro-[*N*,*N*-bis(diphenylphosphino)-4-fluoroaniline-κ^2*P*,*P'*]palladium(II)

The procedure was analogous to that presented in **Section 4.6.1** utilizing *N*,*N*-Bis(diphenylphosphino)-4-fluoroaniline (33.6 mg, 7.01x10^{-5} mol) was used. An orange powder (40.8 mg , 88.7 %) was obtained. ^{1}H NMR (300 MHz CD_2Cl_2) δ_H 6.44 (2 H, m, 2 CH), 6.79 (2 H, m, 2 CH), 7.55 (8 H, m, 8 CH), 7.68 (4 H, m, 4 CH), 7.87 (8 H, m, 8 CH). ^{31}P NMR (121.49 MHz, CD_2Cl_2) δ_P 36.57 (s).

4.6.4 Dichloro-[*N*,*N*-bis(diphenylphosphino)-4-chloroaniline-κ^2*P,P'*]palladium(II)

The procedure was analogous to that presented in **Section 4.6.1** except *N*,*N*-Bis(diphenylphosphino)-4-chloroaniline (34.74 mg, 7.01×10^{-5} mol) was used. Dissolving the product in dichloromethane and layering the solution with methanol resulted in yellow crystals (45.8 mg, 97.1%) suitable for X-ray diffraction. ^{1}H NMR (300 MHz CD_2Cl_2) δ_H 6.44 (2 H, d, *J* = 8.7 Hz, 2 CH), 7.06 (2 H, d, *J* = 8.7 Hz, 2 CH), 7.57 (8 H, m, 8 CH), 7.70 (4 H, m, 4 CH), 7.87 (8 H, m, 8 CH). ^{31}P NMR (121.49 MHz, CD_2Cl_2) δ_P 36.07 (s).

4.6.5 Dichloro-[*N*,*N*-bis(diphenylphosphino)-*p*-toluidine-κ^2*P,P'*]palladium(II)

The procedure was analogous to that presented in **Section 4.6.1** except *N*,*N*-Bis(diphenylphosphino)-*p*- toluidine (33.6 mg, 7.01×10^{-5} mol) was used. An orange solid product with a yield of (38.7 mg, 84.6 %) was obtained. ^{1}H NMR (300 MHz CD_2Cl_2) δ_H 2.20 (3 H, s, CH_3), 6.37 (2 H, d, *J* = 8.7 Hz, 2 CH), 6.87 (2 H, d, *J* = 8.7 Hz, 2 CH), 7.53 (8 H, m, 8 CH), 7.68 (4 H, m, 4 CH), 7.88 (8 H, m, 8 CH). ^{31}P NMR (121.49 MHz, CD_2Cl_2) δ_P 34.82 (s).

4.6.6 Dichloro-[*N*,*N*-bis(di-*p*-tolylphosphino)cyclohexylamine-κ^2*P,P'*]palladium(II)

The procedure was analogous to that presented in **Section 4.6.1** utilizing *N*,*N*-Bis(diphenylphosphino)cyclohexylamine (9.20 mg, 1.75×10^{-5} mol). Dissolving the product in dichloromethane and layering the solution with methanol resulted in light yellow crystals suitable for X-ray diffraction. Yield of (10.1 mg, 82.3 %). ^{1}H NMR (600 MHz CD_2Cl_2) δ_H 0.72 (1 H, m, 1 CH), 0.90 (4 H, m, 4 CH), 1.34 (5 H, m, 5 CH), 2.46 (12 H, s, 3 CH_3), 3.21 (1 H, m, 1 CH), 7.39 (8 H, t, *J* = 12.1 Hz, 8 CH), 7.91 (8 H, dt, *J* = 13.1, 8.4 Hz, 8 CH). ^{31}P NMR (243 MHz, CD_2Cl_2) δ_P 28.10 (s).

4.6.7 Dichloro-[*N*,*N*-bis(di-*p*-tolylphosphino)cyclobutylamine-κ^2*P,P'*]palladium(II)

The procedure was analogous to that presented in **Section 4.6.1** utilizing *N*,*N*-Bis(diphenylphosphino)cyclobutylamine (8.90 mg, 1.75×10^{-5} mol). Dissolving the product in

dichloromethane layering the solution with methanol resulted in light yellow crystals with a yield of (8.42 mg, 71.5%). ^{1}H NMR (600 MHz CD_2Cl_2) δ_H 1.32 (2 H, m, 2 CH), 1.71 (4 H, m, 4 CH), 2.46 (12 H, s, 4 CH_3), 3.77 (1 H, m, 1 CH), 7.40 (8 H, d, J = 6.6 Hz, 8 CH), 7.84 (8 H, m, 8 CH). ^{31}P NMR (243 MHz, CD_2Cl_2) δ_P 27.52 (s).

4.7 Discussion

In this study, seven PNP ligands, fourteen metal complexes ([Pt(PNP)Cl_2], [Pd(PNP)Cl_2]) were synthesized (see **Figure 4.3**), all with good yields ranging from 40.6 and 89.5 % for the free ligands and 46.4 to 97.1 % for the metal complexes. Special care was taken during the synthesis of all ligands to ensure that the P atom precursors (e.g. Ph_2PCl) did not undergo an oxidation reaction with the atmosphere. These ligands were strategically selected for 1-octene hydroformylation reaction based on the following reasons (**1**) to investigate the effects of PNP ligands with different electronic effects on the N atom (**2**) to investigate the effects of PNP ligands with different steric demands on the N atom. Three of the synthesized ligands system namely Cl-Ph-PNP, CH_3-Ph-PNP and F-Ph-PNP have previously been reported in the literature with a wide range of applications, but mainly catalysis' (cobalt based ethylene tetramerization) and luminescence. [11,12,13,14] The above mentioned ligands were re-synthesized and characterized in order to investigate their effects on hydroformylation of 1-octene and solid state of the Pt(II) and Pd(II) complexes. The following PNP ligands, 5-*p*-tolyl-PNP, 4-*p*-tolyl-*o*-tol, Chzyl-4-*p*-tolyl and Cbutyl-4-*p*-tolyl are novel and are described extensively during this study. All the Pd(II) and Pt(II) complexes synthesised in this study are novel and were specifically synthesized for the purpose of this study.

^{31}P NMR (**Table 4.3**) data of both the free PNP ligands and the palladium complexes were relatively easily interpretable as they yielded singlet ^{31}P resonance peaks. The free PNP ligands yielded singlet peaks with chemical shifts ranging between 48.14 and 70.59 ppm. While the palladium complexes yielded singlet peaks with chemical shift ranging from 27.5 to 36.57 ppm.

[11] S. Ghosh, G. Hogarth, N. Hollingsworth, K. B. Holt, I. Richards, M. G. Richmond, B. E. Sancheza, D. Unwina, *Dalton Trans*., **2013**, *42*, 6775.

[12] V. Wing-Wah Yam, W. Kit-Mai Fung, M. Wong, *J. Organomet. Chem*, **1997,** *16*, 1772.

[13] E. Chung-Chin Cheng, W. Lo, T. Kwok-Ming Lee, N. Zhu, V. Wing-Wah Yam, *Inorg. Chem*. **2014**, *53*, 3854.

[14] M. GuoLiang, N. YingNan, H. WenBo, L. ShanMing, S. XianFeng, N. Bo, J. Tao, *Chin Sci Bult*, **2008**, *53*, 3511.

A significant shift between the free ligand ^{31}P and the palladium coordinated ^{31}P NMR peak were observed, indicating electronic changes between the free PNP ligand and the palladium coordinated ligand. No second order $^{31}P - ^{31}P$ coupling was observed for all free and coordinated ligands.

The ^{195}Pt nucleus has a natural abundance of 34 % and a nuclear spin of a ½, so one should consider the 66 % of the magnetically inactive platinum isotope.[15,16] This means if a P atom is coordinated to the Pt metal centre, the ^{31}P NMR will show three resonance peaks (meaning a triplet). The central resonance peak of this triplet will correspond to the 66% magnetically inactive isotopes that did not couple to the P atom, while the other two peaks will in total amount to the 34% (17% each) representing the 34% magnetically active isotopes that coupled to the P atom. Hence the platinum coordinated ligands were easily identified by the ^{31}P NMR (**Table 4.3**). The *J*(Pt–P) of the synthesized platinum complexes ranged from 1650.0 to 1693.60 Hz, indicating significant electronic difference between the free and coordinated ligand. These coupling constants are caused by various indirect nuclear spin-spin couplings; best described by the so called 'Fermi-Contact' interactions in the s-orbitals. The Fermi-Contact interaction theory states that out of all first-order coupling constants contributors, the main contribution comes from the overlap in the s-orbital.[17] Hence in Pt-P the Fermi-Contact term represents the relation between the bond distance Pt-P and the first-order coupling constant *J* (Pt-P).

The electron withdrawing ability of ligand Cl-Ph-PNP, CH_3-Ph-PNP and F-Ph-PNP follows the following order CH_3-Ph-PNP << Cl-Ph-PNP < F-Ph-PNP because CH_3 has been reported to be having an inductive electron-withdrawing character and periodically F is more electronegative that Cl.[18] The effects of these differences on the *J*(Pt–P) coupling constants is summarized in **Table 4.2**.

[15] J.W. Akitt, B.E. Mann, *NMR and chemistry: introduction to modern NMR spectroscopy*, 4th Ed, Eastbourne: Stanley and Thornes Publishers, **2000**.

[16] P.J. Hore, *Nuclear Magnetic Resonance*, Oxford University Press, **1995**.

[17] M.Gielen, R. Willem, B. Wrackmeyer, *Physical Properties in Organometallic Chemistry*, Great Britain: John Wiley & Sons Publishers, **2002**.

[18] O. Nicolas, M. Marcos, M.A. Ricardo, *J. Phys. Chem. A*, **2007**, *111* (25), 5557.

Table 4.2: ^{31}P NMR *J*(Pt–P) data for CH_3-Ph-PNP, Cl-Ph-PNP and F-Ph-PNP ligands.

Compound	***J*(Pt–P) (Hz)**
CH_3-Ph-PNP	1665.6
Cl-Ph-PNP	1683.2
F-Ph-PNP	1684.5

From Table 4.2 it is clear that the *J*(Pt–P) increase as the ligand's electron withdrawing ability increases. These will later be correlated to the catalysts activity and selectivity in the Rh-PNP based 1-octene hydroformylation reaction in **Chapter 6**.

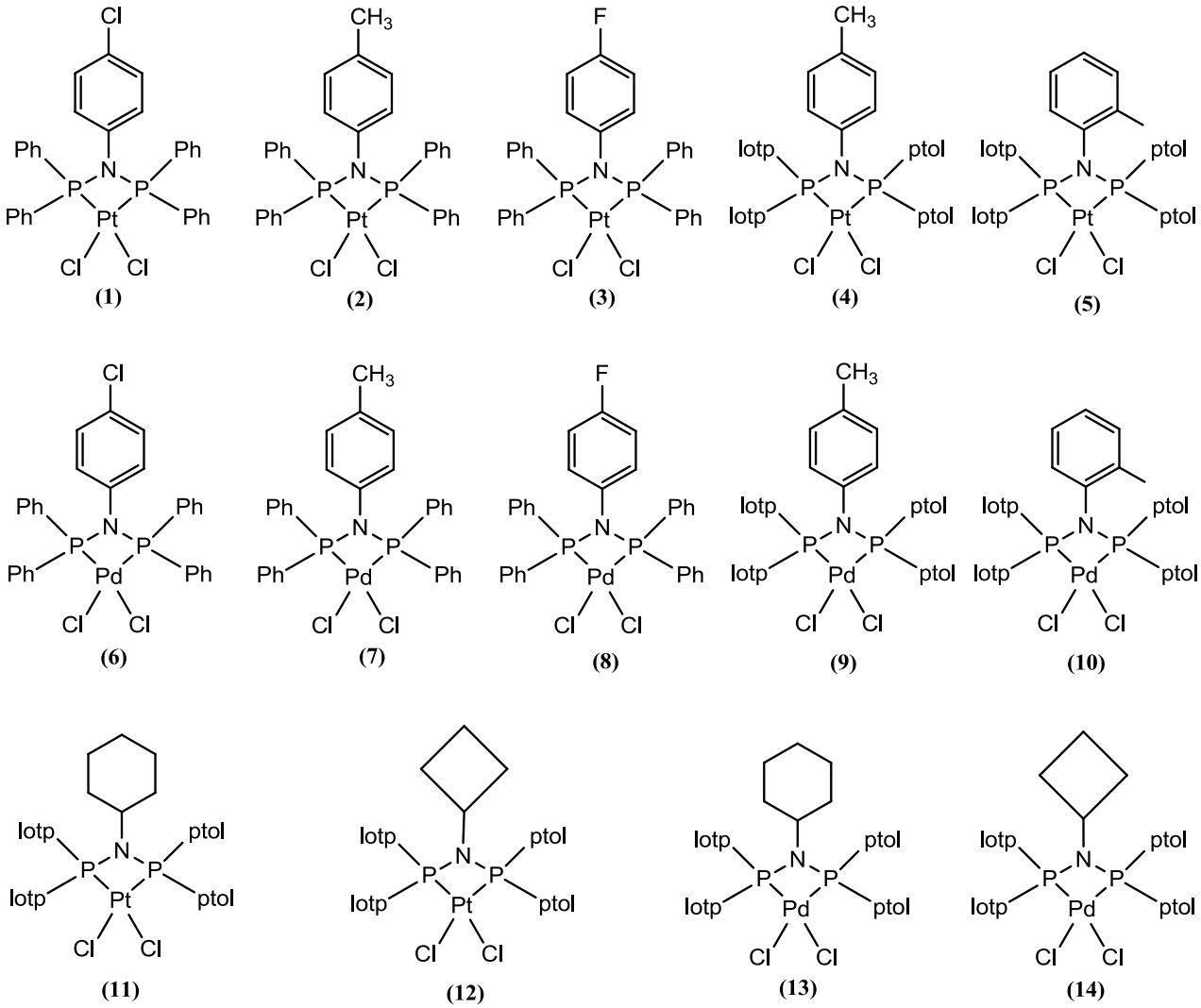

Figure 4.3: A schematic representation of all the synthesized metal-PNP ligand. **(1)** [Pt(Cl-Ph-PNP)Cl_2] **(2)** [Pt(CH_3-Ph-PNP)Cl_2] **(3)** [Pt(F-Ph-PNP)Cl_2] **(4)** [Pt(5-*p*-tolyl-PNP)Cl_2] **(5)** [Pt(4-*p*-tolyl-*o*-tol)Cl_2] **(6)** [Pd(Cl-Ph-PNP)Cl_2] **(7)** [Pd(CH_3-Ph-PNP)Cl_2] **(8)** [Pd(F-Ph-PNP)Cl_2] **(9)** [Pd(5-*p*-tolyl-PNP)Cl_2] **(10)** [Pt(4-*p*-tolyl-*o*-tol)Cl_2] **(11)** [Pt(Chzyl-4-*p*-tolyl)Cl_2] **(12)** [Pt(Cbutyl-4-*p*-tolyl)Cl_2] **(13)** [Pd(Chzyl-4-*p*-tolyl)Cl_2] **(14)** [Pd(Cbutyl-4-*p*-tolyl)Cl_2].

Table 4.3: ^{31}P NMR data for both the free PNP ligand and the metal (Pt(II) and Pd(II)) coordinated PNP metal complexes.

Compound	δ_P (ppm)	*J*(Pt–P) (Hz)
5-*p*tolyl-PNP	67.4	
4-*p*tolyl-*o*tol-PNP	59.9	
F-Ph-PNP[a]	70.6	
Cl-Ph-PNP[b]	69.9	
CH_3-Ph-PNP[c]	68.6	
Chzyl-4-*p*-tolyl-PNP	49.7	
Cbutyl-4-*p*-tolyl-PNP	48.1	
[Pt(5-*p*-tolyl-PNP)Cl_2]	19.7	1678.4
[Pt(4-*p*-tolyl-*o*-tol)Cl_2]	20.4	1693.6
[Pt(F-Ph-PNP)Cl_2]	20.3	1684.5
[Pt(Cl-Ph-PNP)Cl_2]	21.9	1683.2
[Pt(Chzyl-4-*p*-tolyl)Cl_2]	13.8	1650.0
[Pt(Cbutyl-4-*p*-tolyl)Cl_2]	13.5	1654.8
[Pt(CH_3-Ph-PNP)Cl_2]	20.8	1665.6
[Pd(5-*p*-tolyl-PNP)Cl_2]	34.3	
[Pd(4-*p*-tolyl-*o*-tol)Cl_2]	35.6	
[Pd(F-Ph-PNP)Cl_2]	36.6	
[Pd(Cl-Ph-PNP)Cl_2]	36.1	
[Pd(Chzyl-4-*p*-tolyl)Cl_2]	28.1	
[Pd(Cbutyl-4-*p*-tolyl)Cl_2]	27.5	
[Pd(CH_3-Ph-PNP)Cl_2]	34.8	

[a] Ref **11**, [b] Ref **12,** [c] ref **10** and **11** .

4.8 Conclusion

In this study, seven PNP ligands and fourteen metal complexes [M(PNP)Cl_2](M = Pt, Pd) were successfully synthesized. ^{31}P NMR data for both the free PNP ligand and the metal (Pt(II) and Pd(II)) coordinated ligand illustrated whether the ligand is coordinated or not. Out of these fourteen metal complexes, six complexes (three [Pt(PNP)Cl_2] and three [Pd(PNP)Cl_2]) formed single crystals suitable for X-ray diffraction studies were obtained and are discussed in detail in **Chapter 5**. In **Chapter 6** all synthesised ligands will be investigated as potential ligands in the rhodium based hydroformylation catalytic reaction of 1-octene.

5 Single crystal X-ray diffraction study of Pt(II) and Pd(II)-PNP complexes

Abstract

In this chapter the crystallographic data of selected [Pt(PNP)Cl_2] and [Pd(PNP)Cl_2] metal complexes are reviewed.

5.1 Introduction

A convenient way of refining the properties of a metal complex is to manipulate the characters of the coordinated ligands. Once this has been performed, parameters that do not only capture the electronic and the steric changes generated by such modifications but also the structural changes are required (*Note: In this study only phosphine ligands are reviewed*).[1] Parameters such as the Tolman cone angle (θ) and Tolman electronic parameter (υ) play a key role on understanding various ligand effects.[2] In this chapter X-ray diffraction is used to illustrate the structural effects and the *effective Tolman-based N-substituent steric effect* ($\theta_{\text{N-sub}}$) is used to illustrate the ligand steric effects.[2] The cone angle is obtained by constructing a three-dimensional cone shape between a metal and the three outermost atoms of the ligand as illustrated by **Figure 5.1** (discussed in detail in **Chapter 2**).[3] The e*ffective Tolman-based N-substituent steric effect* was calculated using a modified Tolman cone angle equation (**Equation 5.1**) using a cone shape constructed through the N atom (*instead of the metal centre*) on the PNP ligand and the R group on the N-atom.

$$\theta = \frac{2}{3}\sum_{i=1}^{3}\frac{\theta_i}{2} \qquad \textbf{Equation 5.1}$$

[1] N. Fey, A.G. Orpen, J.N. Harvey, *Coord Chem Rev*, **2009**, *253*, 704.
[2] N. Cloete, H.G. Visser, I. Engelbrecht, M.J. Overett, W. F. Gabrielli, A. Roodt, *Inorg. Chem*. **2013**, *52*, 2268.
[3] C.A. Tolman, *Chem. Rev*., **1977**, *77*, 313.

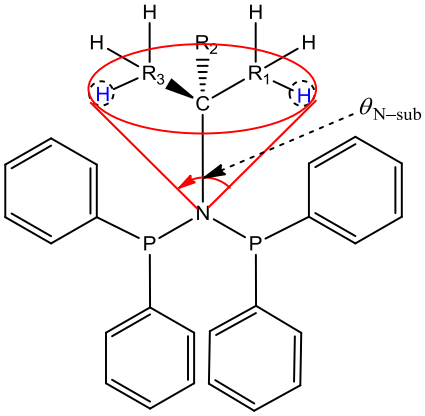

Figure 5.1: The Effective Tolman-Based N-substituent ($\theta_{N\text{-}sub}$) is a steric parameter

To understand the structural behavior of metal complexes due to ligand alterations the molecular forces involved within the molecule must be understood and evaluated.

Table 5.1: The general properties and classifications of three major types of H-bonds, X-H...A as described by Grabowski and Desiraju.[4,5] Only the comparative values are presented.

H-bonds parameters	**Strong**	**Moderate**	**Weak**
Interaction type	Strongly covalent	Mostly electrostatic	Electrostatic / dispersed
Examples	$[F\ldots H\ldots F]^+$	N-H…O=C	C-H….O
	$[N\ldots H\ldots N]^+$		N-H…F-C
			O-H…π
Bond energy (Kcal.mol^{-1})	15-40	4-15	<4
X-H *vs*. H…A	X-H ≈ H…A	X-H < H…A	X-H << H…A
Lengthening of X-H (Å)	0.08-0.25	0.02-0.08	≤0.02
X…A range (Å)	2.2-2.5	2.5-3.2	>3.2
H…A range (Å)	1.2-1.5	1.5-2.2	>2.2
X-H…A angles range (°)	170-180	>130	>90
Effect on crystal packing	Strong	Distinctive	Variable
Covalency	Pronounced	Weak	Vanishing
Electrostatic contribution	Significant	Dominant	Moderate
IR *vs*. relative shift (cm^{-1})	25%	10-25%	< 10%

[4] S.J. Grabowski, J. Leszcynski., *Hydrogen Bonding – New Insights*, Dordrecht : SpringerLink Publishers, **2006.**

[5] G.R. Desiraju, T. Steiner, *The Weak Hydrogen Bond: In Structural Chemistry and Biology*, Oxford Science Publications, **1999**.

Table **5.1** illustrates the properties and classifications of the three major hydrogen bonding responsible for the stabilization of a molecule.

A range of systematically altered phosphine ligands (PNP) were synthesized during this study (see **Figure 4.1** and **Figure 4.2**). One of the primary objectives of this research was to crystallize crystals suitable for single-crystal X-ray diffraction of all the metal (Platinum and Palladium)-ligand (PNP) complexes and all the ligands produced. Unfortunately due to time constraints and to some extend the complexity involved crystallization only a certain number of single crystals were obtained and evaluated.

Although hydroformylation of 1-octene is typically conducted using a rhodium-PNP complex as a catalyst; Pt(II) and Pd(II)-PNP complexes were synthesized to serve as models for the evaluation of the solid state characteristics of all PNP ligand synthesized. Because of the expensiveness of the rhodium precursors, rhodium-PNP complexes were only synthesized *in situ* during the catalytic evaluation. However, catalytic evaluations of both Pt(II) and Pd(II) complexes are reserved for the future plans of this study.

To evaluate the electronic effects induced by PNP ligands, three PNP ligands with different electronic properties on the nitrogen atom were synthesized (see **Figure 4.1**), and to study the steric effects induced four PNP ligands with different steric properties on both the N and the P atoms were synthesized (see **Figure 4.2**). To fully understand the behavior of a catalyst, one should thoroughly evaluate the coordination chemistry between the metal center and the involved ligands. This means determining the molecular structure of both the free ligand and the coordinated complex.

5.2 Crystallographic Data

In **Chapter 4**, the methods used to synthesize single crystals suitable for X-ray diffraction were reported. **Figure 5.2** shows all complexes that provided single crystals that were analyzed by an X-ray diffraction instrument, whereas **Table 5.3** and **5.4** provides a summary of the crystallographic data of these complexes. A number of similar complexes have been reported in literature and will be compared to those synthesized in this study.[6,7,8,9,10,11] Supplementary data

[6] F. Durap, N. Biricik, B. Gümgüm, S. Özkar, W.Han Ang, Z. Fei. R. Scopelliti, *Polyhedron*, **2008**, *27*, 196.

[7] D.M. Tooke, E.J. Zijp, J.I. van der Vlugt, D. Vogt, A. Spek, *Acta. Cryst*, **2007**, *E63*, m86.

[8] F. Fei, W. Han Ang, D. Zhao, R. Scopelliti, P.J. Dyson, *Inorg. Chim. Acta*, **2006**, *359*, 2635.

(**Appendix A**) provides all the crystallographic data in details i.e. bond distances, torsion angles and anisotropic displacement parameters.

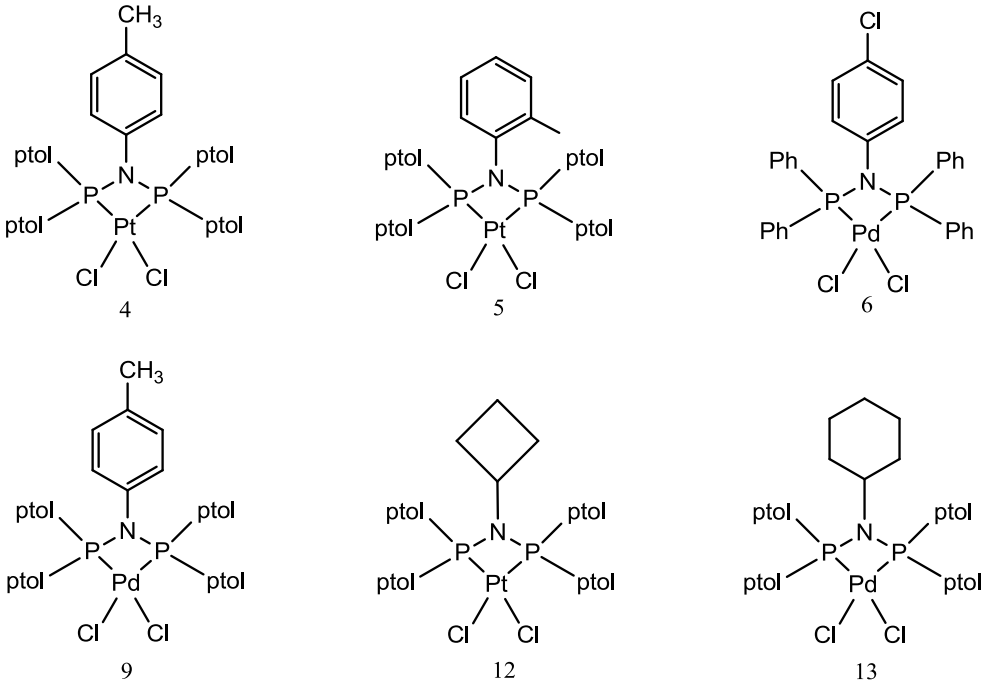

Figure 5.2: All complexes that provided single crystals that were analyzed by X-ray diffraction. Naming of these compounds is shown in **Table 5.2** below (Note: Numbering is related to the synthesized complexes as listed in Chapter 4 **Figure 4.3**).

Table 5.2: Abbreviations and definition of complexes shown in **Figure 5.2**.

No:	Abbreviations	Definition
4	[Pt(5-*p*-tolyl-PNP)Cl_2]	Dichloro-[*N*,*N*-Bis(di-*p*-tolylphosphino)-*p*-toluidine-κ^2P,P']platinum(II)
5	[Pt(4-*p*-tolyl-*o*-tol)Cl_2]	Dichloro-[*N*,*N*-Bis(di-*p*-tolylphosphino)-*o*-toluidine-κ^2P,P']platinum(II)
6	[Pd(Cl-Ph-PNP)Cl_2]	Dichloro-[*N*,*N*-Bis(diphenylphosphino)-4-chloroaniline-κ^2P,P']palladium(II)
9	[Pd(5-*p*-tolyl-PNP)Cl_2]	Dichloro-[*N*,*N*-Bis(diphenylphosphino)-*p*-toluidine-κ^2P,P']palladium(II)
12	[Pt(Cbutyl-4-*p*-tolyl)Cl_2]	Dichloro-[*N*,*N*-Bis(di-*p*-tolylphosphino)cyclobutylamine-κ^2P,P']platinum(II)
13	[Pd(Chzyl-4-*p*-tolyl)Cl_2]	Dichloro-[*N*,*N*-Bis(di-*p*-tolylphosphino)cyclohexylamine-κ^2P,P']palladium(II)

[9] G. Calabrò, D. Drommi, C. Graiff, F. Faraone, A. Tiripicchio, *Eur. J. Inorg, Chem*., **2004**, 1447.

[10] R.P.K. Babu, S.S. Krishnamurthy, M. Nethaji, *Tetrahedron*, **1995**, *6*, 427.

[11] C.S. Browning, D.H. Farrar, D.C. Frankel, *Acta Cryst*, **1992**, *C48*, 806.

Bruker X8 Apex II 4K Kappa CCD diffractometer fitted with a graphite monochromated Mo Kα radiation, with a ω and φ scans at wavelength (λ) of 0.71073 Å was used to collect the intensity data of all single crystals at 100K. Cell refinements were completed with SAINT-Plus[12] while SAINT-Plus and XPREP2 were used for data reduction. All the absorption corrections were obtained from the use of a multi-scan technique and the SADABS[13] software package. To solve and refine structures the following software packages SIR-97[14], SHELXL-97[15] and WinGX[16] were utilized. A DIAMOND[17] software package was used to draw all molecular diagrams. Unless stated otherwise, all the molecular structures were shown with thermal ellipsoid drawn at 50% probability level and all non-hydrogen atoms refined anisotropically. Methyl, methylene and methine atoms were placed in a geometrically idealized positions as well as all aromatic hydrogen atoms, C-H = 0.95 to 1.00 Å, and constrained to ride on their parent atoms, Uiso(H) = 1.5 Ueq(C) and 1.2 Ueq(C) respectively. For the numbering of the phenyl rings, the first digit refers to the ring number while the second digit refers to the carbon atom in the ring.

[12] Bruker, *SAINT-Plus*, Version 7.12 (including XPREP), Bruker AXS Inc., Madison, Wisconsin, USA, **2004**.

[13] Bruker, *SADABS*, Version 2004/1, Bruker AXS Inc., Madison, Wisconsin, USA, **1998**.

[14] A. Altomare, M.C. Burla, M. Camalli, G.L. Cascarano, C. Giacovazzo, A. Guagliardi, A.G.G. Moliterni, G. Polidori, R. Spagna, *J. Appl. Cryst*., **1999**, *32*, 837.

[15] Sheldrick, G.M., *SHELXL97, Program for the refinement of crystal structures*, University of Göttingen, Germany, **1997**.

[16] L.J. Farrugia, *J. Appl. Cryst*., **1999**, *32*, 837.

[17] K. Brandenburg, H. Putz, DIAMOND, Release 3.0c, Crystal Impact GbR, Bonn, Germany, **2006**.

Table 5.3: Crystallographic data of [Pd(Cl-Ph-PNP)Cl_2], [Pt(5-*p*-tolyl-PNP)Cl_2] and [Pd(5-*p*-tolyl-PNP)Cl_2].

Crystallographic data	**[Pd(Cl-Ph-PNP)Cl_2] (6)**	**[Pt(5-*p*-tolyl-PNP)Cl_2] (4)**	**[Pd(5-*p*-tolyl-PNP)Cl_2] (9)**
Empirical formula	$C_{61}H_{52}Cl_{16}N_2OP_4Pd_2$	$C_{35}H_{35}Cl_2NP_2Pt$	$C_{35}H_{35}Cl_2NP_2Pd$
Formula weight (g mol^{-1})	1378.42	797.57	708.88
Temperature (K)	100(2)	100(2)	100(2)
Crystal system	Monoclinic	Orthorhombic	Orthorhombic
Space group	$P2_1/c$	*Pbca*	*Pbca*
Unit cell dimensions			
a (Å)	9.990(2)	18.5299(9)	18.4310(9)
b (Å)	14.950(3)	14.8938(6)	14.8778(6)
c (Å)	20.307(4)	23.1057(12)	23.1047(11)
α (°)	90.00	90.00	90.00
β (°)	99.80(3)	90.00	90.00
γ (°)	90.00	90.00	90.00
Volume ($Å^3$)	2988.6(11)	6376.7(5)	6335.6(5)
Z	4	8	8
Density (g cm^{-3})	1.532	1.662	1.486
Crystal colour	Yellow	Colourless	Yellow
Crystal morphology	Cuboid	Cuboid	Cuboid
Crystal size (mm^3)	0.302 x 0.238 x 0.050	0.266 x 0.116 x 0.043	0.278 x 0.174 x 0.126
μ (mm^{-1})	1.019	4.695	0.881
F(000)	1388	3152	2896
θ range (°)	1.700-25.998	2.935-25.535	2.745-28.000
	$-12 \le h \le 12$	$-22 \le h \le 21$	$-24 \le h \le 24$
Index ranges	$-18 \le k \le 18$	$-17 \le k \le 16$	$-19 \le k \le 19$
	$-25 \le l \le 25$	$-28 \le l \le 27$	$-30 \le l \le 30$
Reflections collected	46799	145933	135854
Unique reflections	5865	5650	7651
Reflections with $I > 2\sigma(I)$	4265	4318	6258
R_{int}	0.1371	0.0923	0.0769
Completeness to theta (°, %)	100.0	98.3	99.8
Data / restraints / parameters	5865 / 13 / 354	5650 / 0 / 375	7651 / 0 / 375
Goodness-of-fit on F2	1.075	1.036	1.059
R [$I > 2\sigma(I)$]	$R_1 = 0.0705$	$R_1 = 0.0271$	$R_1 = 0.0290$
	$wR_2 = 0.1556$	$wR_2 = 0.0416$	$wR_2 = 0.0613$
R (all data)	$R_1 = 0.1010$	$R_1 = 0.0495$	$R_1 = 0.0409$
	$wR_2 = 0.1719$	$wR_2 = 0.0472$	$wR_2 = 0.0680$
ρmax, ρmin ($e.Å^{-3}$)	1.373, -1.508	0.836, -1.422	0.458, -0.484

[Pd(Cl-Ph-PNP)Cl_2] **(6)** = Dichloro-[*N*,*N*-Bis(diphenylphosphino)-4-chloroaniline-$\kappa^2 P,P'$]palladium(II).

[Pt(5-*p*-tolyl-PNP)Cl_2] **(4)** = Dichloro -[*N*,*N*-Bis(di-*p*-tolylphosphino)-*p*-toluidine-$\kappa^2 P,P'$]platinum(II).

[Pd(5-*p*-tolyl-PNP)Cl_2] **(9)** = Dichloro-[*N*,*N*-Bis(diphenylphosphino)-*p*-toluidine-$\kappa^2 P,P'$]palladium(II).

Table 5.4; Crystallographic data of [Pt(4-*p*-tolyl-*o*-tol)Cl_2], [Pt(Cbutyl-4-*p*-tolyl)Cl_2] and [Pd(Chzyl-4-*p*-tolyl)Cl_2].

Crystallographic data	**[Pt(4-*p*-tolyl-*o*-tol)Cl_2] (5)**	**[Pt(Cbutyl-4-*p*-tolyl)Cl_2] (12)**	**[Pd(Chzyl-4-*p*-tolyl)Cl_2] (13)**
Empirical formula	$C_{35}H_{35}Cl_2NP_2Pt$	$C_{32}H_{35}Cl_2NP_2Pt$	$C_{34}H_{42}Cl_2NOP_2Pd$
Formula weight (g mol^{-1})	797.57	761.54	719.92
Temperature (K)	100(2)	100(2)	100(2)
Crystal system	Monoclinic	Monoclinic	Monoclinic
Space group	$P2_1/c$	$P2_1/c$	$P2_1/c$
Unit cell dimensions			
a (Å)	10.3035(9)	12.6144(6)	9.7949(35)
b (Å)	20.5508(16)	14.0308(5)	16.9268(54)
c (Å)	15.398(5)	17.9954(7)	21.2270(79)
α (°)	90.000	90.000	90.000
β (°)	100.476(3)	104.843(14)	99.321(12)
γ (°)	90.000	90.000	90.000
Volume ($Å^3$)	3206.0(11)	3078(18)	3473(2)
Z	4	4	4
Density (g cm^{-3})	1.652	1.643	1.377
Crystal colour	Colourless	Colourless	Yellow
Crystal morphology	Plate	Cuboid	Cuboid
Crystal size (mm^3)	0.078 x 0.255 x 0.499	0.121 x 0.207 x 0.336	0.179 x 0.529 x 0.559
μ (mm^{-1})	4.669	4.857	0.807
F(000)	1576	1504	1484
θ range (°)	1.982-27.999	2.895-28.00	2.738-27.998
	$-13 \leq h \leq 13$	$-16 \leq h \leq 16$	$-12 \leq h \leq 12$
Index ranges	$-27 \leq k \leq 27$	$-18 \leq k \leq 18$	$-22 \leq k \leq 22$
	$-20 \leq l \leq 20$	$-25 \leq l \leq 25$	$-28 \leq l \leq 28$
Reflections collected	66551	69023	69100
Unique reflections	7735	7431	8367
Reflections with $I > 2\sigma(I)$	5448	6380	7363
R_{int}	0.1003	0.0601	0.0467
Completeness to theta (°, %)	99.8	99.8	99.8
Data / restraints / parameters	7735 / 0 / 375	7431 / 0 / 347	8367 / 0 / 386
Goodness-of-fit on F2	1.038	1.028	1.090
R [$I > 2\sigma(I)$]	$R_1 = 0.0371$	$R_1 = 0.0267$	$R_1 = 0.0375$
R (all data)	$wR_2 = 0.0711$	$wR_2 = 0.0648$	$wR_2 = 0.0968$
	$R_1 = 0.0664$	$R_1 = 0.0348$	$R_1 = 0.0441$
	$wR_2 = 0.0827$	$wR_2 = 0.0694$	wR_2 0.0968
ρmax, ρmin (e.$Å^{-3}$)	1.143, -1.144	1.734, -1.403	1.675, -0.724

[Pt(4-*p*-tolyl-*o*-tol)Cl_2] **(4)** = Dichloro-[*N*,*N*-Bis(di-*p*-tolylphosphino)-*o*-toluidine-$\kappa^2 P,P'$]platinum(II).

[Pt(Cbutyl-4-*p*-tolyl)Cl_2] **(12)** = Dichloro-[*N*,*N*-Bis(di-*p*-tolylphosphino)cyclobutylamine-$\kappa^2 P,P'$]platinum(II).

[Pd(Chzyl-4-*p*-tolyl)Cl_2] **(13)** = Dichloro-[*N*,*N*-Bis(di-*p*-tolylphosphino)cyclohexylamine-$\kappa^2 P,P'$]palladium(II).

5.3 Dichloro-[*N*,*N*-bis(diphenylphosphino)-4-chloroaniline-κ^2*P*,*P'*]palladium(II)

The synthesis of the title compound [Pd(Cl-Ph-PNP)Cl_2], (see **Figure 5.5**) resulted in light yellow crystals suitable for X-ray data analysis [**Chapter 4.6.4]**. The complex crystallizes in a monoclinic crystal system in the $P2_1/c$ space group with four molecules in a unit cell (Z = 4). The asymmetric unit contains one independent molecule and a methanol moiety (MeOH). **Figure 5.5** also shows the numbering system on the title complex. The *Effective Tolman-based N-substituent steric effect* ($\theta_{N\text{-}sub}$) was calculated using **Equation 5.1** and found to be 36.7°.

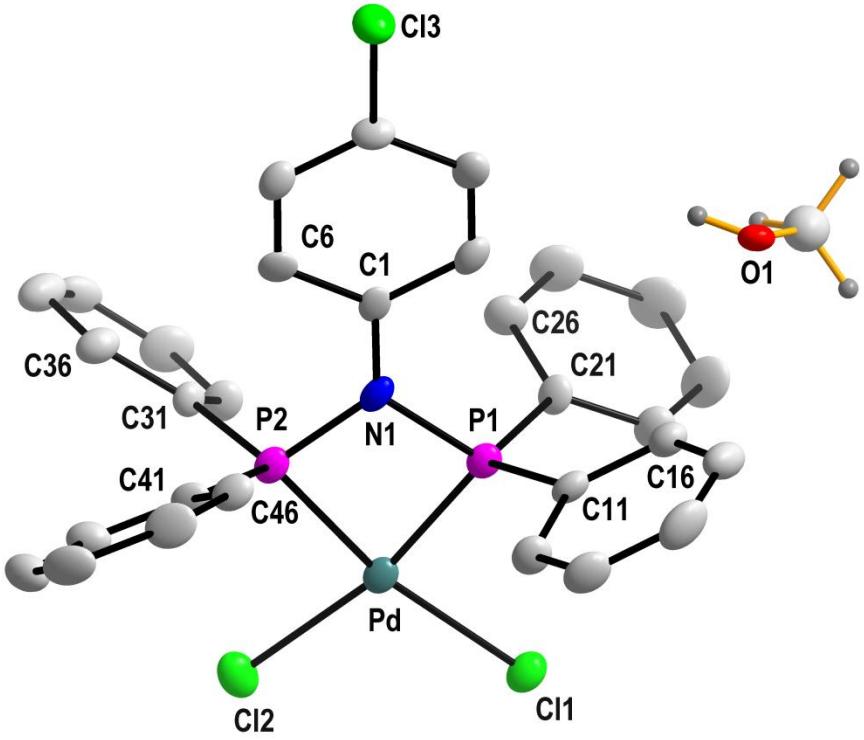

Figure 5.5: Molecular representation of [Pd(Cl-Ph-PNP)Cl_2] metal complex, hydrogen atoms and numbering for certain carbon atoms were omitted for clarity. For aromatic rings, the first digit represents the ring number and the second digit represents the specific C-atom in the ring. All displacement ellipsoid were drawn at 50% probability level.

Table 5.5*:* Important bond lengths and bond angles for the crystal structure of [Pd(Cl-Ph-PNP)Cl_2] (Å and °)

Atoms	**Bond length (Å)**	**Atoms**	**Bond angle (°)**
Pd – P1	2.149(2)	P1 – Pd – P2	81.30(8)
Pd – P2	2.179(2)	P1 – N1 – P2	107.5(3)
Pd – Cl1	2.409(2)	C1 – N1 – P1	126.8(5)
Pd – Cl2	2.385(2)	C1 – N1 – P2	125.7(5)
N1 – C1	1.329(9)	N1 – P1 – C11	112.1(3)
N1 – P1	1.752(6)	N1 – P1 – C21	112.6(3)
N1 – P2	1.743(6)	N1 – P2 – C31	112.9(3)
P1 – C11	1.844(7)	N1 – P2 – C41	113.4(3)
P1 – C21	1.829(7)	C11 – P1 – C21	108.2(3)
P2 – C31	1.842(7)	C31 – P2 – C41	107.7(3)
P2 – C41	1.849(7)	CL1 – Pd – CL2	106.0(8)

Some of the important bond lengths and angles are reported in **Table 5.5**. The Pd-Cl1 and Pd-Cl2 bond lengths are 2.409(2) and 2.385(2) Å respectively and are in agreement with the reported Pd-Cl bond lengths of these types of metal complexes.[18,19] The P1-Pd-P2 and Cl1-Pd-Cl2 angles are 81.30(8) and 106.0(8) ° respectively indicating the highly distorted square planar geometry of the metal complex around the Pd atom, while the P1-N1-P2 bite angle is 107.5(3) ° indicating a small contraction from the ideal 109.4 ° angle expected for a tetrahedral geometry around the N atom.[20,21,22] The N atom is positioned along the Pd/P1/P2 plane, while the *p*-chlorophenyl substituent on the N atom is twisted at an angle of 5.934 ° with respect to the Pd/P1/P2 plane to accommodate the steric bulk properties of the entire metal complex, thus stabilizing the molecule (see **Figure 5.6**).

[18] H.T. Al-Masri, *Z. Anorg. Allg. Chem,* **2012**, *638* (6), 1012.

[19] M. Aydemir, A. Baysal, F. Durap, B. Gumgum, S. Ozkar, L.T. Yildirim, *Appl. Organometal. Chem,* **2009**, *23*, 467.

[20] J.C. Kotz, P.M. Treichel, J.R. Townsed, *Chemistry and Chemical reactivity*, Canada: Thomson Brooks/Cole Publishers, **2009**.

[21] F.A. Carey, R.J. Sundberg, *Advanced Organic Chemistry* 5th Ed., New York: Springer Science + Business media, **2007**.

[22] C.E. Housecroft, A.G. Sharpe, *Inorgani Chemistry* 2nd Ed., Gosport: Pearson Prentice Hall Publishers, **2005**.

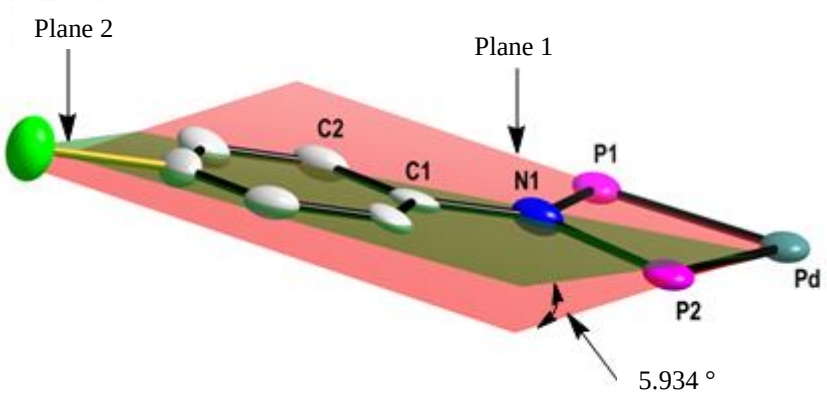

Figure 5.6: Graphical representation of the N atom adaptation technique in ligand steric bulk influence. Plane 1 and plane 2 are constructed through atoms Pd/P1/P2 and C1/C2/C3/C4/C5/C6 respectively.

Figure 5.7 illustrates the space taken by the *p*-chlorophenyl group using a space-filling model.[17] The hydrogen and carbon atoms are displayed as dark grey and grey colors respectively, while the chlorine atom is presented as a green colored sphere. A red stick-wire model is used for the remaining parts of the molecule for clarity.

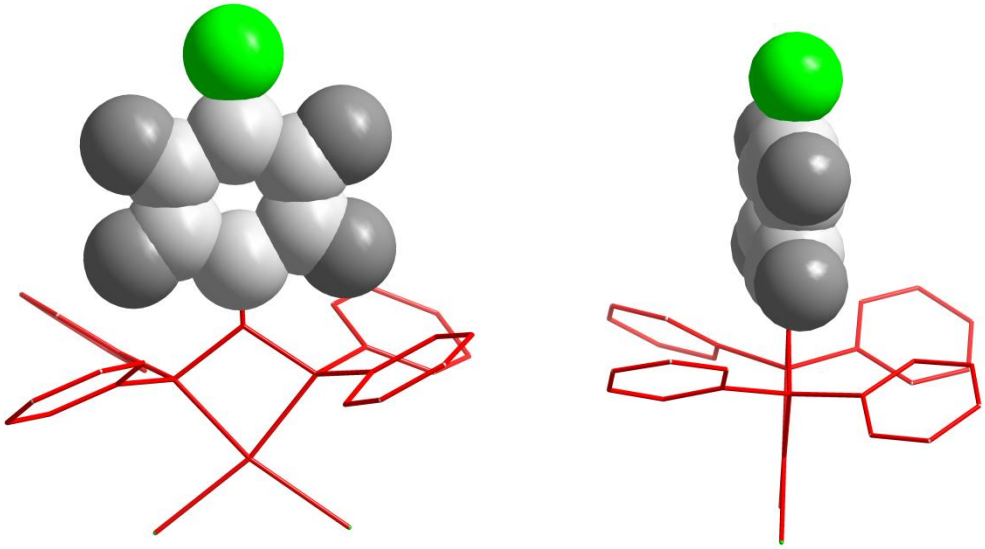

Figure 5.7: Graphical representation of the complex [Pd(Cl-Ph-PNP)Cl_2]. A stick-wire and space-filling models are used for the P-phenyl rings and the R-N group respectively.

The crystal structure is stabilized by five classical intermolecular hydrogen bonding, one intramolecular hydrogen bonding and three C-H…π interactions as indicated by the bond distances and bond angles in **Table 5.7** and **5.8**. Intermolecular and intramolecular hydrogen

bond interactions contributing to the molecular packing of this metal complex are illustrated in **Figure 5.8** and **5.9**.

Table 5.7: Intra and Intermolecular hydrogen bonding for **[**Pd(Cl-Ph-PNP)Cl_2**]**

D-H…A	d(D-H) (Å)	d(H…A) (Å)	d(D…A) (Å)	< (DHA)
C(16)-H(6) … O(1)#1	0.95	2.37	3.269(12)	157
C(24)-H(10) … Cl(2)#2	0.95	2.82	3.763(8)	176
C(3)-H(15) … Cl(2)#3	0.95	2.83	3.561(8)	135
C(36)-H(24) … Cl(1)#4	0.95	2.80	3.530(8)	134
O(1)-H(1) … Cl(2)#3	0.95	2.37	3.269(12)	157
C(61)-H(31C) … Cl(1)#3	0.95	2.82	3.763(8)	176

Symmetry transformation used to generate equivalent to atoms: **#1** x, y, z **#2** –x + 1, +y + 0.5, -z+0.5 **#3** x, -y +1.5, z+0.5 **#4** x-1, y, z.

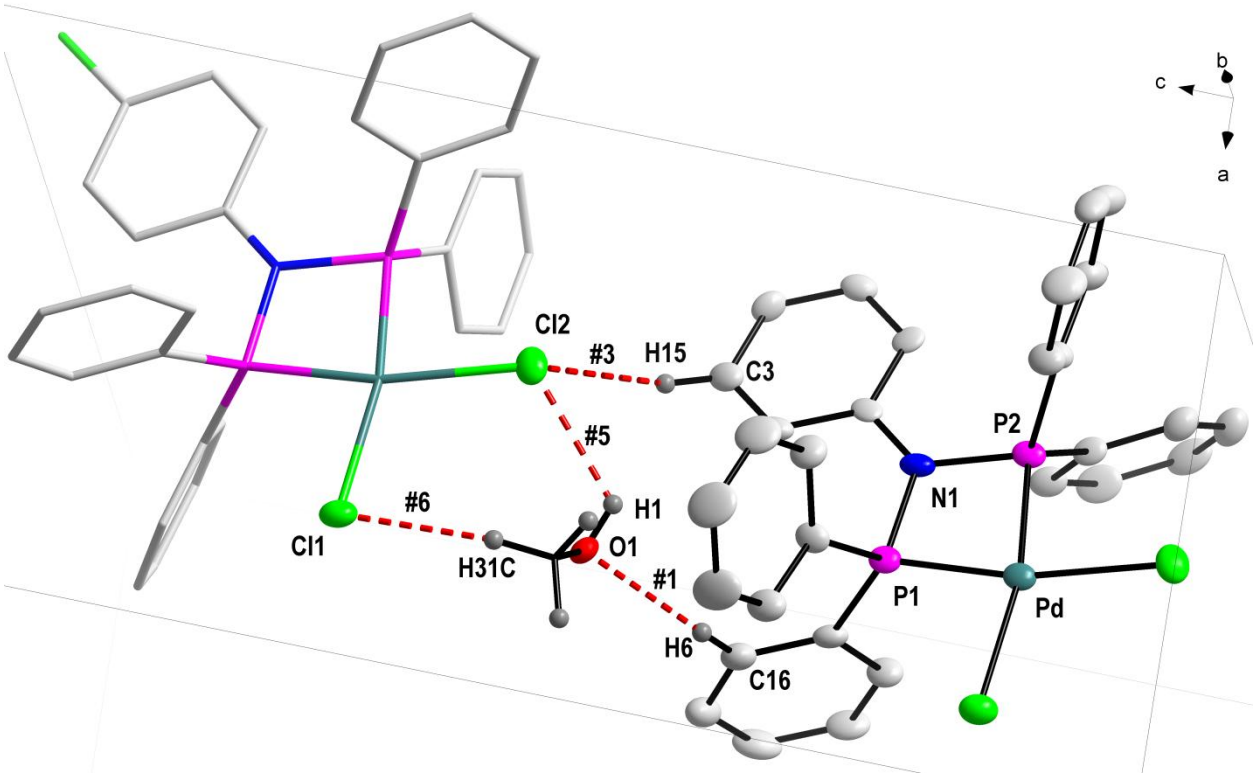

Figure 5.8: Graphical representation of the intra and the intermolecular hydrogen bonding (indicated by the red dash bonds) observed for [Pd(Cl-Ph-PNP)Cl_2].

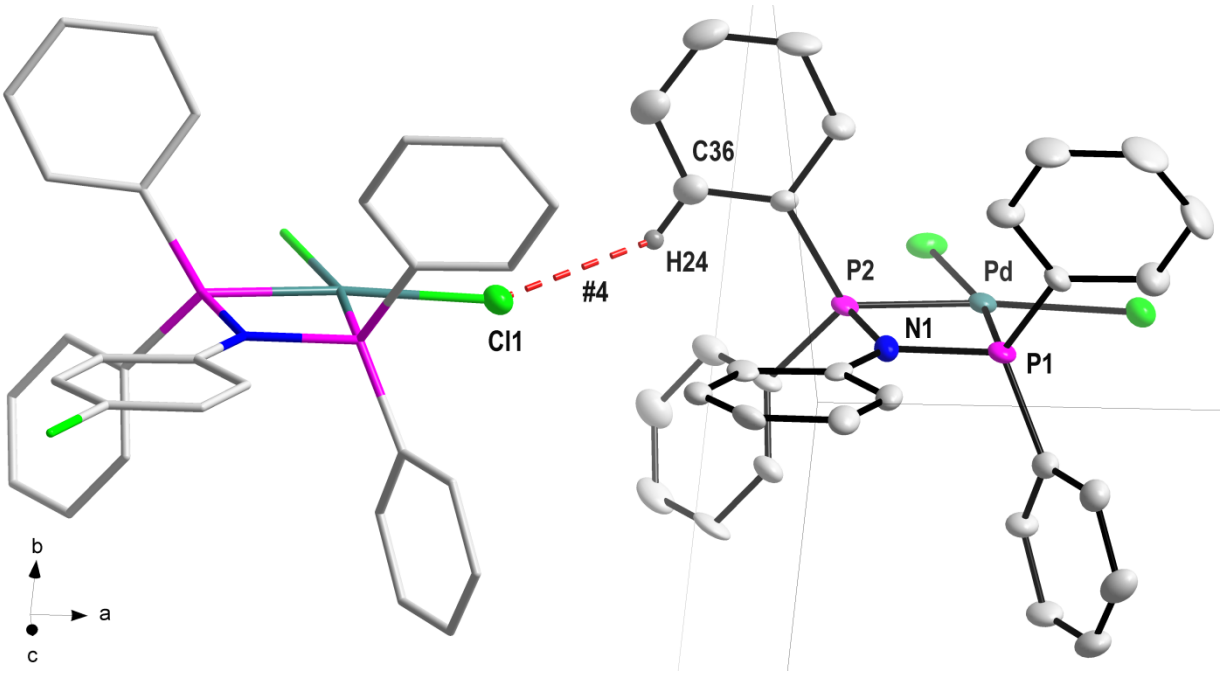

Figure 5.9: Graphical representation of some of the intermolecular hydrogen bonding (indicated by the red dash bonds) observed for [Pd(Cl-Ph-PNP)Cl_2].

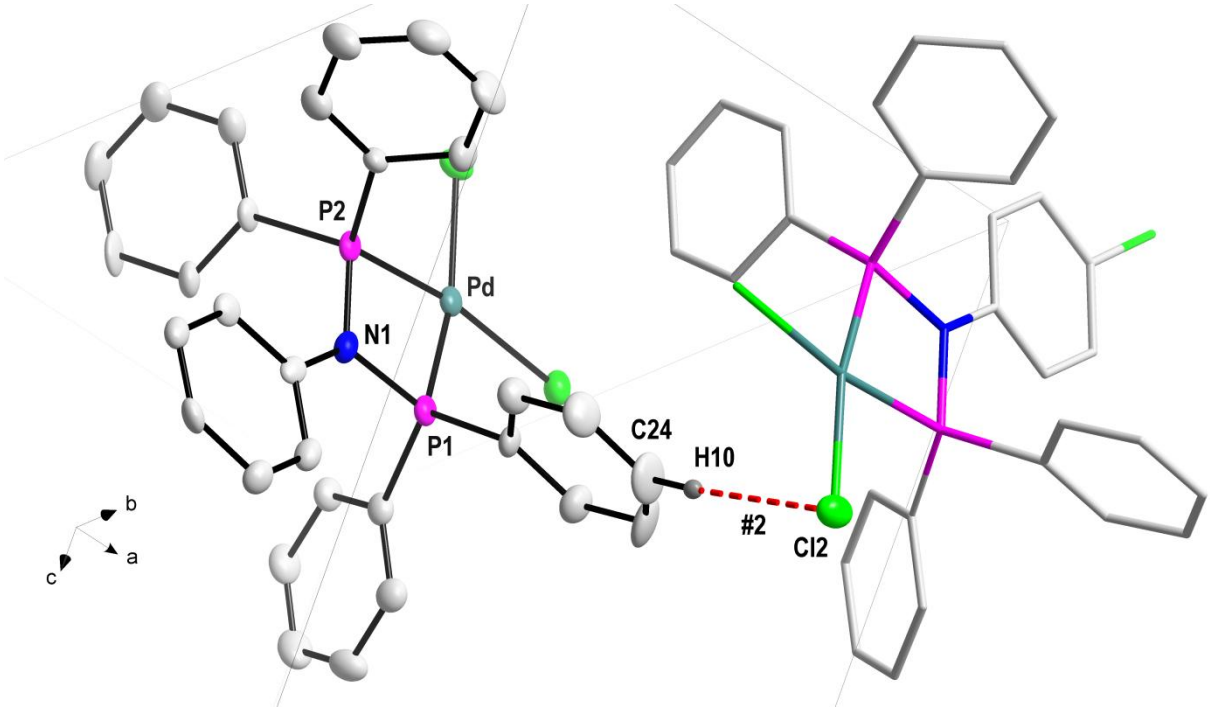

Figure 5.9: Graphical representation of some of the intermolecular hydrogen bonding (indicated by the red dash bonds) observed for [Pd(Cl-Ph-PNP)Cl_2].

The crystal structure is further stabilized by a C-H….Cg (π-ring) interactions as illustrated in **Figure 5.10** and **Table 5.8**. A very weak C-Cl…Cg interaction between C(4)-Cl(3)…Cg(5) where Cg(5) equals to the centroid atom of C31, C32, C33, C34, C35, C36 exists with a weak C…Cg interaction of 4.706(7) Å and will not be shown graphically.

Table 5.8: Representations of C-H...Cg(π-ring) interactions for **[**Pd(Cl-Ph-PNP)Cl_2**]**

C-H…Cg	d(H…Cg) (Å)	d(C…Cg) (Å)	<(C-H…Cg) (Å)
C(12)-H(2)…Cg(1)#1	2.95	3.300(7)	104
C(34)-H(22)…Cg(2)#5	2.85	3.576(8)	134
C(61)-H(31A)…Cg(4)#1	2.72	3.407(18)	128

Symmetry transformation used to generate equivalent to atoms: **#1** x, y, z **#5** -x, y + 0.5, -z + 0.5; Cg1 = centroid atoms of Pd, P1, N1, P2; Cg2 = centroid atom of C1, C2, C3, C4, C5, C6; Cg4 = centroid atom of C21, C22, C23, C24, C26, C26.

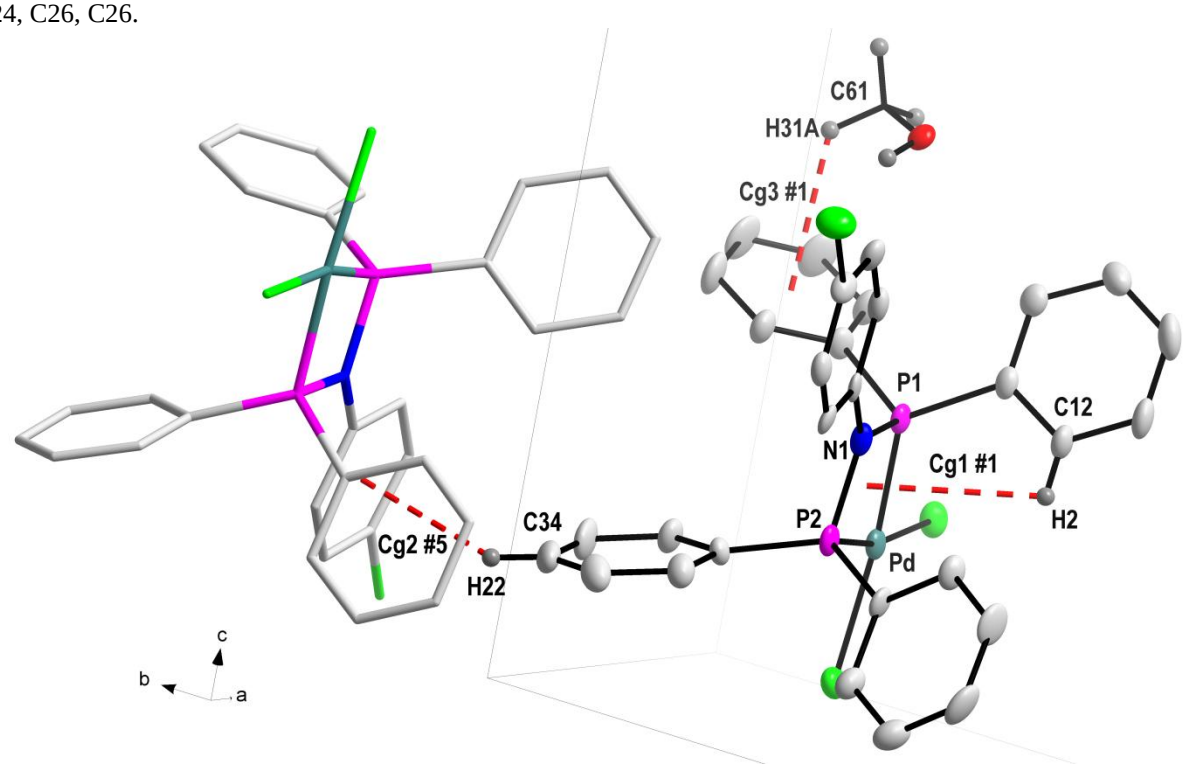

Figure 5.10: Graphical representation of the C-H...Cg interactions (indicated by the red dash bonds) observed for [Pd(Cl-Ph-PNP)Cl_2]. Only the H atoms relevant for the interactions are drawn in an ellipsoid model.

The molecules pack in a head to tail formation along the *c*-axis as shown in **Figure 5.11.**

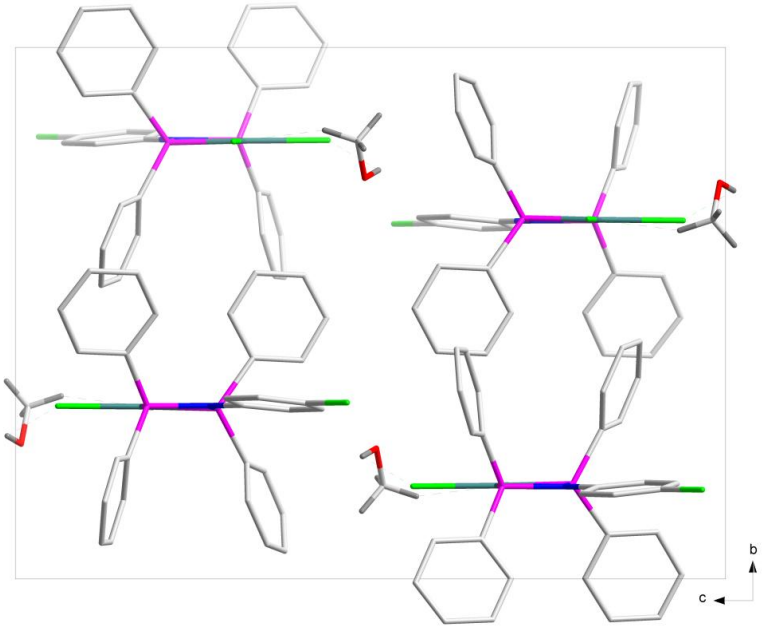

Figure 5.11: Graphical representation of the [Pd(Cl-Ph-PNP)Cl_2] molecular packing. For clarity, all the H atoms are omitted.

5.4 Dichloro-[*N*,*N*-bis(di-*p*-tolylphosphino)-*p*-toluidine-κ^2*P*,*P'*]platinum(II)

The synthesis of the title compound [Pt(5-*p*-tolyl-PNP)Cl_2], (see **Figure 5.12**) gave colourless crystals suitable for X-ray data analysis [**Chapter 4.5.1**]. The complex crystallizes in an orthorhombic crystal system in the *Pbca* space group with eight molecules in the unit cell (Z = 8). The asymmetric unit contains one independent molecule. **Figure 5.12** shows the molecular structure and the numbering system on the title complex. The *Effective Tolman-based N-substituent steric effect* ($\theta_{N\text{-}sub}$) was calculated using **Equation 5.1** and found to be 33.7 °.

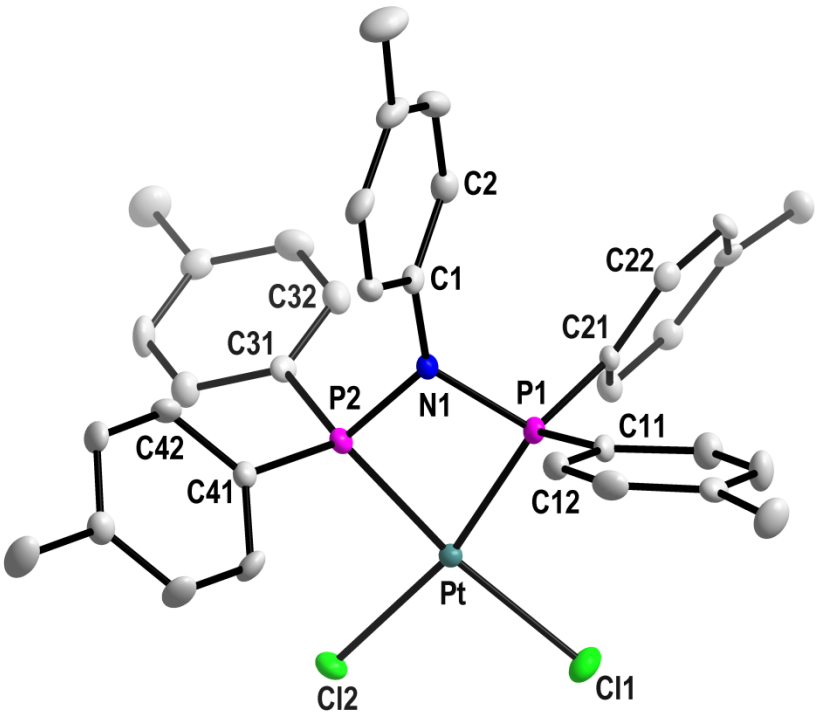

Figure 5.12: Molecular representation of [Pt(5-*p*-tolyl-PNP)Cl_2] metal complex, hydrogen atoms and numbering for certain carbon atoms were omitted for clarity. For aromatic rings, the first digit represents the ring number and the second digit represents the specific C-atom in the ring. All displacement ellipsoid were drawn at 50% probability level.

Table 5.9: Important bond lengths and bond angles for the crystal structure of [Pt(5-*p*-tolyl-PNP)Cl_2] (Å and °)

Atoms	Bond length (Å)	Atoms	Bond angle (°)
Pt – P1	2.215(1)	P1 – Pt – P2	72.95(4)
Pt – P2	2.195(1)	P1 – N1 – P2	100.2(2)
Pt – Cl1	2.361(9)	C1 – N1 – P1	130.1(2)
Pt – Cl2	2.355(9)	C1 – N1 – P2	129.6(2)
N1 – C1	1.441(5)	N1 – P1 – C11	108.5(2)
N1 – P1	1.714(3)	N1 – P1 – C21	110.1(2)
N1 – P2	1.704(3)	N1 – P2 – C31	107.5(2)
P1 – C11	1.793(4)	N1 – P2 – C41	110.7(2)
P1 – C21	1.797(4)	C11 – P1 – C21	107.6(2)
P2 – C31	1.802(4)	C31 – P2 – C41	107.1(2)
P2 – C41	1.791(4)	Cl1 – Pt – Cl2	93.64(3)

Some of the important bond lengths and angles are reported in **Table 5.9**. The Pt-Cl1 and Pt-Cl2 bond lengths are 2.361(9) and 2.355(9) Å respectively and are in agreement with the reported Pt-Cl bond lengths of these types of metal complexes.[18,19,23,24] The P1-Pt-P2 and Cl1-Pt-Cl2 angles are 72.95(4) and 93.64(3) ° respectively indicating the highly distorted square planar geometry of the metal complex around the Pt atom, while the P1-N1-P2 bite angle is 100.2(2) ° indicating a significant contraction from the ideal 109.4 ° angle expected for a tetrahedral geometry around the N atom.[20,21,22] The N atom is positioned along the Pd/P1/P2 plane adopting an almost planar geometry with these atoms, while the *p*-tolyl substituent on the N atom is twisted at an angle of 70.77 ° with respect to the Pd/P1/P2 plane to accommodate the steric bulk properties of the entire metal complex, thus stabilizing the molecule (see **Figure 5.13**).

[23] N. Cloete, H.G. Visser, A. Roodt, *Acta Cryst*, **2010**, *E66*, m51.

[24] V. Callo, P. Mastrorilli, C.F. Nobile, P. Braunstein, U. Englert, *Dalton Trans*, **2006**, 2342.

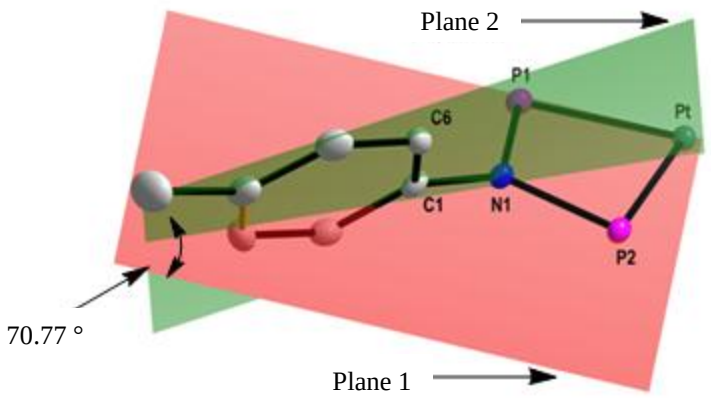

Figure 5.13: Graphical representation of the N atom adaptation technique in ligand steric bulk influence. Plane 1 and plane 2 are constructed through atoms Pt/P1/P2 and C1/C2/C3/C4/C5/C6 respectively.

Figure 5.14 illustrates the space taken by the *p*-tolyl group using a space-filling model.[17] The hydrogen and carbon atoms are displayed as dark grey and grey colors respectively. A red stick-wire model is used for the remaining parts of the molecule for clarity.

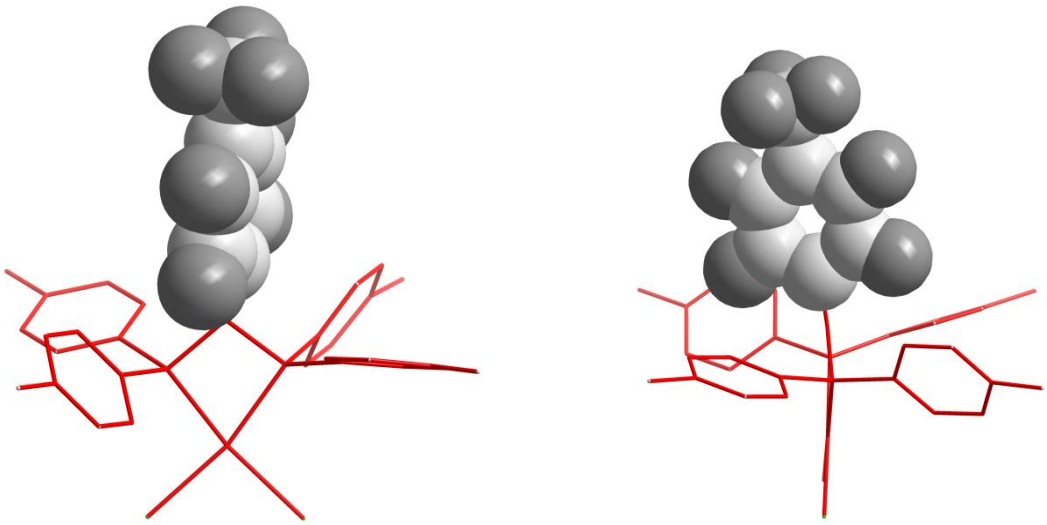

Figure 5.14: Graphical representation of the P-phenyl rings and the R-N group adaptation technique to ligand steric bulk influence on the complex [Pt(5-*p*-tolyl-PNP)Cl_2]. A stick-wire and space-filling model are used for the P-phenyl rings and the R-N group respectively.

No intramolecular hydrogen bonding is observed however the crystal structure is stabilized by one intermolecular hydrogen bonding and five C-H…π interactions as indicated by the bond distances and bond angles in **Table 5.11** and **5.12** respectively. Intermolecular hydrogen bond

interaction contributing to the molecular packing of this metal complex is illustrated in **Figure 5.15**.

Table 5.11: Intermolecular hydrogen bonding for **[**Pt(5-*p*-tolyl-PNP)Cl_2**]**

D-H…A	d(D-H) (Å)	d(H…A) (Å)	d(D…A) (Å)	< (DHA)
C(17)-H(14A) … Cl(2)#1	0.98	2.81	3.762(4)	165

Symmetry transformation used to generate equivalent to atoms: **#1** -x, y + 0.5, -z + 0.5

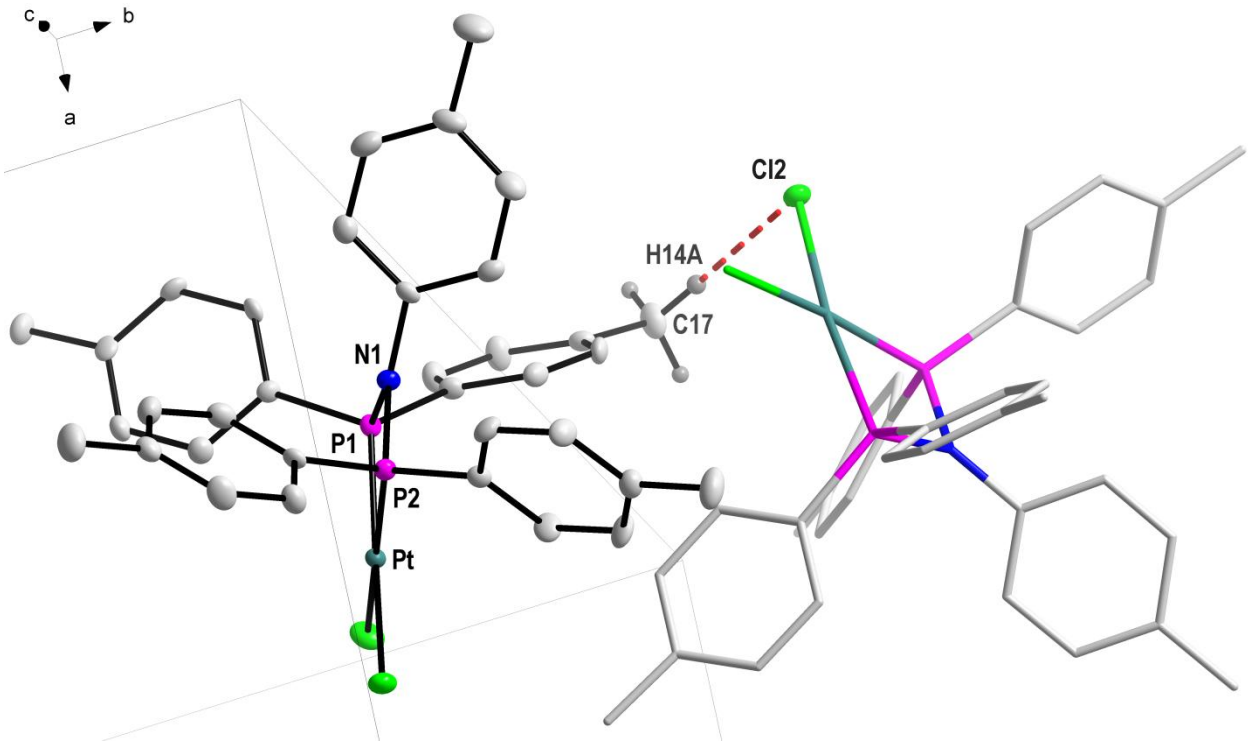

Figure 5.15: Graphical representation of the intermolecular hydrogen bonding (indicated by the red dash bonds) observed for [Pt(5-*p*-tolyl-PNP)Cl_2].

The crystal structure is further stabilized by a C-H….Cg (π-ring) interactions illustrated in **Figure 5.16**, **5.17** and **5.18** with **Table 5.12** showing the respective values.

Table 5.12: Representations of C-H...Cg(pi-ring) interactions for **[**Pt(5-*p*-tolyl-PNP)Cl_2**]**

C-H…Cg	d(H…Cg) (Å)	d(C…Cg) (Å)	<(C-H…Cg) (Å)
C(27)-H(7A)…Cg(2)#2	2.57	3.398(4)	142
C(27)-H(7C)…Cg(3)#2	2.94	3.588(4)	124
C(45)-H(24)…Cg(4)#3	2.99	3.665(4)	129
C(43)-H(26)…Cg(2)#4	2.82	3.409(4)	121
C(32)-H(34)…Cg(1)#5	2.95	3.250(4)	100

Symmetry transformation used to generate equivalent to atoms: **#2** -0.5 - x, -0.5 + y, z **#3** -x, 0.5+y, 0.5-z **#4** -x, 2 - y , 1 – z, **#5** x, y, z. Cg1 = centroid atoms of Pt, P1, N1, P2; Cg2 = centroid atom of C1, C2, C3, C4, C5, C6; Cg3 = centroid atom of C11 C12 C13 C14 C15 C16; Cg4 = centroid atom of C21, C22, C23, C24, C26, C26.

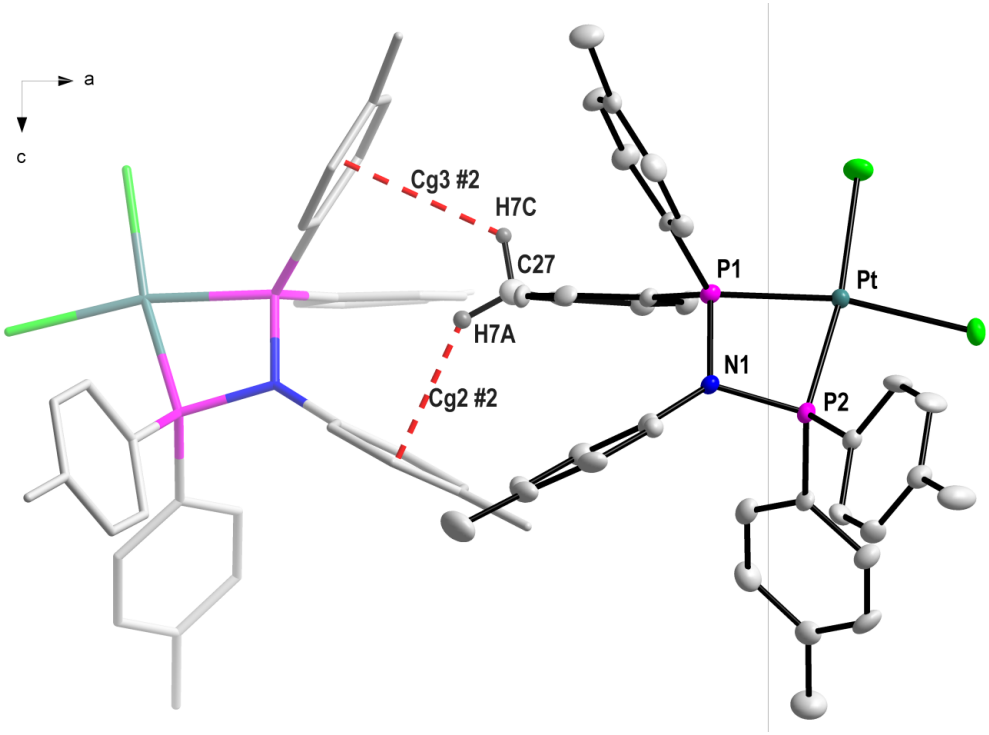

Figure 5.16 Graphical representation of some of the all the C-H...Cg interactions (indicated by the red dash bonds) observed for [Pt(5-*p*-tolyl-PNP)Cl_2].

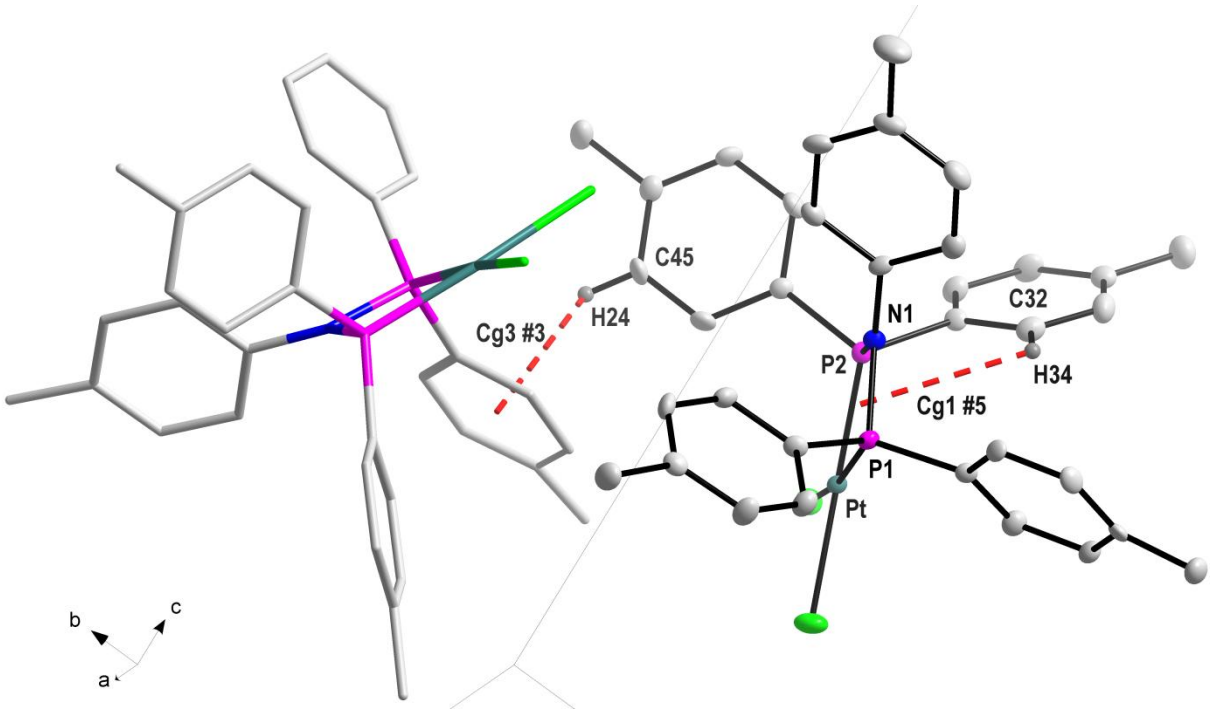

Figure 5.17 Graphical representation of some of the all the C-H...Cg interactions (indicated by the red dash bonds) observed for [Pt(5-*p*-tolyl-PNP)Cl_2].

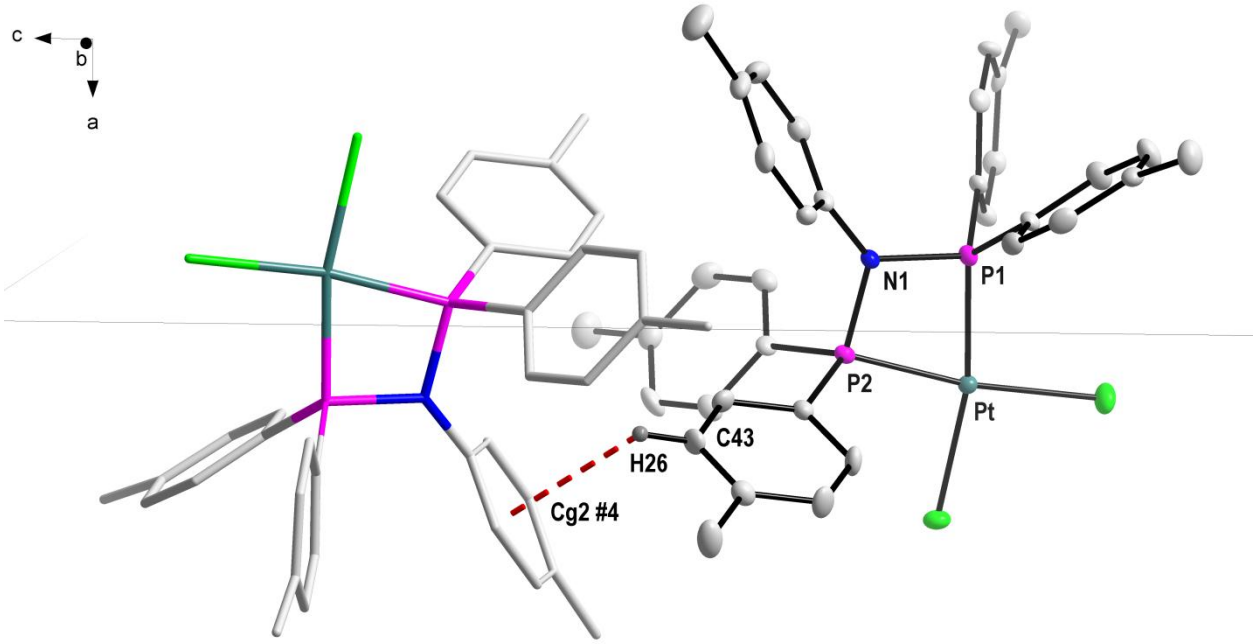

Figure 5.18 Graphical representation of some of the all the C-H...Cg interactions (indicated by the red dash bonds) observed for [Pt(5-*p*-tolyl-PNP)Cl_2].

The molecules pack in a tail to tail formation along the *a*-axis as shown in **Figure 5.19.**

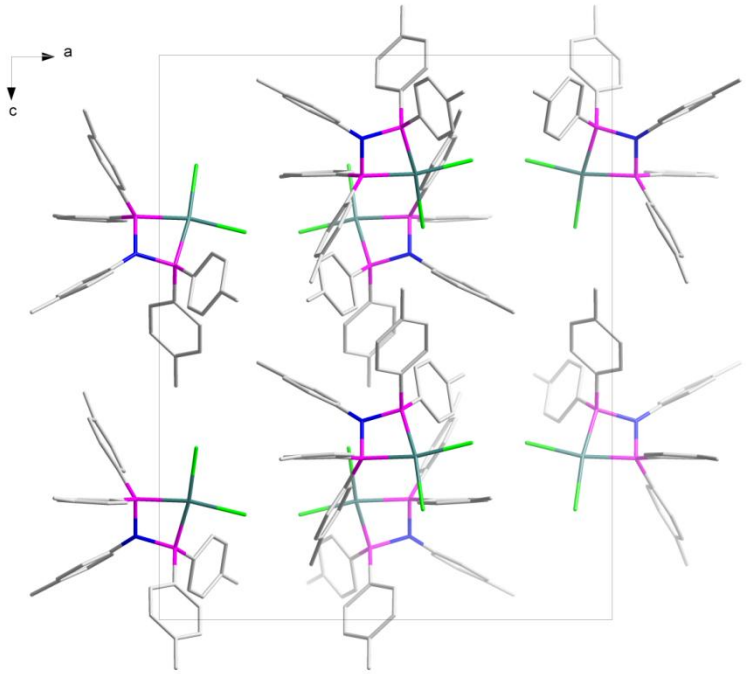

Figure 5.19: Graphical representation of the [Pt(5-*p*-tolyl-PNP)Cl_2] molecular packing. For clarity, all the H atoms are omitted.

5.5 Dichloro-[*N*,*N*-bis(diphenylphosphino)-*p*-toluidine-κ^2*P*,*P'*]palladium(II)

The synthesis of the title compound [Pd(5-*p*-tolyl-PNP)Cl_2], (see **Figure 5.20**) gave light orange crystals suitable for X-ray data analysis [**Chapter 4.6.1]**. The complex crystallizes in an orthorhombic crystal system in the *Pbca* space group with eight molecules in a unit cell (Z = 8). The asymmetric unit contains one independent molecule. Figure **5.20** shows the molecular structure and the numbering system on the title complex. The *Effective Tolman-based N-substituent steric effect* ($\theta_{N\text{-}sub}$) was calculated using **Equation 5.1** and found to be 33.7°.

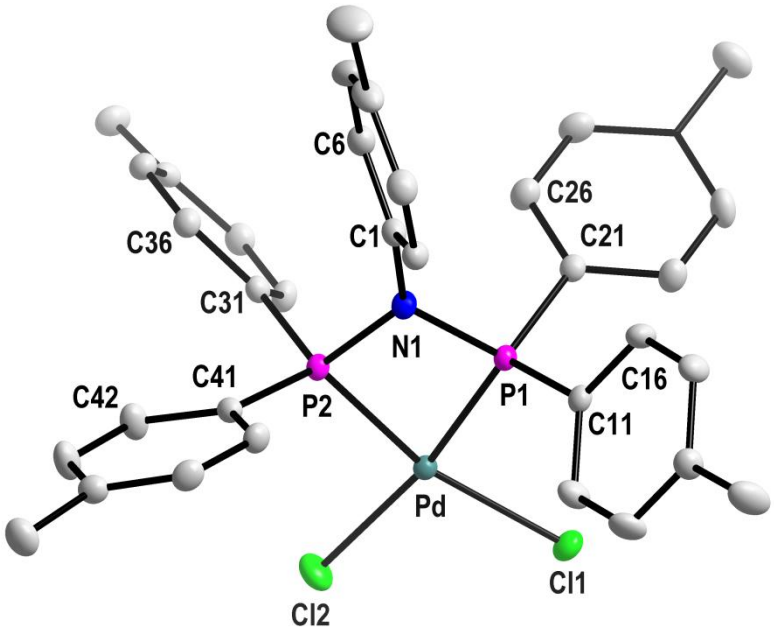

Figure 5.20: Molecular representation of [Pt(5-*p*-tolyl-PNP)Cl_2] metal complex, hydrogen atoms and numbering for some carbon atoms were omitted for clarity. For aromatic rings, the first digit represents the ring number and the second digit represents the specific C-atom in the ring. All displacement ellipsoid were drawn at 50% probability level.

Table 5.13: Important bond lengths and bond angles for the crystal structure of [Pd(5-*p*-tolyl-PNP)Cl_2] (Å and °)

Atoms	Bond length (Å)	Atoms	Bond angle (°)
Pd – P1	2.200(6)	P1 – Pd – P2	72.48(2)
Pd – P2	2.226(6)	P1 – N1 – P2	100.1(9)
Pd – Cl1	2.354(5)	C1 – N1 – P1	129.9(1)
Pd – Cl2	2.359(6)	C1 – N1 – P2	129.9(1)
N1 – C1	1.440(3)	N1 – P1 – C11	110.0(9)
N1 – P1	1.701(2)	N1 – P1 – C21	108.2(1)
N1 – P2	1.710(2)	N1 – P2 – C31	110.4(9)
P1 – C11	1.791(2)	N1 – P2 – C41	108.4(9)
P1 – C21	1.801(2)	C11 – P1 – C21	107.2(1)
P2 – C31	1.797(2)	C31 – P2 – C41	107.9(1)
P2 – C41	1.793(2)	Cl1 – Pd – Cl2	97.49(2)

Some of the important bond lengths and angles are reported in **Table 5.13**. The Pd-Cl1 and Pd-Cl2 bond lengths are 2.354(5) and 2.359(6) Å respectively and are in agreement with the reported Pt-Cl bond lengths of these types of metal complexes.[6,9,18,19] The P1-Pd-P2 and Cl1-Pd-Cl2 angles are 72.48(4) and 97.49(3) ° respectively indicating the highly distorted square planar geometry of the metal complex around the Pt atom, while the P1-N1-P2 bite angle is 100.1(9) ° indicating a significant contraction from the ideal 109.4 ° angle expected for a tetrahedral geometry around the N atom.[20,21,22] The N atom is positioned along the Pd/P1/P2 plane adopting an almost planar geometry with these atoms, while the *p*-tolyl substituent on the N atom is twisted at an angle of 70.83 ° with respect to the Pd/P1/P2 plane to accommodate the steric bulk properties of the entire metal complex, thus stabilizing the molecule (see **Figure 5.21**).

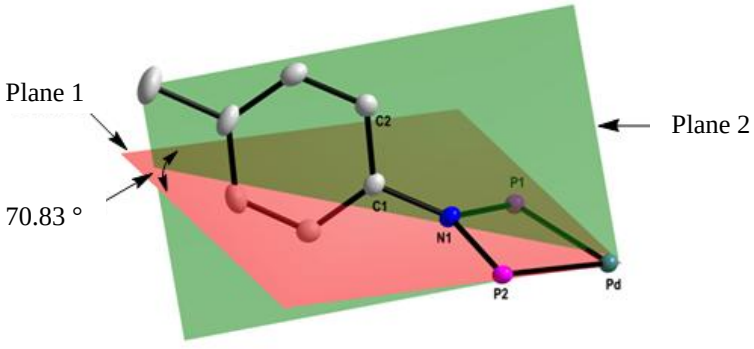

Figure 5.21: Graphical representation of the N atom adaptation technique in ligand steric bulk influence. Plane 1 and plane 2 are constructed through atoms Pd/P1/P2 and C1/C2/C3/C4/C5/C6 respectively.

Figure 5.22 illustrates the space taken by the *p*-tolyl group using a space-filling model.[17] The hydrogen and carbon are displayed as dark grey and grey colors respectively. A red stick-wire model is used for the remaining parts of the molecule for clarity.

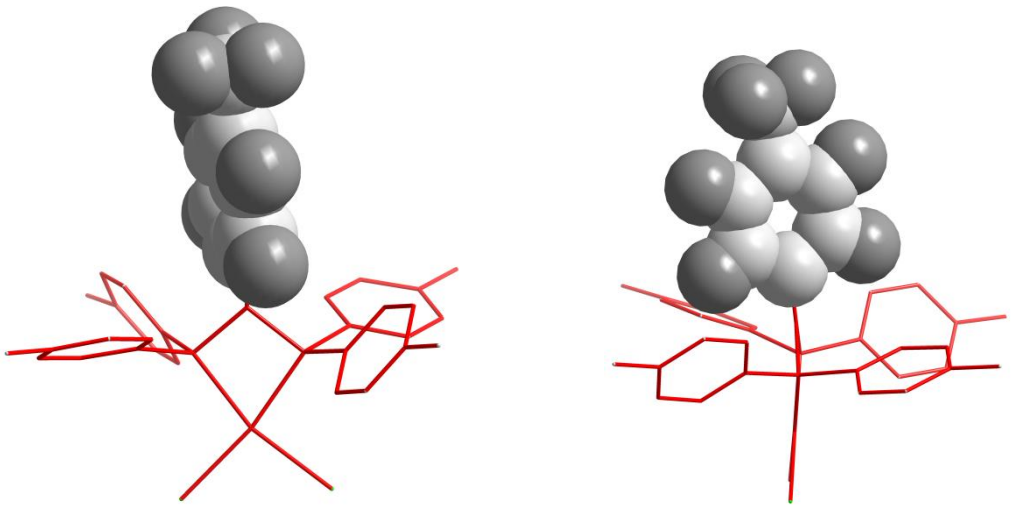

Figure 5.22: Graphical representation of the P-phenyl rings and the R-N group adaptation technique to ligand steric bulk influence on the complex [Pd(5-*p*-tolyl-PNP)Cl_2]. A stick-wire and space-filling model are used for the P-phenyl rings and the R-N group respectively.

No intramolecular hydrogen bonding is observed however the crystal structure is stabilized by one intermolecular hydrogen bonding and five C-H…π interactions as indicated by the bond distances and bond angles in **Table 5.15** and **5.16** respectively. Intermolecular hydrogen bond interaction contributing to the molecular packing of this metal complex is illustrated in **Figure 5.23**.

Table 5.15: Intermolecular hydrogen bonding for **[**Pd(5-*p*-tolyl-PNP)Cl_2**]**

D-H…A	**d(D-H) (Å)**	**d(H…A) (Å)**	**d(D…A) (Å)**	**< (DHA)**
C(47)-H(37C)… Cl(1)#1	0.98	2.77	3.732(2)	166

Symmetry transformation used to generate equivalent to atoms: **#1** -x, y + 0.5, -z + 0.5

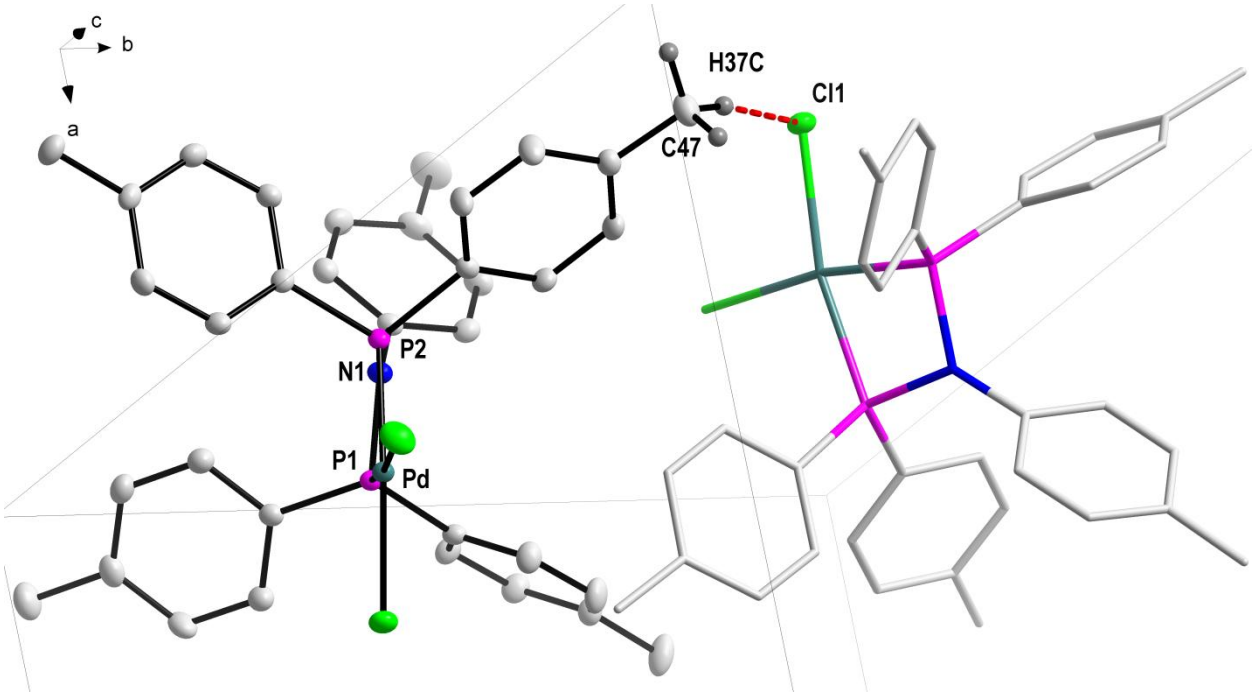

Figure 5.23: Graphical representation of the intermolecular hydrogen bonding (indicated by the red dash bonds) observed for [Pd(5-*p*-tolyl-PNP)Cl2].

The crystal structure is further stabilized by a C-H….Cg (pi-ring) interactions illustrated in **Figure 5.24, 5.25** and **5.26** with **Table 5.16** containing all the respective values.

Table 5.16: Representations of C-H...Cg(pi-ring) interactions for **[**Pd(5-*p*-tolyl-PNP)Cl_2**]**

C-H…Cg	**d(H…Cg) (Å)**	**d(C…Cg) (Å)**	**<(C-H…Cg) (Å)**
C(13)-H(13)…Cg(5)#1	2.98	3.650(2)	129
C(15)-H(15)…Cg(2)#2	2.80	3.400(2)	122
C(26)-H(26)…Cg(1)#3	2.96	3.255(2)	100
C(37)-H(47A)…Cg(6)#4	2.95	3.597(3)	124
C(37)-H(47C)…Cg(2)#4	2.56	3.391(3)	142

Symmetry transformation used to generate equivalent to atoms: **#2** -x, 1 - y, - z **#3** x, y , z, **#4** -0.5 - x,-0.5 + y, z. Cg1 = centroid atoms of Pd, P1, N1, P2; Cg2 = centroid atom of C1, C2, C3, C4, C5, C6; Cg5 = centroid atom of C31 C32 C33 C34 C35 C36; Cg6 = centroid atom of C41, C42, C43, C44, C46, C46.

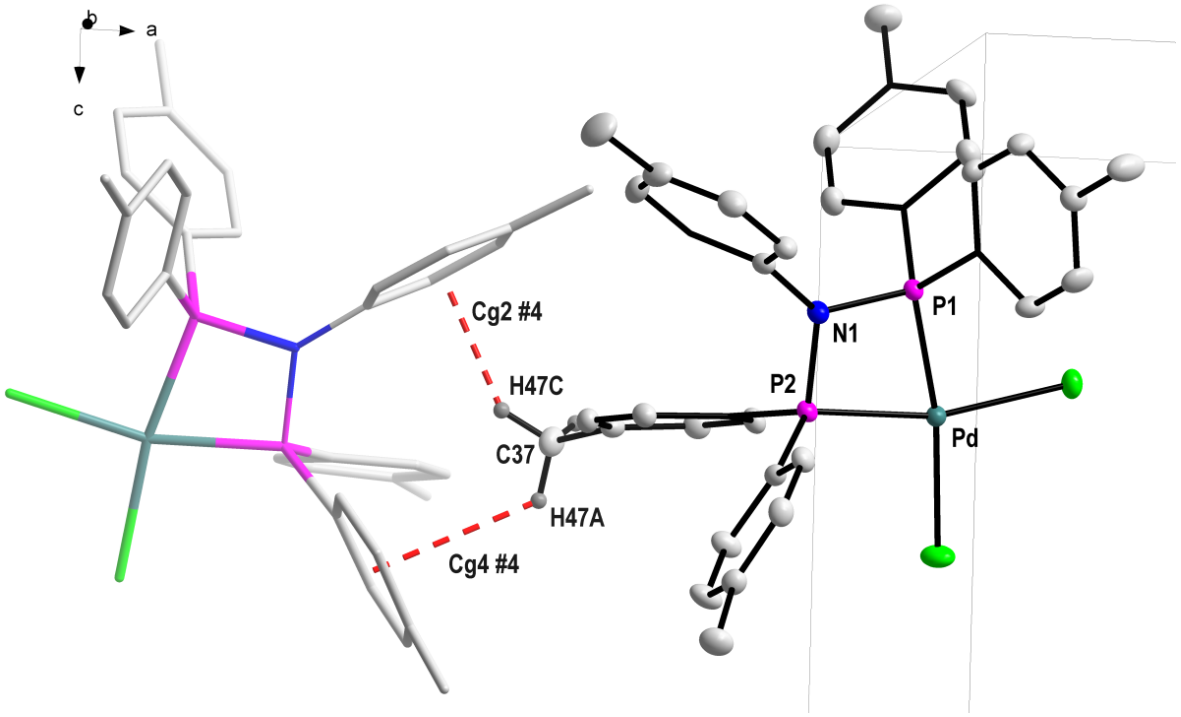

Figure 5.24: Graphical representation of the all the C-H...Cg interactions (indicated by the red dash bonds) observed for [Pd(5-*p*-tolyl-PNP)Cl_2].

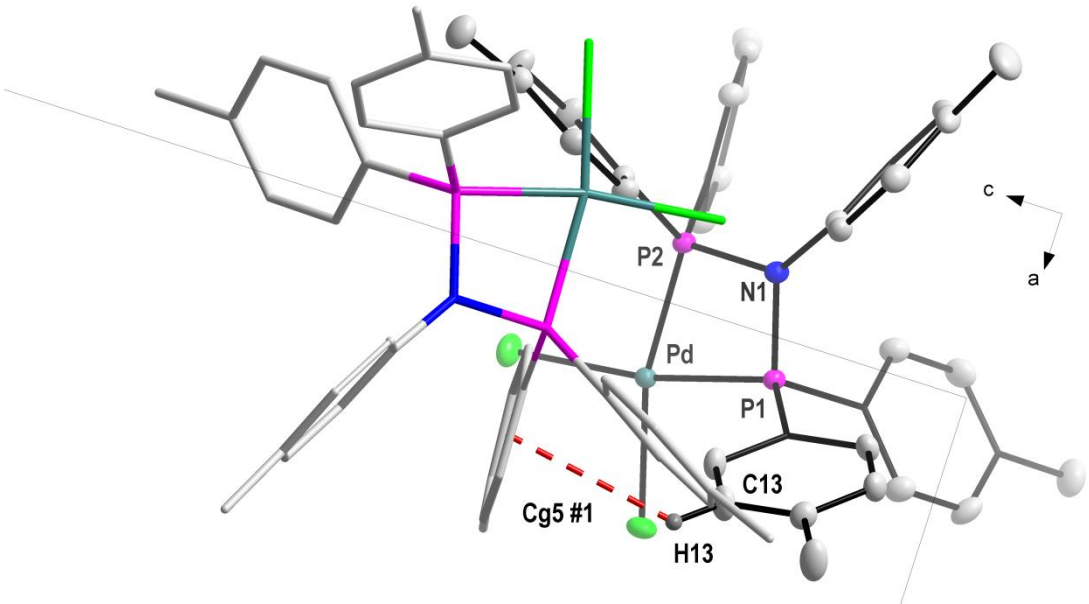

Figure 5.25: Graphical representation of the all the C-H...Cg interactions (indicated by the red dash bonds) observed for [Pd(5-*p*-tolyl-PNP)Cl_2].

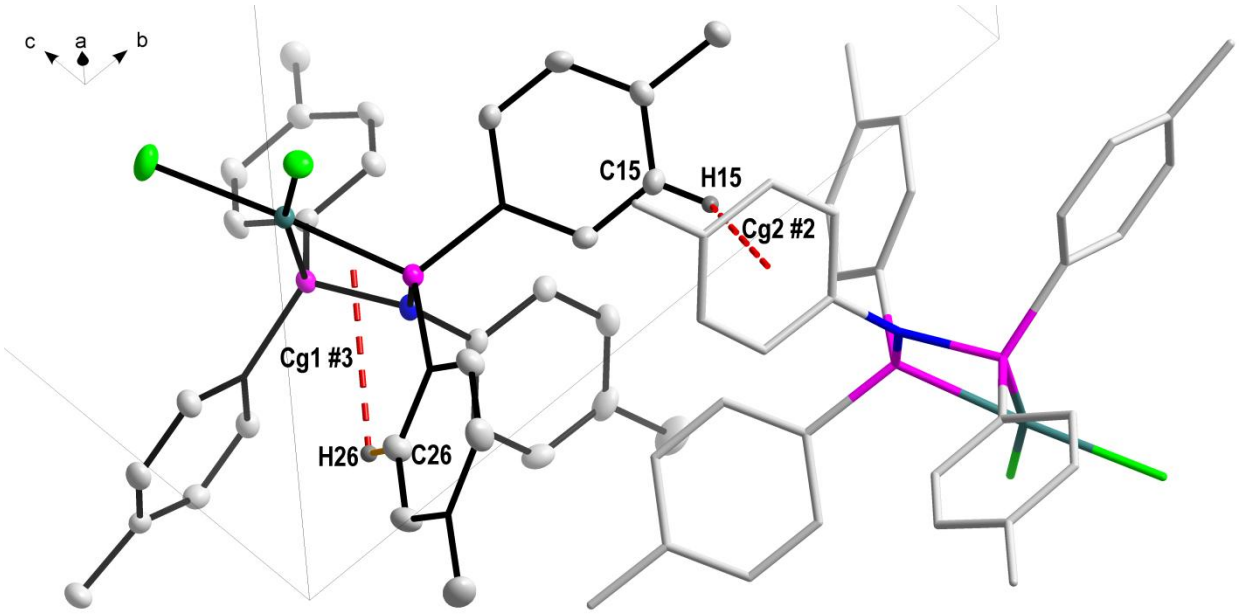

Figure 5.26: Graphical representation of the all the C-H...Cg interactions (indicated by the red dash bonds) observed for [Pd(5-*p*-tolyl-PNP)Cl_2].

The molecules pack in tail to tail formation along the *a*-axis as shown in **Figure 5.27.**

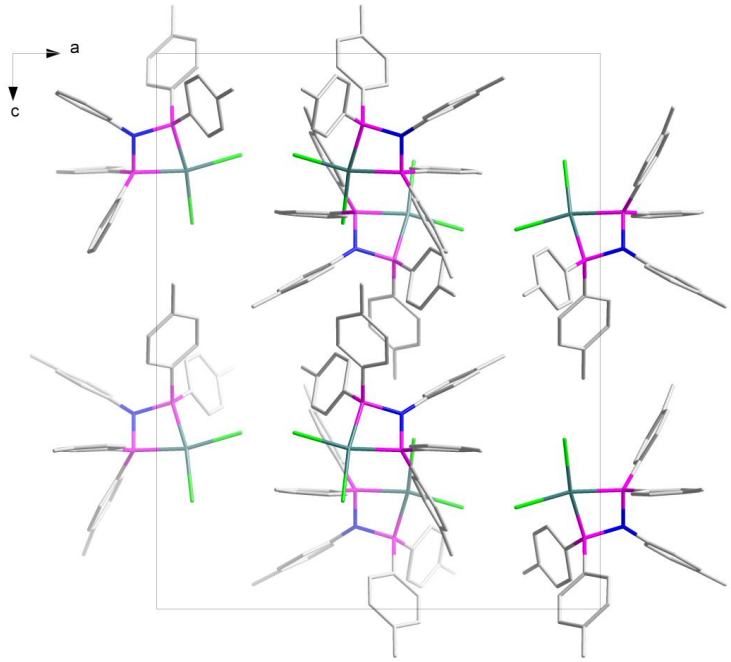

Figure 5.27: Graphical representation of the [Pd(5-*p*-tolyl-PNP)Cl_2] molecular packing. For clarity, all the H atoms are omitted.

5.6 Dichloro-[*N*,*N*-bis(di-*p*-tolylphosphino)-*o*-toluidine-κ^2*P*,*P'*]platinum(II)

The synthesis of the title compound [Pt(4-*p*-tolyl-*o*-tol)Cl_2], (see **Figure 5.28**) resulted in oval shaped colourless crystals suitable for X-ray data analysis [**Chapter 4.5.2]**. The complex crystallizes in a monoclinic crystal system in the $P2_1/c$ space group with four molecules in a unit cell (Z = 4). The asymmetric unit contains one independent molecule. **Figure 5.28** also shows the numbering system on the title complex, the solvent is omitted for clarity. The *Effective Tolman-based N-substituent steric effect* ($\theta_{N\text{-sub}}$) was calculated using **Equation 5.1** and found to be 42.2°.

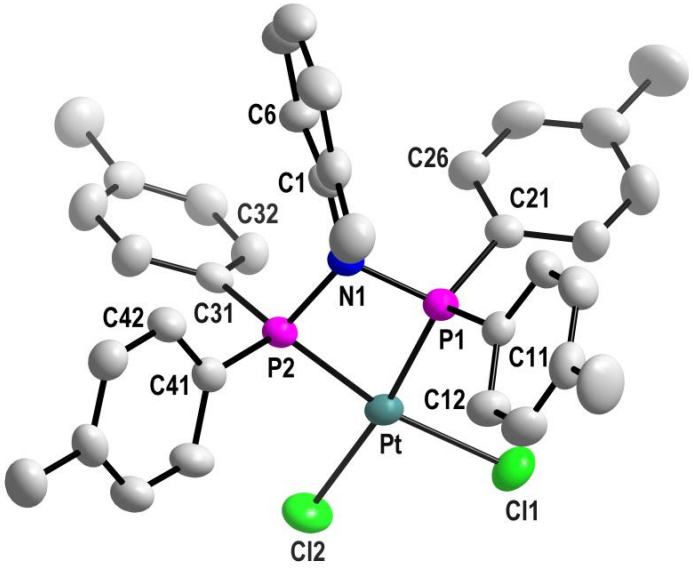

Figure 5.28: Molecular representation of [Pt(4-*p*-tolyl-*o*-tol)Cl_2] metal complex, hydrogen atoms and numbering for some carbon atoms were omitted for clarity. For aromatic rings, the first digit represents the ring number and the second digit represents the specific C-atom in the ring. All displacement ellipsoid were drawn at 50% probability level.

Table 5.17: Important bond lengths and bond angles for the crystal structure of [Pt(4-*p*-tolyl-*o*-tol)Cl_2] (Å and °)

Atoms	Bond length (Å)	Atoms	Bond angle (°)
Pt – P1	2.195(1)	P1 – Pt – P2	72.97(5)
Pt – P2	2.207(1)	P1 – N1 – P2	99.44(2)
Pt – Cl1	2.342(2)	C1 – N1 – P1	130.5(3)
Pt – Cl2	2.350(1)	C1 – N1 – P2	129.7(3)
N1 – C1	1.451(5)	N1 – P1 – C11	110.1(2)
N1 – P1	1.714(4)	N1 – P1 – C21	110.4(2)
N1 – P2	1.717(4)	N1 – P2 – C31	108.1(2)
P1 – C11	1.802(4)	N1 – P2 – C41	110.1(2)
P1 – C21	1.797(5)	C11 – P1 – C21	106.3(2)
P2 – C31	1.806(5)	C31 – P2 – C41	105.9(2)
P2 – C41	1.800(5)	Cl1 – Pt – Cl2	92.88(5)

Some of the important bond lengths and angles are reported in **Table 5.17**. The Pt-Cl1 and Pt-Cl2 bond lengths are 2.342(2) and 2.350(1) Å respectively and are in agreement with the reported Pt-Cl bond lengths of these types of metal complexes.[6,9,23,24] The P1-Pt-P2 and Cl1-Pt-Cl2 angles are 72.97(5) and 92.88(5) ° respectively indicating the highly distorted square planar geometry of the metal complex around the Pt atom, while the P1-N1-P2 bite angle is 99.44(2) ° indicating a significant contraction from the ideal 109.4 ° angle expected for a tetrahedral geometry around the N atom.[20,21,22] The N atom is positioned along the Pd/P1/P2 plane adopting an almost planar geometry with these atoms, while the *o*-tolyl substituent on the N atom is twisted at an angle of 74.15 ° with respect to the Pd/P1/P2 plane to accommodate the steric bulk properties of the entire metal complex, thus stabilizing the molecule (see **Figure 5.29**).

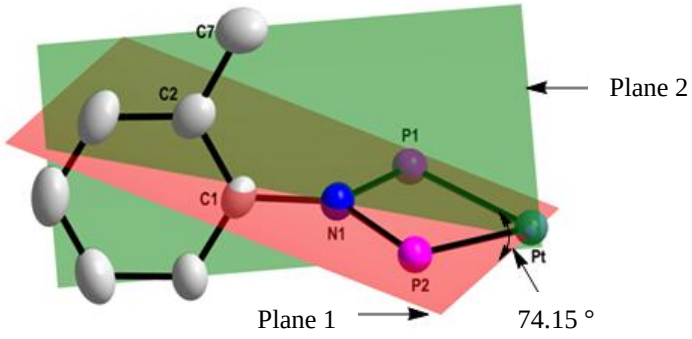

Figure 5.29: Graphical representation of the N atom adaptation technique in ligand steric bulk influence. Plane 1 and plane 2 are constructed through atoms Pt/P1/P2 and C1/C2/C3/C4/C5/C6 respectively.

Figure 5.30 illustrates the space taken by the *o*-tolyl group using the space-filling model.[17] The hydrogen and carbon atoms care displayed as dark grey and grey colors respectively. A red stick-wire model is used for the remaining parts of the molecule for clarity.

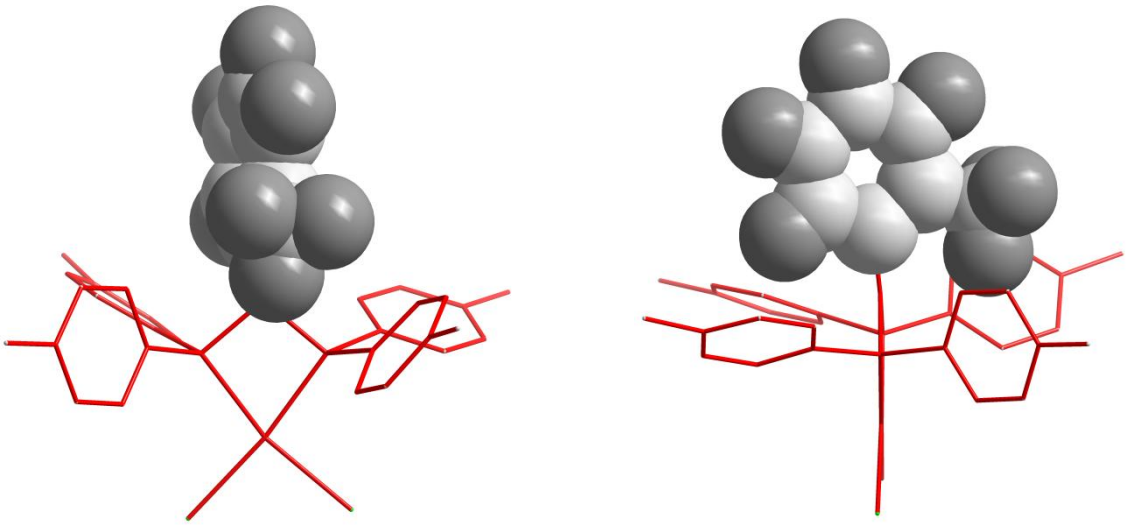

Figure 5.30: Graphical representation of the P-phenyl rings and the R-N group adaptation technique to ligand steric bulk influence on the complex [Pt(4-*p*-tolyl-*o*-tol)Cl_2]. A stick-wire and space-filling model are used for the P-phenyl rings and the R-N group respectively.

The crystal structure is stabilized by one classical intermolecular hydrogen bonding, one intramolecular hydrogen and five C-H…π interactions as indicated by the bond distances and bond angles in **Table 5.19** and **5.20**. Intermolecular and intramolecular hydrogen bond interactions contributing to the molecular packing of this metal complex are illustrated in **Figure 5.31**.

Table 5.19: Intra and Intermolecular hydrogen bonding for **[**Pt(4-*p*-tolyl-*o*-tol)Cl_2**]**

D-H…A	d(D-H) (Å)	d(H…A) (Å)	d(D…A) (Å)	< (DHA)
C(7)-H(32A)…N(1)#1	0.96	2.54	2.987(7)	108
C(25)-H(35)…Cl(1)#2	0.93	2.82	3.711(6)	162

Symmetry transformation used to generate equivalent to atoms: **#1** x, y, z **#2** x, -y + 0.5, z - 0.5

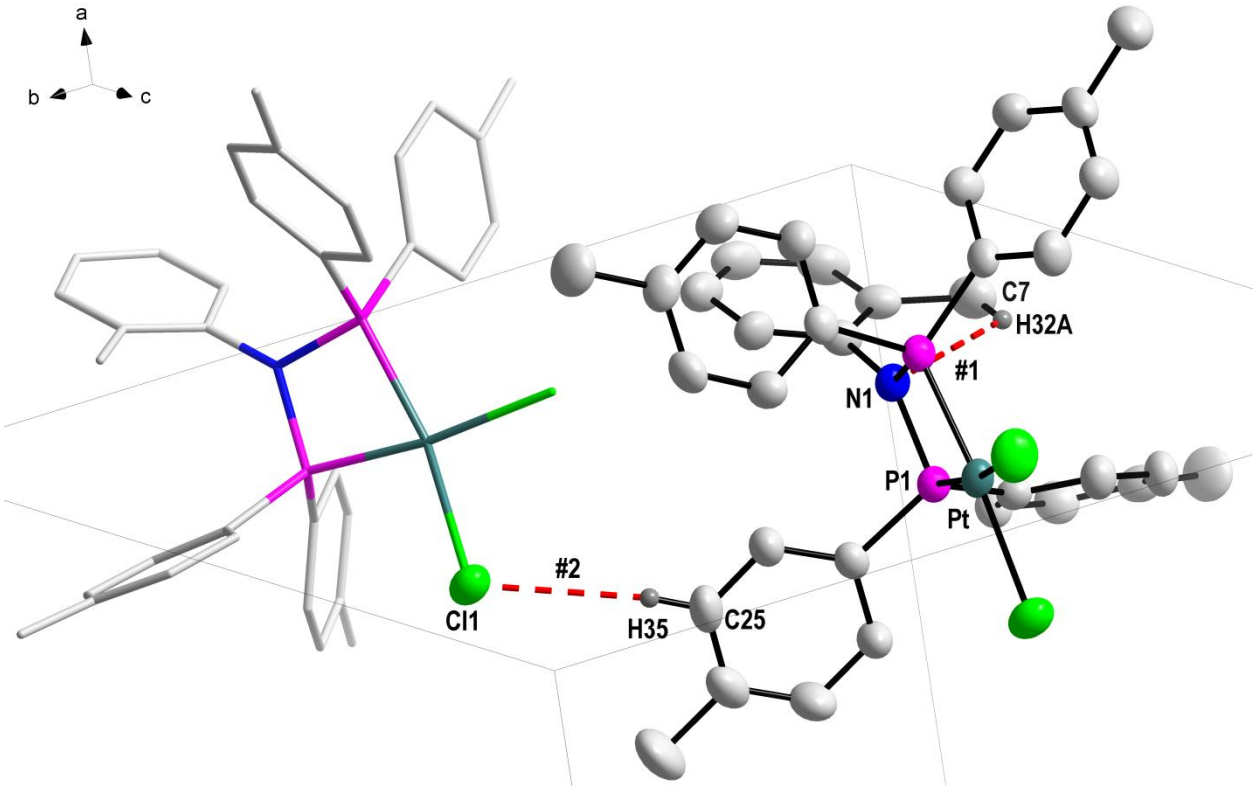

Figure 5.31: Graphical representation of the Intra and the intermolecular hydrogen bonding (indicated by the red dash bonds) observed for [Pt(4-*p*-tolyl-*o*-tol)Cl_2].

The crystal structure is further stabilized by a C-H….Cg (pi-ring) interactions as illustrated in **Figure 5.32**, **5.33** and **Table 5.20**.

Table 5.20: Representations of C-H...Cg(pi-ring) interactions for **[**Pt(4-*p*-tolyl-*o*-tol)Cl_2**]**

C-H…Cg	**d(H…Cg) (Å)**	**d(C…Cg) (Å)**	**<(C-H…Cg) (Å)**
C(32)-H(15)…Cg(1)#1	2.97	3.266(5)	100
C(37)-H(30C)…Cg(6)#3	2.94	3.612(7)	129
C(7)-H(32A)…Cg(3)#1	2.99	3.427(7)	109
C(7)-H(32C)…Cg(3)#1	2.99	3.427(7)	109
C(15)-H(43)…Cg(2)#4	2.81	3.441(6)	126

Symmetry transformation used to generate equivalent to atoms: **#1** x, y, z **#3** 2 - x, 0.5 + y, 0.5- z **#4** 1 - x, - y , -z, Cg1 = centroid atoms of Pt, P1, N1, P2; Cg2 = centroid atom of C1, C2, C3, C4, C5, C6; Cg3 = centroid atom of C11 C12 C13 C14 C15 C16; Cg6 = centroid atom of C41, C42, C43, C44, C46, C46.

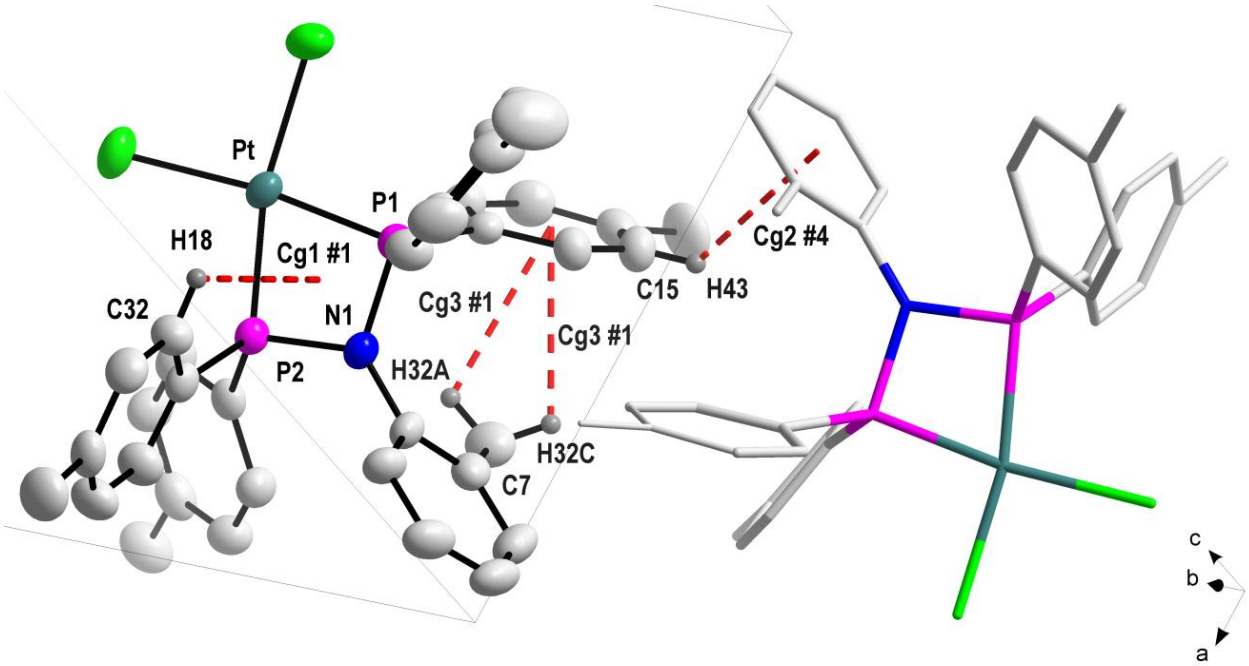

Figure 5.32: Graphical representation of the C-H...Cg interactions (indicated by the red dash bonds) observed for [Pt(4-*p*-tolyl-*o*-tol)Cl_2].

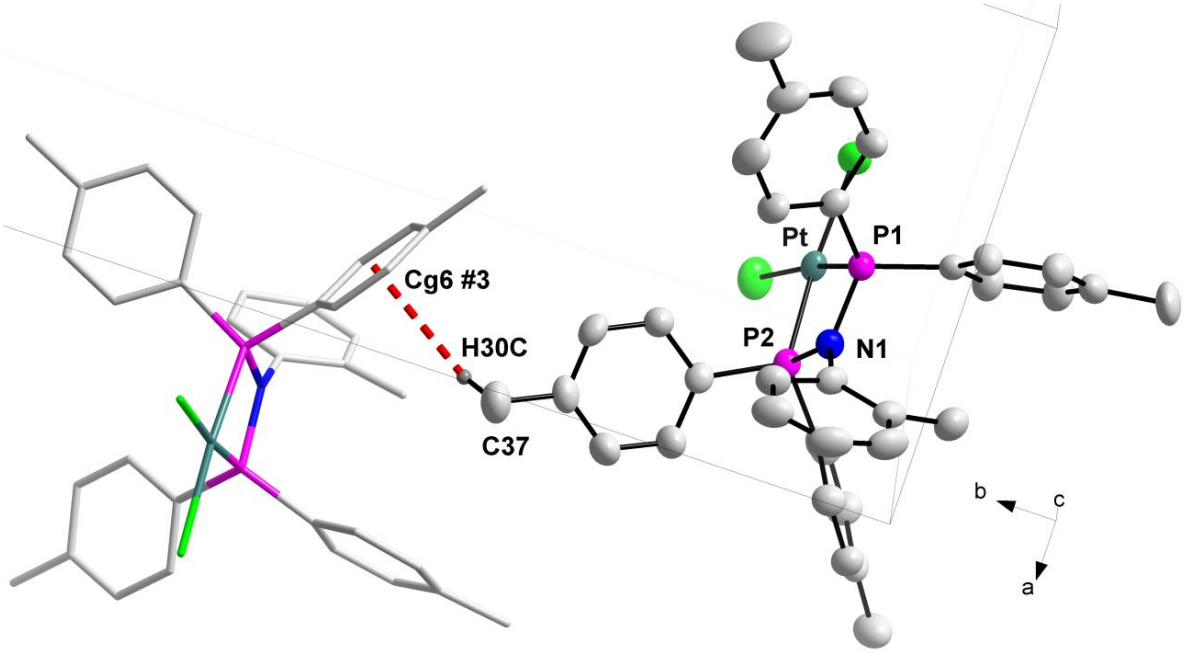

Figure 5.33: Graphical representation of the C-H...Cg interactions (indicated by the red dash bonds) observed for [Pt(4-*p*-tolyl-*o*-tol)Cl_2].

The molecules pack in a head to head formation along the *c*-axis as shown in **Figure 5.34**.

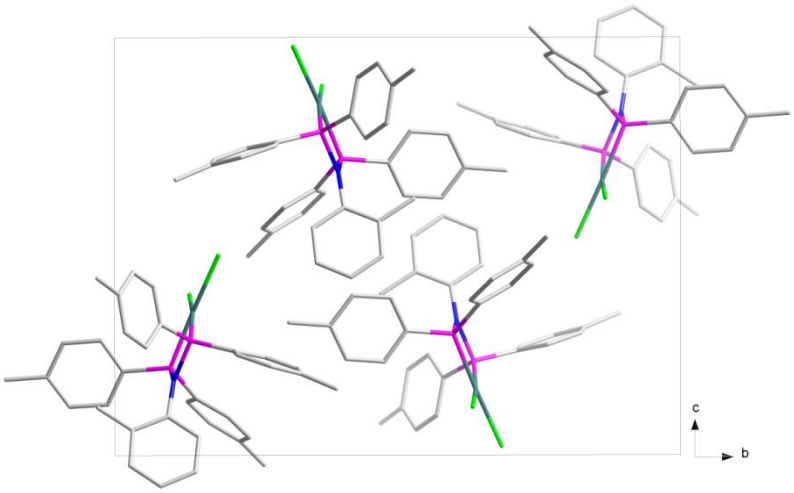

Figure 5.34: Graphical representation of the [Pt(4-*p*-tolyl-*o*-tol)Cl_2] molecular packing. For clarity, all the H atoms are omitted.

5.7 Dichloro-[*N*,*N*-bis(di-*p*-tolylphosphino)cyclobutylamine-κ^2*P*,*P'*]platinum(II)

The synthesis of the title compound [Pt(Cbutyl-4-*p*-tolyl)Cl_2], (see **Figure 5.36**) gave colourless crystals suitable for X-ray data analysis [**Chapter 4.5.4]**. The complex crystallizes in a monoclinic crystal system in the *P*21/*c* space group with four molecules in a unit cell (Z = 4). The asymmetric unit contains one independent molecule. **Figure 5.36** shows the molecular structure and the numbering system on the title complex. The *Effective Tolman-based N-substituent steric effect* ($\theta_{N\text{-sub}}$) was calculated using **Equation 5.1** and found to be 73.2 °.

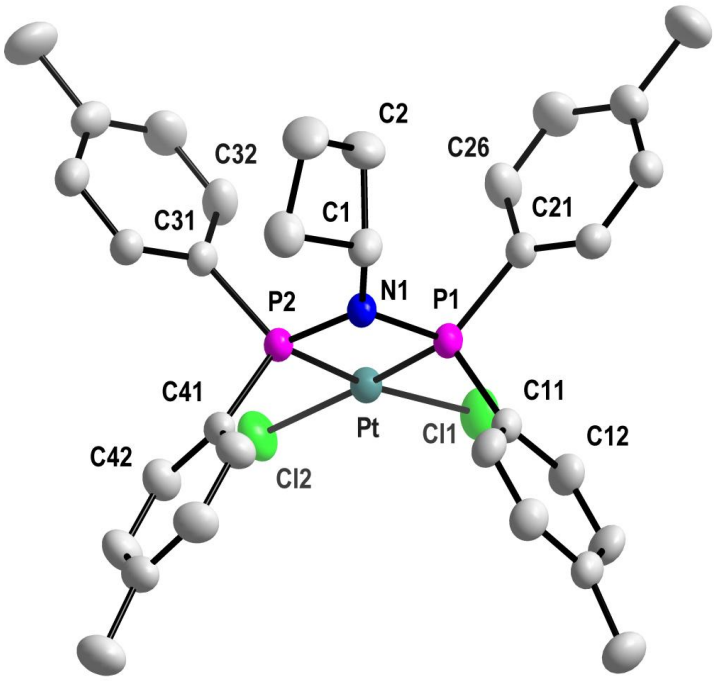

Figure 5.36: Molecular representation of [Pt(Cbutyl-4-*p*-tolyl)Cl_2] metal complex, hydrogen atoms and numbering for some carbon atoms were omitted for clarity. For aromatic rings, the first digit represents the ring number and the second digit represents the specific C-atom in the ring. All displacement ellipsoid were drawn at 50% probability level.

Table 5.21: Important bond lengths and bond angles for the crystal structure of [Pt(Cbutyl-4-*p*-tolyl)Cl_2] (Å and °)

Atoms	Bond length (Å)	Atoms	Bond angle (°)
Pt – P1	2.2038(11)	P1 – Pt – P2	71.73(4)
Pt – P2	2.2111(11)	P1 – N1 – P2	99.49(17)
Pt – Cl1	2.3639(12)	C1 – N1 – P1	125.5(3)
Pt – Cl2	2.3646(12)	C1 – N1 – P2	132.2(3)
N1 – C1	1.475(5)	N1 – P1 – C11	108.75(19)
N1 – P1	1.693(3)	N1 – P1 – C21	108.32(17)
N1 – P2	1.696(3)	N1 – P2 – C31	111.19(17)
P1 – C11	1.807(4)	N1 – P2 – C41	108.80(19)
P1 – C21	1.803(4)	C11 – P1 – C21	107.62(18)
P2 – C31	1.806(4)	C31 – P2 – C41	107.51(18)
P2 – C41	1.800(4)	Cl1 – Pt – Cl2	92.10(5)

Some of the important bond lengths and angles are reported in **Table 5.21**. The Pt-Cl1 and Pt-Cl2 bond lengths are 2.3639(12) and 2.3646(12) Å respectively and are in agreement with the reported Pt-Cl bond lengths of these types of metal complexes.[6,9,23,24] The P1-Pt-P2 and Cl1-Pt-Cl2 angles are 71.73(4) and 92.10(5) ° respectively indicating the highly distorted square planar geometry of the metal complex around the Pt atom, while the P1-N1-P2 bite angle is 99.49(17) ° indicating a significant contraction from the ideal 109.4 ° angle expected for a tetrahedral geometry around the N atom.[20,21,22] The N atom is positioned slightly below the Pd/P1/P2 plane, at a distance of 0.113 Å adopting an almost planar geometry with these atoms. The cyclobutyl substituent on the N atom is bent creating a C1-N1-Pt angle of 162.16 ° to accommodate the steric bulk properties of the entire metal complex, to aid in stabilizing the molecule (see **Figure 5.37**).

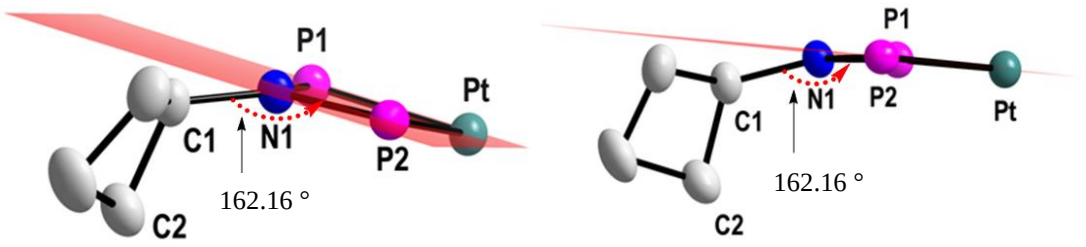

Figure 5.37: Graphical representation of the N atom adaptation technique in ligand steric bulk influence. The Plane is constructed through atoms Pt/P1/P2.

Figure 5.38 illustrates the space taken by the cyclobutyl group using a space-filling model.[17] The hydrogen and carbon atoms are displayed as dark grey and grey colors respectively. A red stick-wire model is used for the remaining parts of the molecule for clarity.

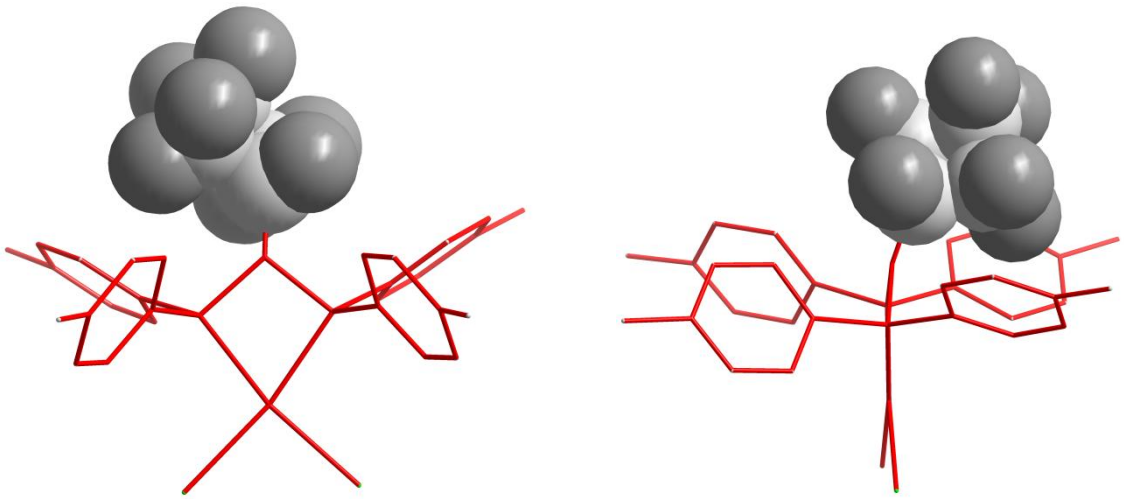

Figure 5.38: Graphical representation of the P-phenyl rings and the R-N group adaptation technique to ligand steric bulk influence on the complex [Pt(Cbutyl-4-*p*-tolyl)Cl_2]. A stick-wire and space-filling model are used for the P-phenyl rings and the R-N group respectively.

No classical intra and intermolecular hydrogen bonding is observed however the crystal structure is stabilized by two C-H…π interactions as indicated by the bond distances and bond angles in **Table 5.23** and **Figure 5.39**.

Table 5.23: Representations of C-H...Cg(pi-ring) interactions for **[**Pt(Cbutyl-4-*p*-tolyl)Cl_2**]**

C-H…Cg	**d(H…Cg) (Å)**	**d(C…Cg) (Å)**	**<(C-H…Cg) (Å)**
C(3)-H(30A)…Cg(6) #1	2.77	3.663(5)	151
C(3)-H(30B)…Cg(3) #1	2.96	3.523(5)	117

Symmetry transformation used to generate equivalent to atoms: **#1** 1 - x, 0.5 + y, 0.5 - z Cg3 = centroid atoms of C11, C12, C13, C14, C15, C16; Cg6 = centroid atom of C41, C42, C43, C44, C46, C46.

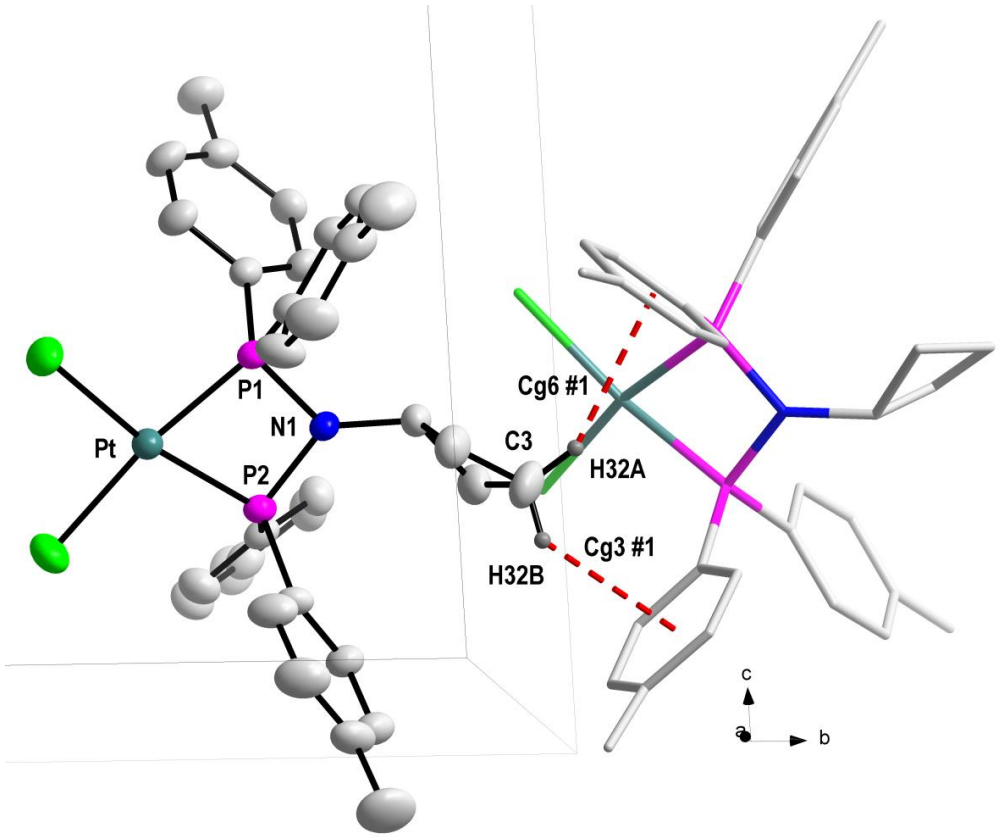

Figure 5.39: Graphical representation of the C-H...Cg interactions (indicated by the red dash bonds) observed for [Pt(Cbutyl-4-*p*-tolyl)Cl_2].

The molecules pack in a head to tail formation along the b-axis as shown in **Figure 5.40**.

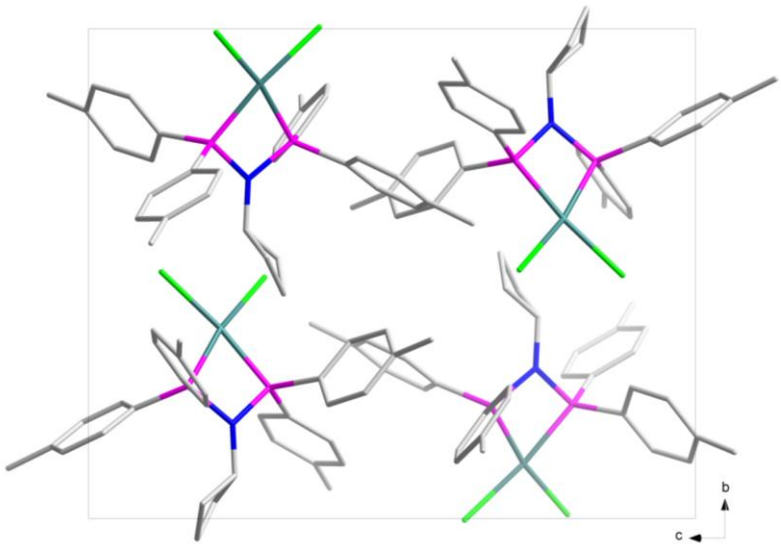

Figure 5.40: Graphical representation of the [Pt(Cbutyl-4-*p*-tolyl)Cl_2] molecular packing. For clarity, all the H atoms are omitted.

5.8 Dichloro-[*N*,*N*-bis(di-*p*-phenylphosphino)cyclohexylamine-κ^2*P*,*P'*]palladium(II)

The synthesis of the title compound [Pd(Chzyl-4-*p*-tolyl)Cl_2], (see **Figure 5.41**) resulted in light yellow crystals suitable for X-ray data analysis [**Chapter 4.6.6]**. The complex crystallizes in a monoclinic crystal system in the $P2_1/c$ space group with four molecules in a unit cell (Z = 4). The asymmetric unit contains one independent molecule and a methanol moiety (MeOH). **Figure 5.41** also shows the numbering system on the title complex. The *Effective Tolman-based N-substituent steric effect* ($\theta_{N\text{-sub}}$) was calculated using **Equation 5.1** and found to be 80.6 °.

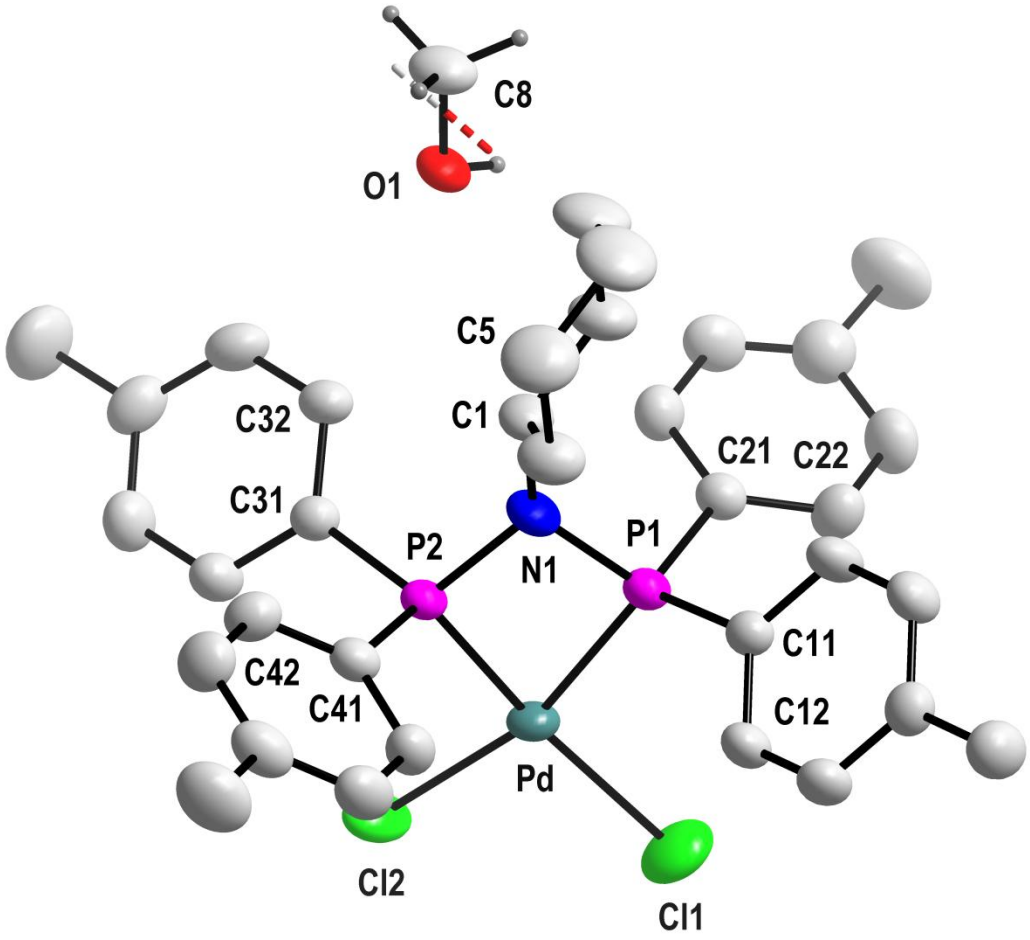

Figure 5.41: Molecular representation of [Pd(Chzyl-4-*p*-tolyl)Cl_2] metal complex, hydrogen atoms and numbering for some carbon atoms were omitted for clarity. For aromatic rings, the first digit represents the ring number and the second digit represents the specific C-atom in the ring. All displacement ellipsoid were drawn at 50% probability level.

Table 5.24*:* Important bond lengths and bond angles for the crystal structure of [Pd(Chzyl-4-*p*-tolyl)Cl_2] (Å and °)

Atoms	**Bond length (Å)**	**Atoms**	**Bond angle (°)**
Pd – P1	2.2239(11)	P1 – Pd – P2	71.80(3)
Pd – P2	2.1975(8)	P1 – N1 – P2	99.27(11)
Pd – Cl1	2.3716(10)	C1 – N1 – P1	132.97(18)
Pd – Cl2	2.3428(14)	C1 – N1 – P2	126.02(18)
N1 – C1	1.494(3)	N1 – P1 – C11	112.70(12)
N1 – P1	1.715(2)	N1 – P1 – C21	108.18(12)
N1 – P2	1.688(2)	N1 – P2 – C31	110.62(12)
P1 – C11	1.802(3)	N1 – P2 – C41	109.15(11)
P1 – C21	1.806(3)	C11 – P1 – C21	107.57(13)
P2 – C31	1.798(3)	C31 – P2 – C41	106.37(12)
P2 – C41	1.814(3)	Cl1 – Pd – Cl2	96.24(4)

Some of the important bond lengths and angles are reported in **Table 5.24**. The Pd-Cl1 and Pd-Cl2 bond lengths are 2.3716(10) and 2.3428(14) Å respectively and are in agreement with the reported Pd-Cl bond lengths of these types of metal complexes.[18,25] The P1-Pd-P2 and Cl1-Pd-Cl2 angles are 71.80(3) and 96.24(4) ° respectively indicating the highly distorted square planar geometry of the metal complex around the Pd atom, while the P1-N1-P2 bite angle is 99.27(11) ° indicating a small contraction from the ideal 109.4 ° angle expected for a tetrahedral geometry around the N atom.[20,21,22] The N atom is positioned slightly below the Pd/P1/P2 plane, at a distance of 0.074 Å adopting an almost planar geometry with these atoms. The cyclohexyl substituent on the N atom is bent creating a C1-N1-Pd angle of 170.64 ° to accommodate the steric bulk properties of the entire metal complex, to aid in stabilizing the molecule (see **Figure 5.42**).

[25] M. Aydemir, A. Baysal, F. Durap, B. Gumgum, S. Ozkar, L.T. Yildirim, *Appl. Organometal. Chem*, **2009**, *23*, 467.

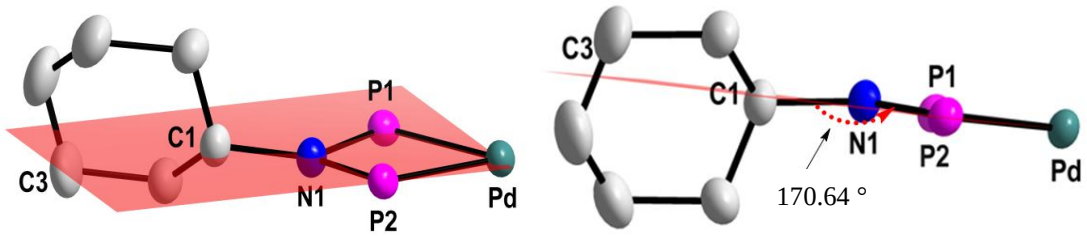

Figure 5.42: Graphical representation of the N atom adaptation technique in ligand steric bulk influence. The plane is constructed through atoms Pd/P1/P2.

Figure 5.43 illustrates the space taken by the cyclohexyl group using a space-filling model.[17] The hydrogen and carbon are displayed as dark grey and grey colors respectively. A red stick-wire model is used for the remaining parts of the molecule for clarity.

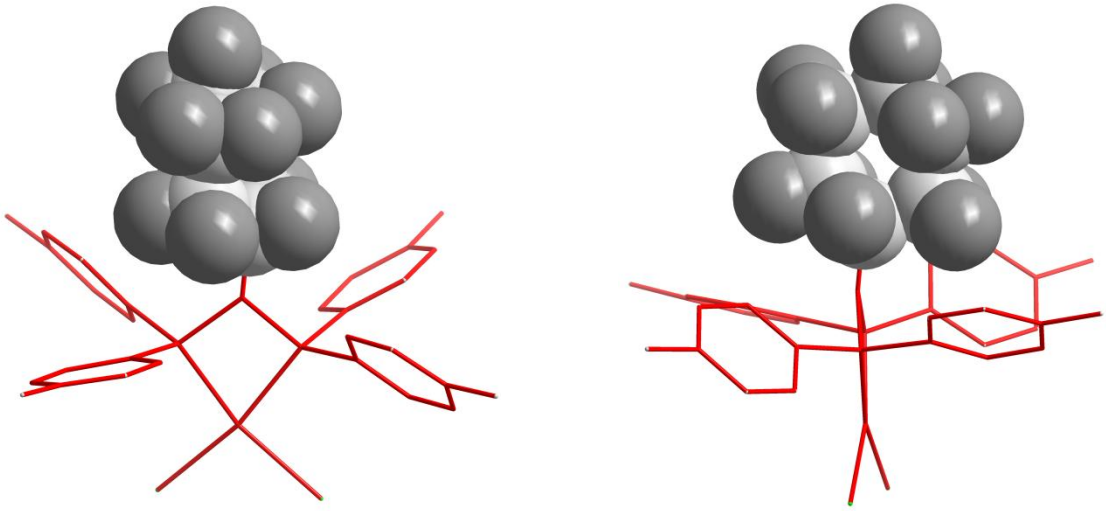

Figure 5.43: Graphical representation of the complex [Pd(Chzyl-4-*p*-tolyl)Cl_2]. A stick-wire and space-filling models are used for the P-phenyl rings and the R-N group respectively.

The crystal structure is stabilized by two classical intermolecular hydrogen bonding, two intramolecular hydrogen bonding and four C-H…π interactions as indicated by the bond distances and bond angles in **Table 5.26** and **5.27**. Inter and intramolecular hydrogen bond interactions are illustrated in **Figure 5.44**.

Table 5.26: Intra and Intermolecular hydrogen bonding for **[**Pd(Chzyl-4-*p*-tolyl)Cl_2**]**

D-H…A	d(D-H) (Å)	d(H…A) (Å)	d(D…A) (Å)	< (DHA)
C(13)-H(015)…Cl(2)#2	0.93	2.77	3.628(4)	155
C(2)-H(02A)…O(1)#1	0.97	2.50	3.398(8)	154
C(17)-H(03C)…Cl(2)#2	0.96	2.80	3.656(5)	150

Symmetry transformation used to generate equivalent to atoms: **#1** x, y, z **#2** 1 - x, -y, 1 - z.

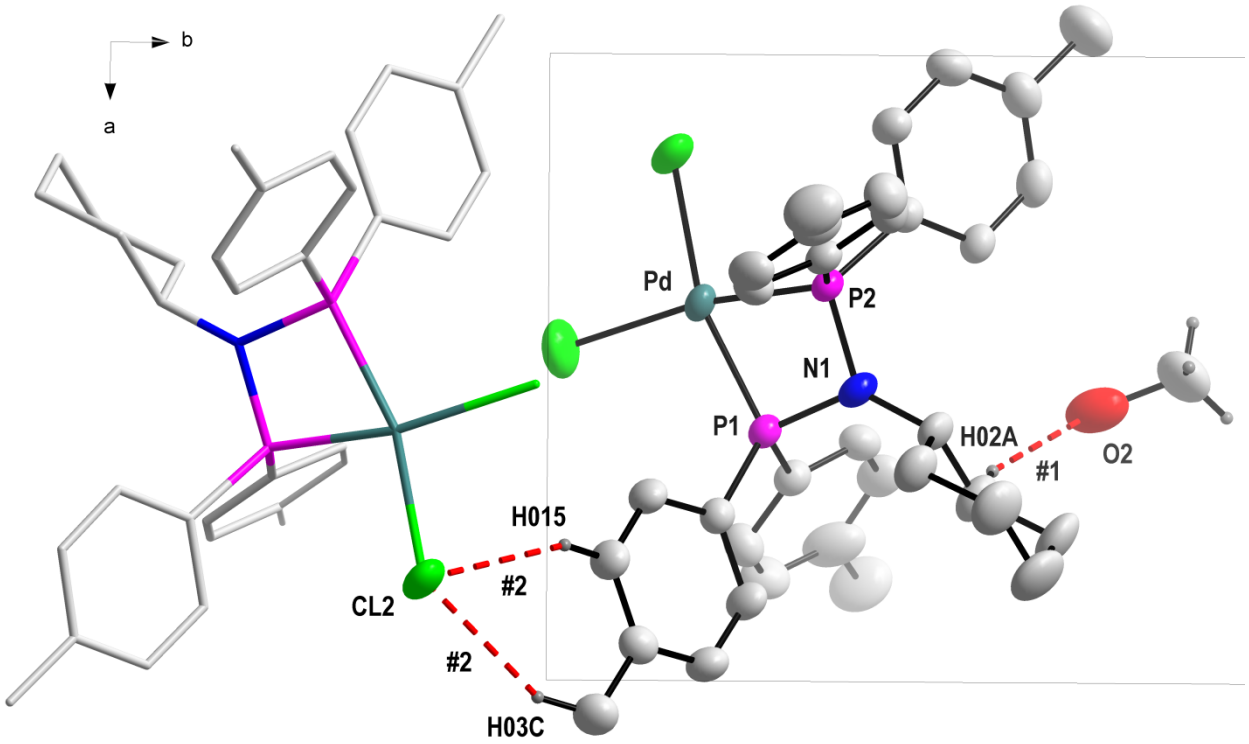

Figure 5.44 Graphical representation of the Intra and the intermolecular hydrogen bonding (indicated by the red dash bonds) observed for [Pd(Chzyl-4-*p*-tolyl)Cl_2].

The crystal structure is further stabilized by four C-H….Cg (pi-ring) interactions as illustrated **Figure 5.45**, **5.46** and **Table 5.27**.

Table 5.27: Representations of C-H...Cg(pi-ring) interactions for **[**Pd(Chzyl-4-*p*-tolyl)Cl_2**]**

C-H…Cg	d(H…Cg) (Å)	d(C…Cg) (Å)	<(C-H…Cg) (Å)
C(35)-H(013)…Cg(4) #3	2.88	3.617(4)	137
C(15)-H(021)…Cg(6) #4	2.74	3.622(4)	159
C(46)-H(022)…Cg(1) #1	2.93	3.227(3)	100
C(26)-H(039)…Cg(1) #1	2.94	3.247(3)	101

Symmetry transformation used to generate equivalent to atoms: **#1** x, y, z **#3** -1 + x, y, z **#4** 1 + x, y, z Cg1 = centroid atoms of Pd, P1, N1, P2; Cg4 = centroid atoms of C21, C22, C23, C24, C25, C26; Cg6 = centroid atom of C41, C42, C43, C44, C46, C46.

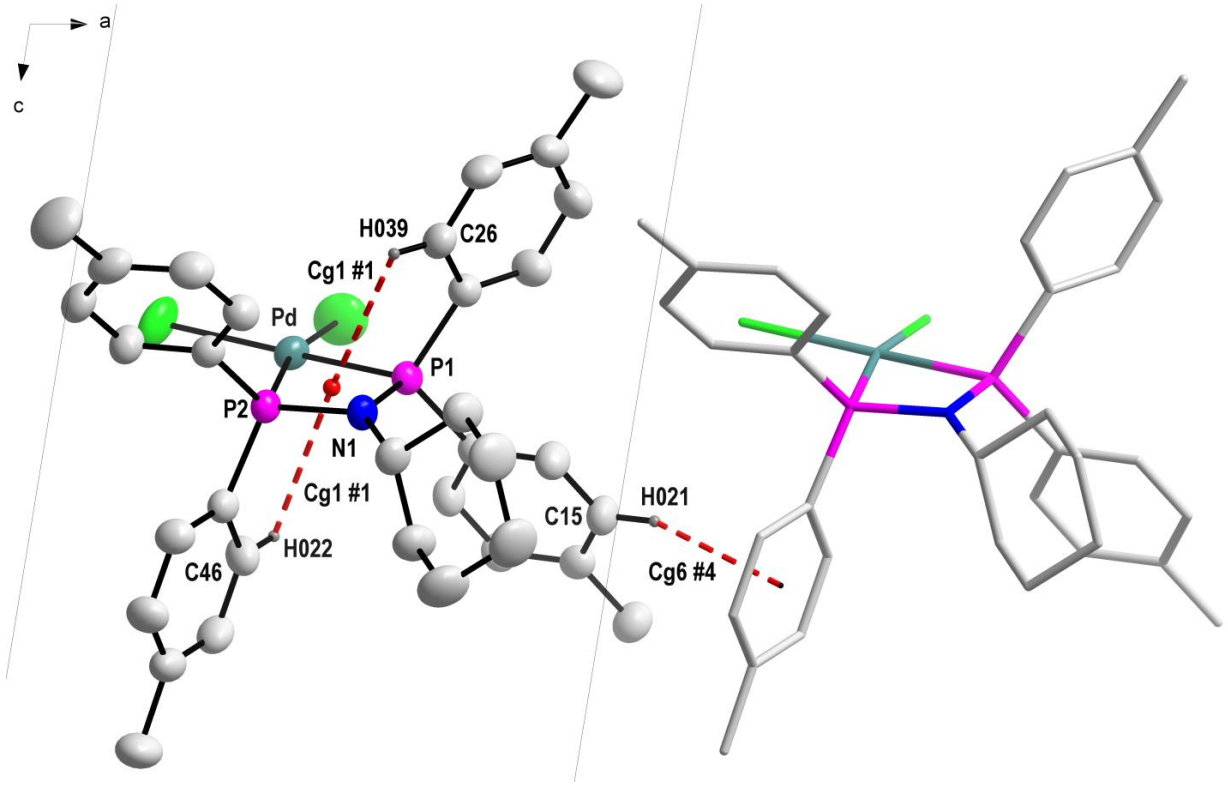

Figure 5.45: Graphical representation of the C-H...Cg interactions (indicated by the red dash bonds) observed for [Pd(Chzyl-4-*p*-tolyl)Cl_2].

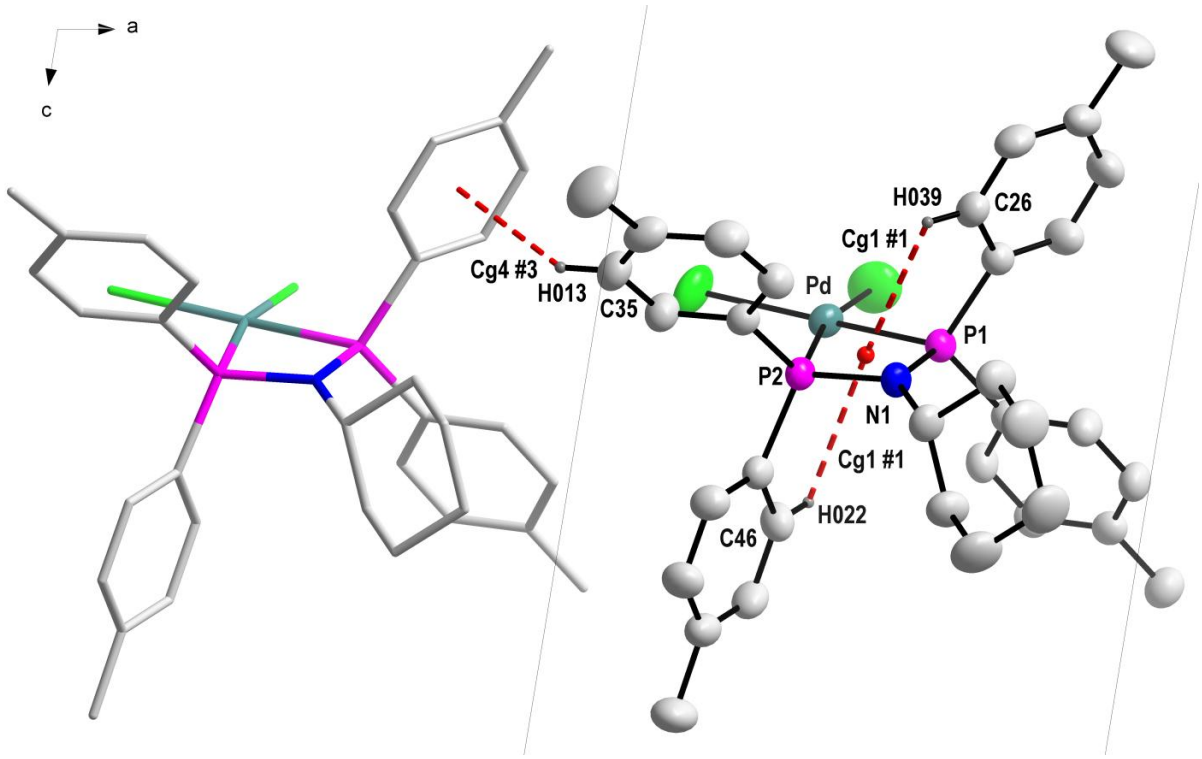

Figure 5.46: Graphical representation of the C-H...Cg interactions (indicated by the red dash bonds) observed for [Pd(Chzyl-4-*p*-tolyl)Cl_2]. Only the H atoms relevant for the interactions are drawn in an ellipsoid model.

The molecules pack in a head to head formation along the b-axis as shown in **Figure 5.47**.

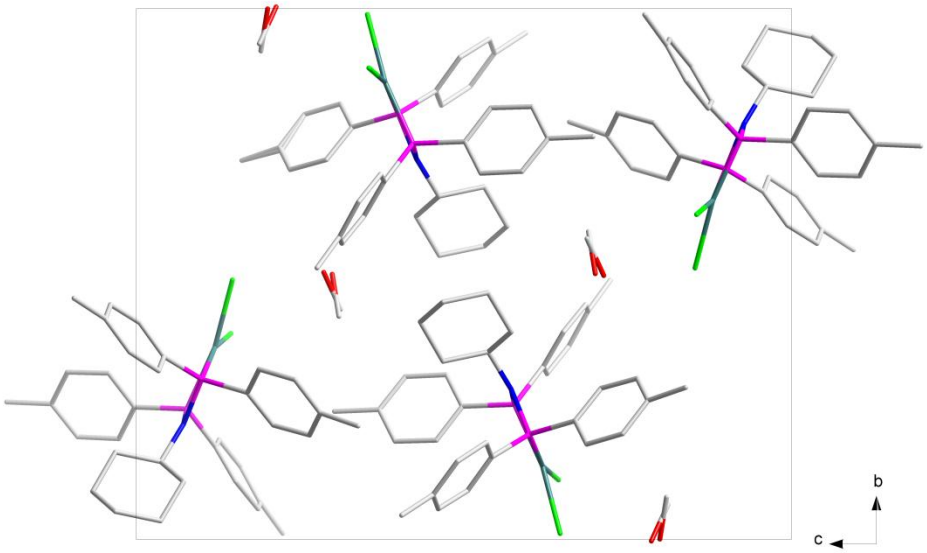

Figure 5.47: Graphical representation of the [Pd(Chzyl-4-*p*-tolyl)Cl_2] molecular packing. For clarity, all the H atoms are omitted.

5.9 Discussion

In this chapter six metal complex crystal structures were evaluated, three were Pt complexes [Pt(5-*p*-tolyl-PNP)Cl_2, (**A**)], [Pt(4-*p*-tolyl-*o*-tol)Cl_2, (**B**)], [Pt(Cbutyl-4-*p*-tolyl)Cl_2, (**C**)] and the other three were Pd complexes [Pd(Cl-Ph-PNP)Cl_2 (**D**)], [Pd(5-*p*-tolyl-PNP)Cl_2, (**E**)], [Pd(Chzyl-4-*p*-tolyl)Cl_2, (**F**)]. Complex **A** and **D** both crystallized in an orthorhombic crystal system and were both refined in the standard space group *Pbca* each with eight molecules per unit cell (Z=8). Complex **B** crystallized in a monoclinic crystal system and was refined in a standard space group $P2_1/c$ with four molecules per unit cell (Z=4). Complex **B** and **C** both crystallized in a monoclinic crystal system and in a non standard space group $P2_1/n$ each with four molecules per unit cell (Z=4), but were refined into a space group $P2_1/c$. All crystal structures were stabilized by a variety of X-H…Cg (π-ring) interactions due to a high number of aromatic rings on the PNP ligands. Furthermore, a range of inter and intramolecular hydrogen bonding also played a role on the solidification of these metal complexes. The bond angles and bond lengths of all crystal structures were in agreement with the reported values of similar complexes in literature.[6,7,9,18,19,23,24]

It was noted that all six complexes solidified into single crystals suitable for X-ray analysis despite the significant square planar geometry distortion around the metal centers (Pt/Pd). The P-M-P bond angles ranged from 72.48 to 81.30 ° indicating a significant contraction from the ideal 90 ° angle for a square planar geometry around the metal center. The P-N-P bond angles ranged from 99.44 to 107.5 ° also indicating a significant contraction from the ideal 109.4 ° angle expected for a tetrahedral geometry around the N atom for most of the complexes. All this strains are caused by both the ligand's steric and electronic properties and the complex adaptation technique to accommodate these factors. **Table 5.9.1** illustrates a summary of all the comparable bond angles and The *Effective Tolman-based N-substituent steric effect* ($\theta_{N\text{-}sub}$) values.

Table 5.9.1: Selected bond angles and *Effective Tolman-based N-substituent steric effect* ($\theta_{N\text{-}sub}$) values for both Pt and Pd – PNP complexes

Metal Complexes	**P1 – M – P2**	**P1 – N1 – P2**	$\theta_{N\text{-}sub}$ **(Coordinated ligands)**
Pd(Cl-Ph-PNP)Cl_2 **(D)**	81.30(8)	107.5(3)	36.7
Pt(5-*p*-tolyl-PNP)Cl_2 **(A)**	72.95(4)	100.2(2)	33.7
Pd(5-*p*-tolyl-PNP)Cl_2 **(E)**	72.48(2)	100.1(9)	33.7
Pt(4-*p*-tolyl-*o*-tol)Cl_2 **(B)**	72.97(5)	99.44(2)	42.2
Pt(Cbutyl-4-*p*-tolyl)Cl_2 **(C)**	71.73(4)	99.49(17)	73.2
Pd(Chzyl-4-*p*-tolyl)Cl_2 **(F)**	71.80(3)	99.27(11)	80.9

Complex **A** and **E** both contain the 5-*p*-tolyl-PNP ligand; the only difference between these two complexes is the metal centre, Platinum and Palladium respectively. Both metals fall under the Platinum Group Metals family (PGM) and thus they have similar properties.[20] The atomic radius and the electronegativity of these metals are highly comparable and thus one would expect complex **A** and **E** to be isostructural. The atomic radius and the electronegativity of Pallatium are 137 pm and 2.2, while for Platinum are 138.5 pm and 2.2 respectively.[26] In order to determine whether these complexes were isostrustural, a visual comparison between complex **A** and **E** was performed, and this initially showed that the two complexes were not isostructural (see **Figure 5.9.1**, RMS = 1.44). But after rotating one of the complexes the two complexes became isostructural as illustrated by **Figure 5.9.1**, for this reason we believe that if we invert one of the complexes then perform a visual comparisons, the structures would become isostructural without any rotation. The RMS value used is a parameter used to quantify structures believed to be similar. The lower the RMS value the more similar are the compared structures.

[26] N.N. Greenwood, A. Earnshaw, *Chemistry of the Elements* 2nd Ed., Great Britain: Butterworth-Heinemann Publishers, **1997**.

Before Rotation **After Rotation**

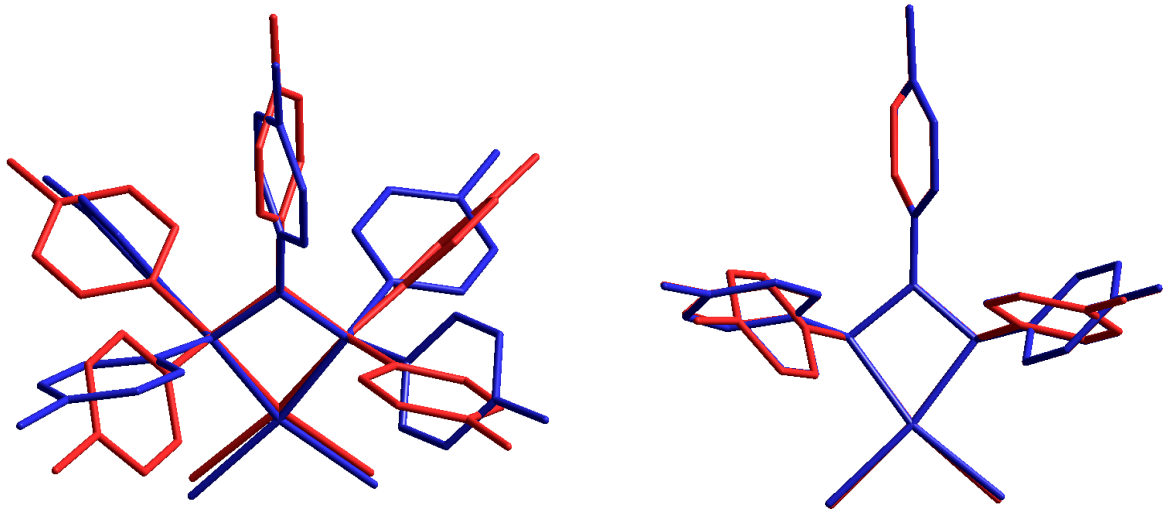

Figure 5.9.1 An overlay of the isostructural complexes [Pd(5-*p*-tolyl-PNP)Cl2] (**blue**) and [Pt(5-*p*-tolyl-PNP)Cl2] (**red**). RMS value = 1.44

5.10 Conclusion

X-ray diffraction studies confirmed the successful synthesis of six single crystals metal complexes. Out of these, five contained unique diphosphinoamine ligands proving further the successful synthesis of five ligands out of seven ligands synthesized in this study and the successful coordination of these ligands to either platinum or palladium metal centers. X-ray diffraction studies further proved the contributions of the steric bulky and the phenyl ring arrangement of diphosphinoamine ligands in stabilizing the molecule. All the crystal structures were stabilized by a few C-H…π interactions and some by further intra and intermolecular hydrogen bondings.

This study further illustrated that two of the synthesized complexes were isostructural. These complexes displayed similar unit cell dimensions, space groups, crystal systems, molecular packing, π-π stacking and intermolecular hydrogen bonding. **Table 5.9.1** contains some of the important values and findings obtained in this study. From **Table 5.9.1** it can be concluded that all the M-P bond lengths were in agreement for each respective metal.

CHAPTER 5

In this chapter, X-ray diffraction studies were used to elucidate the structures of diphosphinoamine ligand containing metal complexes synthesized in **Chapter 4**. Ligand steric and electronic effects on the catalytic hydroformylation reaction will be investigated and discussed in **Chapter 5**.

6 Hydroformylation of 1-octene

Abstract

In this chapter the catalytic evaluation of various Rh-PNP on the hydroformylation of 1-octene is presented. The relation between the measured ligand steric parameter and the catalyst reactivity is also discussed.

6.1 Introduction

As stated in **Chapter 2**, hydroformylation reaction is the addition of a formyl group (CHO) on alkenes (olefins) to form an aldehyde.[1] In this study, the preliminary catalytic hydroformylation of 1-octene with various diphosphinoamine (PNP) were performed and are discussed. All the PNP ligands used, were synthesized as described in **Chapter 4** and are displayed in **Figures 6.1** and **6.2**. The PNP ligands were strategically synthesized based on the steric and electronic properties as it has been reported in literature that these two parameters have a significant influence on the activity and selectivity of phosphine ligand containing catalysts in a hydroformylation reaction.[2,3,4] A modified Tolman steric parameter was used in **Chapter 5** to calculate the steric demands of all synthesized PNP ligands, and the values obtained will be correlated to the activity and selectivity of the catalyst in this chapter. The electronic properties of these synthesized ligands (see **Figure 6.1**) have not been fully studied. However, from using the ^{31}P NMR of Pt-PNP we can confidently say that their electronic properties are considerably different.

[1] R. Meijboom, M. Haumann, A. Roodt, L. Damoense. *Helv. Chim. Acta*., **2005**, *88* , 676.

[2] A. van Rooy, J.N.H. de Bruijn, C.F. Roobeek, P.C. Kamer, P.W.N.M. van Leeuwen. *J. Organomet. Chem*., **1996**, *507*, 69.

[3] M. Kranenburg, P.C.J. Kamer, P.W.N.M. van Leeuwen, D. Vogtb, W. Keim, *J. Chem. Soc., Chem. Commun*., **1995**, 2177.

[4] 3 T. Hayashi, T. Kawabata, T. Isoyama, I. Ogata, *Bull Chem. Soc. Jpn*., **1981**, *54*, 3438.

Casey *et al*. observed that the selectivity towards linear aldehyde production in catalytic hydroformylation with rigid diphosphanes was significantly high for ligands with chelate bite angles close to 120 °.[5,6,7] However, the bite angles of the ligands synthesized in this study range from 71.80(3) to 81.30(8) °. Since these are small values when compared to the 120 ° reported by Casey *et al*. the effect of bite angles will not be evaluated.

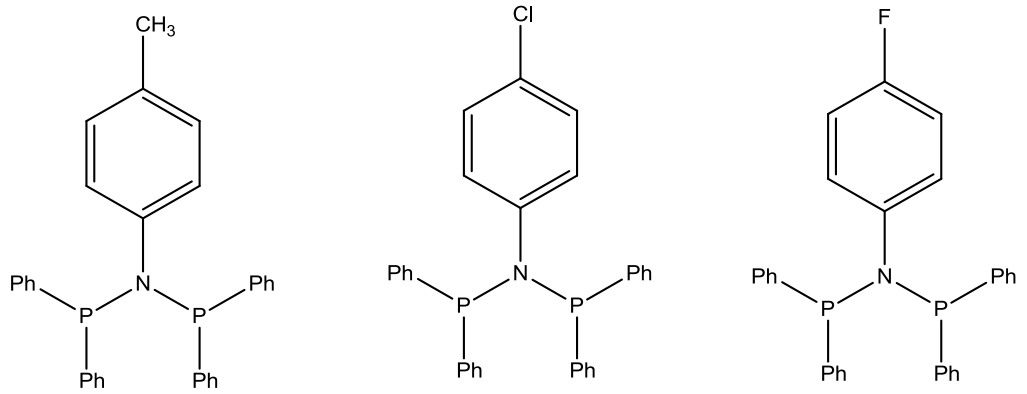

Figure 6.1: Diphosphinoamine ligands (PNP ligands) synthesized in this study for ligand electronic effects on hydroformylation: **1** CH_3-Ph-PNP, **2** Cl-Ph-PNP, **3** F-Ph-PNP.

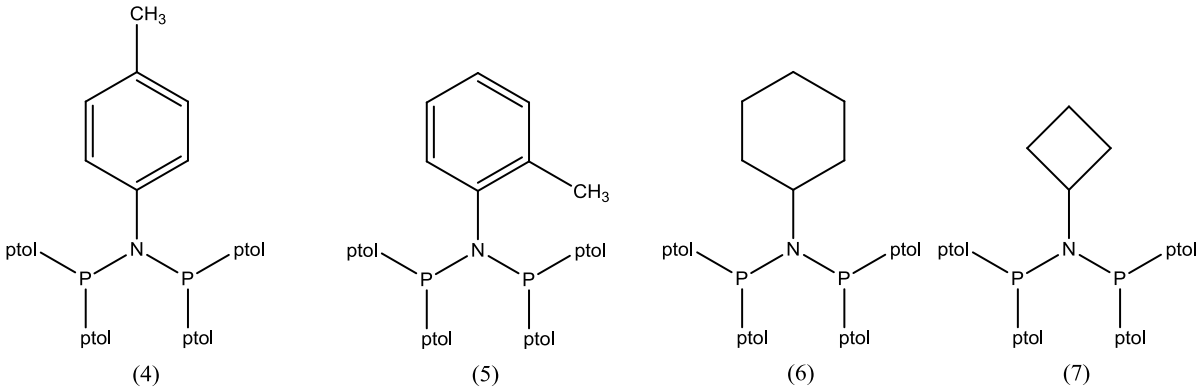

Figure 6.2: Diphosphinoamine ligands (PNP ligands) synthesized in this study for ligand steric effects on hydroformylation: **4** *5-p*-tolyl-PNP, **5** 4-*p*-tolyl-*o*tol, **6** Chzyl-4-*p*-tolyl and **7** Cbutyl-4-*p*-tolyl.

[5] L.A. Van der Veen, P.C.J. Kamer, P.W.N.M. Van Leeuwen. *Angew. Chem. Int. Ed*., **1999**, *38*, 3

[6] C. P. Casey, G. T.Whiteker, M. G. Melville, L. M. Petrovich, J. A. Gavney Jr., D. R.Powell. *J. Am. Chem. Soc*., **1992**, *114*, 5535

[7] C. P. Casey, L. M. Petrovich. *J. Am. Chem. Soc*., **1995**, *117*, 6007.

Generally every catalytic reaction requires its own optimization studies and this requires extensive reaction conditions analysis. Thus, the results that are reported in this chapter are of a preliminary level. A more complete investigation will also be reported in the near future.

6.2 Experimental

6.2.1 General

Unless stated otherwise, all chemicals were GC grade and were used without further purification. Toluene, 1-octene and dodecane were purchased from Sigma Aldrich, while rhodium(III)chloride hydrate was obtained from Strem Chemicals. See **Chapter 4** for synthesis and characterisation of all PNP ligands used. Hydroformylation reaction samples were analysed on a Shimadzu GC-2010 gas chromatography fitted with a Flame Ionisation Detector (FID) and Agilent Technologies HP-1 30 m column with a 0.252 mm internal diameter and 0.25 μm film thickness. Supplementary data (**Appendix A**) provides all the areas of the stating material, the internal standards and the product; together with the calculated percentage yields.

6.2.2 (Acetylacetonato)dicarbonylrhodium(I) ([Rh(acac)(CO_2)]) synthesis

A drop of water was added to a mixture of rhodium(III)chloride hydrate (0.1002 g, 0.3806 mmol) and dimethylformamide (2 ml). The reaction mixture was then refluxed at 180 °C for 30 min (until the color of the solution was yellow). Acetylacetone (42.7 μl, 0.4290 mmol) was then added with vigorous mixing. A small amount of ice cold water was added to the reaction mixture and the formed precipitates was collected by centrifuging. After decanting the water, the product was dissolved in dichloromethane (5 ml) and left overnight to crystallize. Yield 80.6 mg (75.9 %). υ_{max}/cm^{-1} 1993, 2061 (CO).

6.2.3 Hydroformylation

All hydroformylation experiments were carried out in a 100 ml PARR model 4560 stainless hastelloy autoclave equipped with a temperature control unit, an internal mechanical stirrer and a sampling valve. Reaction mixtures loaded in to a reactor contained a PNP ligand (0.05 mmol), 1000 eq. 1-octene, toluene (40 ml) and dodecane (~2.0 g) as an internal standard. The reactor was flushed three times with argon and heated to 80 °C while stirring at ~250 rpm. When the chosen temperature was reached, a substrate vessel containing 1 eq. [Rh(acac)($CO)_2$] in toluene

(10 ml) was fitted and the catalyst precursor was injected into the reactor by a CO/H_2 (1:1) gas at a constant pressure of about 20.0 bar for 24 hours. Unless stated otherwise, sampling was performed at 30 min intervals for the first 3 hours then the last sample was taken on the 24th hours. Samples vials containing 250 µl of the reaction mixture and toluene (750 µl) were analyzed on a temperature controlled GC. General calculations were completed using the following equations:

- % Conversion = [n(1-octene)$_{out}$ / n(1-octene)$_{in}$] x 100
- % Nonanal Yield = [n(nonanal)$_{out}$ / n(1-octene)$_{converted}$] x 100
- % Isomerisation = [n(2-octene)$_{out}$ / n(1-octene)$_{converted}$] x 100
- Turn over number (TON) = (% conv /100) x n(1-octene) / n(catalyst)
- Turn over frequency (TOF) = TON / time (h)
- Linear:Branched ratio (l:b) = 1-nonanal / 2-methyloctanal

6.3 Results

The aim of this study was to investigate the PNP ligand steric and electronic influence on the selectivity of a Rh-PNP catalyst in hydroformylation of 1-octene towards the desired linear product. To achieve this, a number of PNP ligands were synthesized (see **Figures 6.1** and **6.2**). It was decided that only the steric influence of the substituent on the N atom of the PNP ligands will be investigated as it has been reported in literature that they have a significant influence on the selectivity of a catalyst.[8] To achieve this, a modified Tolman cone angle (*The Effective Tolman cone angle* [$\theta_{N\text{-sub}}$]) was utilized to calculate the steric bulk of these substituents.[9] **Table 6.1** shows the calculated $\theta_{N\text{-sub}}$ for only the PNP ligands that were analyzed with X-ray diffraction in **Chapter 5**. Note these $\theta_{N\text{-sub}}$ values will later be correlated to the selectivity of their respective catalysts and that the subject of the subsequent studies is to calculate $\theta_{N\text{-sub}}$ for all synthesized ligands. These ($\theta_{N\text{-sub}}$) values were not calculated for free PNP ligands but PNP coordinated ligands to Pt(II) and Pd(II) metal centres. However, we assume the values for the

[8] S. Kuhlmann, K. Blann, A. Bollmann, J.T. Dixon, E, Killian, M.C. Maumela, H. Maumela, D.H. Morgan, M. Pretorius. *J. Catal*., **2007**, *245*, 279.

[9] N. Cloete, H.G. Visser, I. Engelbrecht, M.J. Overett, W. F. Gabrielli, A. Roodt., *Inorg. Chem*. **2013**, *52*, 2268.

free and metal coordinated ligands will be the similar as it was observed by Cloete *et al*.[9,10] In the case of 5-*p*-tolyl-PNP an average of the values reported in **Chapter 5** was taken.

Table 6.1: *Effective Tolman-based N-substituent steric effect* ($\theta_{N\text{-}sub}$) values for some PNP ligands

PNP ligands	$\theta_{N\text{-}sub}$
Cl-Ph-PNP (**2**)	36.7
5-*p*-tolyl-PNP (**4**)	33.7
4-*p*-tolyl-*o*-tol (**5**)	42.2
Chzyl-4-*p*-tolyl (**6**)	80.6
Cbutyl-4-*p*-tolyl (**7**)	73.2

The current industrial rhodium catalyst used is [$RhHCO(PPh_3)_3$]. Therefore, it is scientifically fair to compare our results to that of a PPh_3 ligand.[11] All reactions were performed in triplicate and **Tables 6.2** and **6.3** show the average of the obtained results.

Table 6.2: Rh-PNP based hydroformylation of 1-octene after 3 hours

Ligand	M:L ratio	Time (min)	Conversion (%)	Linear aldehyde (%)	Isomerisation (%)	l:b ratio[b]	TOF (h^{-1})	$\theta_{N\text{-}sub}$ (°)
1	1:1	180	98	20.8	62.0	1.2:1	313	33.1[c]
2	1:1	180	98	34.8	45.5	1.8:1	310	36.7
3	1:1	180	97	35.1	38.2	1.4:1	318	-
4	1:1	180	98	20.3	63.8	1.3:1	320	33.7
5	1:1	180	98	22.8	59.4	1.3:1	324	42.2
6	1:1	180	97	28.5	53.6	1.6:1	310	80.6
7	1:1	180	98	25.5	58.3	1.7:1	310	73.2
PPh_3	1:2	120	98	50.8	26.3	1.9:1	470	145[a]

[a] Ref 12 and 13, [b] 1:b = linear-to-branched (2-methyloctanal) selectivity, c Ref 15, all values reported are an average of 3 set of reactions.

[10] N. Cloete. *PhD thesis*, University of the Free State, Bloemfontein, South Africa, **2009**.

[11] P.W.N.M. van Leeuwen, C. Claver (Eds.). *Rhodium Catalyzed Hydroformylation*, Kluwer Academics Publishers, Dordrecht, **2000**.

[12] C.A. Tolman, *Chem. Rev*., **1977**, *77*, 313.

Because PPh_3 is used in large scales in industry, our values are compared to those reported by Engelbrecht *et al*. who used a 1:2 eq ($M:PPh_3$) which is comparable to the 1:1 ratio used in this study.[13]

Table 6.3: Rh-PNP based hydroformylation of 1-octene after 24 hours.

Ligands	M:L ratio	Time (h)	Conversion (%)	Linear aldehyde (%)	Isomerisation (%)	l:b ratio[b]	TOF (h^{-1})	$\theta_{N\text{-}sub}$ (°)
4	1:1	24	99	42.3	11.9	0.92:1	41	33.7
5	1:1	24	99	37.1	22.6	0.92:1	41	42.2
6	1:1	24	99	39.8	12.5	1.1:1	39	80.6
7	1:1	24	99	39.5	19.9	1.0:1	39	73.2
PPh_3	1:2	2	98	50.8	26.3	1.9:1	470	145[a]

[a] Ref 12 and 13, [b] 1:b = linear-to-branched (2-methyloctanal) selectivity, all values reported are an average of 3 set of reactions.

When arranged in an electron withdrawing order, the substituents on ligand **1**, **2** and **3** follows the trend $–CH_3 << –Cl < –F$.[14] The selectivity towards linear products increases with an increase in the electron withdrawing properties from 20.8 % ($–CH_3$) to 35.1 % (–F). The $\theta_{N\text{-}sub}$ steric properties of ligand **1** (33.1°)[15], **2** (36.7°) and **3** (not reported) are comparable; and the assumption is therefore made that the primary differences in chemical character is due to the specific electronic property of the respective ligand. **Figure 6.3** shows a combined relation between the linear and the isomerized products for ligand **1**, **2** and **3**, while **Figure 6.4** shows a graph of the relationship between the production of nonanal (linear product) and electron withdrawing groups. The production of the isomerized products tends to decrease with an increase in the electron withdrawing ability of the ligands. For ligand **1**, **2** and **3** the percentage production of the isomerized product is 62.0, 45.5 and 38.2 % respectively.

[13] I. Engelbrecht, *PhD thesis*, University of the Free State, Bloemfontein, South Africa, **2013**.

[14] O. Nicolas, M. Marcos, M.A. Ricardo, *J. Phys. Chem. A*, **2007**, *111* (25), 5557.

[15] V.W.W. Yam, E.C.C. Cheng, N. Zhu, *Angew. Chem. Int. Ed*, **2001**, *40*, 1763.

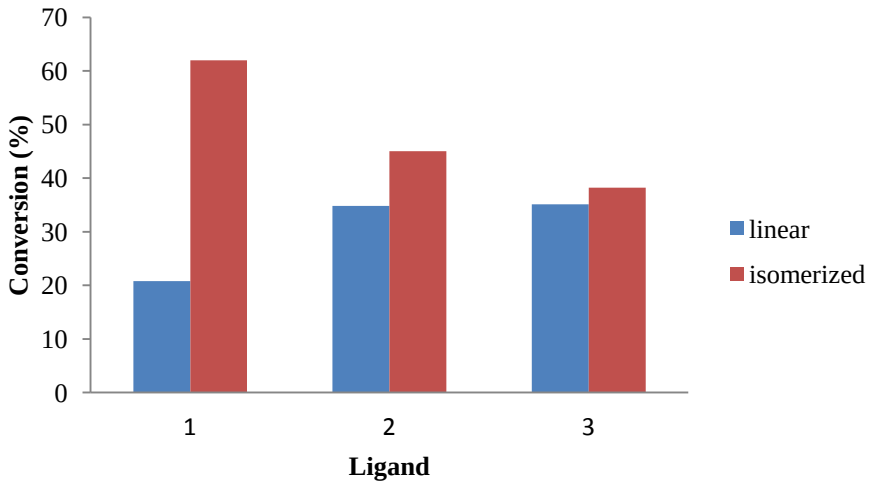

Figure 6.3: Combined results for hydroformylation of 1-octene with a Rh-(PNP) catalyst, PNP = ligand **1**(Cl-Ph-PNP), **2** (CH_3-Ph-PNP) and **3** (F-Ph-PNP).

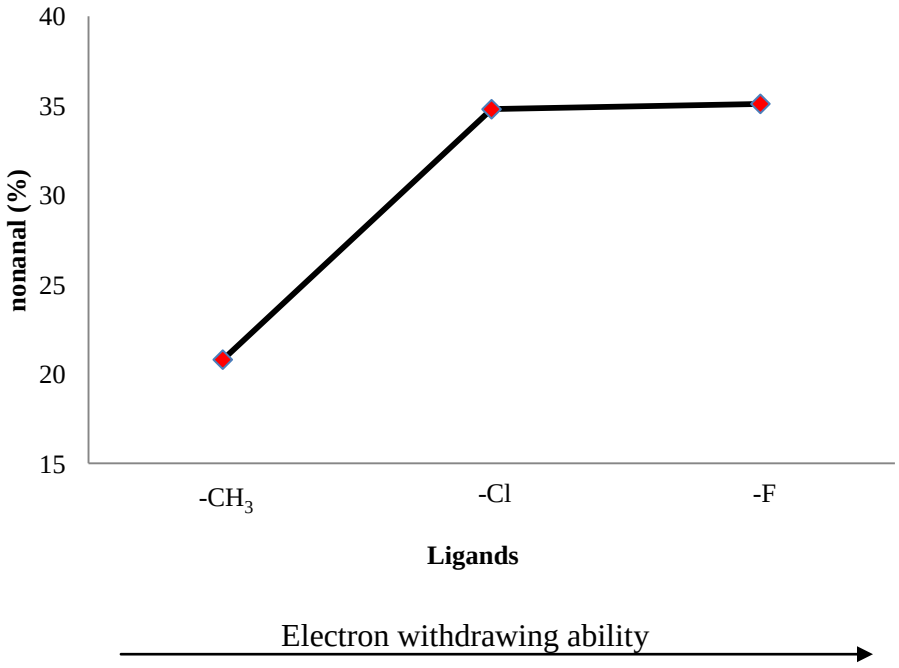

Figure 6.4: A graph of the relationship between the production of nonanal (linear product) and electron withdrawing groups.

The ligands **4**, **5**, **6** and **7** all produced low amounts of linear product after 3 hours as indicated in **Figure 6.5**, but with significantly different percentage yield. The production of the linear product seems to increase with an increase in the steric bulk on the N atoms of the PNP ligand as shown

in **Figure 6.6**. The linear product production remained more than the branched product for the first 3 hours and the percentage conversion reached close to 98 % for all these reactions during the sampling period (see **Figure 6.7**).

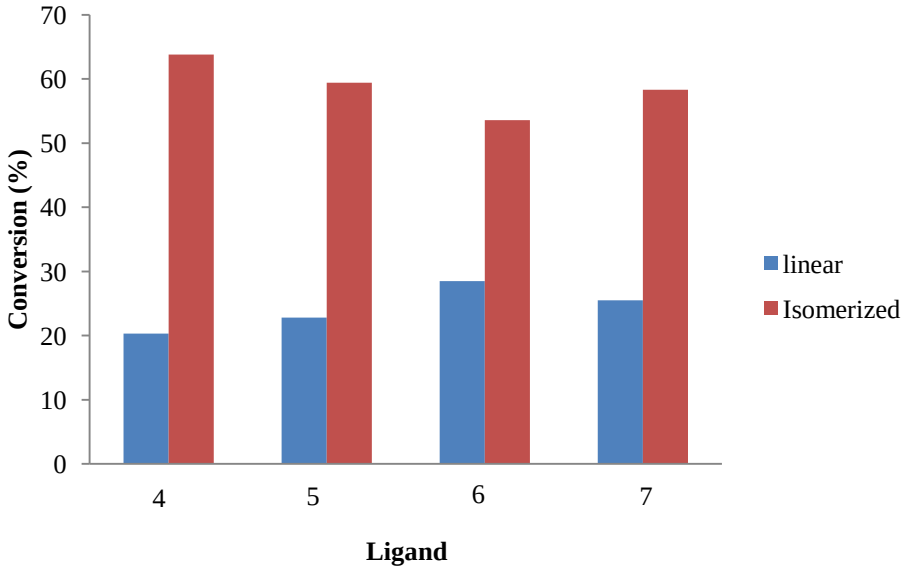

Figure 6.5: Combined results for hydroformylation of 1-octene with a Rh-(PNP) catalyst, PNP = ligand **4**, **5**, **6** and **7** after 3 hours.

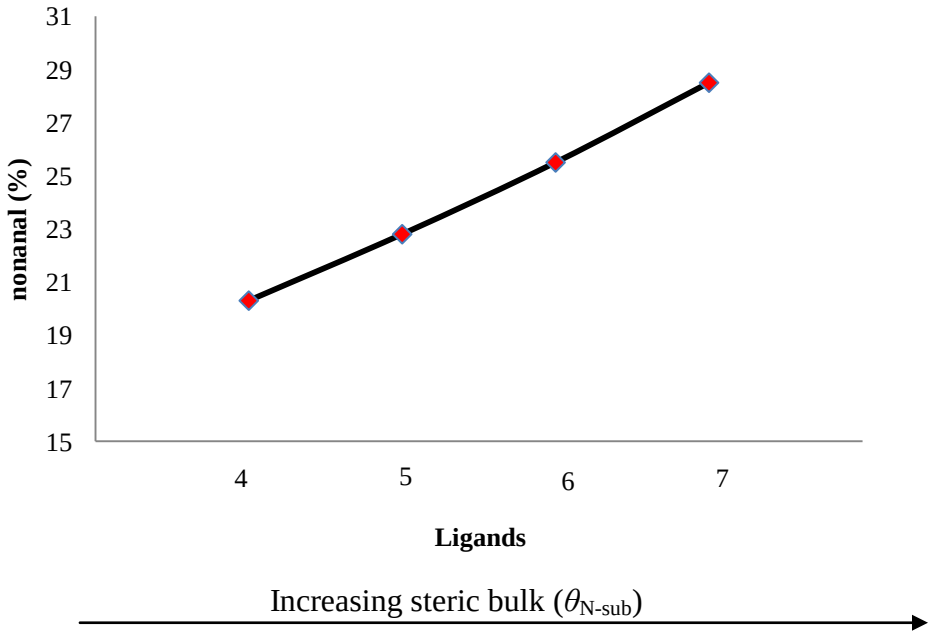

Figure 6.6: A graph of the relationship between the production of nonanal (linear product) and steric bulk on the N atom of the PNP ligand.

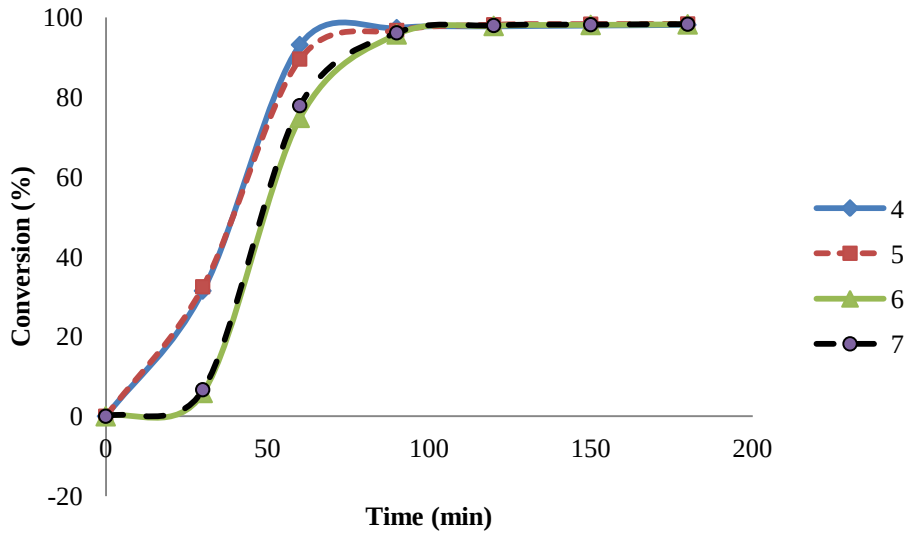

Figure 6.7: Conversion as a function of time for hydroformylation of 1-octene with a Rh-(PNP) catalyst, PNP = ligand **4**, **5**, **6** and **7**.

When experiments with ligand **4**, **5**, **6** and **7** were left to run overnight (24 h), an increase in both the branched and the linear products was observed as shown in **Figure 6.8**. All the ligands showed a higher selectivity towards the branched product. A 99 % conversion was observed after 24 h for all reactions.

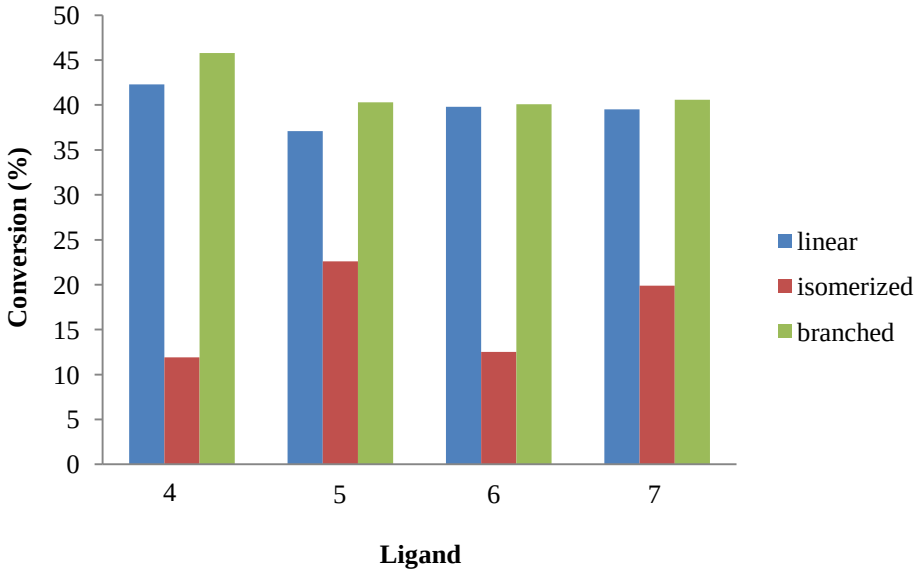

Figure 6.8: Combined results for hydroformylation of 1-octene with a Rh-(PNP) catalyst, PNP = ligand **4**, **5**, **6** and **7** after 24 hours. Note that branched = Product 2 from **Figure 6.9**.

6.4 Discussion

In this study, seven different PNP ligands were investigated as potential ligands on the Rh-PNP based hydroformylation of 1-octene. Ligand **1**, **2** and **3** had different electronic effects on the N atom of the PNP ligands (see **Figure 6.1**), while Ligand **4** to Ligand **7** had different steric demands on the N atom of the PNP ligands (see **Figure 6.1**). Improved linear product yields were obtained when the electron withdrawing ability and the steric demands on the N atom were higher. All reactions proceeded to a conversion of approximately 98% in 3h. However, in all reactions isomerization of 1-octene was faster and thus gave higher product yields (indicated in **Figure 6.3** and **6.5**) than the intended 1-octene to nonanal hydroformylation reaction (**Figure 6.9**).

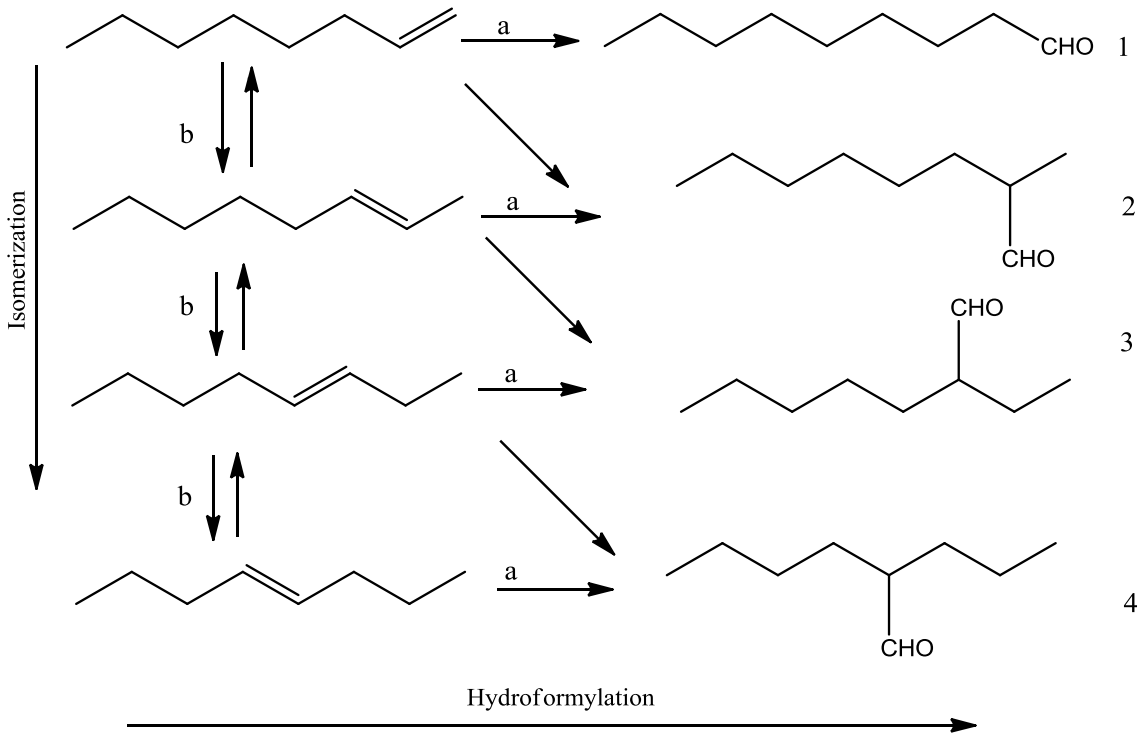

Figure 6.9: 1-Octene hydroformylation and isomerization reaction; (a) hydroformylation, (b) isomerization.[16,17]

[16] S. Shirakawa, S. Shimizu, Y. Sasaki, *New J. Chem.*, **2001**, *25*, 777.

[17] S.L. Desset, S.W. Reader, D.J. Cole-Hamilton, *Green Chem,*. **2009**, *11*, 630.

The problem faced in hydroformylation reactions is that all the used and tested catalysts do not only catalyze linear alkenes to aldehydes, but they also isomerize the starting material. This was also observed in our study where:

- Ligand **1** gave 20.8% nonanal and 79.2% isomerized and branched products;
- Ligand **2** gave 34.8% nonanal and 65.2% isomerized and branched products;
- Ligand **3** gave 35.1% nonanal and 64.9% isomerized and branched products;
- Ligand **4** gave 20.3% nonanal and 79.7% isomerized and branched products;
- Ligand **5** gave 22.8% nonanal and 77.2% isomerized and branched products;
- Ligand **6** gave 28.5% nonanal and 71.5% isomerized and branched products;
- Ligand **7** gave 25.5% nonanal and 74.5% isomerized and branched products.

The results were all obtained in 3 h. Ligand **3** gave the highest nonanal production even though it is believed to have a low steric bulk on the N atom comparable to ligand **1** and **2**. The only difference between ligand **3** and the others is the electronic effects on the N atom.

As mentioned before, an increase of the linear product production was observed when a systematic increase in ligand electron withdrawing ability and steric bulk were systematically increased. However, it is believed that the electron withdrawing factor has greater influence than the steric bulk as shown by the best three ligands indicated in **Table 6.4**. The ligands that gave higher linear product yields had relatively small steric bulkiness on the N atom but significantly distinct electronic effects. The findings agree with those reported by Engelbrecht *et al*. which suggests that the steric effects of the PNP ligand functionalities area significant contributing factor to the linear product selectivity.[13]

Table 6.4: Rh-PNP based hydroformylation of 1-octene after 3 hours, the best three ligands with the highest selectivity.

Ligand	M:L ratio	Time (min)	Conversion (%)	Linear aldehyde (%)	Isomerisation (%)	l:b ratio[a]	TOF (h^{-1})	$\theta_{N\text{-}sub}$ (°)
3	1:1	180	97	**35.1**	38.2	1.4:1	318	-
2	1:1	180	98	**34.8**	45.5	1.8:1	310	36.7
6	1:1	180	98	**28.5**	53.6	1.7:1	310	80.6

[a] 1:b = linear-to-branched (2-methyloctanal) selectivity, all values reported are an average of 3 set of reactions.

When ligands **4**, **5**, **6** and **7** hydroformylation reactions were allowed to run for 24 hours, not only were higher linear product yields obtained, but higher branched (**product 2** from **Figure 6.9)** product yield was also observed. The branched product yield was higher than the linear product in all reactions but calculation of TOF on the reaction indicated a very low TOF value.

6.5 Conclusion

In conclusion, a range of PNP ligands were investigated with regards to their rhodium based alkene hydroformylation reaction using 1-octene as a substrate. Higher reaction rates were obtained by careful choice of a more sterically bulky or a more electron withdrawing PNP ligand especially when these effects were on the N atom of the ligand. The most promising ligand had high electron withdrawing ability, thus we propose that electronic effects may affect the activity of a catalyst at the same level as the steric property as observed by Cloete *et al.* [9] on ethylene tri- and tetramerization with sterically bulky PNP ligands. Although after 24 h over 90% aldehydes (this includes aldehydes from the isomerized alkene, see **Figure 6.9**) were formed, the level of selectivity for a linear product (1-nonanal) was still not sufficient enough for studies to be conducted on scaled up volumes.

Chapter 7 will highlight some of the objectives that are currently in progress and the future work to be put in place concerning the improvement of the catalyst's selectivity for the desired linear aldehyde.

7 Evaluation of this study

Abstract

In this chapter, the results obtained during the course of this study, are evaluated on the basis of their scientific relevance and success.

7.1 Scientific relevance and results obtained

The aim of this study was to synthesize and evaluate various diphosphinoamine (PNP) ligands with regards to their rhodium based 1-octene hydroformylation reaction. The main focus was on the investigation of the structural effects (i.e. the electronic and steric properties) when the R_2 group (see **Figure 7.1**) on the N atom is systematically varied. The following ligands were successfully synthesised for this purpose: CH_3-Ph-PNP (**1**), Cl-Ph-PNP (**2**), F-Ph-PNP (**3**), 5-*p*-tolyl-PNP (**4**), 4-*p*-tolyl-*o*-tol (**5**), Chzyl-4-*p*-tolyl (**6**) and Cbutyl-4-*p*-tolyl (**7**). Ligand **1**, **2** and **3** were chosen as electronically distinct ligands, while ligand **4**, **5**, **6** and **7** were chosen as sterically distinct ligands. To study the coordination chemistry of the bidentate ligands, a selected range of complexes of the type [Pt(PNP)Cl_2] and [Pd(PNP)Cl_2] were synthesized and crystallized for X-ray diffraction studies.

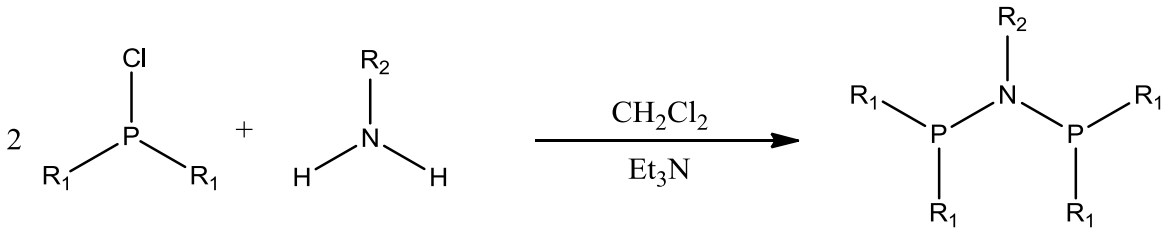

Figure 7.1: General method for the synthesis of diphosphinoamine (PNP) ligands

All the given aims of this study were successfully reached. The ^{31}P and ^{1}H NMR studies confirmed the successful synthesis of all seven ligands, while XRD studies were conducted on five out of seven of these ligands. The Gas-Chromatography (GC) studies verified the successful

conversion of 1-octene to 1-nonanal, the isomerisation of 1-octene and the conversion of these isomerized products to their respective aldehydes. Interesting results were obtained when the electronic and the steric effects of the R_2 group were systematically increased. An increase in the electron withdrawing ability of the R_2 group resulted in an increase in the production of the desired linear 1-octene hydroformylation product. Similarly, an increase in the steric bulk of the R_2 group resulted in an increase on the production of this desired product. Additionally, six crystal structures namely [Pt(5-*p*-tolyl-PNP)Cl_2], [Pt(4-*p*-tolyl-*o*-tol)Cl_2], [Pt(Cbutyl-4-*p*-tolyl)Cl_2], [Pd(5-*p*-tolyl-PNP)Cl_2], [Pd(Cl-Ph-PNP)Cl_2] and [Pd(Chzyl-4-*p*-tolyl)Cl_2] were successfully analyzed and this assisted with the calculation of the *effective Tolman-based N-substituent steric effect* ($\theta_{N\text{-}sub}$) (discussed in detail in **Chapter 2**).

Unfortunately, we were unable to calculate $\theta_{N\text{-}sub}$ for metal complexes containing ligand **1** and **3** but from literature studies we were able to obtain $\theta_{N\text{-}sub}$ for ligand **1**. One of the major challenges of working with tertiary phosphine ligands is that they are usually air and moisture sensitive. This was observed in this study with some of the phosphine precursors; all of the alkylated phosphine precursors oxidized during sampling before they could even react with the chosen amine precursor. Another challenge was observed during crystallization, some of the metal complexes could not be dissolved in any available solvent and thus their crystal structures were not obtained.

7.2 Future research

Based on the challenges and the results obtained in this study, the following set of objectives will be attempted for future research:

- Synthesize more electronically and sterically distinct PNP ligands;
- Conduct [Pt(PNP)Cl_2] and [Pd(PNP)Cl_2] based catalytic reactions;
- Investigate further the correlation between the ligands electronic effects and the catalyst selectivity;
- Perform theoretical calculations for the synthesized ligands and compare the $\theta_{N\text{-}sub}$ values with the experimental ones;

- Optimize the catalysts selectivity by varying the reaction conditions such as the temperature, pressure and catalyst concentration;
- Investigate the synthesized ligands as potential ligands in chromium base ethylene tri- and tetramerization;
- Perform High Pressure (HP) NMR and HP IR studies to gain further insight regarding possible intermediates;
- Synthesize Rh-PNP complexes for X-ray diffraction studies.

Hydroformylation has been intensively studied since the discovery by Otto Roelen. Although the understanding of the reaction mechanism is believed to be nearing completion, there's still room for catalyst improvement. Since some of the reported data in this study are novel, the results obtained are hoped to one day assists in the synthesis of a highly active and selective hydroformylation catalyst.

APPENDIX

A: Crystallographic data for [Pd(Cl-Ph-PNP)Cl_2]

Table A.1: Fractional Atomic Coordinates ($\times 10^4$) and Equivalent Isotropic Displacement Parameters ($Å^2 \times 10^3$) for [Pd(Cl-Ph-PNP)Cl_2].

Atom	*x*	*y*	*z*	U(eq)
C1	1432(7)	6727(4)	3188(3)	18.3(14)
C2	2143(7)	6816(5)	3866(4)	23.5(15)
C3	1408(8)	6799(5)	4316(4)	25.1(16)
C4	-35(7)	6689(5)	4090(3)	23.1(15)
C5	-753(8)	6587(4)	3426(4)	23.0(16)
C6	-17(7)	6602(4)	2971(4)	20.3(15)
C11	4778(7)	5839(5)	3347(4)	21.8(15)
C12	4574(8)	5012(4)	3022(4)	25.5(16)
C13	5019(8)	4241(5)	3382(4)	32.1(19)
C14	5705(9)	4285(5)	4063(5)	39(2)
C15	5954(8)	5088(5)	4382(4)	31.8(18)
C16	5482(8)	5883(5)	4035(4)	26.4(17)
C21	4659(7)	7824(5)	3259(4)	22.5(16)
C22	6100(8)	7969(5)	3508(4)	31.4(18)
C23	6630(9)	8790(6)	3769(5)	44(2)
C24	5711(10)	9472(5)	3792(5)	46(2)
C25	4246(10)	9344(5)	3544(5)	41(2)
C26	3737(9)	8528(5)	3272(4)	29.9(18)
C31	565(7)	7719(4)	1577(3)	18.7(15)
C32	1288(8)	8515(5)	1522(4)	27.3(17)
C33	559(10)	9303(5)	1339(4)	38(2)
C34	-880(9)	9321(5)	1213(4)	35(2)
C35	-1623(9)	8543(6)	1258(4)	35(2)
C36	-885(8)	7749(5)	1434(4)	28.3(17)
C41	608(7)	5751(4)	1560(4)	20.5(15)
C42	-208(8)	5715(5)	890(4)	27.5(17)
C43	-935(9)	4930(5)	632(4)	32.6(19)
C44	-832(9)	4205(5)	1049(4)	36(2)
C45	-19(8)	4238(5)	1716(4)	34(2)
C46	713(8)	5011(4)	1980(4)	24.5(16)
C61	6236(18)	8242(11)	5181(9)	42(4)
N1	2213(6)	6741(4)	2719(3)	21.3(12)
P1	3991.2(19)	6790.1(12)	2847.1(9)	19.4(4)
P2	1638.4(18)	6744.7(11)	1859.3(9)	19.8(4)
Cl1	6229.3(18)	6771.5(12)	1932.1(9)	27.9(4)
Cl2	3021(2)	6745.4(12)	598.0(9)	30.8(4)

Cl3	-951(2)	6680.2(15)	4671.5(9)	35.8(5)
Pd	3784.6(6)	6756.9(3)	1776.7(3)	19.86(16)
O1	5466(10)	7541(6)	5082(5)	22(2)

Table A.2: Hydrogen Atom Coordinates (Å×10^4) and Isotropic Displacement Parameters (Å^2×10^3) for [Pd(Cl-Ph-PNP)Cl_2].

Atom	***x***	***y***	***z***	**U(eq)**
H14	3102	6882	3969	28
H15	1784	6855	4776	30
H17	-1711	6512	3329	28
H18	-398	6535	2512	24
H2	4144	4977	2568	31
H3	4864	3674	3171	38
H4	5990	3747	4294	46
H5	6433	5114	4828	38
H6	5627	6446	4252	32
H8	6709	7485	3492	38
H9	7575	8871	3923	53
H10	6026	10035	3971	56
H11	3638	9827	3570	49
H12	2797	8454	3102	36
H20	2253	8518	1608	33
H21	1044	9841	1298	46
H22	-1342	9869	1097	42
H23	-2588	8546	1173	43
H24	-1375	7209	1459	34
H26	-257	6232	615	33
H27	-1459	4913	195	39
H28	-1300	3669	900	43
H29	24	3718	1988	40
H30	1241	5020	2415	29
H31A	5850	8720	4878	64
H31B	7147	8093	5097	64
H31C	6294	8442	5645	64
H1	4689	7692	4888	33

Table A.3: Anisotropic Displacement Parameters (Å^2×10^3) for [Pd(Cl-Ph-PNP)Cl_2].

Atom	**U_{11}**	**U_{22}**	**U_{33}**	**U_{23}**	**U_{13}**	**U_{12}**
C1	20(4)	5(3)	28(4)	-1(3)	0(3)	3(3)
C2	18(4)	13(3)	38(4)	0(3)	3(3)	3(3)
C3	26(4)	15(3)	34(4)	-7(3)	2(3)	1(3)
C4	28(4)	16(3)	29(4)	3(3)	14(3)	-3(3)

C5	21(4)	12(3)	36(4)	2(3)	4(3)	0(3)
C6	27(4)	6(3)	29(4)	-4(3)	8(3)	2(3)
C11	18(4)	16(3)	33(4)	1(3)	8(3)	2(3)
C12	28(4)	13(3)	36(4)	0(3)	5(3)	1(3)
C13	33(5)	13(4)	51(5)	1(3)	11(4)	4(3)
C14	32(5)	23(4)	62(6)	13(4)	9(4)	9(4)
C15	32(5)	35(5)	30(4)	7(3)	9(4)	10(4)
C16	22(4)	24(4)	33(4)	-1(3)	7(3)	3(3)
C21	20(4)	14(3)	32(4)	0(3)	1(3)	-6(3)
C22	29(5)	21(4)	44(5)	-8(3)	3(4)	-1(3)
C23	31(5)	30(5)	70(6)	-17(4)	7(5)	-18(4)
C24	57(6)	15(4)	68(6)	-15(4)	12(5)	-13(4)
C25	51(6)	12(4)	59(6)	-6(4)	10(5)	3(4)
C26	37(5)	16(4)	37(4)	-4(3)	6(4)	1(3)
C31	20(4)	13(3)	22(4)	4(3)	2(3)	1(3)
C32	29(4)	14(3)	39(4)	-3(3)	4(4)	-2(3)
C33	53(6)	11(4)	52(5)	4(3)	13(5)	2(4)
C34	49(6)	23(4)	32(4)	0(3)	9(4)	15(4)
C35	36(5)	36(5)	38(5)	9(4)	15(4)	10(4)
C36	29(4)	24(4)	34(4)	4(3)	12(4)	3(3)
C41	24(4)	8(3)	31(4)	-3(3)	8(3)	-4(3)
C42	33(5)	20(4)	32(4)	-3(3)	12(4)	-4(3)
C43	35(5)	32(4)	32(4)	-8(3)	11(4)	-9(4)
C44	37(5)	17(4)	57(6)	-15(4)	17(4)	-11(3)
C45	36(5)	11(4)	56(5)	-1(3)	16(4)	-13(3)
C46	22(4)	16(3)	37(4)	1(3)	10(3)	-5(3)
C61	42(4)	44(4)	41(4)	1(2)	8(2)	1(2)
N1	15(3)	14(3)	35(3)	-1(3)	4(3)	0(2)
P1	20.7(9)	9.1(8)	28.4(9)	0.0(7)	4.1(7)	-1.8(7)
P2	19.8(9)	8.1(8)	31.1(9)	0.4(7)	3.4(7)	-2.1(7)
Cl1	23.0(9)	22.0(9)	39.2(10)	2.9(8)	7.3(8)	-2.1(8)
Cl2	42.8(11)	17.9(8)	29.6(9)	4.3(7)	0.3(8)	-0.3(8)
Cl3	32.3(11)	47.2(12)	29.5(10)	-0.3(9)	10.0(8)	-3.9(10)
Pd	20.9(3)	9.6(2)	29.0(3)	2.0(2)	4.0(2)	-1.5(2)
O1	24(3)	22(3)	22(3)	-4.6(18)	8.3(19)	2.9(18)

Table A.4: Bond Lengths for [Pd(Cl-Ph-PNP)Cl_2].

Atom	Atom	Length/Å	Atom	Atom	Length/Å
C1	C2	1.446(10)	C31	C32	1.405(10)
C1	C6	1.451(9)	C31	C36	1.429(10)
C1	N1	1.329(9)	C31	P2	1.842(7)
C2	C3	1.265(10)	C32	C33	1.403(10)

C3	C4	1.446(10)	C33	C34	1.417(12)
C4	C5	1.423(10)	C34	C35	1.391(12)
C4	Cl3	1.612(7)	C35	C36	1.411(11)
C5	C6	1.276(10)	C41	C42	1.464(10)
C11	C12	1.400(10)	C41	C46	1.390(10)
C11	C16	1.453(10)	C41	P2	1.849(7)
C11	P1	1.844(7)	C42	C43	1.432(10)
C12	C13	1.397(10)	C43	C44	1.368(11)
C13	C14	1.436(12)	C44	C45	1.457(12)
C14	C15	1.368(11)	C45	C46	1.423(10)
C15	C16	1.422(10)	C61	O1	1.295(14)
C21	C22	1.458(10)	N1	P1	1.752(6)
C21	C26	1.402(10)	N1	P2	1.743(6)
C21	P1	1.829(7)	P1	Pd	2.1488(19)
C22	C23	1.405(10)	P2	Pd	2.179(2)
C23	C24	1.378(13)	Cl1	Pd	2.4089(19)
C24	C25	1.476(13)	Cl2	Pd	2.3854(19)
C25	C26	1.399(10)			

Table A.5: Bond Angles for [Pd(Cl-Ph-PNP)Cl_2].

Atom	**Atom**	**Atom**	**Angle/°**	**Atom**	**Atom**	**Atom**	**Angle/°**
C2	C1	C6	127.2(6)	C34	C35	C36	117.3(8)
N1	C1	C2	115.3(6)	C35	C36	C31	123.0(7)
N1	C1	C6	117.5(6)	C42	C41	P2	121.7(5)
C3	C2	C1	115.7(7)	C46	C41	C42	120.8(6)
C2	C3	C4	116.3(7)	C46	C41	P2	117.3(5)
C3	C4	Cl3	115.4(5)	C43	C42	C41	122.5(7)
C5	C4	C3	128.8(7)	C44	C43	C42	116.3(7)
C5	C4	Cl3	115.8(6)	C43	C44	C45	121.3(7)
C6	C5	C4	115.1(7)	C46	C45	C44	123.2(7)
C5	C6	C1	116.8(7)	C41	C46	C45	115.8(7)
C12	C11	C16	120.1(6)	C1	N1	P1	126.8(5)
C12	C11	P1	113.9(5)	C1	N1	P2	125.7(5)
C16	C11	P1	125.8(5)	P2	N1	P1	107.5(3)
C13	C12	C11	118.2(7)	C11	P1	Pd	119.9(2)
C12	C13	C14	121.6(7)	C21	P1	C11	108.2(3)
C15	C14	C13	121.0(7)	C21	P1	Pd	116.5(2)
C14	C15	C16	118.7(7)	N1	P1	C11	112.1(3)
C15	C16	C11	120.3(7)	N1	P1	C21	112.6(3)
C22	C21	P1	123.1(5)	N1	P1	Pd	85.9(2)
C26	C21	C22	119.7(7)	C31	P2	C41	105.7(3)
C26	C21	P1	116.9(6)	C31	P2	Pd	119.8(2)

C23	C22	C21	123.2(7)	C41	P2	Pd	118.8(2)
C24	C23	C22	116.6(8)	N1	P2	C31	112.9(3)
C23	C24	C25	121.4(7)	N1	P2	C41	113.4(3)
C26	C25	C24	121.3(8)	N1	P2	Pd	85.2(2)
C25	C26	C21	117.8(8)	P1	Pd	P2	81.30(8)
C32	C31	C36	118.4(6)	P1	Pd	Cl1	86.94(7)
C32	C31	P2	114.5(5)	P1	Pd	Cl2	167.02(7)
C36	C31	P2	127.1(5)	P2	Pd	Cl1	168.23(7)
C33	C32	C31	118.8(7)	P2	Pd	Cl2	85.77(8)
C32	C33	C34	121.9(8)	Cl2	Pd	Cl1	106.00(8)
C35	C34	C33	120.6(7)				

B: Crystallographic data for [Pt(5-*p*-tolyl-PNP)Cl_2]

Table B.1: Fractional Atomic Coordinates ($\times 10^4$) and Equivalent Isotropic Displacement Parameters ($Å^2 \times 10^3$) for [Pt(5-*p*-tolyl-PNP)Cl_2].

Atom	***x***	***y***	***z***	**U(eq)**
C11	-903(2)	8811(2)	2333.7(15)	13.4(9)
C12	-778(2)	9733(2)	2366.7(16)	15.9(9)
C13	-1037(2)	10300(3)	1941.9(17)	18.4(9)
C14	-1412(2)	9971(2)	1467.1(16)	15.4(9)
C15	-1543(2)	9059(3)	1441.3(17)	21(1)
C16	-1291(2)	8486(3)	1863.7(17)	20.0(9)
C17	-1645(2)	10593(3)	987.0(17)	24.5(10)
C21	-1082.5(19)	7079(2)	2885.9(15)	12.2(8)
C22	-1835.9(19)	7100(2)	2870.8(15)	12.8(8)
C23	-2230(2)	6313(2)	2876.6(16)	15.8(9)
C24	-1889(2)	5482(2)	2896.3(16)	14.6(8)
C25	-1139(2)	5460(2)	2933.7(16)	15.9(9)
C26	-735(2)	6248(2)	2924.9(16)	17.0(9)
C27	-2311(2)	4623(2)	2845.7(17)	20.6(9)
C31	336.0(19)	7732(2)	4363.9(15)	12.9(8)
C32	-192(2)	7090(3)	4442.1(17)	19.2(9)
C33	-183(2)	6519(3)	4917.2(17)	23(1)
C34	364(2)	6569(3)	5327.3(16)	18.5(9)
C35	898(2)	7206(3)	5247.1(16)	21.7(10)
C36	898(2)	7777(3)	4772.2(16)	18.8(9)
C37	370(3)	5964(3)	5851.3(18)	30.9(11)
C41	763(2)	9468(2)	3922.5(15)	13.4(9)
C42	657(2)	9855(3)	4465.3(16)	18.1(9)
C43	954(2)	10684(3)	4590.0(17)	18.4(9)
C44	1374(2)	11138(3)	4190.7(16)	17.6(9)

C45	1479(2)	10748(3)	3650.8(16)	21.5(10)
C46	1177(2)	9922(3)	3513.8(16)	18.7(9)
C47	1711(3)	12031(3)	4343.7(18)	28.5(11)
C1	-1090(2)	9097(2)	3802.7(15)	12.8(9)
C2	-1691(2)	8664(3)	4026.4(16)	17.7(9)
C3	-2243(2)	9172(3)	4275.8(17)	22(1)
C4	-2204(2)	10100(3)	4301.9(17)	21.3(10)
C5	-1592(2)	10517(3)	4085.1(16)	20.8(10)
C6	-1039(2)	10028(3)	3833.6(16)	15.4(9)
C7	-2813(3)	10654(3)	4552.9(19)	35.4(12)
N1	-527.1(16)	8592.5(19)	3520.4(12)	12.1(7)
P1	-523.6(5)	8064.2(6)	2861.2(4)	11.9(2)
P2	346.3(5)	8426.2(6)	3725.3(4)	12.3(2)
Cl1	818.8(5)	7226.0(7)	1957.3(4)	23.4(2)
Cl2	1886.1(5)	7699.7(6)	3135.7(4)	18.6(2)
Pt	655.8(2)	7825.2(2)	2894.1(2)	10.93(5)

Table B.2: Hydrogen Atom Coordinates ($Å \times 10^4$) and Isotropic Displacement Parameters ($Å^2 \times 10^3$) for [Pt(5-*p*-tolyl-PNP)Cl_2].

Atom	***x***	***y***	***z***	**U(eq)**
H13	-514	9972	2683	19
H12	-956	10928	1975	22
H10	-1813	8822	1126	25
H9	-1384	7860	1833	24
H14A	-1759	11185	1149	37
H14B	-2074	10347	796	37
H14C	-1254	10652	704	37
H6	-2079	7661	2856	15
H5	-2742	6340	2867	19
H3	-899	4899	2966	19
H2	-223	6221	2945	20
H7A	-2774	4688	3047	31
H7B	-2036	4131	3021	31
H7C	-2399	4490	2436	31
H34	-569	7038	4166	23
H33	-556	6087	4962	28
H31	1275	7254	5524	26
H30	1278	8198	4723	23
H35A	200	6300	6190	46
H35B	863	5751	5921	46
H35C	52	5449	5783	46
H27	381	9548	4750	22
H26	868	10947	4958	22

H24	1763	11053	3370	26
H23	1252	9668	3142	22
H28A	2059	12201	4043	43
H28B	1960	11981	4717	43
H28C	1334	12490	4370	43
H16	-1728	8028	4010	21
H17	-2653	8876	4431	26
H19	-1551	11151	4110	25
H20	-627	10327	3683	19
H21A	-2999	11064	4256	53
H21B	-2633	11002	4883	53
H21C	-3201	10254	4682	53

Table B.3: Anisotropic Displacement Parameters ($Å^2 \times 10^3$) for [Pt(5-*p*-tolyl-PNP)Cl_2].

Atom	**U_{11}**	**U_{22}**	**U_{33}**	**U_{23}**	**U_{13}**	**U_{12}**
C11	11(2)	17(2)	12(2)	-0.9(17)	-3.4(16)	1.2(17)
C12	16(2)	15(2)	16(2)	-4.4(17)	0.6(17)	-2.2(18)
C13	21(2)	9.5(19)	24(2)	2.6(18)	4.4(19)	-2.6(18)
C14	11(2)	20(2)	15(2)	1.5(18)	0.3(17)	2.4(18)
C15	28(3)	17(2)	18(2)	-0.2(19)	-8.9(19)	-2.6(19)
C16	24(2)	15(2)	21(2)	-0.9(19)	-3.8(19)	-0.8(19)
C17	37(3)	18(2)	18(2)	3.5(19)	-2(2)	2(2)
C21	11(2)	14.4(19)	11.1(19)	-2.0(17)	-2.0(16)	-1.4(17)
C22	17(2)	9.4(18)	12.4(19)	3.0(17)	-2.6(17)	3.7(17)
C23	9(2)	22(2)	16(2)	1.4(18)	-1.8(17)	-5.0(18)
C24	20(2)	17(2)	6.9(19)	0.7(17)	5.0(18)	-1.6(18)
C25	20(2)	11.1(19)	17(2)	0.4(17)	-0.2(18)	1.9(17)
C26	16(2)	17(2)	18(2)	-0.7(17)	-4.0(18)	-1.4(18)
C27	24(2)	17(2)	21(2)	-1.7(19)	0.4(19)	-7.2(19)
C31	11(2)	14(2)	14(2)	2.0(17)	-2.2(16)	4.2(18)
C32	16(2)	20(2)	21(2)	-3.1(19)	-3.8(18)	2(2)
C33	23(3)	18(2)	28(2)	4(2)	4(2)	-2(2)
C34	21(2)	16(2)	18(2)	0.1(18)	1.6(18)	4.8(19)
C35	26(2)	22(2)	18(2)	-1(2)	-11.6(18)	0(2)
C36	21(2)	16(2)	19(2)	1.1(19)	-5.0(18)	0.9(19)
C37	41(3)	25(2)	26(3)	7(2)	1(2)	-1(2)
C41	12(2)	14.7(19)	14(2)	-1.3(17)	-2.2(17)	1.0(17)
C42	16(2)	23(2)	15(2)	2.3(18)	3.6(18)	-4(2)
C43	21(2)	18(2)	17(2)	-7.8(18)	-0.9(18)	-3.3(19)
C44	19(2)	16(2)	17(2)	1.9(18)	-3.5(18)	-1.2(19)
C45	32(3)	20(2)	13(2)	4.8(18)	4.8(19)	-7(2)
C46	27(2)	20(2)	9(2)	-2.5(18)	2.3(18)	-0.2(19)

C47	46(3)	21(2)	19(2)	1.4(19)	1(2)	-11(2)
C1	13(2)	13(2)	13(2)	-2.1(17)	-3.8(17)	4.0(18)
C2	21(2)	17(2)	16(2)	1.4(18)	-3.3(18)	-0.4(19)
C3	16(2)	32(3)	19(2)	3(2)	2.5(18)	-2(2)
C4	22(2)	28(2)	14(2)	-1.2(19)	0.7(19)	10(2)
C5	28(3)	21(2)	14(2)	-5.4(18)	-1.4(19)	6(2)
C6	12(2)	21(2)	13(2)	0.9(18)	-0.3(17)	-0.9(18)
C7	36(3)	40(3)	30(3)	-1(2)	11(2)	14(2)
N1	10.7(18)	14.3(16)	11.3(16)	-1.0(14)	-2.0(13)	0.5(14)
P1	13.2(5)	11.0(5)	11.7(5)	-2.0(4)	-1.6(4)	-0.4(4)
P2	10.5(5)	13.4(5)	13.0(5)	0.2(4)	-2.0(4)	-0.2(4)
Cl1	27.7(6)	26.9(5)	15.4(5)	-6.0(4)	0.3(4)	7.7(5)
Cl2	11.1(5)	21.6(5)	23.2(5)	-0.7(4)	0.5(4)	1.2(4)
Pt	10.62(8)	10.51(8)	11.65(8)	-0.92(6)	0.11(6)	0.71(6)

Table B.4: Bond Lengths for [Pt(5-*p*-tolyl-PNP)Cl_2].

Atom	**Atom**	**Length/Å**	**Atom**	**Atom**	**Length/Å**
C11	C12	1.395(5)	C35	C36	1.388(5)
C11	C16	1.390(5)	C41	C42	1.394(5)
C11	P1	1.793(4)	C41	C46	1.392(5)
C12	C13	1.381(5)	C41	P2	1.791(4)
C13	C14	1.388(5)	C42	C43	1.382(5)
C14	C15	1.382(5)	C43	C44	1.383(5)
C14	C17	1.509(5)	C44	C45	1.390(5)
C15	C16	1.378(5)	C44	C47	1.512(5)
C21	C22	1.397(5)	C45	C46	1.388(5)
C21	C26	1.398(5)	C1	C2	1.387(5)
C21	P1	1.797(4)	C1	C6	1.392(5)
C22	C23	1.381(5)	C1	N1	1.441(5)
C23	C24	1.390(5)	C2	C3	1.396(6)
C24	C25	1.394(5)	C3	C4	1.385(6)
C24	C27	1.505(5)	C4	C5	1.386(6)
C25	C26	1.391(5)	C4	C7	1.513(6)
C31	C32	1.379(5)	C5	C6	1.385(5)
C31	C36	1.406(5)	N1	P1	1.714(3)
C31	P2	1.802(4)	N1	P2	1.704(3)
C32	C33	1.389(5)	P1	Pt	2.2154(10)
C33	C34	1.389(6)	P2	Pt	2.1951(10)
C34	C35	1.384(6)	Cl1	Pt	2.3606(9)
C34	C37	1.509(5)	Cl2	Pt	2.3546(9)

Table B.5: Bond Angles for [Pt(5-*p*-tolyl-PNP)Cl_2].

Atom	Atom	Atom	Angle/°	Atom	Atom	Atom	Angle/°
C12	C11	P1	120.6(3)	C43	C44	C47	120.5(3)
C16	C11	C12	118.1(3)	C45	C44	C47	121.3(4)
C16	C11	P1	121.2(3)	C46	C45	C44	121.2(4)
C13	C12	C11	120.4(4)	C45	C46	C41	119.9(4)
C12	C13	C14	121.3(3)	C2	C1	C6	119.9(3)
C13	C14	C17	120.5(3)	C2	C1	N1	120.5(3)
C15	C14	C13	118.0(4)	C6	C1	N1	119.5(3)
C15	C14	C17	121.5(3)	C1	C2	C3	119.3(4)
C16	C15	C14	121.3(4)	C4	C3	C2	121.4(4)
C15	C16	C11	120.9(4)	C3	C4	C5	118.2(4)
C22	C21	C26	118.8(3)	C3	C4	C7	121.4(4)
C22	C21	P1	123.9(3)	C5	C4	C7	120.3(4)
C26	C21	P1	117.4(3)	C6	C5	C4	121.4(4)
C23	C22	C21	120.6(3)	C5	C6	C1	119.7(4)
C22	C23	C24	121.1(3)	C1	N1	P1	130.1(2)
C23	C24	C25	118.4(3)	C1	N1	P2	129.6(2)
C23	C24	C27	121.2(3)	P2	N1	P1	100.17(16)
C25	C24	C27	120.2(3)	C11	P1	C21	107.58(17)
C26	C25	C24	121.0(3)	C11	P1	Pt	120.62(13)
C25	C26	C21	120.0(3)	C21	P1	Pt	115.87(12)
C32	C31	C36	118.0(3)	N1	P1	C11	108.53(16)
C32	C31	P2	120.8(3)	N1	P1	C21	110.14(16)
C36	C31	P2	120.9(3)	N1	P1	Pt	92.70(11)
C31	C32	C33	121.3(4)	C31	P2	Pt	119.02(12)
C34	C33	C32	121.0(4)	C41	P2	C31	107.06(17)
C33	C34	C37	121.4(4)	C41	P2	Pt	117.58(13)
C35	C34	C33	117.9(4)	N1	P2	C31	107.50(16)
C35	C34	C37	120.7(4)	N1	P2	C41	110.74(16)
C34	C35	C36	121.7(4)	N1	P2	Pt	93.69(10)
C35	C36	C31	120.1(4)	P1	Pt	Cl1	98.95(4)
C42	C41	P2	121.7(3)	P1	Pt	Cl2	167.41(3)
C46	C41	C42	119.1(3)	P2	Pt	P1	72.95(4)
C46	C41	P2	119.1(3)	P2	Pt	Cl1	171.81(4)
C43	C42	C41	120.1(4)	P2	Pt	Cl2	94.47(3)
C42	C43	C44	121.4(4)	Cl2	Pt	Cl1	93.64(3)
C43	C44	C45	118.3(3)				

C: Crystallographic data for [Pd(5-*p*-tolyl-PNP)Cl_2]

Table C.1: Fractional Atomic Coordinates ($\times 10^4$) and Equivalent Isotropic Displacement Parameters ($Å^2 \times 10^3$) for [Pd(5-*p*-tolyl-PNP)Cl_2].

Atom	*x*	*y*	*z*	U(eq)
C11	769.2(11)	4474.8(14)	1080.5(9)	14.1(4)
C12	1184.2(13)	4935.4(15)	1487.8(10)	19.4(5)
C13	1481.1(14)	5766.3(15)	1352.4(10)	22.8(5)
C14	1373.5(12)	6148.2(14)	809.9(10)	18.3(5)
C15	956.5(12)	5685.3(15)	406.9(10)	19.2(5)
C16	659.9(12)	4854.9(15)	536.4(10)	18.1(4)
C17	1707.6(16)	7039.2(15)	651.0(11)	28.8(6)
C21	344.8(11)	2732.8(14)	642.3(9)	14.7(4)
C22	910.1(13)	2771.6(15)	239.8(10)	20.1(5)
C23	912.1(14)	2201.2(15)	-234.5(10)	22.9(5)
C24	366.7(13)	1567.1(15)	-319(1)	20.8(5)
C25	-183.6(13)	1521.9(16)	90.8(11)	22.6(5)
C26	-196.9(12)	2095.4(15)	564.3(10)	20.3(5)
C27	376.2(15)	959.6(17)	-840.3(11)	29.1(6)
C31	-1081.4(11)	2096.8(14)	2119.6(9)	14.4(4)
C32	-732.5(12)	1265.7(14)	2071.8(10)	17.2(4)
C33	-1130.2(12)	476.4(14)	2060(1)	18.1(4)
C34	-1885.4(12)	493.5(14)	2102.5(9)	15.8(4)
C35	-2230.4(12)	1325.4(15)	2133.3(9)	17.9(4)
C36	-1839.4(12)	2119.7(14)	2144.0(9)	16.2(4)
C37	-2304.8(13)	-370.2(15)	2149.4(11)	22.0(5)
C41	-900.8(11)	3836.4(14)	2668.9(9)	14.1(4)
C42	-1275.4(13)	3496.0(15)	3146.2(10)	20.1(5)
C43	-1528.9(14)	4071.7(15)	3571.4(10)	23.0(5)
C44	-1412.8(12)	4994.7(15)	3537.8(10)	17.8(4)
C45	-1056.0(12)	5328.2(14)	3055.1(10)	18.4(5)
C46	-789.0(12)	4762.6(14)	2629(1)	17.2(4)
C47	-1647.1(14)	5611.0(15)	4018.0(11)	25.0(5)
C1	-1089.6(11)	4111.2(14)	1200.9(9)	14.8(4)
C6	-1695.5(12)	3678.9(15)	975.7(10)	17.8(4)
C5	-2249.2(12)	4186.6(16)	725(1)	22.0(5)
C4	-2205.7(13)	5116.4(16)	694.2(10)	22.7(5)
C3	-1590.0(13)	5534.2(15)	911.6(10)	21.0(5)
C2	-1034.4(12)	5045.2(15)	1162.8(9)	17.2(4)
C7	-2819.7(15)	5669.2(19)	444.4(13)	35.6(6)
N1	-522.5(9)	3612.3(11)	1484.9(8)	14.3(4)
P1	351.7(3)	3432.4(4)	1278.5(2)	12.73(11)

P2	-521.8(3)	3084.9(4)	2142.6(2)	12.54(11)
Cl1	1891.7(3)	2725.6(4)	1829.0(2)	20.03(12)
Cl2	800.3(3)	2233.9(4)	3050.9(2)	25.61(13)
Pd	668.2(2)	2835.2(2)	2112.1(2)	12.10(5)

Table C.2: Hydrogen Atom Coordinates ($Å \times 10^4$) and Isotropic Displacement Parameters ($Å^2 \times 10^3$) for [Pd(5-*p*-tolyl-PNP)Cl_2].

Atom	***x***	***y***	***z***	**U(eq)**
H12	1264	4680	1859	23
H13	1761	6078	1634	27
H15	874	5943	37	23
H16	382	4544	254	22
H17A	1326	7496	622	43
H17B	1957	6985	278	43
H17C	2057	7216	950	43
H22	1294	3190	292	24
H23	1295	2244	-509	27
H25	-559	1089	46	27
H26	-580	2052	838	24
H27A	264	1310	-1188	44
H27B	13	484	-792	44
H27C	858	689	-881	44
H42	-218	1242	2047	21
H43	-886	-83	2022	22
H45	-2745	1348	2147	21
H46	-2086	2680	2168	19
H47A	-2390	-510	2558	33
H47B	-2026	-858	1971	33
H47C	-2771	-306	1950	33
H32	-1357	2868	3179	24
H33	-1787	3832	3892	28
H35	-993	5959	3016	22
H36	-530	5005	2310	21
H37A	-1260	5653	4307	37
H37B	-2087	5372	4200	37
H37C	-1747	6209	3860	37
H52	-1732	3043	992	21
H53	-2664	3890	573	26
H55	-1549	6170	887	25
H56	-617	5344	1309	21
H57A	-3068	5991	757	53
H57B	-3165	5271	248	53
H57C	-2624	6103	166	53

Table C.3: Anisotropic Displacement Parameters ($Å^2 \times 10^3$) for [Pd(5-*p*-tolyl-PNP)Cl_2].

Atom	U_{11}	U_{22}	U_{33}	U_{23}	U_{13}	U_{12}
C11	12.1(10)	14.4(10)	15.7(10)	1.4(8)	1.9(8)	0.5(8)
C12	26.5(12)	17.2(11)	14.3(11)	2.0(9)	-2.9(9)	-2.0(9)
C13	31.0(13)	19.0(11)	18.3(12)	-3.6(9)	-6.8(10)	-4.5(10)
C14	21.7(11)	14.1(10)	19.1(11)	0.2(9)	1.1(9)	-1.3(9)
C15	22.4(11)	19.7(11)	15.6(11)	4.1(9)	-2.6(9)	-1.9(9)
C16	17.6(11)	20.1(11)	16.5(11)	0.8(9)	-3.6(9)	-3.8(9)
C17	44.9(16)	18.7(12)	22.8(13)	1.8(10)	-6.8(11)	-10.1(11)
C21	13.6(10)	14.8(10)	15.7(11)	1.1(8)	0.5(8)	1.6(8)
C22	19.6(11)	17.7(11)	23.0(12)	-0.8(9)	3.8(9)	-1.9(9)
C23	26.8(12)	21.6(11)	20.4(12)	-0.4(9)	10(1)	0.6(10)
C24	27.3(12)	16.1(10)	19.0(11)	-0.5(9)	-2.6(10)	4.1(9)
C25	21.0(12)	18.9(11)	27.9(13)	-3.8(10)	-2.3(10)	-3.5(9)
C26	17.9(11)	19.5(11)	23.5(12)	-1.0(9)	2.2(9)	-1.3(9)
C27	40.2(15)	25.9(13)	21.4(13)	-5.7(10)	-1.1(11)	1.1(11)
C31	16.3(10)	14.1(10)	12.7(10)	1.7(8)	0.9(8)	-1.2(8)
C32	15.8(10)	16.2(10)	19.5(11)	1.5(9)	3.8(9)	-0.2(8)
C33	21.0(11)	13.5(10)	19.8(12)	-0.4(9)	1.7(9)	2.3(8)
C34	19.0(11)	16.4(10)	11.9(10)	0.5(8)	-1.4(8)	-3.6(8)
C35	14.6(10)	21.6(11)	17.5(11)	0.0(9)	-0.2(9)	-1.4(8)
C36	16.1(10)	15.4(10)	17.3(11)	1.1(9)	1.3(8)	2.1(8)
C37	21.5(12)	17.9(11)	26.5(13)	2.0(9)	-2.9(10)	-5.5(9)
C41	13.3(10)	15.7(10)	13.4(10)	-0.6(8)	0.0(8)	1.3(8)
C42	27.8(12)	12.6(10)	19.8(12)	-0.2(9)	6(1)	-2.7(9)
C43	32.6(13)	18.5(11)	18.0(12)	0.5(9)	8.3(10)	-4.4(10)
C44	18.1(11)	16.2(10)	19.0(11)	-1.6(9)	-0.9(9)	0.9(9)
C45	18.9(11)	11.4(10)	24.9(12)	-0.5(9)	0.2(9)	-1.2(8)
C46	17.1(11)	15.3(10)	19.2(11)	1.9(9)	2.1(9)	-3.1(8)
C47	33.7(14)	20.0(11)	21.2(12)	-3.2(10)	4(1)	0.9(10)
C1	14.9(10)	16.3(10)	13.3(10)	1.4(8)	1.6(8)	2.9(8)
C6	19.2(11)	16.8(10)	17.4(11)	-0.5(9)	1.7(9)	0.6(9)
C5	16.6(11)	28.7(12)	20.9(12)	-4.5(10)	-3.0(9)	-0.5(9)
C4	21.8(12)	28.3(12)	17.9(11)	3.2(10)	-0.9(9)	10.7(10)
C3	23.7(12)	17.5(11)	21.9(12)	3.6(9)	2.5(10)	4.0(9)
C2	16.8(10)	19.1(11)	15.9(11)	2.7(9)	0.7(8)	-1.3(9)
C7	31.0(14)	40.7(15)	35.0(16)	3.2(13)	-10.4(12)	14.9(12)
N1	13.3(9)	13.8(8)	15.9(9)	2.7(7)	1.2(7)	2.2(7)
P1	11.7(2)	13.3(2)	13.2(3)	1.2(2)	1.1(2)	0.0(2)
P2	12.5(2)	11.5(2)	13.7(3)	1.3(2)	1.8(2)	0.06(19)
Cl1	12.4(2)	22.4(3)	25.3(3)	-0.4(2)	0.7(2)	1.3(2)
Cl2	31.8(3)	28.7(3)	16.3(3)	6.2(2)	0.2(2)	8.2(2)
Pd	11.55(8)	11.64(8)	13.10(8)	1.18(6)	-0.04(6)	0.85(6)

Table C.4: Bond Lengths for [Pd(5-*p*-tolyl-PNP)Cl_2].

Atom	Atom	Length/Å	Atom	Atom	Length/Å
C11	C12	1.393(3)	C41	C42	1.396(3)
C11	C16	1.393(3)	C41	C46	1.396(3)
C11	P1	1.791(2)	C41	P2	1.793(2)
C12	C13	1.388(3)	C42	C43	1.385(3)
C13	C14	1.390(3)	C43	C44	1.392(3)
C14	C15	1.390(3)	C44	C45	1.387(3)
C14	C17	1.507(3)	C44	C47	1.503(3)
C15	C16	1.384(3)	C45	C46	1.385(3)
C21	C22	1.398(3)	C1	C6	1.390(3)
C21	C26	1.389(3)	C1	C2	1.396(3)
C21	P1	1.801(2)	C1	N1	1.440(3)
C22	C23	1.386(3)	C6	C5	1.395(3)
C23	C24	1.392(3)	C5	C4	1.387(3)
C24	C25	1.389(3)	C4	C3	1.388(3)
C24	C27	1.506(3)	C4	C7	1.513(3)
C25	C26	1.388(3)	C3	C2	1.384(3)
C31	C32	1.398(3)	N1	P1	1.7014(18)
C31	C36	1.399(3)	N1	P2	1.7103(18)
C31	P2	1.797(2)	P1	P2	2.6162(8)
C32	C33	1.385(3)	P1	Pd	2.1997(6)
C33	C34	1.396(3)	P2	Pd	2.2256(6)
C34	C35	1.393(3)	Cl1	Pd	2.3536(5)
C34	C37	1.503(3)	Cl2	Pd	2.3590(6)
C35	C36	1.384(3)			

Table C.5: Bond Angles for [Pd(5-*p*-tolyl-PNP)Cl_2].

Atom	Atom	Atom	Angle/°	Atom	Atom	Atom	Angle/°
C12	C11	P1	119.30(16)	C6	C1	C2	119.7(2)
C16	C11	C12	119.30(19)	C6	C1	N1	121.01(19)
C16	C11	P1	121.34(16)	C2	C1	N1	119.27(19)
C13	C12	C11	120.2(2)	C1	C6	C5	119.5(2)
C12	C13	C14	120.7(2)	C4	C5	C6	121.2(2)
C13	C14	C17	121.4(2)	C5	C4	C3	118.4(2)
C15	C14	C13	118.7(2)	C5	C4	C7	121.2(2)
C15	C14	C17	119.9(2)	C3	C4	C7	120.4(2)
C16	C15	C14	121.1(2)	C2	C3	C4	121.4(2)
C15	C16	C11	120.0(2)	C3	C2	C1	119.7(2)
C22	C21	P1	120.92(17)	C1	N1	P1	129.85(14)
C26	C21	C22	118.6(2)	C1	N1	P2	129.92(14)
C26	C21	P1	120.36(17)	P1	N1	P2	100.14(9)

C23	C22	C21	120.2(2)	C11	P1	C21	107.15(10)
C22	C23	C24	121.6(2)	C11	P1	P2	129.09(7)
C23	C24	C27	120.7(2)	C11	P1	Pd	117.36(7)
C25	C24	C23	117.7(2)	C21	P1	P2	120.28(7)
C25	C24	C27	121.6(2)	C21	P1	Pd	118.88(7)
C26	C25	C24	121.4(2)	N1	P1	C11	110.01(9)
C25	C26	C21	120.6(2)	N1	P1	C21	108.23(10)
C32	C31	C36	118.97(19)	N1	P1	P2	40.05(6)
C32	C31	P2	117.51(16)	N1	P1	Pd	93.98(6)
C36	C31	P2	123.52(16)	Pd	P1	P2	54.217(17)
C33	C32	C31	120.5(2)	C31	P2	P1	119.50(7)
C32	C33	C34	120.7(2)	C31	P2	Pd	115.35(7)
C33	C34	C37	120.15(19)	C41	P2	C31	107.85(10)
C35	C34	C33	118.35(19)	C41	P2	P1	129.33(7)
C35	C34	C37	121.4(2)	C41	P2	Pd	120.62(7)
C36	C35	C34	121.4(2)	N1	P2	C31	110.41(9)
C35	C36	C31	119.9(2)	N1	P2	C41	108.43(9)
C42	C41	C46	118.9(2)	N1	P2	P1	39.80(6)
C42	C41	P2	120.13(16)	N1	P2	Pd	92.82(6)
C46	C41	P2	120.87(16)	Pd	P2	P1	53.303(17)
C43	C42	C41	120.2(2)	P1	Pd	P2	72.48(2)
C42	C43	C44	121.3(2)	P1	Pd	Cl1	92.22(2)
C43	C44	C47	121.1(2)	P1	Pd	Cl2	170.27(2)
C45	C44	C43	118.1(2)	P2	Pd	Cl1	164.69(2)
C45	C44	C47	120.8(2)	P2	Pd	Cl2	97.81(2)
C46	C45	C44	121.5(2)	Cl1	Pd	Cl2	97.49(2)
C45	C46	C41	120.0(2)				

D: Crystallographic data for [Pt(4-*p*-tolyl-*o*-tol)Cl_2]

Table D.1: Fractional Atomic Coordinates ($\times 10^4$) and Equivalent Isotropic Displacement Parameters ($Å^2 \times 10^3$) for [Pt(4-*p*-tolyl-*o*-tol)Cl_2].

Atom	***x***	***y***	***z***	**U(eq)**
C11	5590(4)	154(2)	2016(3)	31.8(10)
C12	5904(5)	-236(2)	2757(3)	44.4(13)
C13	5629(6)	-903(3)	2693(3)	49.6(14)
C14	5083(5)	-1187(2)	1891(4)	45.8(13)
C15	4743(5)	-786(2)	1171(3)	46.5(13)
C16	4988(5)	-119(2)	1225(3)	39.7(12)
C17	4871(6)	-1912(3)	1820(4)	69.9(18)
C21	4940(5)	1448(2)	1362(3)	34.8(11)
C22	3611(5)	1295(2)	1287(3)	45.5(13)

C23	2665(6)	1679(3)	783(4)	59.6(15)
C24	3000(6)	2224(3)	342(3)	56.0(15)
C25	4321(6)	2377(3)	434(3)	57.3(16)
C26	5273(5)	2000(2)	932(3)	44.4(13)
C27	1961(7)	2636(4)	-225(4)	94(3)
C31	9291(5)	2109(2)	2497(3)	33.3(11)
C32	8483(5)	2652(2)	2352(3)	42.4(12)
C33	8940(5)	3233(2)	2075(3)	43.4(13)
C34	10232(6)	3290(2)	1954(3)	43.1(13)
C35	11046(6)	2759(3)	2135(3)	51.1(14)
C36	10597(5)	2172(3)	2407(3)	46.4(13)
C37	10692(6)	3912(3)	1596(4)	62.9(17)
C41	9937(5)	814(2)	3144(3)	33.9(11)
C42	10748(5)	551(2)	2595(3)	41.3(12)
C43	11848(5)	186(2)	2950(3)	44.2(13)
C44	12165(5)	80(2)	3856(3)	44.4(13)
C45	11361(5)	332(3)	4387(3)	47.1(13)
C46	10247(5)	692(2)	4045(3)	44.5(13)
C47	13353(6)	-297(3)	4238(4)	62.2(16)
C1	8039(5)	943(2)	932(3)	35.3(11)
C2	8203(5)	322(2)	607(3)	42.3(12)
C3	8486(5)	273(3)	-241(3)	53.6(15)
C4	8647(5)	817(3)	-732(3)	55.0(15)
C5	8551(6)	1423(3)	-391(3)	52.6(15)
C6	8246(5)	1489(2)	444(3)	42.3(13)
C7	8166(6)	-286(3)	1138(4)	56.5(15)
N1	7663(4)	1044.1(18)	1786(2)	32.9(9)
P1	6152.0(12)	986.0(6)	2097.0(7)	31.6(3)
P2	8570.2(13)	1346.3(6)	2746.7(7)	31.2(3)
Cl1	4786.2(14)	1326.1(6)	3841.5(9)	50.7(3)
Cl2	7861.3(16)	1835.5(7)	4780.2(8)	55.9(4)
Pt	6858.4(2)	1379.7(2)	3423.9(2)	32.57(7)

Table D.2: Hydrogen Atom Coordinates ($Å \times 10^4$) and Isotropic Displacement Parameters ($Å^2 \times 10^3$) for [Pt(4-*p*-tolyl-*o*-tol)Cl_2].

Atom	***x***	***y***	***z***	**U(eq)**
H14	6297	-56	3295	53
H36	5815	-1161	3197	59
H43	4340	-964	634	56
H33	4747	142	728	48
H22A	5575	-2108	1580	105
H22B	4044	-2001	1438	105
H22C	4859	-2089	2395	105

H44	3358	933	1579	55
H27	1780	1570	738	72
H35	4572	2744	152	69
H40	6156	2115	982	53
H49A	1930	2531	-836	140
H49B	2176	3088	-129	140
H49C	1116	2551	-70	140
H18	7617	2624	2444	51
H26	8375	3588	1969	52
H50	11925	2795	2074	61
H34	11170	1821	2529	56
H30A	10208	3984	1010	94
H30B	11617	3880	1579	94
H30C	10545	4268	1969	94
H28	10548	622	1989	50
H21	12378	11	2581	53
H42	11567	259	4993	57
H16	9707	852	4419	53
H37A	13647	-543	3780	93
H37B	13146	-588	4680	93
H37C	14040	-4	4501	93
H46	8569	-137	-480	64
H41	8822	770	-1300	66
H101	8689	1789	-717	63
H25	8181	1902	680	51
H32A	8057	-175	1726	85
H32B	8977	-521	1163	85
H32C	7440	-553	866	85

Table D.3: Anisotropic Displacement Parameters ($Å^2 \times 10^3$) for [Pt(4-*p*-tolyl-*o*-tol)Cl_2].

Atom	**U_{11}**	**U_{22}**	**U_{33}**	**U_{23}**	**U_{13}**	**U_{12}**
C11	30(3)	32(2)	35(2)	-2(2)	9(2)	2(2)
C12	54(4)	40(3)	40(3)	5(2)	11(3)	1(3)
C13	57(4)	40(3)	52(3)	14(3)	12(3)	3(3)
C14	38(3)	40(3)	61(3)	-7(3)	14(3)	-4(3)
C15	46(3)	44(3)	46(3)	-8(3)	2(3)	-4(3)
C16	40(3)	38(3)	39(3)	2(2)	2(2)	-2(2)
C17	73(5)	36(3)	100(5)	-4(3)	12(4)	-20(3)
C21	39(3)	34(3)	31(2)	1(2)	7(2)	6(2)
C22	37(3)	43(3)	55(3)	15(3)	8(3)	3(3)
C23	38(3)	64(4)	74(4)	11(3)	3(3)	6(3)
C24	57(4)	63(4)	48(3)	11(3)	10(3)	23(3)

C25	70(4)	52(3)	54(3)	24(3)	22(3)	15(3)
C26	45(3)	41(3)	49(3)	12(2)	11(3)	6(3)
C27	79(5)	110(6)	89(5)	44(5)	6(4)	42(5)
C31	40(3)	35(3)	23(2)	-0.5(19)	0(2)	0(2)
C32	39(3)	39(3)	50(3)	0(2)	9(2)	0(3)
C33	50(4)	31(3)	48(3)	1(2)	4(3)	8(3)
C34	53(4)	36(3)	38(3)	-3(2)	4(3)	-12(3)
C35	44(3)	46(3)	66(3)	3(3)	16(3)	-6(3)
C36	46(3)	41(3)	54(3)	7(2)	11(3)	-3(3)
C37	73(5)	42(3)	74(4)	0(3)	16(3)	-11(3)
C41	37(3)	28(2)	35(2)	3(2)	2(2)	-6(2)
C42	41(3)	49(3)	32(2)	-1(2)	4(2)	1(3)
C43	42(3)	43(3)	49(3)	3(2)	12(3)	3(3)
C44	39(3)	36(3)	54(3)	11(2)	-4(3)	-2(3)
C45	50(4)	53(3)	37(3)	5(2)	5(3)	6(3)
C46	56(4)	45(3)	31(2)	1(2)	5(2)	0(3)
C47	48(4)	65(4)	71(4)	14(3)	3(3)	2(3)
C1	35(3)	42(3)	28(2)	-7(2)	3(2)	3(2)
C2	32(3)	47(3)	47(3)	-8(2)	7(2)	2(3)
C3	50(4)	66(4)	44(3)	-16(3)	8(3)	13(3)
C4	46(3)	83(4)	38(3)	-5(3)	13(3)	12(3)
C5	46(3)	73(4)	40(3)	11(3)	13(3)	8(3)
C6	44(3)	52(3)	34(2)	0(2)	13(2)	2(3)
C7	55(4)	46(3)	70(4)	-2(3)	17(3)	7(3)
N1	38(2)	35(2)	26.3(18)	-2.0(16)	5.7(17)	-1.0(19)
P1	35.3(7)	30.8(6)	28.9(6)	0.1(5)	6.3(5)	-0.5(6)
P2	35.3(7)	31.8(6)	25.9(5)	0.2(5)	4.2(5)	-0.9(6)
Cl1	51.8(9)	49.9(8)	56.7(8)	-5.5(6)	26.8(7)	-2.3(7)
Cl2	74.9(11)	55.0(8)	36.3(6)	-13.4(6)	5.7(7)	-8.1(8)
Pt	42.55(12)	28.67(10)	27.61(10)	-0.75(8)	9.36(8)	-0.35(9)

Table D.4: Bond Lengths for [Pt(4-*p*-tolyl-*o*-tol)Cl_2].

Atom	Atom	Length/Å	Atom	Atom	Length/Å
C11	C12	1.385(6)	C41	C42	1.401(6)
C11	C16	1.382(6)	C41	C46	1.389(6)
C11	P1	1.802(4)	C41	P2	1.800(5)
C12	C13	1.399(7)	C42	C43	1.386(7)
C13	C14	1.390(7)	C43	C44	1.391(7)
C14	C15	1.376(7)	C44	C45	1.367(7)
C14	C17	1.506(7)	C44	C47	1.477(7)
C15	C16	1.393(7)	C45	C46	1.388(7)
C21	C22	1.390(7)	C1	C2	1.391(6)

C21	C26	1.386(6)	C1	C6	1.389(6)
C21	P1	1.797(5)	C1	N1	1.451(5)
C22	C23	1.378(7)	C2	C3	1.392(6)
C23	C24	1.385(7)	C2	C7	1.499(7)
C24	C25	1.379(8)	C3	C4	1.377(7)
C24	C27	1.512(7)	C4	C5	1.362(7)
C25	C26	1.370(7)	C5	C6	1.385(6)
C31	C32	1.384(6)	N1	P1	1.714(4)
C31	C36	1.384(7)	N1	P2	1.717(4)
C31	P2	1.806(5)	P1	P2	2.617(2)
C32	C33	1.379(6)	P1	Pt	2.1949(13)
C33	C34	1.382(7)	P2	Pt	2.2072(14)
C34	C35	1.373(7)	Cl1	Pt	2.3418(16)
C34	C37	1.503(7)	Cl2	Pt	2.3500(14)
C35	C36	1.384(7)			

Table D.5: Bond Angles for [Pt(4-*p*-tolyl-*o*-tol)Cl_2].

Atom	**Atom**	**Atom**	**Angle/°**	**Atom**	**Atom**	**Atom**	**Angle/°**
C12	C11	P1	118.0(4)	C2	C1	N1	121.8(4)
C16	C11	C12	119.4(4)	C6	C1	C2	120.3(4)
C16	C11	P1	122.3(3)	C6	C1	N1	117.8(4)
C11	C12	C13	119.7(5)	C1	C2	C3	117.7(5)
C14	C13	C12	121.2(5)	C1	C2	C7	123.5(4)
C13	C14	C17	120.7(5)	C3	C2	C7	118.7(5)
C15	C14	C13	117.8(5)	C4	C3	C2	121.5(5)
C15	C14	C17	121.5(5)	C5	C4	C3	120.4(5)
C14	C15	C16	121.7(5)	C4	C5	C6	119.5(5)
C11	C16	C15	120.0(4)	C5	C6	C1	120.4(5)
C22	C21	P1	119.6(4)	C1	N1	P1	130.5(3)
C26	C21	C22	118.1(5)	C1	N1	P2	129.7(3)
C26	C21	P1	121.9(4)	P1	N1	P2	99.44(18)
C23	C22	C21	120.1(5)	C11	P1	P2	124.51(16)
C22	C23	C24	121.7(6)	C11	P1	Pt	117.52(14)
C23	C24	C27	121.5(6)	C21	P1	C11	106.3(2)
C25	C24	C23	117.6(5)	C21	P1	P2	126.53(17)
C25	C24	C27	120.9(6)	C21	P1	Pt	117.80(15)
C26	C25	C24	121.4(5)	N1	P1	C11	110.09(19)
C25	C26	C21	121.0(5)	N1	P1	C21	110.4(2)
C32	C31	P2	118.4(4)	N1	P1	P2	40.32(12)
C36	C31	C32	118.4(4)	N1	P1	Pt	94.04(13)
C36	C31	P2	123.2(4)	Pt	P1	P2	53.73(4)
C33	C32	C31	121.2(5)	C31	P2	P1	124.32(16)

C32	C33	C34	120.4(5)	C31	P2	Pt	117.93(16)
C33	C34	C37	119.8(5)	C41	P2	C31	105.9(2)
C35	C34	C33	118.2(5)	C41	P2	P1	126.13(16)
C35	C34	C37	121.9(5)	C41	P2	Pt	120.10(15)
C34	C35	C36	121.9(5)	N1	P2	C31	108.12(18)
C31	C36	C35	119.8(5)	N1	P2	C41	110.1(2)
C42	C41	P2	123.0(3)	N1	P2	P1	40.24(13)
C46	C41	C42	118.7(5)	N1	P2	Pt	93.53(14)
C46	C41	P2	118.2(4)	Pt	P2	P1	53.30(4)
C43	C42	C41	120.3(4)	P1	Pt	P2	72.97(5)
C42	C43	C44	120.5(5)	P1	Pt	Cl1	94.23(5)
C43	C44	C47	120.5(5)	P1	Pt	Cl2	172.74(5)
C45	C44	C43	118.9(5)	P2	Pt	Cl1	167.19(5)
C45	C44	C47	120.6(5)	P2	Pt	Cl2	99.91(6)
C44	C45	C46	121.6(5)	Cl1	Pt	Cl2	92.88(5)
C45	C46	C41	120.0(5)				

E: Crystallographic data for [Pd(Chzyl-4-*p*-tolyl)Cl_2]

Table E.1: Fractional Atomic Coordinates ($\times 10^4$) and Equivalent Isotropic Displacement Parameters ($Å^2 \times 10^3$) for [Pd(Chzyl-4-*p*-tolyl)Cl_2].

Atom	***x***	***y***	***z***	**U(eq)**
C1	5991(4)	3534.4(19)	4623.6(17)	38.5(7)
C2	7060(4)	3912(2)	4273.9(19)	50.3(9)
C3	7690(5)	4650(3)	4629(2)	63.2(12)
C4	8283(5)	4472(3)	5316(2)	71.3(14)
C5	7212(5)	4097(3)	5663(2)	66.1(12)
C6	6593(4)	3356(2)	5314.9(18)	48.8(9)
C7	5099(15)	5795(9)	3096(8)	75.9(14)
C8	5633(11)	5663(7)	3119(5)	50.3(9)
C11	7366(3)	1552.3(18)	4573.1(15)	33.5(6)
C12	7060(3)	919(2)	4941.7(17)	39.8(7)
C13	8079(4)	576(2)	5388.6(18)	42.8(8)
C14	9435(4)	842(2)	5468.4(16)	38.1(7)
C15	9737(4)	1470(2)	5096.1(18)	43.1(8)
C16	8727(4)	1824(2)	4658.0(17)	42.1(8)
C17	10549(4)	456(2)	5946(2)	51.0(9)
C21	6753(3)	2234.8(19)	3299.8(15)	34.7(6)
C22	7830(4)	1794(2)	3121.2(18)	44.4(8)
C23	8350(4)	1992(3)	2573.7(19)	51.2(9)
C24	7810(5)	2617(4)	2187(2)	70.9(11)
C25	6711(4)	3034(2)	2353.0(17)	47.3(9)

C26	6182(3)	2848(2)	2903.4(16)	40.2(7)
C27	8441(6)	2863(4)	1614(2)	74.6(14)
C31	2541(3)	3256.7(18)	3785.8(15)	32.2(6)
C32	2994(4)	3909.3(19)	3477.8(16)	37.7(7)
C33	2030(4)	4422(2)	3139.8(18)	46.2(8)
C34	622(4)	4302(2)	3104.4(18)	47.6(9)
C35	189(4)	3639(2)	3396.9(19)	47.1(8)
C36	1127(4)	3122(2)	3730.3(17)	41.8(8)
C37	-412(5)	4884(3)	2762(3)	75.9(14)
C41	3228(3)	2507.6(19)	5020.4(15)	34.0(6)
C42	2496(4)	3103(2)	5263.5(17)	41.3(7)
C43	2241(4)	3067(2)	5888.9(18)	48.2(8)
C44	2729(4)	2446(2)	6289.2(17)	46.7(8)
C45	3454(4)	1849(2)	6045.9(18)	47.7(9)
C46	3700(4)	1869(2)	5416.7(18)	42.3(8)
C47	2479(5)	2411(3)	6972(2)	66.2(12)
Cl1	4717.0(14)	113.4(6)	3529.7(7)	70.3(3)
Cl2	1592.3(10)	1120.7(6)	3553.0(6)	58.1(3)
N1	5343(3)	2825.4(17)	4275.6(14)	39.0(6)
O1	4960(7)	4971(4)	2864(3)	39.0(6)
O2	5642(7)	5007(4)	2992(3)	70.9(11)
P1	6013.3(8)	1982.0(5)	3999.1(4)	31.12(17)
P2	3677.3(8)	2542.4(4)	4225.0(4)	29.49(16)
Pd1	3967.6(2)	1383.8(2)	3799.1(2)	32.86(8)

Table E.2: Hydrogen Atom Coordinates ($Å \times 10^4$) and Isotropic Displacement Parameters ($Å^2 \times 10^3$) for [Pd(Chzyl-4-*p*-tolyl)Cl_2].

Atom	***x***	***y***	***z***	**U(eq)**
H1	5254	3924	4630	46
H2A	6627	4057	3846	60
H2B	7787	3534	4238	60
H3A	8416	4856	4414	76
H3B	6983	5053	4615	76
H4A	8612	4958	5531	86
H4B	9065	4118	5331	86
H5A	6481	4475	5692	79
H5B	7639	3958	6093	79
H6A	7305	2956	5328	59
H6B	5871	3148	5532	59
H7A	4947	5841	3530	114
H7B	4240	5873	2813	114
H7C	5753	6188	3012	114

H8A	5624	5683	3570	75
H8B	5161	6117	2918	75
H8C	6572	5660	3042	75
H12	6162	723	4889	48
H13	7848	162	5639	51
H15	10641	1658	5142	52
H16	8956	2248	4417	51
H17A	10672	751	6338	77
H17B	11402	448	5779	77
H17C	10279	-75	6026	77
H22	8198	1368	3369	53
H23	9078	1700	2462	61
H25	6320	3444	2093	57
H26	5441	3135	3009	48
H27A	7733	3073	1292	112
H27B	8860	2413	1447	112
H27C	9132	3260	1739	112
H32	3936	4002	3498	45
H33	2339	4855	2933	55
H35	-752	3540	3368	57
H36	810	2678	3920	50
H37A	-606	5283	3056	114
H37B	-1251	4612	2592	114
H37C	-34	5127	2419	114
H42	2171	3530	5007	50
H43	1733	3468	6042	58
H45	3783	1425	6306	57
H46	4178	1458	5260	51
H47A	2034	1921	7044	99
H47B	1898	2844	7052	99
H47C	3347	2446	7255	99
H1A	5362	4793	2584	59
H2	6469	5040	2971	106

Table E.3: Anisotropic Displacement Parameters ($Å^2 \times 10^3$) for [Pd(Chzyl-4-*p*-tolyl)Cl_2].

Atom	**U_{11}**	**U_{22}**	**U_{33}**	**U_{23}**	**U_{13}**	**U_{12}**
C1	38.1(16)	32.8(16)	43.3(18)	-7.8(13)	2.9(14)	-9.4(13)
C2	56(2)	43.4(19)	50(2)	-4.2(15)	5.1(17)	-19.7(16)
C3	67(3)	49(2)	72(3)	-6(2)	7(2)	-32(2)
C4	66(3)	71(3)	71(3)	-22(2)	-5(2)	-31(2)
C5	75(3)	66(3)	52(2)	-20(2)	-4(2)	-17(2)
C6	57(2)	47(2)	40.5(19)	-6.0(16)	2.4(16)	-14.3(17)

C7	67(3)	73(3)	82(3)	19(3)	-4(2)	21(2)
C8	56(2)	43.4(19)	50(2)	-4.2(15)	5.1(17)	-19.7(16)
C11	34.0(15)	31.6(15)	35.4(16)	0.9(12)	7.4(12)	-1.7(12)
C12	32.4(16)	38.9(17)	49.2(19)	6.9(15)	9.8(14)	-4.7(13)
C13	41.6(18)	40.6(18)	47.2(19)	11.4(15)	10.1(15)	-3.3(14)
C14	38.7(17)	40.3(17)	35.2(16)	-1.6(13)	5.6(13)	3.4(14)
C15	32.0(16)	48(2)	49(2)	4.4(16)	4.6(14)	-6.7(14)
C16	38.0(17)	43.1(18)	45.1(19)	11.8(15)	6.1(14)	-8.3(14)
C17	45(2)	54(2)	52(2)	8.0(18)	0.2(17)	0.2(17)
C21	34.3(15)	35.5(16)	34.3(16)	-0.2(12)	5.7(12)	-3.9(12)
C22	50(2)	42.1(19)	42.6(19)	3.5(15)	10.7(15)	7.9(16)
C23	48(2)	63(2)	46(2)	-2.1(18)	16.1(17)	5.3(18)
C24	54(2)	102(3)	53(2)	16(2)	-2.8(16)	-16(2)
C25	47(2)	56(2)	36.1(17)	11.0(16)	-3.3(15)	-3.9(17)
C26	33.9(16)	44.9(18)	40.4(17)	0.9(14)	2.2(13)	2.9(14)
C27	80(3)	101(4)	47(2)	11(2)	21(2)	-18(3)
C31	33.4(15)	30.5(14)	32.2(15)	-0.2(12)	3.8(12)	-2.6(12)
C32	40.4(17)	32.0(15)	41.1(17)	1.2(13)	7.8(14)	-5.7(13)
C33	60(2)	34.4(17)	43.6(19)	5.2(14)	6.5(17)	-2.9(16)
C34	55(2)	42.1(19)	41.3(19)	0.4(15)	-4.6(16)	7.8(16)
C35	36.0(17)	55(2)	48(2)	3.5(17)	-0.6(15)	3.9(16)
C36	36.0(17)	40.8(18)	47.3(19)	7.7(15)	2.9(14)	-3.8(14)
C37	67(3)	73(3)	82(3)	19(3)	-4(2)	21(2)
C41	30.3(14)	35.0(15)	36.0(16)	3.1(12)	3.8(12)	-6.2(12)
C42	47.9(19)	36.4(17)	38.5(17)	2.3(14)	4.1(14)	-0.4(14)
C43	55(2)	49(2)	41.3(19)	-4.5(16)	11.0(16)	3.2(17)
C44	41.7(18)	61(2)	36.0(17)	2.8(16)	3.7(14)	-12.6(17)
C45	39.9(18)	54(2)	47(2)	16.8(17)	-0.7(15)	-1.6(16)
C46	37.1(17)	42.4(18)	49(2)	10.3(15)	10.4(15)	3.5(14)
C47	69(3)	91(4)	39(2)	8(2)	9.1(19)	-12(3)
Cl1	89.9(8)	36.9(5)	83.4(8)	-16.9(5)	11.7(6)	5.9(5)
Cl2	42.6(5)	45.3(5)	78.5(7)	4.6(5)	-13.9(5)	-18.7(4)
N1	32.0(12)	39.1(13)	45.1(14)	-2.9(11)	4.2(11)	-12.4(10)
O1	32.0(12)	39.1(13)	45.1(14)	-2.9(11)	4.2(11)	-12.4(10)
O2	54(2)	102(3)	53(2)	16(2)	-2.8(16)	-16(2)
P1	29.9(4)	28.8(4)	34.6(4)	-0.2(3)	5.1(3)	-4.9(3)
P2	27.6(3)	26.7(3)	33.9(4)	0.0(3)	4.0(3)	-5.4(3)
Pd1	36.09(14)	25.32(12)	35.84(14)	-1.29(9)	1.78(9)	-7.57(9)

Table E.4: Bond Lengths for [Pd(Chzyl-4-*p*-tolyl)Cl_2].

Atom	Atom	Length/Å	Atom	Atom	Length/Å
C1	C2	1.519(5)	C25	C26	1.389(5)
C1	C6	1.520(5)	C31	C32	1.392(4)
C1	N1	1.496(4)	C31	C36	1.390(5)
C2	C3	1.535(5)	C31	P2	1.798(3)
C3	C4	1.511(7)	C32	C33	1.393(5)
C4	C5	1.514(7)	C33	C34	1.384(6)
C5	C6	1.530(5)	C34	C35	1.381(6)
C7	O2	1.466(16)	C34	C37	1.513(6)
C8	O1	1.409(11)	C35	C36	1.379(5)
C11	C12	1.388(4)	C41	C42	1.384(5)
C11	C16	1.394(5)	C41	C46	1.401(5)
C11	P1	1.801(3)	C41	P2	1.814(3)
C12	C13	1.388(5)	C42	C43	1.391(5)
C13	C14	1.387(5)	C43	C44	1.388(6)
C14	C15	1.386(5)	C44	C45	1.383(6)
C14	C17	1.512(5)	C44	C47	1.510(5)
C15	C16	1.380(5)	C45	C46	1.395(5)
C21	C22	1.394(5)	Cl1	Pd1	2.3720(12)
C21	C26	1.395(5)	Cl2	Pd1	2.3432(15)
C21	P1	1.806(3)	N1	P1	1.714(3)
C22	C23	1.383(5)	N1	P2	1.687(3)
C23	C24	1.391(7)	P1	P2	2.5924(16)
C24	C25	1.380(7)	P1	Pd1	2.2238(12)
C24	C27	1.509(6)	P2	Pd1	2.1972(10)

Table E.5: Bond Angles for [Pd(Chzyl-4-*p*-tolyl)Cl_2].

Atom	Atom	Atom	Angle/°	Atom	Atom	Atom	Angle/°
C2	C1	C6	111.4(3)	C42	C41	P2	122.8(3)
N1	C1	C2	111.6(3)	C46	C41	P2	118.5(3)
N1	C1	C6	112.6(3)	C41	C42	C43	120.6(3)
C1	C2	C3	110.9(3)	C44	C43	C42	121.3(4)
C4	C3	C2	111.9(4)	C43	C44	C47	121.6(4)
C3	C4	C5	111.4(4)	C45	C44	C43	118.2(3)
C4	C5	C6	111.2(4)	C45	C44	C47	120.2(4)
C1	C6	C5	111.4(3)	C44	C45	C46	121.2(3)
C12	C11	C16	118.1(3)	C45	C46	C41	120.2(3)
C12	C11	P1	119.4(2)	C1	N1	P1	133.0(2)
C16	C11	P1	122.5(2)	C1	N1	P2	126.0(2)
C11	C12	C13	120.7(3)	P2	N1	P1	99.32(15)
C14	C13	C12	121.1(3)	C11	P1	C21	107.62(15)

C13	C14	C17	121.0(3)	C11	P1	P2	126.66(11)
C15	C14	C13	117.9(3)	C11	P1	Pd1	119.10(11)
C15	C14	C17	121.1(3)	C21	P1	P2	123.31(11)
C16	C15	C14	121.4(3)	C21	P1	Pd1	114.84(11)
C15	C16	C11	120.7(3)	N1	P1	C11	112.66(15)
C22	C21	C26	118.8(3)	N1	P1	C21	108.13(15)
C22	C21	P1	121.3(3)	N1	P1	P2	39.94(9)
C26	C21	P1	119.8(3)	N1	P1	Pd1	93.51(10)
C23	C22	C21	119.8(3)	Pd1	P1	P2	53.63(4)
C22	C23	C24	121.6(4)	C31	P2	C41	106.35(15)
C23	C24	C27	121.3(5)	C31	P2	P1	129.85(11)
C25	C24	C23	118.4(4)	C31	P2	Pd1	119.82(11)
C25	C24	C27	120.2(5)	C41	P2	P1	120.99(11)
C24	C25	C26	120.8(4)	C41	P2	Pd1	114.91(11)
C25	C26	C21	120.5(3)	N1	P2	C31	110.67(15)
C32	C31	P2	124.0(2)	N1	P2	C41	109.15(14)
C36	C31	C32	118.6(3)	N1	P2	P1	40.73(11)
C36	C31	P2	117.3(2)	N1	P2	Pd1	95.24(11)
C31	C32	C33	119.7(3)	Pd1	P2	P1	54.58(3)
C34	C33	C32	121.5(3)	Cl2	Pd1	Cl1	96.25(5)
C33	C34	C37	120.9(4)	P1	Pd1	Cl1	98.88(5)
C35	C34	C33	118.1(3)	P1	Pd1	Cl2	163.85(4)
C35	C34	C37	121.0(4)	P2	Pd1	Cl1	166.94(4)
C36	C35	C34	121.2(4)	P2	Pd1	Cl2	94.09(4)
C35	C36	C31	120.8(3)	P2	Pd1	P1	71.80(4)
C42	C41	C46	118.6(3)				

F: Crystallographic data for [Pt(Cbutyl-4-*p*-tolyl)Cl_2]

Table F.1: Fractional Atomic Coordinates ($\times 10^4$) and Equivalent Isotropic Displacement Parameters ($Å^2 \times 10^3$) for [Pt(Cbutyl-4-*p*-tolyl)Cl_2].

Atom	***x***	***y***	***z***	**U(eq)**
C1	6132(4)	9117(3)	2410(2)	33.6(9)
C2	7308(5)	9661(3)	2075(3)	45.3(11)
C3	6700(6)	10411(3)	1787(3)	56.2(14)
C4	5740(5)	9697(3)	1876(3)	44.2(11)
C11	5054(4)	7141(3)	3820(2)	30.4(8)
C12	4985(4)	6391(3)	4312(3)	39(1)
C13	3939(5)	6171(3)	4916(3)	43.2(12)
C14	2935(4)	6666(3)	5041(2)	37.2(10)
C15	3011(4)	7431(3)	4560(3)	38.9(10)
C16	4061(4)	7672(3)	3957(2)	36.5(9)
C17	1769(5)	6351(4)	5649(3)	50.8(12)

C21	7407(4)	7908(3)	3296(2)	31.6(8)
C22	7002(4)	8404(3)	3983(2)	36.9(9)
C23	7781(5)	8882(3)	4195(3)	39.9(11)
C24	8967(5)	8876(3)	3730(3)	45.3(12)
C25	9353(5)	8381(4)	3035(3)	54.4(13)
C26	8585(5)	7907(4)	2828(3)	47.6(12)
C27	9816(6)	9378(5)	3973(4)	65.3(16)
C31	7452(4)	7763(3)	739(2)	31.2(8)
C32	8626(4)	7644(4)	557(3)	47.4(12)
C33	9459(5)	8038(4)	-106(3)	55.5(13)
C34	9139(5)	8537(4)	-604(3)	46.0(11)
C35	7975(5)	8649(3)	-431(3)	40.5(10)
C36	7124(4)	8256(3)	234(2)	34.1(9)
C37	10057(6)	8977(4)	-1326(4)	71.0(19)
C41	5041(4)	7140(3)	1536(2)	30.8(8)
C42	4961(4)	6381(3)	1094(3)	41.5(10)
C43	3915(5)	6165(3)	1067(3)	46.4(12)
C44	2910(4)	6678(3)	1489(3)	39.6(10)
C45	2992(4)	7446(3)	1916(3)	42.8(10)
C46	4051(4)	7676(3)	1941(3)	37.2(9)
C47	1763(5)	6384(4)	1498(4)	53.9(13)
N1	6153(3)	8067(2)	2370.7(17)	27.8(7)
P1	6407(1)	7327.1(7)	2982.6(5)	27.8(2)
P2	6386.3(10)	7297.7(7)	1637.6(5)	27.4(2)
Cl1	7568.8(13)	5077.5(8)	2897.5(7)	49.3(3)
Cl2	7313.8(12)	4966.4(8)	1198.3(7)	47.5(3)
Pt1	6948.8(2)	6120.0(2)	2172.2(2)	29.06(7)

Table F.2: Hydrogen Atom Coordinates ($Å \times 10^4$) and Isotropic Displacement Parameters ($Å^2 \times 10^3$) for [Pt(Cbutyl-4-*p*-tolyl)Cl_2].

Atom	***x***	***y***	***z***	**U(eq)**
H27	5679	9318	2944	40
H8A	7555	9895	2460	54
H8B	7934	9322	1669	54
H32A	6425	10961	2122	67
H32B	7157	10607	1259	67
H10A	5852	9370	1404	53
H10B	4957	9954	2129	53
H7	5648	6036	4232	47
H11	3911	5676	5246	52
H22	2347	7788	4645	47
H29	4099	8190	3644	44
H6A	1474	5831	5455	76

H6B	1229	6873	5779	76
H6C	1862	6147	6099	76
H13	6208	8415	4302	44
H31	7504	9213	4657	48
H19	10145	8373	2710	65
H103	8860	7580	2363	57
H10A	10472	8969	3882	98
H10B	9437	9530	4511	98
H10C	10082	9954	3681	98
H21	8857	7295	883	57
H28	10245	7965	-216	67
H102	7752	8992	-764	49
H25	6339	8324	339	41
H4A	9727	9097	-1687	107
H4B	10704	8546	-1549	107
H4C	10323	9565	-1198	107
H23	5619	6017	814	50
H12	3881	5664	759	56
H10	2334	7814	2188	51
H26	4092	8193	2233	45
H10D	1540	5776	1746	81
H10E	1834	6339	980	81
H10F	1180	6849	1775	81

Table F.3: Anisotropic Displacement Parameters ($Å^2 \times 10^3$) for [Pt(Cbutyl-4-*p*-tolyl)Cl_2].

Atom	**U_{11}**	**U_{22}**	**U_{33}**	**U_{23}**	**U_{13}**	**U_{12}**
C1	45(3)	25.9(18)	31(2)	-0.1(16)	-16.6(19)	2.0(18)
C2	54(3)	34(2)	53(3)	3(2)	-28(2)	-7(2)
C3	81(4)	32(2)	65(3)	14(2)	-41(3)	-11(2)
C4	55(3)	35(2)	47(3)	-2.3(19)	-26(2)	11(2)
C11	38(2)	29.7(19)	26.1(18)	1.0(15)	-15.4(17)	-2.8(17)
C12	40(3)	45(2)	37(2)	8.2(19)	-20(2)	3(2)
C13	50(3)	45(3)	36(2)	14.8(18)	-19(2)	-5(2)
C14	46(3)	39(2)	26.1(19)	1.1(16)	-14.7(19)	-6(2)
C15	40(3)	39(2)	36(2)	-2.5(18)	-14.1(19)	7.1(19)
C16	47(3)	32(2)	31(2)	7.5(16)	-16.2(19)	-0.9(19)
C17	46(3)	58(3)	38(3)	8(2)	-7(2)	-7(2)
C21	36(2)	33(2)	27.6(19)	4.4(16)	-15.6(17)	-1.5(17)
C22	37(2)	41(2)	30(2)	3.8(17)	-12.6(18)	-6.2(19)
C23	48(3)	43(3)	32(2)	3.4(17)	-21(2)	-10(2)
C24	46(3)	54(3)	45(3)	8(2)	-28(2)	-8(2)
C25	32(3)	79(4)	50(3)	0(3)	-16(2)	-2(3)
C26	40(3)	69(3)	35(2)	-9(2)	-16(2)	2(2)

C27	56(4)	85(4)	70(4)	8(3)	-41(3)	-22(3)
C31	32(2)	39(2)	21.8(17)	-0.7(15)	-9.4(16)	-3.6(17)
C32	39(3)	72(3)	34(2)	1(2)	-18(2)	3(2)
C33	33(3)	87(4)	44(3)	0(3)	-13(2)	-5(3)
C34	47(3)	52(3)	30(2)	0(2)	-7(2)	-14(2)
C35	48(3)	43(2)	31(2)	4.4(18)	-17(2)	-8(2)
C36	34(2)	40(2)	29(2)	3.7(16)	-14.0(18)	-3.0(18)
C37	52(4)	92(5)	50(4)	16(3)	-3(3)	-23(3)
C41	33(2)	34(2)	28.1(19)	7.3(15)	-16.0(17)	-5.0(17)
C42	38(3)	49(2)	37(2)	-8(2)	-15(2)	3(2)
C43	49(3)	49(3)	48(3)	-9(2)	-27(3)	-4(2)
C44	40(3)	42(2)	44(2)	8.1(19)	-25(2)	-5(2)
C45	35(3)	41(2)	53(3)	-1(2)	-19(2)	6(2)
C46	37(3)	35(2)	45(2)	-2.7(18)	-22(2)	1.0(18)
C47	47(3)	55(3)	69(4)	1(3)	-34(3)	-7(3)
N1	36.1(19)	25.2(15)	25.1(15)	2.1(12)	-15.8(14)	-0.5(13)
P1	34.0(6)	28.3(5)	23.4(4)	1.6(4)	-14.0(4)	0.2(4)
P2	30.5(6)	30.6(5)	23.1(5)	0.9(4)	-13.0(4)	-0.9(4)
Cl1	68.5(9)	42.1(6)	46.1(6)	1.9(5)	-32.7(6)	14.5(6)
Cl2	59.6(8)	43.9(6)	46.8(6)	-16.0(5)	-29.9(6)	12.1(5)
Pt1	33.93(11)	27.70(11)	27.84(10)	-0.22(5)	-15.17(8)	2.12(6)

Table F.4: Bond Lengths for [Pt(Cbutyl-4-*p*-tolyl)Cl_2].

Atom	Atom	Length/Å	Atom	Atom	Length/Å
C1	C2	1.549(7)	C31	C36	1.385(6)
C1	C4	1.542(6)	C31	P2	1.806(4)
C1	N1	1.475(5)	C32	C33	1.380(7)
C2	C3	1.535(7)	C33	C34	1.372(7)
C3	C4	1.525(8)	C34	C35	1.373(7)
C11	C12	1.389(6)	C34	C37	1.515(7)
C11	C16	1.385(6)	C35	C36	1.391(6)
C11	P1	1.807(4)	C41	C42	1.390(6)
C12	C13	1.378(7)	C41	C46	1.385(6)
C13	C14	1.374(7)	C41	P2	1.800(4)
C14	C15	1.391(6)	C42	C43	1.376(7)
C14	C17	1.512(7)	C43	C44	1.386(7)
C15	C16	1.387(7)	C44	C45	1.383(6)
C21	C22	1.384(6)	C44	C47	1.496(7)
C21	C26	1.377(7)	C45	C46	1.395(7)
C21	P1	1.803(4)	N1	P1	1.693(3)
C22	C23	1.383(6)	N1	P2	1.696(3)
C23	C24	1.384(8)	P1	P2	2.5867(14)
C24	C25	1.396(7)	P1	Pt1	2.2038(11)

C24	C27	1.510(7)	P2	Pt1	2.2111(11)
C25	C26	1.364(7)	Cl1	Pt1	2.3639(12)
C31	C32	1.383(7)	Cl2	Pt1	2.3646(12)

Table F.5: Bond Angles for [Pt(Cbutyl-4-*p*-tolyl)Cl_2].

Atom	**Atom**	**Atom**	**Angle/°**	**Atom**	**Atom**	**Atom**	**Angle/°**
C4	C1	C2	89.0(3)	C46	C41	P2	122.9(3)
N1	C1	C2	118.5(4)	C43	C42	C41	120.4(5)
N1	C1	C4	119.8(3)	C42	C43	C44	121.5(4)
C3	C2	C1	87.2(4)	C43	C44	C47	120.5(4)
C4	C3	C2	90.1(3)	C45	C44	C43	118.2(4)
C3	C4	C1	87.8(4)	C45	C44	C47	121.2(5)
C12	C11	P1	118.7(3)	C44	C45	C46	120.7(5)
C16	C11	C12	118.9(4)	C41	C46	C45	120.5(4)
C16	C11	P1	122.2(3)	C1	N1	P1	125.5(3)
C13	C12	C11	120.4(4)	C1	N1	P2	132.2(3)
C14	C13	C12	121.5(4)	P1	N1	P2	99.49(17)
C13	C14	C15	118.1(4)	C11	P1	P2	118.87(14)
C13	C14	C17	121.0(4)	C11	P1	Pt1	114.43(13)
C15	C14	C17	120.7(5)	C21	P1	C11	107.62(18)
C16	C15	C14	121.1(4)	C21	P1	P2	129.67(14)
C11	C16	C15	120.0(4)	C21	P1	Pt1	121.84(15)
C22	C21	P1	120.8(3)	N1	P1	C11	108.75(19)
C26	C21	C22	119.2(4)	N1	P1	C21	108.32(17)
C26	C21	P1	119.8(3)	N1	P1	P2	40.30(11)
C23	C22	C21	119.8(4)	N1	P1	Pt1	94.40(11)
C22	C23	C24	121.2(4)	Pt1	P1	P2	54.27(3)
C23	C24	C25	118.0(5)	C31	P2	P1	129.05(14)
C23	C24	C27	121.0(5)	C31	P2	Pt1	117.14(15)
C25	C24	C27	121.1(5)	C41	P2	C31	107.51(18)
C26	C25	C24	120.8(5)	C41	P2	P1	120.79(14)
C25	C26	C21	121.0(4)	C41	P2	Pt1	117.23(13)
C32	C31	C36	119.0(4)	N1	P2	C31	111.19(17)
C32	C31	P2	119.3(3)	N1	P2	C41	108.80(19)
C36	C31	P2	121.7(3)	N1	P2	P1	40.21(11)
C33	C32	C31	120.4(4)	N1	P2	Pt1	94.06(11)
C34	C33	C32	120.8(5)	Pt1	P2	P1	54.00(3)
C33	C34	C35	119.1(4)	P1	Pt1	P2	71.73(4)
C33	C34	C37	120.5(5)	P1	Pt1	Cl1	98.24(4)
C35	C34	C37	120.4(5)	P1	Pt1	Cl2	169.16(4)
C34	C35	C36	120.9(4)	P2	Pt1	Cl1	169.55(4)
C31	C36	C35	119.7(4)	P2	Pt1	Cl2	98.10(4)

C42	C41	P2	118.1(3)	Cl1	Pt1	Cl2	92.10(5)
C46	C41	C42	118.6(4)				

G: Supplementary GC data for 1-octene hydroformylation with a Rh-PNP as a catalyst.

G. CH_3-Ph-PNP

NONANAL (CH_3-Ph-PNP) Experiment 1

Time (min)	Area Starting Material	Area Of Internal Standard	Area of Product	Mol Product	Mol starting Material	Starting used	% yield
0	0	0	0	0	0	0	0
30	2868286	1165484	29393	0.000674965	0.045282734	0.004719938	1.3
60	442397	1107065	307530	0.00743461	0.007352848	0.042649825	14.9
90	87068	1093991	380539	0.009309562	0.001464405	0.048538267	18.6
120	52859	1016698	388751	0.01023348	0.000956629	0.049046044	20.5
150	52531	1111384	446920	0.010762408	0.000869697	0.049132976	21.5
180	46805	1102539	472617	0.011472529	0.000781115	0.049221558	22.9
BRANCHED							
180		1102539	387403	0.009404004	0.000781115	0.049221558	18.8
ISOMERISATION							
	180min						
n/i	1.2						
Other %	58.2						

NONANAL (CH_3-Ph-PNP) Experiment 2

Time (min)	Area Starting Material	Area Of Internal Standard	Area of Product	Mol Product	Mol starting Material	Starting used	% yield
0	0	0	0	0	0	0	0
30	1423517	1144145	160734	0.003760225	0.02289504	0.027145053	7.5
60	221903	1113912	297194	0.007141283	0.003665828	0.046374265	14.3
90	76588	1106758	338645	0.00818991	0.001273409	0.048766684	16.4
120	59469	1106606	367068	0.008878521	0.000988911	0.049051181	17.7
150	51607	1019593	356454	0.009357584	0.000931411	0.049108681	18.7
180	49075	1047937	387103	0.009887317	0.000861757	0.049178335	19.8
BRANCHED							
180		1047937	317754	0.008116017	0.000861757	0.049178335	16.2
ISOMERISATION							
	180min						
n/i	1.2						
Other %	64.0						

NONANAL (CH_3-Ph-PNP) Experiment 3

Time (min)	Area Starting Material	Area Of Internal Standard	Area of Product	Mol Product	Mol starting Material	Starting used	% yield
0	0	0	0	0	0	0	0
30	2737520	1051173	11880	0.000302141	0.047865545	0.002162075	0.6
60	410258	1081376	270588	0.006689582	0.006973009	0.04305461	13.4
90	77344	1027317	320094	0.008329909	0.001383764	0.048643855	16.7
120	60870	1094301	366249	0.008947606	0.001022366	0.049005253	17.9
150	50891	988941	348223	0.009413568	0.000945824	0.049081795	18.8
180	52080	1119856	415181	0.009911571	0.000854769	0.049172851	19.8
BRANCHED							
180		1119856	343311	0.008195826	0.000854769	0.049172851	16.4
ISOMERISATION							
	180min						
n/i	1.2						
Other %	63.8						

G: Cl-Ph-PNP

NONANAL (Cl-Ph-PNP) Experiment 1

Time (min)	Area Starting Material	Area Of Internal Standard	Area of Product	Mol Product	Mol starting Material	Starting used	% yield
0	0	0	0	0	0	0	0
30	1844503	1175535	220321	0.005110606	0.029414981	0.020508397	10.2
60	229677	1124321	525305	0.012740113	0.003829587	0.046093791	25.5
90	65889	1129850	609004	0.014697769	0.001093243	0.048830135	29.4
120	46557	1132533	662311	0.015946419	0.000770653	0.049152725	31.9
150	42238	1116204	677505	0.016550877	0.000709389	0.049213989	33.2
180	36351	1049467	665822	0.017299814	0.00064934	0.049274038	34.7
BRANCHED							
180		1049467	457809	0.011895087	0.00064934	0.049274038	23.8
ISOMERISATION							
	180min						
n/i	1.5						
Other %	41.5						

NONANAL (Cl-Ph-PNP) Experiment 2

Time (min)	Area Starting Material	Area Of Internal Standard	Area of Product	Mol Product	Mol starting Material	Starting used	% yield
0	0	0	0	0	0	0	0
30	2096432	1171072	118998	0.002715365	0.032888341	0.017016328	5.4
60	355782	1095426	320854	0.007827021	0.005966858	0.043937811	15.7

90	72231	1131595	435015	0.010272716	0.001172674	0.048731994	20.6
120	48702	1133141	477565	0.011262132	0.000789601	0.049115068	22.6
150	42940	1135632	516846	0.012161737	0.000694655	0.049210014	24.4
180	16075	246453	164897	0.017879309	0.001198289	0.048706379	35.8
BRANCHED							
180		1155458	373690	0.008642301	0.001198289	0.048706379	17.3
ISOMERISATION							
	180min						
n/i	2.1						
Other %	46.9						

NONANAL (Cl-Ph-PNP) Experiment 3

Time (min)	Area Starting Material	Area Of Internal Standard	Area of Product	Mol Product	Mol starting Material	Starting used	% yield
0	0	0	0	0	0	0	0
30	1959503	307288	9357	0.000833728	0.120034633	-0.06989119	1.7
60	804628	237578	64495	0.007432816	0.063752197	-0.013608754	14.8
90	114181	247077	123502	0.013685958	0.008698969	0.041444474	27.3
120	27551	243642	140993	0.015844514	0.002128587	0.048014855	31.6
150	21830	304923	171851	0.015431048	0.001347627	0.048795815	30.8
180	18546	294442	183600	0.017072867	0.001185651	0.048957792	34.0
BRANCHED							
180		1026338	338261	0.009023916	0.001185651	0.048957792	18.0
ISOMERISATION							
	180min						
n/i	1.9						
Other %	48.0						

G: F-Ph-PNP

NONANAL (F-Ph-PNP) Experiment 1

Time (min)	Area Starting Material	Area Of Internal Standard	Area of Product	Mol Product	Mol starting Material	Starting used	% yield
0	0	0	0	0	0	0	0
30	1934691	256709	0	0	0.139196867	-0.089100645	0.0
60	993897	252414	45783	0.004872783	0.072725528	-0.022629306	9.7
90	39292	231870	109996	0.012744376	0.003129814	0.046966408	25.4
120	25605	249703	131715	0.014170909	0.001893913	0.04820231	28.3
150	22533	257572	142442	0.014856813	0.001615769	0.048480453	29.7
180	20715	264526	154658	0.015706892	0.001446357	0.048649865	31.4
BRANCHED							
180		264526	157219	0.015966985	0.001446357	0.048649865	31.9

Appendix

ISOMERISATION

	180min
n/i	1.0
Other %	36.8

NONANAL (F-Ph-PNP) Experiment 2

Time (min)	Area Starting Material	Area Of Internal Standard	Area of Product	Mol Product	Mol starting Material	Starting used	% yield
0	0	0	0	0	0	0	0
30	1727812	267264	19023	0.001901431	0.118732788	-0.068731007	3.8
60	258459	260357	109476	0.011232893	0.018232115	0.031769667	22.5
90	43950	260202	137126	0.014078329	0.003102151	0.046899631	28.2
120	27857	264060	151909	0.015368194	0.001937521	0.048064261	30.7
150	24745	252163	155533	0.016477189	0.001802274	0.048199508	33.0
180	22450	263118	171481	0.017410346	0.001567041	0.048434741	34.8
BRANCHED							
180		263118	150453	0.015275387	0.001567041	0.048434741	30.5

ISOMERISATION

	180min
n/i	1.1
Other %	34.6

NONANAL (F-Ph-PNP) Experiment 3

Time (min)	Area Starting Material	Area Of Internal Standard	Area of Product	Mol Product	Mol starting Material	Starting used	% yield
0	0	0	0	0	0	0	0
30	2145625	318424	12595	0.001059191	0.124051677	-0.07413008	2.1
60	457020	308824	133061	0.011537764	0.027244496	0.022677101	23.1
90	59342	285686	173724	0.016283688	0.003824088	0.046097509	32.6
120	31628	343311	222034	0.017318636	0.00169605	0.048225547	34.7
150	24693	259447	194146	0.020038338	0.001752184	0.048169412	40.1
180	22194	305547	222419	0.019492869	0.001337249	0.048584348	39.0
BRANCHED							
180		1026338	338261	0.008825584	0.001337249	0.048584348	17.7

ISOMERISATION

	180min
n/i	2.2
Other %	43.3

G: *5-p*-tolyl-PNP

NONANAL (*5-p*-tolyl-PNP) Experiment 1

Time (min)	Area Starting Material	Area Of Internal Standard	Area of Product	Mol Product	Mol starting Material	Starting used	% yield
0	0	0	0	0	0	0	0
30	1983854	1014982	55917	0.001482975	0.036171978	0.013830694	3.0
60	283584	1002107	231699	0.006223838	0.005237072	0.044765601	12.4
90	73346	1002892	283161	0.007600243	0.001353453	0.04864922	15.2
120	59797	1003090	312037	0.008373642	0.001103216	0.048899457	16.7
150	54317	996111	330671	0.008935864	0.001009134	0.048993539	17.9
180	50764	1011281	356821	0.009497882	0.000928977	0.049073696	19.0
1440	17154	1168502	792414	0.018254539	0.000271679	0.049730993	36.5
BRANCHED							
180		1011281	290202	0.007724613	0.000928977	0.049073696	15.4
1440		1168502	945157	0.021773221	0.000271679	0.049730993	43.5
ISOMERISATION							
	180min	1440min					
n/i	1.2	0.838394045					
Other %	65.6	19.9					

NONANAL (*5-p*-tolyl-PNP) Experiment 2

Time (min)	Area Starting Material	Area Of Internal Standard	Area of Product	Mol Product	Mol starting Material	Starting used	% yield
0	0	0	0	0	0	0	0
30	2530685	1176795	191187	0.004451087	0.040505926	0.010010824	8.8
60	182749	1137566	408624	0.009841377	0.003025936	0.047490814	19.5
90	83627	1173968	479694	0.011194807	0.00134175	0.049175	22.2
120	70451	1171813	482290	0.01127609	0.001132427	0.049384323	22.3
150	62466	1157306	511708	0.012113861	0.001016662	0.049500087	24.0
180	58657	1175560	508803	0.011858055	0.000939845	0.049576905	23.5
1440	10669	1032951	885236	0.023479451	0.000194547	0.050322202	46.5
BRANCHED							
180		1175560	362320	0.008444153	0.000939845	0.049576905	16.7
1440		1032951	906505	0.024043576	0.000194547	0.050322202	47.6
ISOMERISATION							
	180min	1440min					
n/i	1.4	0.976537361					
Other %	59.8	5.9					

NONANAL (*5-p*-tolyl-PNP) Experiment 3

Time (min)	Area Starting Material	Area Of Internal Standard	Area of Product	Mol Product	Mol starting Material	Starting used	% yield
0	0	0	0	0	0	0	0
30	1666975	1181700	151814	0.003535189	0.026687173	0.023509726	7.0
60	134485	1212029	313735	0.007122919	0.002099141	0.048097759	14.2
90	81569	1199121	370839	0.008510017	0.001286894	0.048910005	17.0
120	73847	1218455	400083	0.009035426	0.001146579	0.04905032	18.0
150	66808	1195692	402047	0.009252637	0.001057036	0.049139863	18.4
180	63728	1245934	420441	0.009285773	0.000967645	0.049229255	18.5
1440	12261	1028791	824915	0.022064295	0.000225465	0.049971434	44.0
BRANCHED							
180		1245934	353118	0.007798891	0.000967645	0.049229255	15.5
1440		1028791	864497	0.023123009	0.000225465	0.049971434	46.1
ISOMERISATION							
	180min	1440min					
n/i	1.2	0.954213838					
Other %	66.0	10.0					

G: 4-*p*-tolyl-*o*-tol

NONANAL (4-*p*-tolyl-*o*-tol) Experiment 1

Time (min)	Area Starting Material	Area Of Internal Standard	Area of Product	Mol Product	Mol starting Material	Starting used	% yield
0	0	0	0	0	0	0	0
30	1397889	1035664	151814	0.003942334	0.024956693	0.025204569	7.9
60	212369	1035516	313735	0.008148294	0.003791993	0.046369268	16.2
90	68113	1019078	370839	0.00978675	0.001235822	0.04892544	19.5
120	50665	1024852	400083	0.010499037	0.000914071	0.04924719	20.9
150	47052	1002817	402047	0.010782406	0.00086754	0.049293721	21.5
180	46267	1026338	420441	0.0110173	0.000833516	0.049327745	22.0
1440	19492	1223857	824915	0.018127547	0.000294482	0.049866779	36.1
BRANCHED							
180		1026338	338261	0.008863843	0.000833516	0.049327745	17.7
1440		1223857	926097	0.020351027	0.000294482	0.049866779	40.6
ISOMERISATION							
	180min	1440min					
n/i	1.2	0.890743626					
Other %	60.4	23.3					

Appendix

NONANAL (4-*p*-tolyl-*o*-tol) Experiment 2

Time (min)	Area Starting Material	Area Of Internal Standard	Area of Product	Mol Product	Mol starting Material	Starting used	% yield
0	0	0	0	0	0	0	0
30	1671197	1182550	191187	0.004422307	0.026576077	0.023682298	8.8
60	277443	1193774	408624	0.00936293	0.004370533	0.045887842	18.6
90	74294	1200038	479694	0.010934006	0.001164237	0.049094138	21.8
120	58452	1155603	482290	0.011415886	0.000951204	0.049307171	22.7
150	56069	1189758	511708	0.011764504	0.000886231	0.049372144	23.4
180	53007	1155458	508803	0.012044965	0.000862704	0.049395671	24.0
1440	17077	1207359	885236	0.020055462	0.000265985	0.049992389	39.9
BRANCHED							
180		1155458	373690	0.008846416	0.000862704	0.049395671	17.6
1440		1207359	961843	0.021791032	0.000265985	0.049992389	43.4
ISOMERISATION							
	180min	1440min					
n/i	1.4	0.920353945					
Other %	58.4	16.7					

NONANAL (4-*p*-tolyl-*o*-tol) Experiment 3

Time (min)	Area Starting Material	Area Of Internal Standard	Area of Product	Mol Product	Mol starting Material	Starting used	% yield
0	0	0	0	0	0	0	0
30	9671675	1212951	11905	0.000264712	0.147848898	-0.097558449	0.5
60	466560	1136432	286483	0.006798958	0.007612437	0.042678012	13.5
90	130814	948635	303271	0.008622212	0.002556906	0.047733543	17.1
120	54114	1085406	417727	0.010379759	0.000924436	0.049366013	20.6
150	50016	1138368	458991	0.010874479	0.000814678	0.049475771	21.6
180	47973	1128494	464267	0.011095721	0.000788238	0.049502211	22.1
1440	20399	1192452	784738	0.017748871	0.000317196	0.049973253	35.3
BRANCHED							
180		1128494	391962	0.009367672	0.000788238	0.049502211	18.6
1440		1192452	820637	0.018560819	0.000317196	0.049973253	36.9
ISOMERISATION							
	180min	1440min					
n/i	1.2	0.956254714					
Other %	59.3	27.8					

G: Chzyl-4-*p*-tolyl

NONANAL (Chzyl-4-*p*-tolyl) Experiment 1

Time (min)	Area Starting Material	Area Of Internal Standard	Area of Product	Mol Product	Mol starting Material	Starting used	% yield
0	0	0	0	0	0	0	0
30	2406614	945500	29518	0.000838376	0.046992793	0.00319787	1.7
60	971521	1118520	414936	0.009962103	0.016035953	0.034154709	19.8
90	144747	1113258	606570	0.014631833	0.002400491	0.047790172	29.2
120	70977	1091859	638153	0.015695382	0.001200155	0.048990508	31.3
150	65400	1135496	682062	0.016130651	0.001063356	0.049127307	32.1
180	61751	1124521	687215	0.016411138	0.001013824	0.049176838	32.7
1440	28507	1161431	890280	0.020584809	0.000453153	0.04973751	41.0
BRANCHED							
180		1124521	361388	0.008630179	0.001013824	0.049176838	17.2
1440		1161431	772081	0.017851845	0.000453153	0.04973751	35.6
ISOMERISATION							
	180min	1440min					
n/i	1.9	1.15309145					
Other %	50.1	23.4					

NONANAL (Chzyl-4-*p*-tolyl) Experiment 2

Time (min)	Area Starting Material	Area Of Internal Standard	Area of Product	Mol Product	Mol starting Material	Starting used	% yield
0	0	0	0	0	0	0	0
30	3060847	1225923	32405	0.000707198	0.045924385	0.003968702	1.4
60	349001	1119063	377434	0.009023576	0.005736369	0.044156718	18.1
90	80502	1086477	436654	0.010752492	0.001362859	0.048530227	21.6
120	55714	1008611	429779	0.011400232	0.001016028	0.048877059	22.8
150	53785	1089584	483036	0.011860718	0.000907957	0.048985129	23.8
180	47323	1077433	505449	0.012551028	0.00080788	0.049085206	25.2
1440	12938	1186895	923601	0.020819213	0.000200502	0.049692584	41.7
BRANCHED							
180		1077433	370006	0.009187783	0.00080788	0.049085206	18.4
1440		1186895	979080	0.022069785	0.000200502	0.049692584	44.2
ISOMERISATION							
	180min	1440min					
n/i	1.4	0.94333558					
Other %	56.4	14.0					

NONANAL (Chzyl-4-*p*-tolyl) Experiment 3

Time (min)	Area Starting Material	Area Of Internal Standard	Area of Product	Mol Product	Mol starting Material	Starting used	% yield
0	0	0	0	0	0	0	0
30	1976183	258987	3572	0.000369294	0.140462542	-0.090447396	0.7
60	820141	285943	73199	0.006854319	0.052798354	-0.002783208	13.7
90	126393	257634	107203	0.011141467	0.009030903	0.040984243	22.3
120	52882	316420	137313	0.011619471	0.003076488	0.046938658	23.2
150	39583	256570	122000	0.012731881	0.002839973	0.047175173	25.5
180	34516	250838	126490	0.013502105	0.002533019	0.047482127	27.0
1440	8086	291116	252383	0.023213074	0.000511304	0.049503842	46.4
BRANCHED							
180		250838	86784	0.00926371	0.002533019	0.047482127	18.5
1440		291116	290728	0.026739877	0.000511304	0.049503842	53.5
ISOMERISATION							
	180min	1440min					
n/i	1.5	0.868106959					
Other %	54.5	0.1					

G: Cbutyl-4-*p*-tolyl

NONANAL (Cbutyl-4-*p*-tolyl) Experiment 1

Time (min)	Area Starting Material	Area Of Internal Standard	Area of Product	Mol Product	Mol starting Material	Starting used	% yield
0	0	0	0	0	0	0	0
30	2741994	1121391	31472	0.000749962	0.044921496	0.005060685	1.5
60	278063	1134900	357364	0.008414441	0.004501222	0.04548096	16.8
90	77834	1126403	417982	0.009915985	0.001269464	0.048712717	19.8
120	58416	1067567	421109	0.010540749	0.001005267	0.048976914	21.1
150	59101	1123731	451747	0.010742491	0.000966223	0.049015958	21.5
180	53833	1107701	462116	0.011148092	0.000892834	0.049089347	22.3
1440	13550	1073517	808779	0.020132282	0.000231886	0.049750295	40.3
BRANCHED							
180		1107701	334249	0.008063427	0.000892834	0.049089347	16.1
1440		1073517	897239	0.022334246	0.000231886	0.049750295	44.7
ISOMERISATION							
	180min	1440min					
n/i	1.4	0.901408655					
Other %	61.6	15.0					

Appendix

NONANAL (Cbutyl-4-*p*-tolyl) Experiment 2

Time (min)	Area Starting Material	Area Of Internal Standard	Area of Product	Mol Product	Mol starting Material	Starting used	% yield
0	0	0	0	0	0	0	0
30	1389625	218118	20408	0.00249724	0.116904203	-0.066870347	5.0
60	878373	271899	69911	0.006862608	0.059278251	-0.009244395	13.7
90	296578	239392	99402	0.011082476	0.02273282	0.027301036	22.1
120	63695	284072	136714	0.012845052	0.004114347	0.045919509	25.7
150	41659	286319	144978	0.013514602	0.002669824	0.047364032	27.0
180	35448	237708	128959	0.014479687	0.002736352	0.047297504	28.9
1440	7670	297747	244521	0.021918967	0.000472685	0.049561171	43.8
BRANCHED							
180		237708	78210	0.008781522	0.002736352	0.047297504	17.6
144		297747	269072	0.024119729	0.000472685	0.049561171	48.2
ISOMERISATION							
	180min	1440min					
n/i	1.6	0.908756764					
Other %	53.5	8.0					

NONANAL (Cbutyl-4-*p*-tolyl) Experiment 3

Time (min)	Area Starting Material	Area Of Internal Standard	Area of Product	Mol Product	Mol starting Material	Starting used	% yield
0	0	0	0	0	0	0	0
30	3050362	1161000	11549	0.000265818	0.048268515	0.001636153	0.5
60	1326688	1123719	255301	0.006071093	0.021689815	0.028214853	12.2
90	187810	1073777	425841	0.010597549	0.003213286	0.046691382	21.2
120	72066	1115379	492183	0.011791695	0.001187006	0.048717663	23.6
150	63698	1095983	501365	0.012224251	0.001067743	0.048836926	24.5
180	58857	1092410	517188	0.012651291	0.000989822	0.048914846	25.4
1440	35288	1176653	754785	0.017141425	0.000550964	0.049353704	34.3
BRANCHED							
180		1092410	302055	0.007388775	0.000989822	0.048914846	14.8
1440		1176653	633978	0.014397857	0.000550964	0.049353704	28.9
ISOMERISATION							
	180min	1440min					
n/i	1.7	1.190553931					
Other %	59.8	36.8					